TOPOLOGICALLY NOVEL PHOSPHORUS COMPOUNDS AND METAL COMPLEXES

A Dissertation

by

SUGAM KHAREL

Submitted to the Office of Graduate and Professional Studies of
Texas A&M University
in partial fulfillment of the requirements for the degree of

DOCTOR OF PHILOSOPHY

Chair of Committee,	John Gladysz
Committee Members,	Janet Bluemel
	Francois Gabbai
	Sarbajit Banerjee
	Melissa Grunlan
Head of Department,	Simon North

August 2018

Major Subject: Chemistry

ABSTRACT

This dissertation details the synthesis of isomeric square planar platinum complexes bearing bridgehead diphosphine ligands with *cis* and *trans* geometries at platinum. The stabilities of these isomers have been discussed in detail. The topological properties of these complexes along with those of corresponding diphosphine ligands are examined. An overview on synthesis of oxide analogs of these ligands is presented.

We first studied the literature to understand the chemistry of novel platinum diphosphine complexes with *cis*- (parachutes) and *trans*- (gyroscopes) geometries at platinum.

Next, we carried out the reactions of *cis*-$PtCl_2(P((CH_2)_mCH=CH_2)_3)_2$ and Grubbs' first generation catalyst and then hydrogenations to afford *cis*-$P\overline{tCl_2(P((CH_2)_n)_3P)}$ (*cis*-**2**; $n = 2m+2$ = **b**/12, **c**/14, **d**/16, **e**/18, **f**/20, **g**/22; 6-40%), derived from three fold *inter*ligand metatheses. The thermal behavior of the complexes is examined. When the bridges are sufficiently long, they rapidly exchange via an unusual "triple jump rope" motion over the PtX_2 moieties. The relative stabilities of *cis*/*trans* and other types of isomers are probed by combinations of molecular dynamics and DFT calculations.

We extended our research to *trans*-platinum complexes. Reactions of $P((CH_2)_mCH=CH_2)_3$ (2.0 equiv; m = **f**/9, **g**/10, **k**/14) and $PtCl_2$ in toluene to give *trans*-$PtCl_2(P((CH_2)_mCH=CH_2)_3)_2$ (*trans*-**1f**,**g**,**k**; 63-49%). Reactions of *trans*-**1f**,**g** with Grubbs' first generation catalyst (CH_2Cl_2/reflux) followed by hydrogenations (cat. PtO_2) afford chromatographically separable gyroscope like *trans*-$P\overline{tCl_2(P((CH_2)_n)_3P)}$ (*trans*-**2f**,**g**, 3-19%; from *inter*ligand metathesis) and *trans*-$P\overline{tCl_2((H_2\underline{C})_nP((CH_2)_n)\underline{P}(CH_2)_n)}$ (*trans*-**2'f**,**g**, 25-12%; from *inter*- and *intra*ligand metathesis), where $n = 2m+2$. Under

analogous conditions, *trans*-**1k** gives only *cis*-$PtCl_2(P((CH_2)_{30})_3P)$ (*cis*-**2k**, 39%). The stability of *cis* vs *trans* is established for **1g** and **2'f**,**g** in CH_2Cl_2 and toluene.

To further probe the applicability of our research, we exploited the rapidly equilibrating *in,in* and *out,out* isomer of $P((CH_2)_{14})_3P$ (**1**). U-tubes are charged with CH_2Cl_2 solutions of **1** (lower phase), an aqueous solution of K_2MCl_4 (charging arm; M = Pt, Pd), and an aqueous solution of excess KCl/KCN (receiving arm). The MCl_2 units are then transported to the receiving arm until equilibrium is reached (up to 22 d vs. 100 h, KCl vs. KCN). Analogous experiments with K_2PtCl_4/K_2PdCl_4 mixtures show $PdCl_2$ transport to be more rapid.

The reactions of $(O=)PH(OCH_2CH_3)_2$ and $BrMg(CH_2)_mCH=CH_2$ (4.9-3.2 equiv; *m* = **a**/4, **b**/5, **c**/6) are carried out to give the dialkylphosphine oxides $(O=)PH((CH_2)_mCH=CH_2)_2$ (**2a-c**; 77-81% after workups), which are treated with NaH and then α,ω-dibromides $Br(CH_2)_nBr$ (0.49-0.32 equiv; *n* = **a'**/8, **b'**/10, **c'**/12, **d'**/14) to yield the bis(trialkylphosphine oxides) $(H_2C=CH(CH_2)_m)_2P(=O)$-$(CH_2)_n(O=)P((CH_2)_mCH=CH_2)_2$ (**3ab'**, **3bc'**, **3cd'**, **3ca'**; 79-84%). Reactions of **3bc'** and **3ca'** with Grubbs' first generation catalyst and then H_2/PtO_2 afford the dibridgehead diphosphine dioxides $(O=)P(CH_2)_n((CH_2)_{n'})_2P(=O)$ (**4bc'**, **4ca'**; 14-19%, $n' = 2m + 2$). Crystal structures of two isomers of the latter are obtained, *out,out*-**4ca'** and a conformer of *in,out*-**4ca'** that features crossed chains, such that the (O=)P vectors appear *out,out*.

Overall, this research summarizes the reactions of *cis*- and *trans*- platinum complexes to create an assembly of macrocyclic cages. These cages can be isomerized under thermal conditions and the chemistry of the empty macrocyclic cages obtained from the demetallation of these metal-containing macrocylic cages can be used to selectively transport metal chlorides.

DEDICATION

I dedicate this dissertation to my lovely wife. We have faced a lot together during the last few years and I thank you for helping me make all the right decisions during these times. This one is for you!!

ACKNOWLEDGEMENTS

I would like to begin by thanking my family for their unconditional love and support. Thanks dad, Mukunda P Kharel and mom, Subhadra Kharel for being the coolest parents. Thanks to my parents in law Raju Bhetuwal and Indira Bhetuwal for the final stage of my graduate career less stressful. Thanks to my lovely wife Rita Bhetuwal and my cute daughter Aanvie Kharel. Life in graduate school was stressful but you provided the exact opposite environment at home. I will have a Ph.D. degree but my graduation cap belongs to you.

I would like to thank my advisor and my co-advisor, Dr. Gladysz and Dr. Bluemel, for all of their support and assistance throughout the years. I have learned invaluable lessons from both of you beyond research that will make me a better scholar.

Furthermore, I want to appreciate my entire committee, Dr. Gabbai, Dr. Banerjee, and Dr. Grunlan. You've provided insightful questions and valuable input about what directions to pursue in my research. Thank you for showing up to my seminars and allowing me the time to present my research to you. Also, thanks to Dr. Yang for supporting me as a committee member during the beginning of my Ph.D. and my preliminary exam. My sincere appreciation goes to my lab members who created the best environment in the lab. Special thanks to Dr. Tathagata Mukherjee and Dr. Hemant Joshi for being good friends and true companion. Thanks to Dr. Arjun Acharya, Dr. Ramesh C. Dhakal, and Dr. Rajan Parajuli for all the time they have spent together with me. My time in Texas A&M has been much easier with the help of excellent graduate office staffs whom I like to express my sincere appreciation. Finally, thanks to all my friends who have contributed to make my journey memorable.

CONTRIBUTORS AND FUNDING SOURCES

Contributors

Part 1, faculty committee recognition

This work was supervised by a dissertation committee consisting of Dr. John A. Gladysz, Dr. Janet Bluemel, Dr. Francois Gabbai, and Dr. Sarbajit Banerjee of the Department of Chemistry and Dr. Melissa Grunlan of the Department of Biomedical Engineering.

Part 2, student/collaborator contributions

The work of section 2 of dissertation was completed by the student, in collaboration with Dr. Hemant Joshi, Dr. Tobias Fiedler, and Andreas Ehnbom of the Department of Chemistry; Ms. Katrin Skopek and Ms. Giesla D. Hess of the Institut für Organische Chemie and Interdisciplinary Center for Molecular Materials, Friedrich-Alexander-Universität Erlangen-Nürnberg, Henkestraße 42, 91054 Erlangen (Germany).

The work of section 3 of dissertation was completed by the student, in collaboration with Dr. Hemant Joshi of the Department of Chemistry.

The work of section 4 of dissertation was completed by the student, in collaboration with Dr. Hemant Joshi and Stephen Bierschenk of the Department of Chemistry.

The work of section 5 of dissertation was completed by the student, in collaboration with Mr. Tiezheng Jia of the Department of Chemistry.

All crystal structures were determined by crystallographer Dr. Nattamai Bhuvanesh, Dr. Joseph Reibenspies, and Dr. Frank Hampel, although all crystallographic data were interpreted by the student.

All other work conducted for the dissertation was completed by the student independently.

Funding Sources

This work was made possible in part by National Science Foundation under Grant Number CHE-1153085 and CHE-1566601.

NOMENCLATURE

δ	chemical shift in ppm
λ	wavelength
^{13}C	NMR active carbon nucleus (NMR)
^{1}H	proton (NMR)
^{31}P	NMR active phosphorus nucleus (NMR)
$\{^{1}H\}$	proton decoupled
$\{^{31}P\}$	phosphorus decoupled
Å	Ångstrom
ACS	American Chemical Society
Anal.	Analysis
ATR	Attenuated Total Reflectance
B3LYP	Becke, three parameter, Lee-Yang-Parr
BET	Brunauer Emmett Teller
br	broad
Bu	butyl
COSY	COrrelation SpectroscopY (2D NMR)
d	doublet (NMR), days
DFT	density functional theory
DSC	differential scanning calorimetry
ESI	electrospray ionization
h	hour
HMBC	Heteronuclear Multiple Bond Correlation (2D NMR)
HSQC	Heteronuclear Single Quantum Coherence (2D NMR)

Hz	Hertz
i	ipso
J	scalar coupling constant
IR	infrared
m	multiplet (NMR), medium (IR)
m	meta
Me	methyl
NMR	nuclear magnetic resonance
o	ortho
Oct	octyl
p	para
Ph	phenyl
ppm	parts per million
R	alkyl group
RT	room temperature
s	singlet (NMR), strong (IR)
t	triplet (NMR)
THF	tetrahydrofuran
UV	ultraviolet
ν	wavenumber
Vis	visible
VT	variable temperature
w	weak (IR)

TABLE OF CONTENTS

LIST OF FIGURES

LIST OF SCHEMES

LIST OF TABLES

1. INTRODUCTION

1.1. Molecular gyroscopes

Machines based upon molecules able to perform functions of a rotor are gaining popularity because of their applications, especially in the field of nanofluidics,[1-3] electronics, and photonics.[4,5] The rotors consist of a "rotator", the internal spinning part and a "stator", defining a stable outer framework. Toy gyroscopes clearly illustrate both components, optimal with a stator providing a degree of steric protection. The first device with resemblance to mechanical gyroscopes was made in 1810 by a German inventor, G. C. Bohnenberger. Jean Foucault, a French physicist, built a gyroscope in 1852 that helped people visualize the rotational axis of earth.[6,7] Termed by Foucault, gyroscope is derived from two Greek words - "gyros" and "skopein", meaning "circle" and "to view" respectively.[8]

Macroscopic gyroscopes can assume a number of physical forms,[9] which include biological assemblies such as the halteres of flying insects.[10] All of these serve to sense and/or maintain the orientation of an object. These gyroscopes conserve angular momentum, such as when the object is displaced from its axis of rotation, there is a restoring force.[11] Since the underlying physics can also be applied at the molecular level,[12] chemists are inspired to miniaturize the gyroscope with no regards to its size.

1.2. Gyroscopes in the chemical literature

There has been a series of gyroscope like molecules developed in the past. In 1985, Rose reported the first molecules called "gyroscope porphyrins" from which gyroscope as a term in chemical literature came into existence (Figure 1.1, top left).[13] Rose's porphyrins are similar to toy gyroscopes with two spokes in terms of their connectivities.

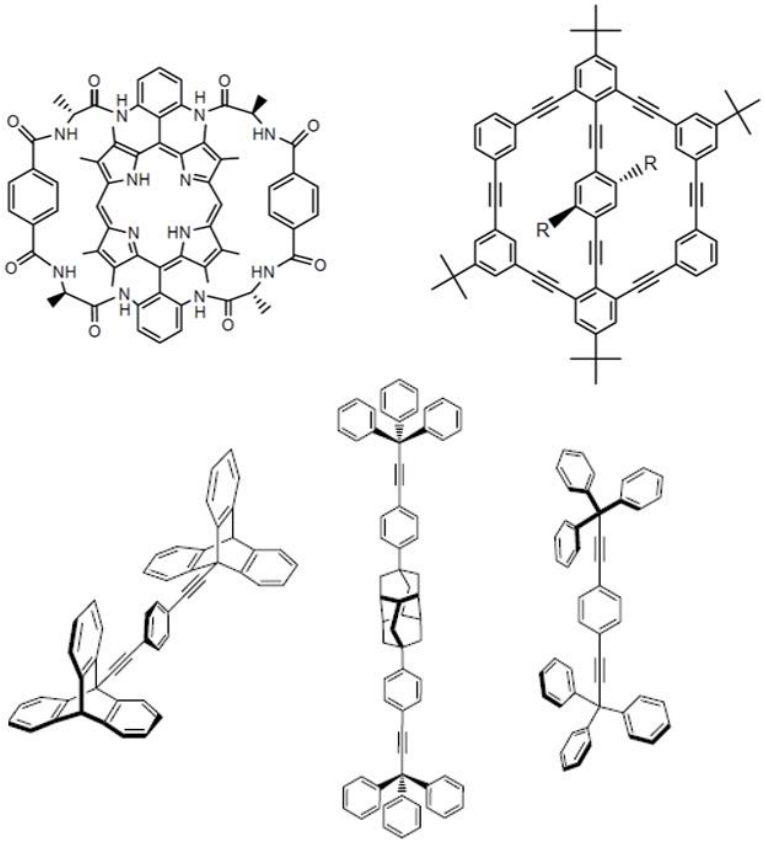

Figure 1.1. Molecular gyroscopes in chemical literature.

In 1995, Moore reported similar molecules (Figure 1.1, top right).[14] These molecules termed as "molecular turnstiles" consisted of a cyclohexa-*m*-phenylene with a C≡C expansion that hosted *p*-phenylene moiety in its center. When R is small, rotation of phenylene is fast on the NMR time scale.

The research group of Miguel Garcia-Garibay has reported configurationally similar models in the recent past (Figure 1.1, bottom).[4,15,16] In place of spokes, they consist of bulky termini in these axes, functioning to protect the rotator because of their steric appearance. This group has studied several properties of these molecules including the speed of rotation of these rotators and even using solid state NMR tactics to measure the rotational barriers.

Gladysz and coworkers developed the first molecule which, in terms of connectivity, is the closest mimic of a toy gyroscope[17] It is comprised of a stator that encapsulates an interior rotator with multiple "spokes", at the same time, duplicating the symmetry and connectivity of a toy gyroscope. This molecule is a trigonal–bipyramidal metal complex with an equatorial ML_3 array. The rotator connects to two phosphorous atoms in axial positions, leading to a P-M-P axis. These phosphorous atoms at the end of the axis are connected by three "spokes", consisting of methylene groups $(CH_2)_n$. The Gladysz group has synthesized a library of these compounds, with different geometric construction at the metal center. The study was extended to square planar metal complexes, where different types of compounds were obtained based on *cis* or *trans* orientation of the two phosphine ligands (Figure 1.1).[18]

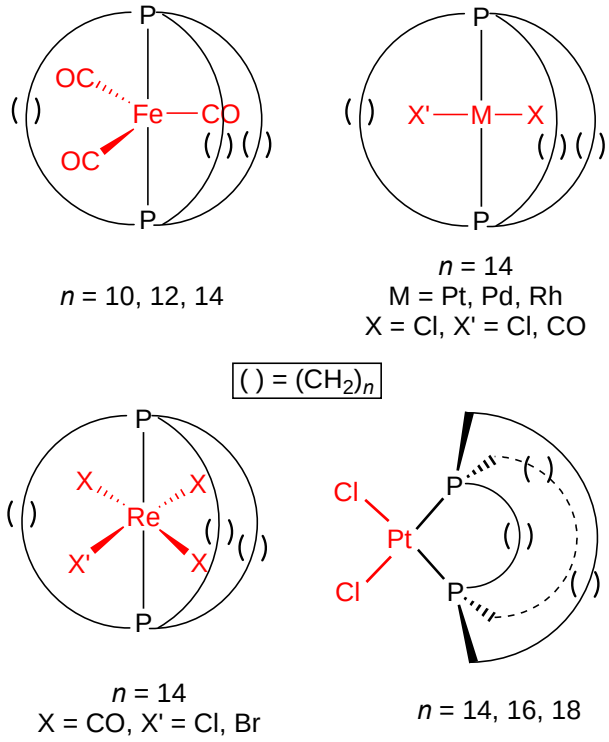

Figure 1.2. Complexes synthesized in Gladysz group; Gyroscope-like (top, bottom left), parachute-like (bottom right).

1.3. Aim of this work

In this thesis, square planar gyroscope like complexes of varying macrocycle sizes have been reported. An obvious aim was to see how flexible the associated diphosphine ligands are conformationally. These phosphines can be isolated by extruding the metal out of the square planar platinum gyroscopes, giving rise to rare dynamic properties. The empty diphosphine cage thus obtained could serve as a host molecule to metals and solvents. Different sized gyroscopes can yield corresponding empty cages that have the potential to capture guest molecules of various sizes which can help in catalysis or transport.

Another question of interest is derived from the geometry of platinum complexes based on *cis* positions of the phosphine ligands. It was of great interest to expand the library of these complexes and probe any attendant unusual types of isomerism. Furthermore, these adducts featuring geometries of a parachute might be active catalytically and provide unexpected reactant or product selectivities.

Furthermore, molecules derived from further coordination of phosphine ligands in empty diphosphine cages should be discussed. This includes synthesizing Lewis acid adducts and also attaining different oxidation states on phosphorus.

1.4. References

(1) Zheng, X.; Mulcahy, M. E.; Horinek, D.; Galeotti, F.; Magnera, T. F.; Michl, J. *J. Am. Chem. Soc*. **2004**, *126*, 4540-4542.

(2) Koumura, N. L.; Geertseman, E. M.; van Gelder, M. B.; Meetsma, A.; Feringa, B. L. *J. Am. Chem. Soc*. **2002**, *124*, 5037-5051.

(3) Feringa, B. L. *Acc. Chem. Res.* **2001**, *34*, 504-513.

(4) (a) Godinez, C. E.; Zepeda, G.; Mortko, C. J.; Dang, H.; Garcia-Garibay, M. A. *J. Org. Chem.* **2004**, *69*, 1652-1662. (b) Dominguez, Z.; Dang, H.; Strouse, M. J.; Garcia-Garibay, M. A. *J. Am. Chem. Soc.* **2002**, *124*, 7719-7727.

(5) (a) Saleh, B. E. A.; Teich, M. C. *Fundamental of Photonics*; Wiley-Interscience: Hoboken, NJ, 2009. (b) Setian, L. *Applications in Electrooptics*; Pearson Prentice Hall: Upper Saddle River, NJ, 2001. (c) Kasap, S. O. *Optoelectronic and Photonics, Principals and Practices*; Pearson Prentice Hall; Upper Saddle River, NJ, **2001**. (d) Weber, M. J. *Handbook of Optical Materials*, CRC Press: Boca Raton, FL, **2002**.

(6) Fabeck, W. Kreiselgeräte, 1. Aufl., Vogel-Verlag, Würzburg, **1980**, 92.

(7) Bergmann, L.; Schäfer, C. Lehrbuch der Experimentalphysik, Band 1, Walter de Gruyter, Berlin, **1990**, 212.

(8) http://www.science.edu.sg

(9) Kottas, G. S.; Clarke, L. I.; Horinek, D.; Michl, J. *Chem. Rev.* **2005**, *105*, 1281-1378.

(10) See http://www.gyroscopes.org/uses.asp.

(11) Alexander, R. M. *Science* **2007**, *315*, 771-772.

(12) (a) Butikov, E. *Eur. J. Phys*. **2006**, *27*, 1071-1081. (b) Kleppner, D.; Kolenkow, R. J. An Introduction to Mechanics, Cambridge University Press, Cambridge, UK; **2010**, Chapters 7.3-7.5.

(13) Boitrel, B.; Lecas, A.; Renko, Z.; Rose, E. *J. Chem. Soc., Chem. Commun.* **1985**, 1820-1821.

(14) Bedard, T. C.; Moore, J. S. *J. Am. Chem. Soc.* **1995**, *117*, 10662-10671.

(15) (a) Dominguez, Z.; Khuong, T.-A.; Dang, H.; Sanrame, C. N.; Nuñez, J. E.; Garcia-Garibay, M. A. *J. Am. Chem. Soc.* **2003**, *125*, 8827-8837. (b) Karlen, S. D.; Ortiz, R.; Chapman, O. L.; Garcia-Garibay, M. A. *J. Am. Chem. Soc.* **2005**, *127*, 6554-6555. (c) Karlen, S. D.; Garcia-Garibay, M. A. *Chem. Commun.* **2005**, 189-191. (d) Karlen, S. D.; Godinez, C. E.; Garcia-Garibay, M. A. *Org. Lett.* **2006**, *8*, 3417-3420.

(16) (a) Garcia-Garibay, M. A. *Proc. Natl. Acad. Sci.* **2005**, *102*, 10771-10776. (b) Khuong, T.-A. V.; Nuñez, J. E.; Godinez, C. E.; Garcia-Garibay, M. A. *Acc. Chem. Res.* **2006**, *39*, 413-422.

(17) Shima, T.; Hampel, F.; Gladysz, J. A. *Angew. Chem. Int. Ed.* **2004**, *43*, 5537; *Angew. Chem.* **2004**, *116*, 5653-5656.

(18) Skopek, K.; Barbasiewicz, M.; Hampel, F.; Gladysz, J. A. *Inorg. Chem*. **2008**, *47*, 3474-3476.

2. THREE FOLD INTRAMOLECULAR RING CLOSING ALKENE METATHESES OF SQUARE PLANAR COMPLEXES WITH *CIS* PHOSPHORUS DONOR LIGANDS $P(X(CH_2)_mCH=CH_2)_3$ (X/*m* = –/5-10, O/3-5); SYNTHESES, STRUCTURES, AND THERMAL BEHAVIOR OF MACROCYCLIC DIBRIDGEHEAD DIPHOSPHORUS COMPLEXES*

2.1. Introduction

Multifold ring closing alkene (C=C) metatheses can lead to a variety of fascinating molecular architectures, especially in metal coordination spheres.[1,2] Over the last fifteen years, we have been especially concerned with metathesis/hydrogenation sequences of the type exemplified in 1.[3-7] These feature educts with *trans* disposed olefinic phosphine ligands of the formula $P((CH_2)_mCH=CH_2)_3$, such as the platinum dichloride complexes *trans*-**1c-e** (indices code to the number of atoms between phosphorus and the vinyl group). The major products are almost always derived from three fold *inter*ligand metatheses, which afford triply *trans* spanning dibridgehead diphosphine ligands. For *trans*-**1c-e**, this corresponds to *trans*-**2c-e**. In some cases, byproducts derived from combinations of *inter*ligand and *intra*ligand metatheses are obtained, such as *trans*-**2'c-e** in 1. Such species carry primed numbers throughout this manuscript. Setaka has realized similar chemistry when the P-M-P linkages are replaced by Si-arylene-Si linkages (e.g., arylene = *p*-C_6H_4).[2d,8]

Analogous reactions of palladium complexes with shorter methylene chains have

*Reproduced with permission from Joshi, H.‡; Kharel, S.‡; Ehnbom, A.; Skopek, K.; Hess, G. D.; Fiedler, T.; Hampel, F.; Bhuvanesh, N.; Gladysz, J. A. *J. Am. Chem. Soc.* **2018**, *140*, in press. DOI: 10.1021/jacs.8b02846. (‡ = equal contribution)

been investigated, but only oligomeric or polymeric products were detected.[4b,9] In any event, the monoplatinum complexes *trans*-**2c-e** represent an interesting class of molecular rotors.[10] In all cases, rotation of the $PtCl_2$ moieties about the P-Pt-P axes is rapid on the NMR time scale, even at –80 °C.[4,11] Given the suggestive geometry, and the potential for closely related systems to function as molecular gyroscopes,[8,10,12,13] we refer to them as gyroscope like.

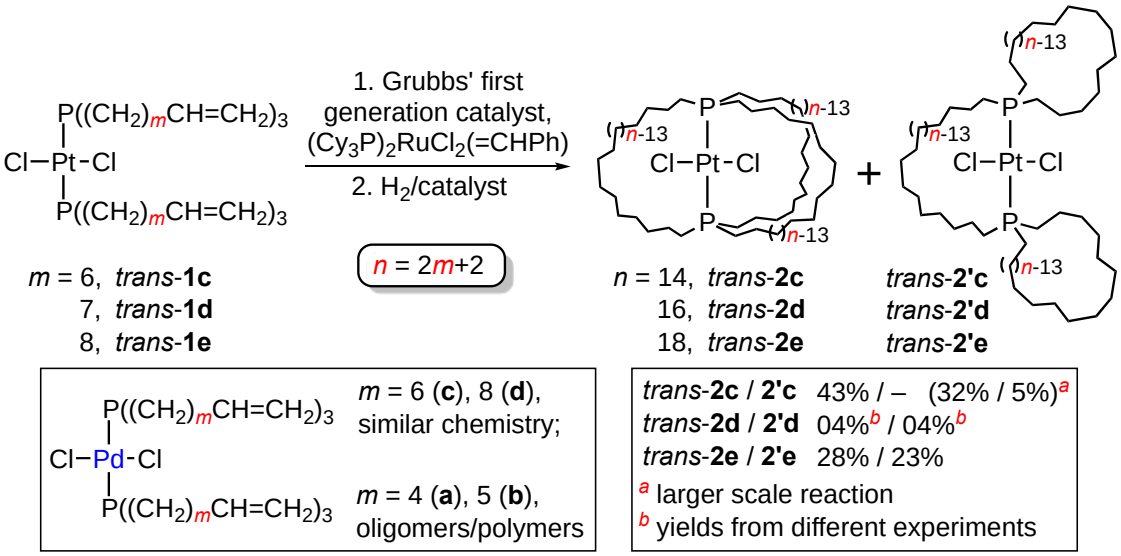

Scheme 2.1. Three fold ring closing metatheses of *trans*-**1c-e**; syntheses of gyroscope like complexes *trans*-**2c-e**.[4]

During the course of the efforts in Scheme 2.1, syntheses of the isomeric educts *cis*-**1** were developed.[14] Hence, it became of interest to investigate analogous metathesis/hydrogenation sequences, as sketched in 2. In the case of three fold *inter*ligand metathesis to give *cis*-**2**, a likely spatial distribution of macrocycles suggests (when the perpendicular Pt-Cl bonds are both directed downwards) a parachute (see **I** in Figure 2.1). Thus, we refer to *cis*-**2** as parachute like.

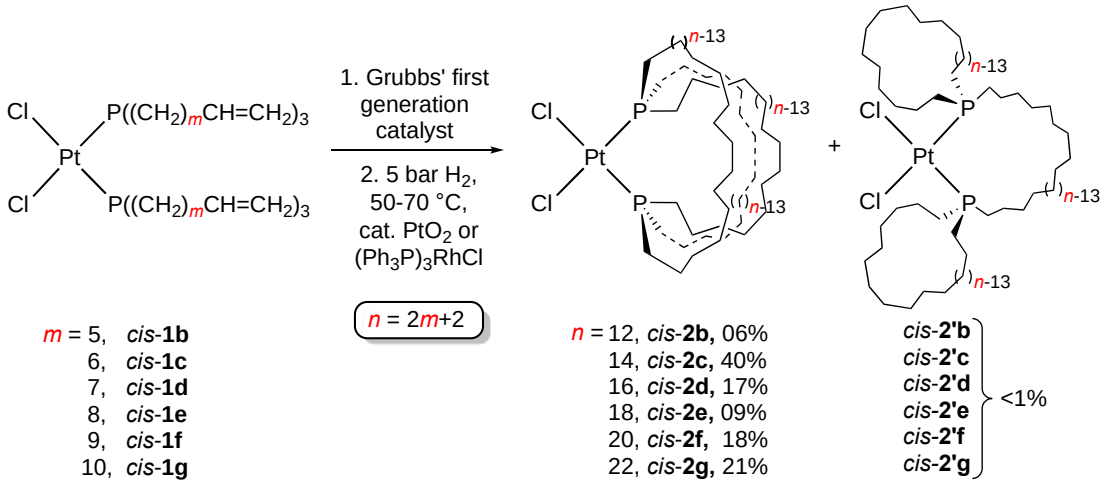

Scheme 2.2. Three fold ring closing metatheses of *cis*-**1b-g**; syntheses of parachute like complexes *cis*-**2b-g**.

Such complexes can also potentially serve as molecular rotors, although this is now in the form of coupled motion about two perpendicular Pt-P bonds. From the frame of reference of the Cl-Pt-Cl moiety, this may be viewed as a three fold "jump rope" process, as illustrated in 3.[15] To wit, one methylene chain occupies a "central" position roughly in the platinum coordination plane, and the other two flanking positions above and below the coordination plane. These undergo clockwise or counterclockwise exchange in the same sense as "jumping rope" (or a tripled rope) in forwards or backwards directions. Others have made "jump rope" analogies for dynamic processes involving a *single* methylene or methylene rich bridge,[15] but *cis*-**2** is perhaps the first system to invoke the rich Olympic traditions of the triple jump or triple axel.

Apart from any dynamic properties, such adducts are of interest in that they help define the geometric flexibility of the dibridgehead diphosphine ligands $P((CH_2)_n)_3P$ (**3c-e**), which can be isolated via various demetallation protocols.[4,16] Both **3c** and **3e** have been found to serve as "container molecules" capable of transporting MCl_2 moieties from

one place to another.

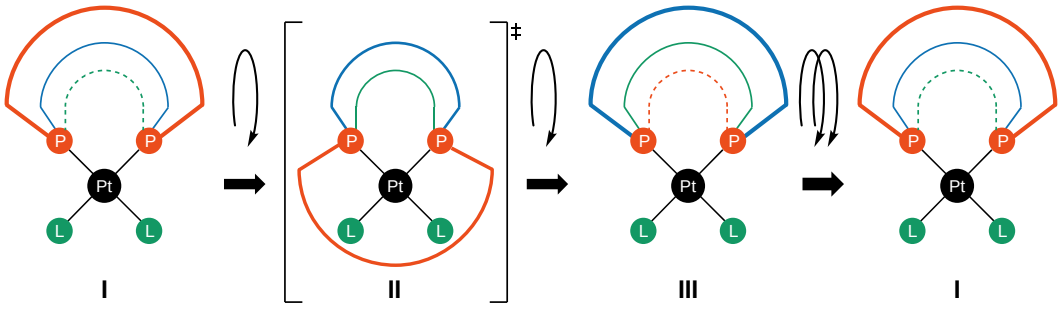

Figure 2.1. Possible "jump rope" dynamic processes involving the macrocycles of parachute like complexes *cis*-**2**.

In all cases, when the "containers" **3c**,**e** are "loaded" (M = Pt, Pd, Ni), the resulting adducts exhibit *trans* Cl-M-Cl and P-M-P linkages (i.e., *trans*-**2c** as opposed to *cis*-**2c**), as exemplified in 3. We have sought to better understand the nuances of this process, especially with respect to kinetic and thermodynamic control of geometric isomerism. The dibridgehead diphosphines are themselves capable of dynamic processes, such as "homeomorphic isomerization",[18] which exchanges *exo* directed (*out*,*out*) and *endo* directed (*in*,*in*) functionality without any intervening inversions of configuration at phosphorus (3). However, these phenomena do not play a role in this study.

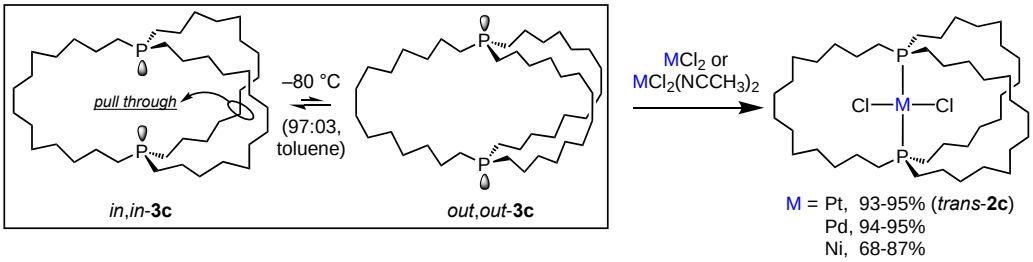

Scheme 2.3. Homeomorphic isomerization of macrocyclic dibridgehead diphosphines, and complexation of MCl_2 units.

Accordingly, we set out to (1) synthesize the parachute like complexes in Scheme 2.2, as well as homologs with dibridgehead diphosphite ligands or octahedral coordination geometries, (2) characterize their spectroscopic, structural, and dynamic properties, and (3) probe their stabilities vis-à-vis gyroscope like isomers by both experimental and computational techniques. A small portion of this work has been communicated.[19]

2.2. Results

2.2.1. Syntheses, dibridgehead diphosphine series. The educts *cis*-$PtCl_2(P((CH_2)_mCH{=}CH_2)_3)_2$ (*cis*-**1**), were prepared from K_2PtCl_4 and the constituent olefinic phosphines in water as reported earlier (*cis*-**1b**-**e**; m = 5-8, 33-70%)[14] or by extending the protocol to phosphines with longer methylene chains (*cis*-**1f**,**g**; m = 9,10, 44-51%; APPENDIX A. Minor amounts of *trans*-**1** were often noted, but were easily separated chromatographically (*trans*-**1** dominates when syntheses are conducted using $PtCl_2$ and the less polar solvent benzene).[14] In accord with literature precedent for bis(phosphine) platinum(II) complexes,[20] the $^1J_{PPt}$ values of *cis*-**1b**-**g** were much greater than those of *trans*-**1b**-**g** (3511-3518 vs. 2375-2382 Hz).[4]

As shown in Scheme 2.2, dilute CH_2Cl_2 solutions of *cis*-**1b**-**g** (0.00073-0.0015 M) and Grubbs' first generation catalyst (7.5-12 mol%) were refluxed. After 12-48 h, workups gave crude metathesis products. The $^{31}P\{^1H\}$ NMR spectra exhibited a multitude of signals,[21] some of which presumably reflect *cis*/*trans* C=C isomers. Hydrogenations were carried out under 1-5 bar of H_2 using PtO_2 or $(Ph_3P)_3RhCl$ as catalysts. Workups gave the target parachute like dibridgehead diphosphine complexes *cis*-$PtCl_2(P((CH_2)_n)_3P)$ (*cis*-**2b**-**g**; $n = 2m+2$) in 6-40% overall yields. The P-Pt-P moieties are part of fifteen to twenty five membered macrocycles. No other monoplatinum products were detected. Hence, the generally low mass balance presumably reflects the formation of oligomers.[21b] Yields were nearly the same when Grubbs' second generation catalyst was employed.

All new complexes that were not mixtures of isomers were characterized by NMR (^{1}H, ^{13}C, ^{31}P) and in many cases by microanalyses, mass spectrometry, and IR spectroscopy, as summarized in the experimental section. The structures of *cis*-**2b-g** readily followed from their spectroscopic properties. For example, the $^{1}J_{PPt}$ values were much greater than those of the *trans* isomers in Scheme 2.1 (3530-3568 vs. 2389-2398 Hz). With *cis*-**2b-d**, two sets of methylene ^{13}C signals were observed, with an intensity ratio of ca. 2:1. With *cis*-**2e-g**, only a single set of methylene signals was observed. This dichotomy is rationalized below. Importantly, the isomeric structures *cis*-**2'b-g** (Scheme 2.2), which are derived from a combination of *inter*ligand and *intra*ligand metatheses, would give two sets of signals for all macrocycle sizes (the less intense from the methylene chain that spans the two phosphorus atoms; the more intense from the phosphacycle methylene chains that circle back to the same phosphorus atom).

2.2.2. Syntheses, dibridgehead diphosphite series. Bis(phosphite) dihaloplatinum complexes are usually obtained as *cis* isomers,[22] consistent with the greater π acidities of phosphite as compared to trialkylphosphine ligands. However, a few special types of *trans* isomers have been reported.[23] The latter feature much lower $^{1}J_{PPt}$ values (4405-4680 vs. 5694-5918 Hz).[22,23] Thus, the olefinic phosphites $P(O(CH_2)_{m*}CH=CH_2)_3$ (*m** = **a**, 3; **b**, 4; **c**, 5)[24] and $PtCl_2$ were combined in toluene. Chromatographic workups afforded the bis(phosphite) complexes *cis*-$PtCl_2(P(O(CH_2)_{m*}CH=CH_2)_3)$ (*cis*-**4a-c**; Scheme 2.4) as light yellow or colorless oils in 60-95% yields, with $^{1}J_{PPt}$ values of 5696-5698 Hz. Note that a ligand or complex with a given index has the same number of atoms between the phosphorus atom and the vinyl groups as with the bis(phosphine) complexes *cis*-**1** (e.g., five for *cis*-**1b** and *cis*-**4b**).

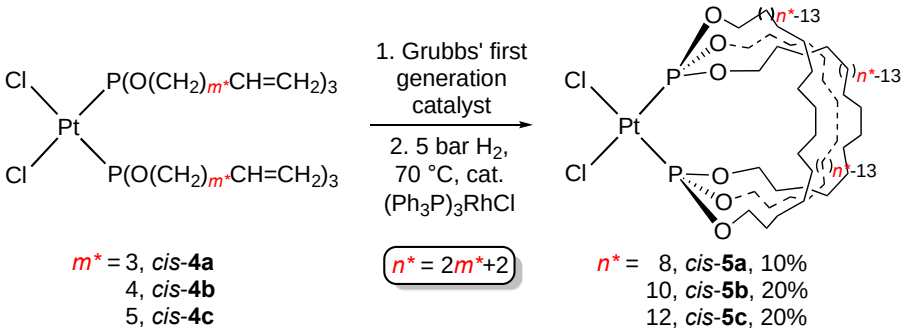

Scheme 2.4. Three fold ring closing metatheses of *cis*-**4a-c**; syntheses of parachute like phosphite complexes *cis*-**5a-c**.

Ring closing metatheses of *cis*-**4a-c** were carried out with Grubbs' first generation catalyst (10-20 mol%) in dilute refluxing CH_2Cl_2 (0.00079-0.00099 M). Hydrogenations were conducted under 5 bar of H_2 using 15-20 mol% of $(Ph_3P)_3RhCl$. As shown in Scheme 2.4, chromatographic workups gave the target parachute like dibridgehead diphosphite complexes *cis*-$PtCl_2(P(O(CH_2)_{n*}O)_3P)$ (*cis*-**5a-c**; $n^* = 2m^*+2$) as white solids or foams in 10-20% overall yields. A lower homolog of *cis*-**4a**, with one less methylene group in each phosphorus substituent, was also synthesized and similarly reacted. Even with a 25% catalyst loading, ^{1}H NMR spectra showed a significant fraction of unreacted $CH=CH_2$ linkages after 72 h.[21a]

The $^1J_{PPt}$ values of *cis*-**5a-c** ranged from 5721 to 5759 Hz. For all three compounds, two sets of methylene ^{13}C signals with a ca. 2:1 intensity ratio were observed, analogous to the two dibridgehead diphosphine complexes with identical macrocycle sizes (*cis*-**2b**,**c**). Importantly, the protons on any CH_2 group of a parachute like (but not gyroscope like) complex are diastereotopic. The couplings are never resolved, but as a result the ^{1}H NMR spectrum of *cis*-**5a** exhibits three well separated OC*HH′* signals (m, 4H each, Δδ ca. 1.0 ppm). The signals become more closely spaced upon going to *cis*-**5b** (Δδ ca. 0.5 ppm) and *cis*-**5c** (2m, 4H/8H, Δδ ca. 0.15 ppm). The diphosphine complex with

the smallest macrocycles, *cis*-**2b**, exhibited three well separated PC*HH′* signals (m, 4H each, Δδ ca. 0.9 ppm).

2.2.3. Substitution reactions. Halide ligands in gyroscope like complexes are usually quite easily substituted by a variety of nucleophiles.[4-6,16] In all cases, the phosphorus donor atoms remain *trans*. As part of this work, it was not sought to develop an extensive substitution chemistry of parachute like complexes, but rather to verify that simple displacements can occur, and the attendant stereochemistry. The latter is relevant to mechanistic issues described below.

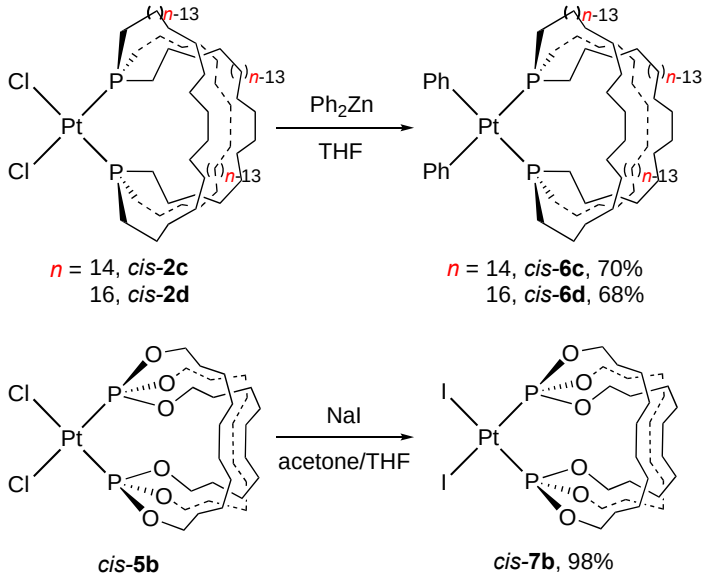

n = 14, *cis*-**2c**
16, *cis*-**2d**

n = 14, *cis*-**6c**, 70%
16, *cis*-**6d**, 68%

cis-**5b**

cis-**7b**, 98%

Scheme 2.5. Substitution reactions of parachute like complexes.

As previously reported,[4b] the gyroscope like dibridgehead diphosphine complex *trans*-**2c** and Ph_2Zn (3.1 equiv) react over the course of 20 h at room temperature to give the diphenyl complex *trans*-$\overline{PtPh_2(P((CH_2)_{14})_3P)}$ (*trans*-**6c**) in 61% yield after workup. As shown in Scheme 2.5, analogous reactions of parachute like *cis*-**2c,d** and Ph_2Zn (18 h)

gave *cis*-**6c,d** as white solids in 68-70% yields. Similarly, a reaction of the dibridgehead diphosphite complex *cis*-**5b** and NaI (4.0 equiv) gave the diiodide complex *cis*-**7b** (Scheme 2.5) as a yellow solid in 98% yield. The NMR spectra of both substitution products exhibited the general features noted in the precursors above. In contrast to the situation with *trans*-**6c**,[4b] there was no sign of restricted rotation about the Pt-C_{ipso} bond on the NMR time scale with *cis*-**6c**.

2.2.4. Crystal Structures. Although all of the structures assigned above seemed quite secure based upon spectroscopic properties, it was still sought to crystallographically characterize as many complexes as possible in order to help define the range of accessible macrocycle conformations. Thus, crystals of *cis*-**1f**, *cis*-**2c**,**d**,**f**, *cis*-**6c**, and *cis*-**5a**,**b** were grown as described in the experimental section. X-ray data were collected, and the structures determined, as summarized in Table 2.1. The molecular structures are depicted in Figures 2-8. Key bond lengths and angles are given in Table 2.1. All of these are very close to those of related platinum(II) complexes, but the averages are valuable for certain structural analyses below.

With *cis*-**2d**,**f** and *cis*-**5a**, two independent molecules were present in the unit cell. Those of *cis*-**2d**,**f** were conformationally similar; over all four atom segments in all three macrocycles, the *gauche*/*anti* sense differed in only three linkages. For the independent molecules of *cis*-**5a**, the macrocycles that were perpendicular to the metal coordination plane showed several points of difference. Complex *cis*-**5b** exhibited a C_2 symmetry axis that passed through the platinum atom and bisected the Cl-Pt-Cl angle. Additional structural features are interpreted in the discussion section.

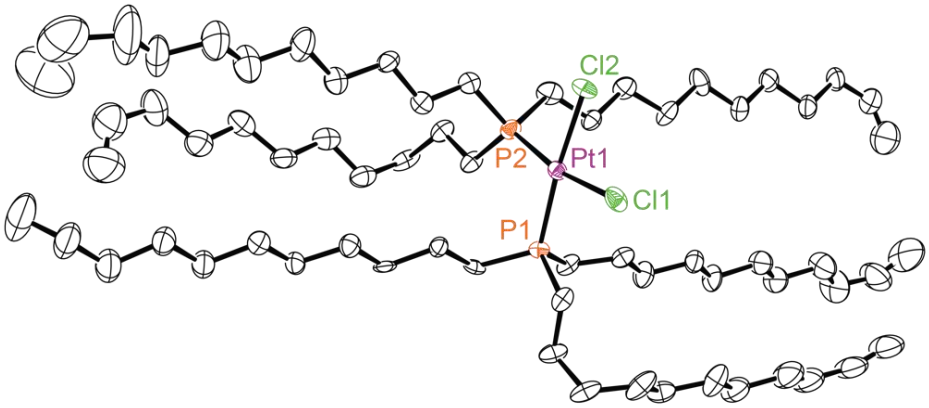

Figure 2.2. Thermal ellipsoid plot (50% probability) of *cis*-**1f**.

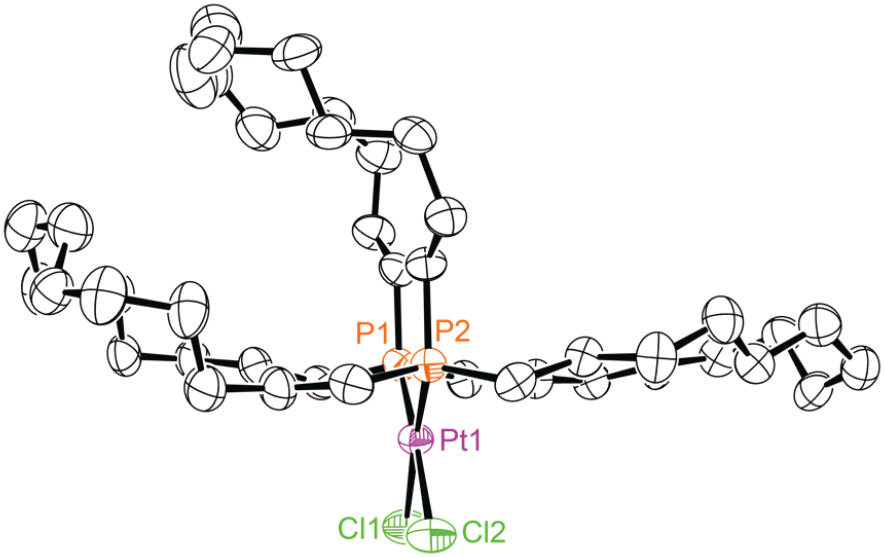

Figure 2.3. Thermal ellipsoid plot (50% probability) of *cis*-**2c**.

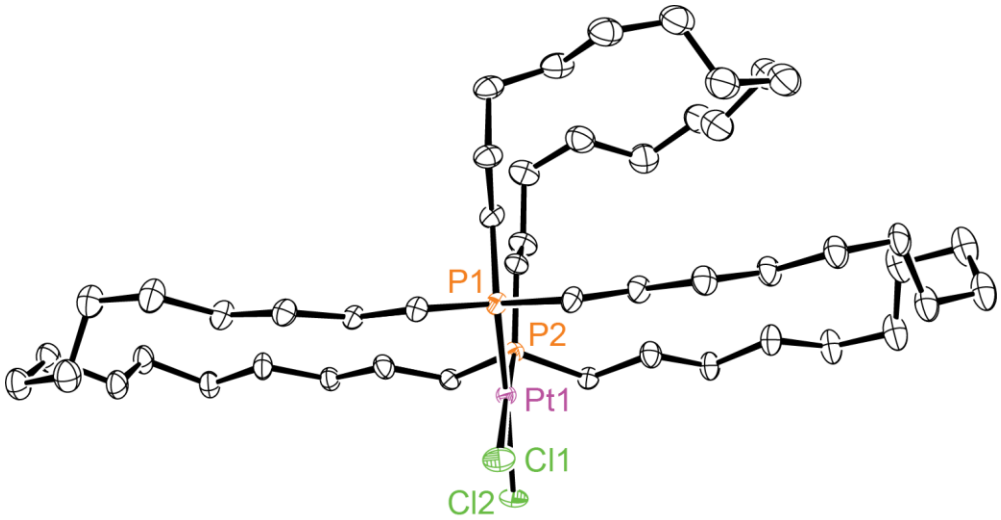

Figure 2.4. Thermal ellipsoid plot (50% probability) of one of the two independent molecules of *cis*-**2d** in the crystal lattice.

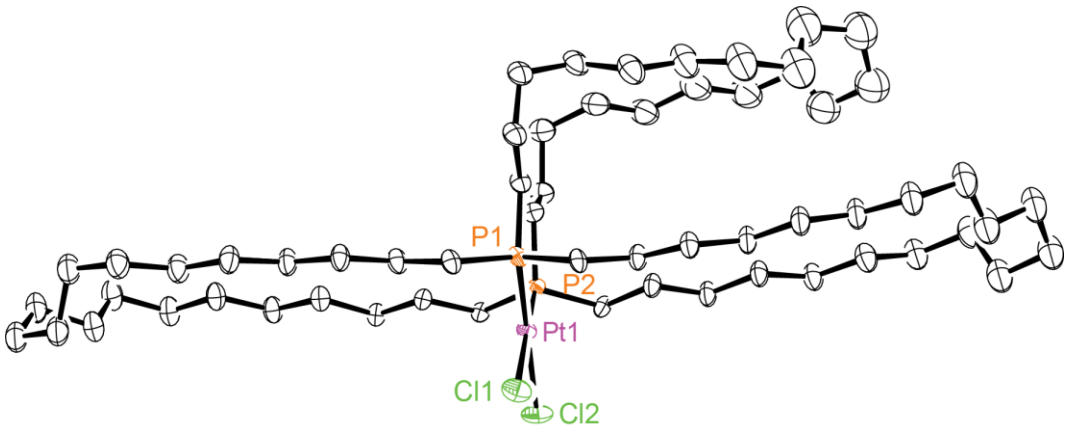

Figure 2.5. Thermal ellipsoid plot (50% probability) of one of the two independent molecules of *cis*-**2f** in the crystal lattice.

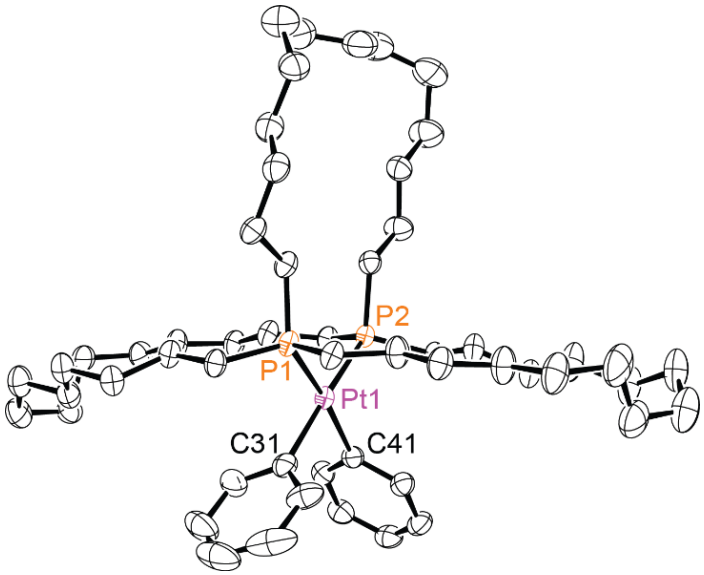

Figure 2.6. Thermal ellipsoid plot (50% probability) of *cis*-**6c**.

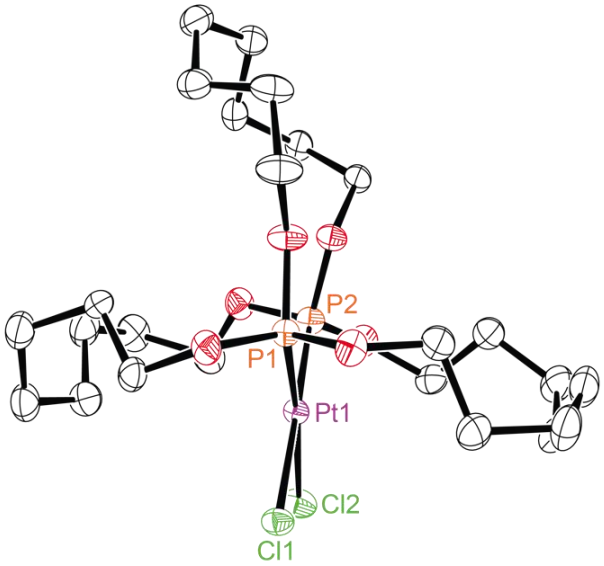

Figure 2.7. Thermal ellipsoid plot (50% probability) of one of the two independent molecules of *cis*-**5a** in the crystal lattice.

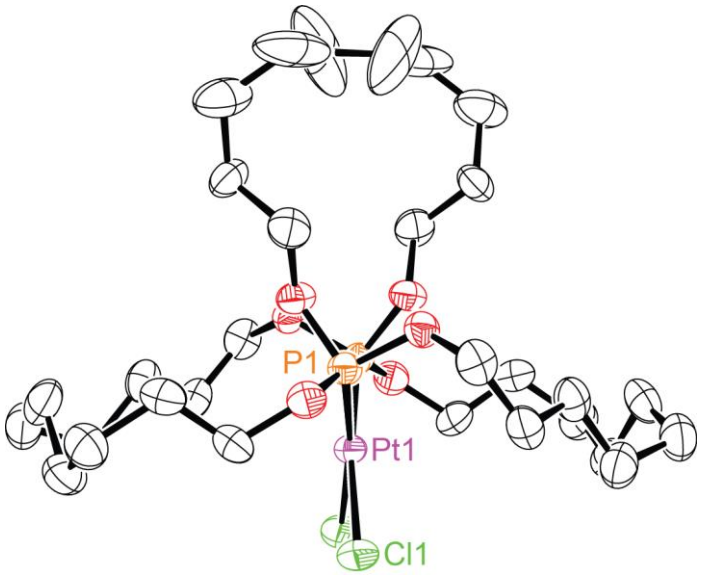

Figure 2.8. Thermal ellipsoid plot (50% probability) of *cis*-**5b**.

2.2.5. Thermolyses. Thermal equilibrations of isomeric gyroscope and parachute like complexes were attempted. An NMR tube was charged with a *o*-$C_6H_4Cl_2$ (*o*-dichlorobenzene) solution of *cis*-**2c**, which features seventeen membered macrocycles, and kept at 185 °C. As shown by the $^{31}P\{^1H\}$ NMR spectra in Figure 2.9, clean isomerization to *trans*-**2c** gradually took place. The *trans*/*cis* ratio plateaued at 89:11 after 5-6 d (6 d spectrum not depicted). An *o*-$C_6H_4Cl_2$ solution of *trans*-**2c** gave 8% isomerization to *cis*-**2c** after 14 h at 180 °C.

Similar experiments were conducted with C_6D_5Br solutions of **2c**,**g**. No isomerizations were observed with *trans*-**2c**,**g** after 48 h at 150 °C. However, *cis*-**2c**,**g** underwent reactions. As shown in Figure 2.10, after 1 d the larger twenty five membered macrocycle *cis*-**2g** gave a 74:7:19 mixture of *trans*-**2g**, *cis*-**2g**, and a species tentatively assigned as an oligomer. After another day, the proportion of oligomer had increased slightly (65:6:29).

Interestingly, *cis*-**2c** gave a somewhat slower isomerization (1 d, 16:78:6

trans/*cis*/oligomer; 2 d, 22:62:16), although the rate was faster than in *o*-$C_6H_4Cl_2$ at 185 °C. As further detailed in the Appendix A and Figure s2.5, continued heating at 185 °C gave a significant amount of the previously characterized gyroscope like di*bromide* complex *trans*-$\overline{PtBr_2(P((CH_2)_{14})_3P)}$ (2.94 ppm; 22:<1: 48:30 *trans*/*cis*/oligomer/dibromide after 3 d).[4b,25]

The preceding experiments indicate that *trans*-**2c**,**g** are thermodynamically more stable than *cis*-**2c**,**g**, with the equilibrium ratio for **2c** being ca. 90:10 (*o*-$C_6H_4Cl_2$, 180-185 °C). DSC analyses of *cis*-**2c** showed an endotherm at 200 °C, nearly coincident with the physically observable melting point at 210 °C. However, no exotherm, which would be expected for an isomerization, was noted. Perhaps the barrier is lower in solution than the solid state. TGA data showed an onset of mass loss close to the melting point, suggesting some concomitant decomposition.

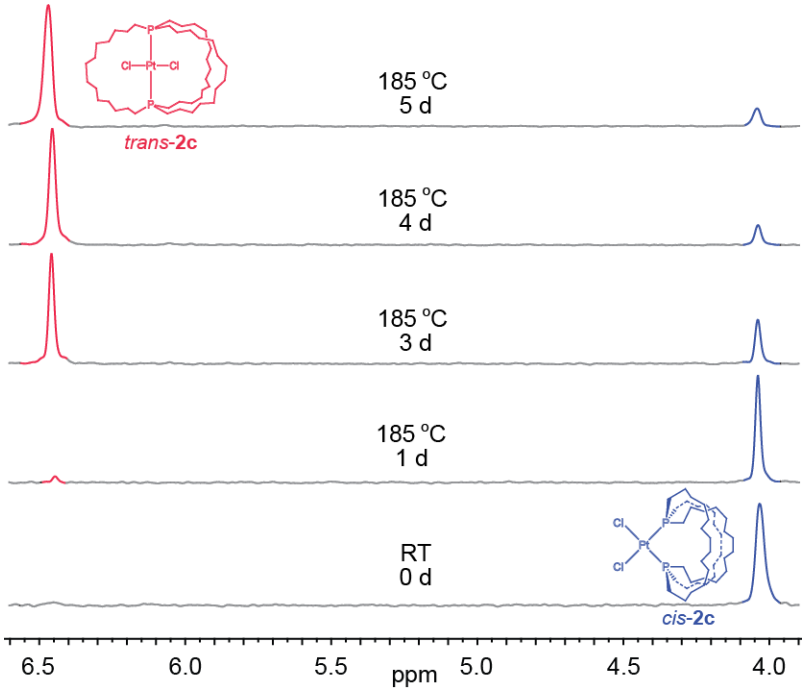

Figure 2.9. Thermolysis of *cis*-**2c** in *o*-$C_6H_4Cl_2$ at 185 °C; $^{31}P\{^1H\}$ NMR data.

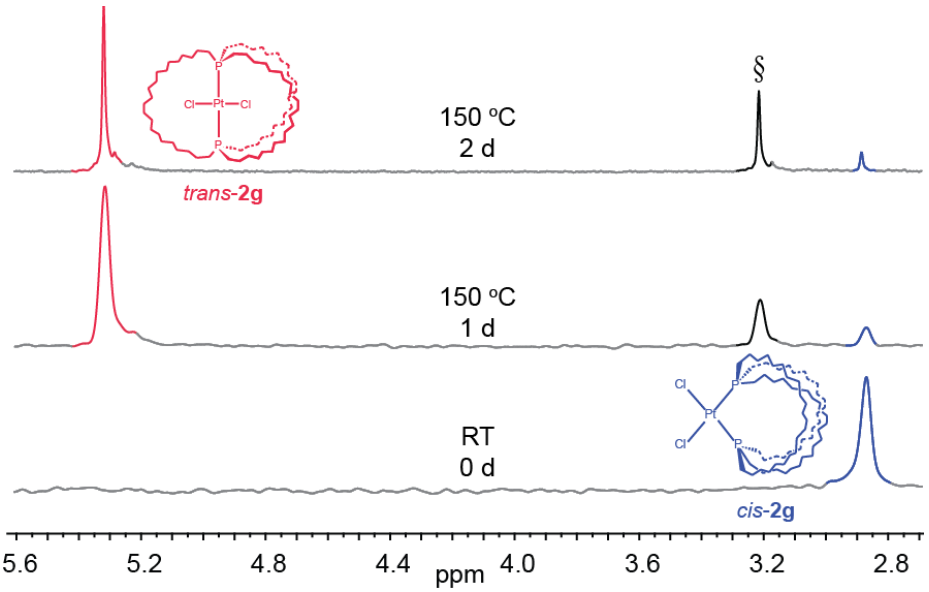

Figure 2.10. Thermolysis of *cis*-**2g** in C_6D_5Br at 150 °C; $^{31}P\{^1H\}$ NMR data (§ denotes an unidentified substance believed to be oligomer).

In a similar experiment, an NMR tube was charged with a *o*-$C_6H_4Cl_2$ solution of the parachute like dibridgehead diphosphite complex *cis*-**5b**. No reaction occurred after 1 d at 100 °C or another 2 d at 185 °C, as assayed by $^{31}P\{^1H\}$ NMR. When the sample was warmed to 200 °C, numerous decomposition products formed.

2.2.6. Dynamic Properties. The parachute like complexes that exhibited two sets of methylene ^{13}C NMR signals (*cis*-**2b-d**, *cis*-**5a-c**) featured smaller macrocycles. Thus, those that exhibited one set of signals (*cis*-**2e-g**) were provisionally assumed to undergo rapid "jump rope" exchange of the methylene bridges per Figure 2.1. Nonetheless, this interpretation would be strengthened if both regimes could be established for a single complex, and activation parameters acquired. Accordingly, samples giving two sets of signals were heated, and those giving one set of signals were cooled, in hopes of observing coalescence/decoalescence phenomena.

As shown in Figures 2.11 and A-2 (APPENDIX A), when C_6D_5Br solutions of *cis*-**2d**, which features nineteen membered macrocycles, were warmed, the two sets of methylene ^{13}C NMR signals coalesced. As previously observed with gyroscope like complexes, the chemical shifts were somewhat temperature dependent.[3,7d] This presumably reflects changes in relative populations of macrocycle conformations (each distinguished by a unique set of chemical shifts) as a result of differential entropies. In contrast, the $^1J_{PPt}$ value, another potentially sensitive probe, was essentially temperature independent (3529 to 3519 Hz, 25 to 100 °C).

The line shapes of the coalescing signals in Figure 2.11 were simulated using gNMR[26] and the rate constants determined at each temperature. An Eyring plot utilizing these rate constants (Figure A-3, APPENDIX A) afforded $\Delta H^{\ddagger}$, $\Delta S^{\ddagger}$, and $\Delta G^{\ddagger}_{298K}$ values of 7.8 kcal/mol, –27.9 eu, and 16.1 kcal/ mol for the process rendering the methylene signals equivalent. As further analyzed below, one would expect a highly negative $\Delta S^{\ddagger}$ for the conformationally restricted transition state **III** in Figure 2.1.

When C_6D_5Br solutions of *cis*-**2c** or *cis*-**6d**, which feature smaller seventeen membered macrocycles or larger phenyl ligands, respectively, were heated to 120-100 °C, no coalescence of methylene ^{13}C NMR signals was observed (Figures s2.1 and s2.4). With *cis*-**2c**, this allowed a lower limit of 19.6 kcal/mol ($\Delta G^{\ddagger}_{393K}$) to be set for any process capable of rendering the methylene groups equivalent, as derived in the APPENDIX A. When CD_2Cl_2 solutions of *cis*-**2e**, which features larger twenty one membered macrocycles and a single

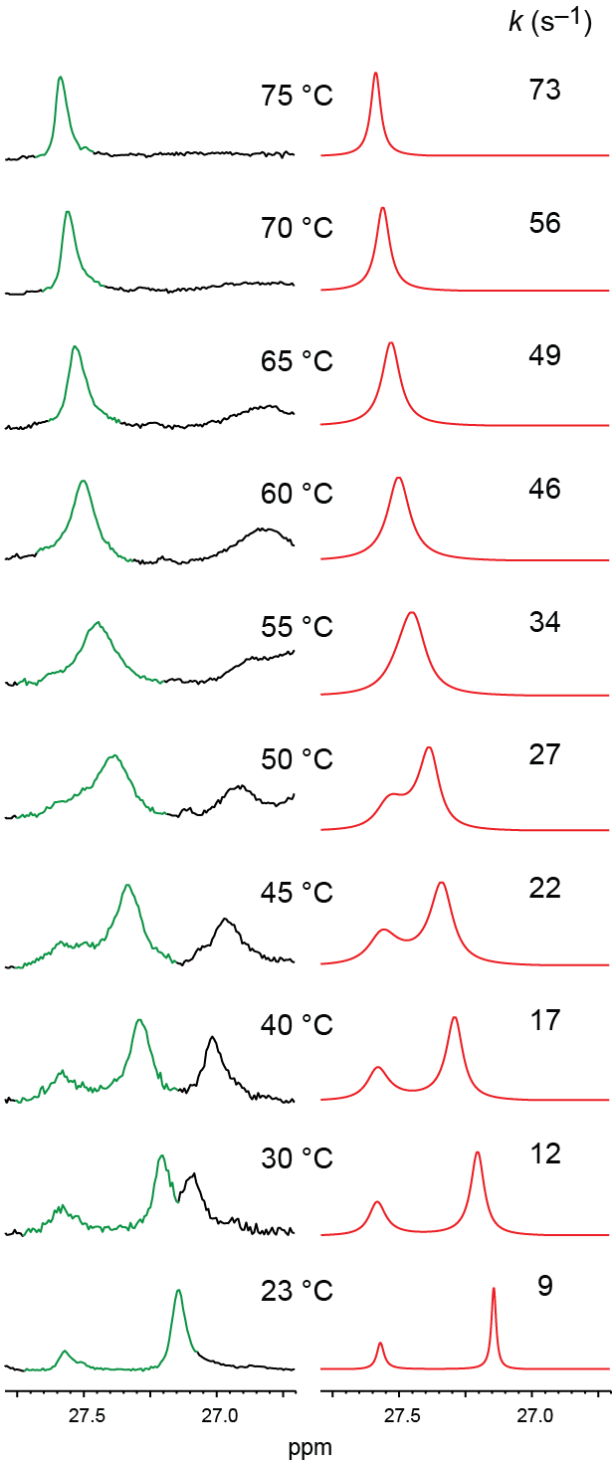

Figure 2.11. Partial $^{13}C\{^{1}H\}$ NMR spectra of *cis*-**2d** (C_6D_5Br) as a function of temperature. Each spectrum (left) is paired with simulated line shapes for the signals of interest (right; compare red and green traces).

set of methylene ^{13}C NMR signals, were cooled to –80 °C, no decoalescence was observed.

2.2.7. Attempted Extension to Octahedral Rhenium Complexes. The ring closing metatheses to give square planar gyroscope like complexes in Scheme 2.1 are easily extended to trigonal bipyramidal and octahedral coordination geometries.[3a-c,6,7b] Thus, we were curious whether the routes to parachute like complexes in Schemes 2.2 and 2.4 could similarly be applied to trigonal bipyramidal or octahedral educts.

Accordingly, the rhenium halide complexes $ReX(CO)_5$ (X = Cl, Br) and the olefinic phosphine $P((CH_2)_6CH=CH_2)_3$ (2.0 equiv) were combined in C_6H_5Cl at 60-80 °C. Workups gave the *cis* bis(phosphine) complexes *fac*-$ReX(CO)_3(P((CH_2)_6CH=CH_2)_3)_2$ (X = Cl, *fac*-**10c**; Br, *fac*-**11c**) in 43-67% yields. As shown in Scheme 2.6, the thermolysis of *fac*-**11c** in C_6H_5Cl at 140 °C afforded the previously characterized[6a,b] isomer *mer,trans*-**11c** in 89% yield. Many earlier studies have shown that *mer*,*trans* isomers of rhenium tricarbonyl bis(phosphine) halide complexes are more stable than *fac* isomers.[27] As noted previously, when *mer,trans*-**11c** is subjected to the standard metathesis/hydrogenation conditions, the corresponding gyroscope like complex *mer, trans*-$\overline{ReBr(CO)_3(P((CH_2)_{14})_3P)}$ (*mer,trans*-**12c**; Scheme 2.6) can be isolated in 37% yield.[6a,b]

In procedures parallel to those in Schemes 2.2 and 2.4, *fac*-**10c** and *fac*-**11c** were treated with Grubbs' first generation catalyst and then H_2/PtO_2. As shown in Scheme 2.6, workups gave products derived from a combination of *inter*ligand and *intra*ligand metatheses, *fac*-**12'c** and *fac*-**13'c**, in 39% and 15% overall yields, respectively. The parachute like complexes *fac*-**12c** and *fac*-**13c** were not detected; due to their lower symmetry vs. *cis*-**2**, three sets of methylene ^{13}C NMR signals – one for each macrocycle

– would be expected. Interestingly, mass spectra of the crude metathesis product derived from *fac*-**10c** exhibited a number of dirhenium ions (e.g., $2\mathbf{M}^{+}$–3CO, 100%).

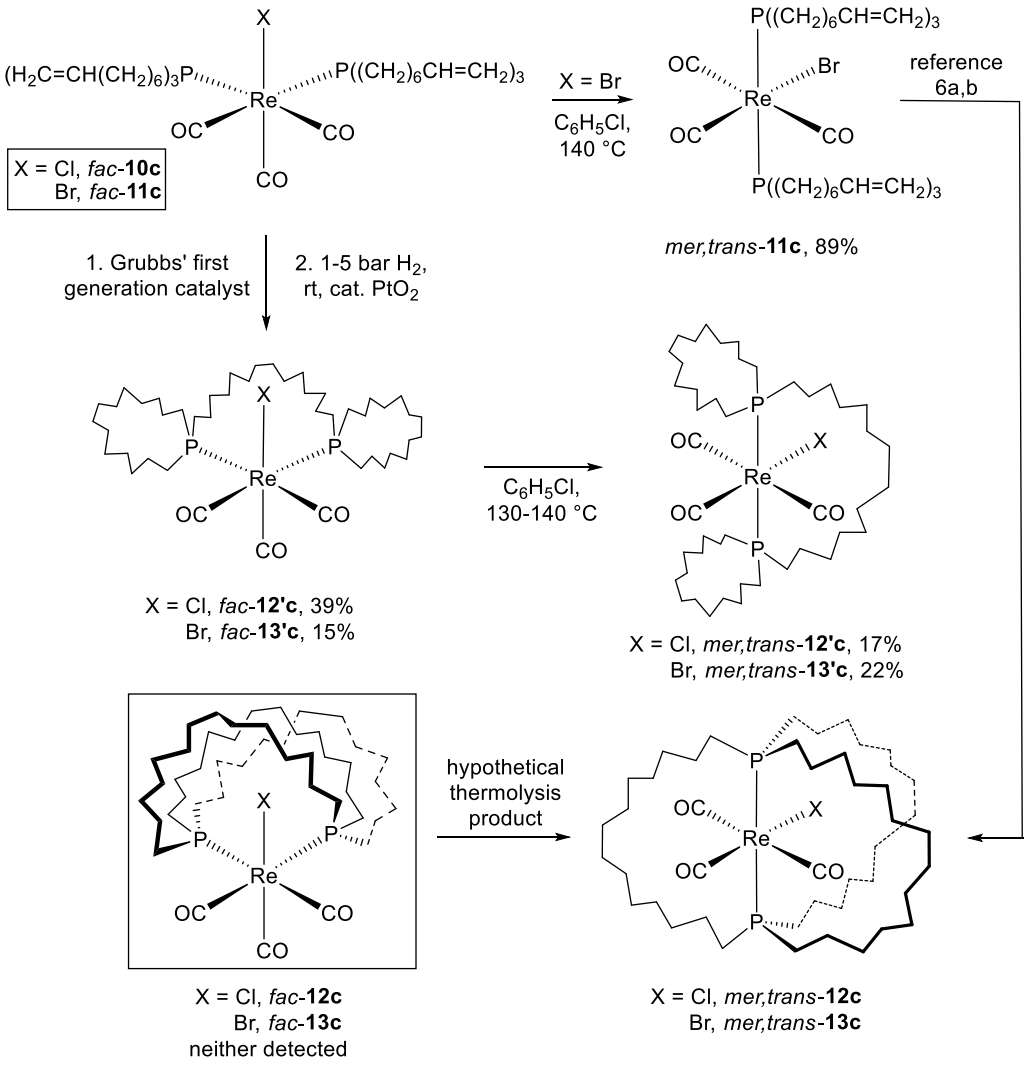

Scheme 2.6. Three fold ring closing metatheses of the octahedral rhenium complexes *fac*-**10c** and *fac*-**11c** and related reactions.

As a further check of structure, *fac*-**12'c** and *fac*-**13'c** were thermolyzed in C_6H_5Cl at 130-140 °C. Similar to the result with *fac*-**11c**, *mer,trans*-**12'c** and *mer,trans*-**13'c** were

isolated in 17-22% yields. The complex *mer,trans*-**12'c** had been independently synthesized earlier (byproduct accompanying *mer*,*trans*-**12c**), as had homologs of *mer,trans*-**13'c** with larger macrocycles.[6b] Thermolyses of the target complexes, *fac*-**12c** and *fac*-**13c**, would have given the known gyroscope like complexes *mer,trans*-**12c** and *mer,trans*-**13c**.[6a,b]

2.2.8. Computational Studies. Further insight was sought regarding the relative stabilities of the various types of isomeric species encountered above. Thus, DFT calculations, including dispersion corrections, were carried out. This was followed by molecular dynamics annealing simulations to maximize the likelihood of correctly identifying the lowest energy conformer. This output was further optimized by additional DFT calculations. As shown in Figure A-9 (APPENDIX A), the dispersion corrections gave structures that more closely modeled those in the crystal structures.

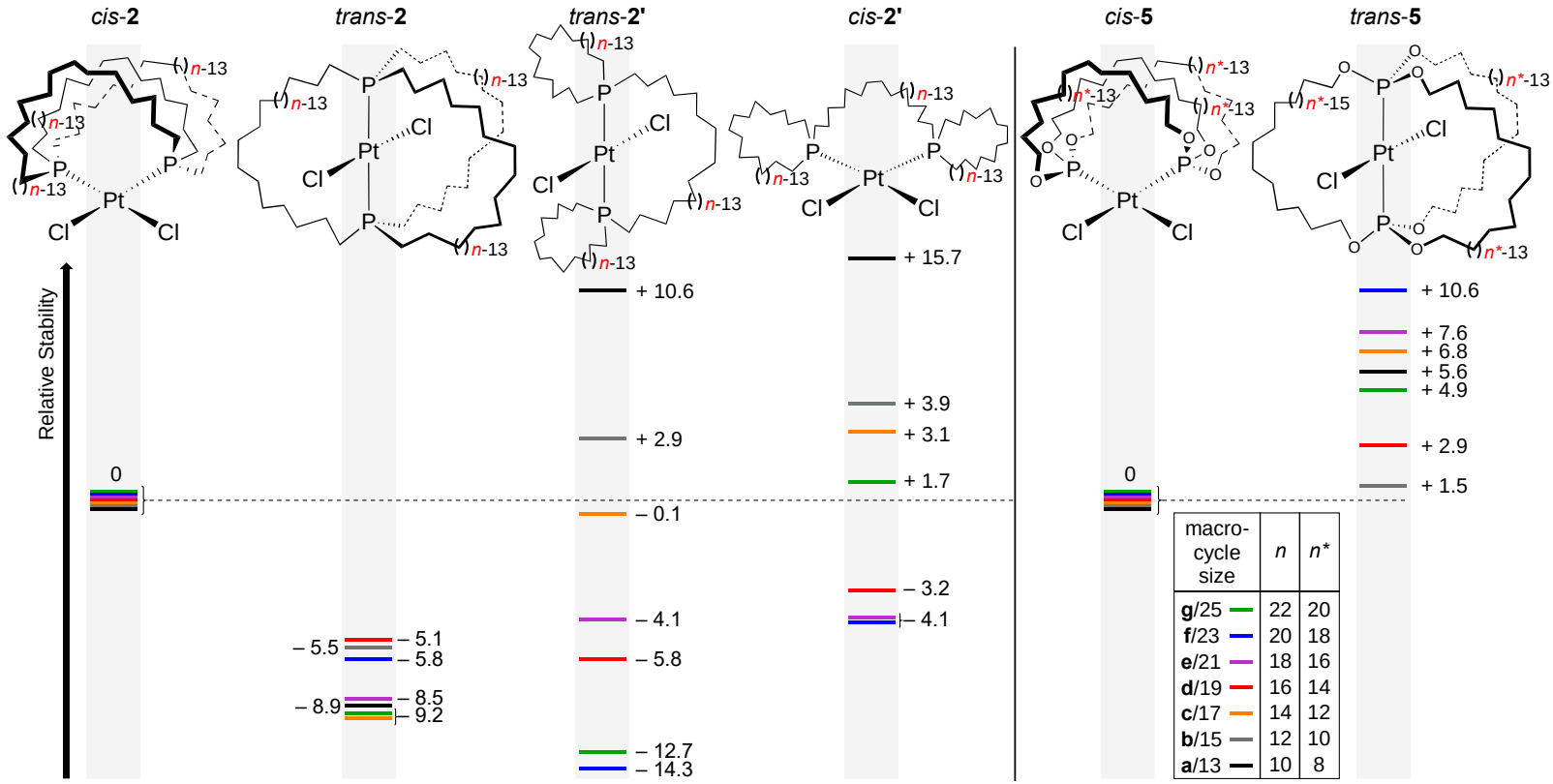

Figure 2.12. Relative energies (kcal/mol) of isomeric platinum dichloride complexes as computed by DFT and molecular dynamics (gas phase).

The relative gas phase stabilities of the parachute and gyroscope like complexes *cis*-**2** and *trans*-**2** are illustrated as a function of macrocycle size in Figure 2.12. As one goes from thirteen to twenty five membered macrocycles (or ten (**a**) to twenty-two (**g**) methylene groups per bridge), the gyroscope like complexes range from 5.1 to 9.2 kcal/mol more stable, consistent with the trends established for **2c**,**g** in haloarenes in Figures 2.9-2.10. However, the energy differences do not vary monotonically. Rather, there is an "even/odd" alternation with respect to *n*/2 (odd, –9.2 to –8.5 kcal/mol; even, –5.8 to –5.1 kcal/mol). No attempt has been made to elucidate a basis for this phenomenon. However, it may be coupled to conformational features of the macrocycles. Physical properties that alternate with even/odd methylene chain lengths have abundant precedent.[28]

Figure 2.12 also displays the relative energies of the alternative cyclization products *trans*-**2'a-g** (Scheme 2.1) and *cis*-**2'a-g** (Scheme 2.2). The former is more stable for all macrocycle sizes. In both cases, the complexes with the two smallest macrocycle sizes, **2'a**,**b**, are considerably higher in energy, also as compared to gyroscope and parachute like **2a**,**b**. This presumably reflects ring strain associated with the monophosphacycles. The energies of **2'a-g** generally decrease with increasing macrocycle size, although not monotonically. Interestingly, *trans*-**2'f,g**, which feature the two largest macrocycle sizes, are computed to be more stable than gyroscope like *trans*-**2f,g** (–5.4 to –3.5 kcal/mol).

Data for the parachute and gyroscope like phosphite complexes *cis*-**5a-g** and *trans*-**5a-g** are also provided in Figure 2.12 (right). Now the former are computed to be more stable, consistent with (1) the preferred geometry for acyclic bis(phosphite) platinum dichloride complexes, and (2) the absence of any thermal isomerization of *cis*-**5b**, as noted above. Thus, a metal based electronic effect dominates over any ring strain trends that may

be operative with the macrocycles.

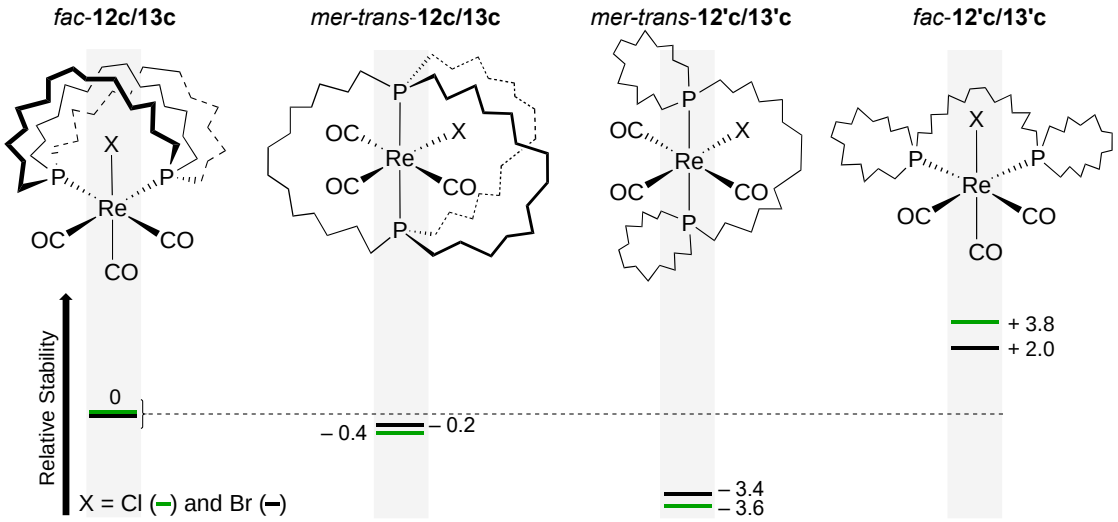

Figure 2.13. Relative energies (kcal/mol) of isomeric rhenium tris(carbonyl) halide complexes as computed by DFT and molecular dynamics (gas phase).

Data for the four types of isomeric rhenium complexes in Scheme 2.6 are provided in Figure 2.13. Consistent with the thermolyses in Scheme 2.6, and the direction of equilibrium for a number of related complexes,[27] *mer*,*trans*-**12'c** and *mer*,*trans*-**13'c** were found to be much more stable than *fac*-**12'c** and *fac*-**13'c** (–5.4 to –7.4 kcal/mol). Interestingly, the energies of the previously synthesized gyroscope like complexes *mer*,*trans*-**12c** and *mer*,*trans*-**13c** were quite close to those of the parachute like complexes *fac*-**12c** and *fac*-**13c** ($\leq$ 0.4 kcal/mol). Thus, the latter remain realistic synthetic targets, although the cyclization mode leading to (after hydrogenation) the much less stable *fac*-**12'c** and *fac*-**13'c** is preferred under the conditions of Scheme 2.6.

2.3. Discussion

2.3.1. Syntheses and Structures. Schemes 2.2 and 2.4 establish that parachute

like square planar platinum complexes are easily accessed, albeit in modest yields, via three fold *inter*ligand ring closing metatheses of precursors with suitable *cis* olefinic phosphine and phosphite ligands. It also appears that they can be accessed with smaller macrocycles than the corresponding gyroscope like complexes, as exemplified by *cis*-**5a** (thirteen membered), *cis*-**5b**, and *cis*-**2b** (both fifteen membered). As noted above, attempts to synthesize gyroscope like square planar complexes with macrocycles of less than seventeen atoms have yet to be successful.

It seems likely that Schemes 2.2 and 2.4 can be extended to other square planar complexes. However, there appear to be greater restrictions with respect to the metal coordination geometry than for gyroscope like complexes, as reflected by the failure to access octahedral analogs in Scheme 2.6. Here, an alternative mode of ring closing metathesis affords *cis* bis(phosphacycle) chelate ligands (*fac*-**12'c** and *fac*-**13'c**). As noted above, related complexes with *trans* spanning chelates, such as *mer,trans*-**12'c**, are sometimes found as byproducts in syntheses of octahedral gyroscope like complexes.[4b,6b,c]

Prior to our work, no aliphatic dibridgehead diphosphines with bridges greater than four atoms had been synthesized, either as complexes or free ligands.[29] Analogous diphosphites were unknown, although macrocyclic aromatic analogs derived from $P(OAr)_3$ units had been reported.[30] This study establishes that such ligands possess incredible flexibility, as illustrated in Scheme 2.7. Naturally the phosphorus-lone pair vectors can orient collinearly with a 180° angle (**V**), as seen in bimetallic complexes.[31] In the parachute like complexes *cis*-**2** and *cis*-**4**, these vectors define 90° angles (**VII**). Intermediate geometries such as **VI** should be possible, in which the lone pairs might be directed at a surface or polymetallic assembly. Continued rotation of the vectors leads to gyroscope like complexes (**VIII**), in which the phosphorus configurations have been

inverted relative to **V**. These changes in vector orientations require specific accompanying changes in the conformations of the methylene bridges – processes that will be fully treated in the future addressing mechanisms of interconversion of **V** and **VIII**.

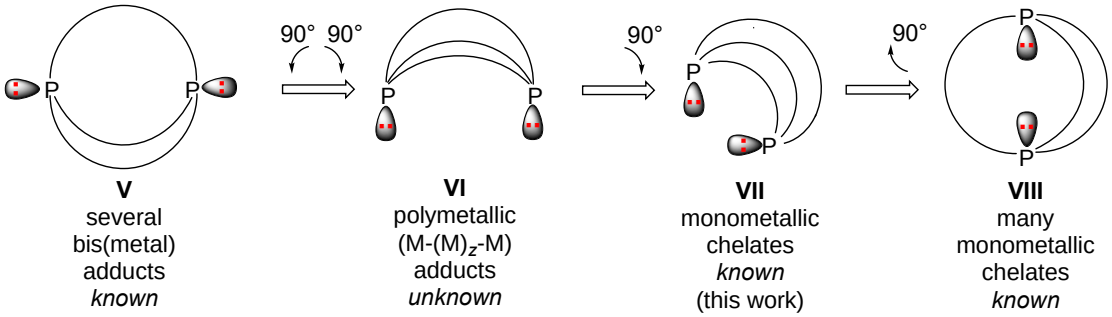

Scheme 2.7. Limiting structures for macrocyclic dibridgehead diphosphorus ligands.

The crystal structures determined include parachute like complexes with thirteen, fifteen, seventeen, nineteen, and twenty three membered macrocycles. These can be compared to the conformational model in Figure 2.1, in which the "middle" macrocycle occupies the metal coordination plane. This is always the case for the first few atoms emanating from phosphorus. However, as shown in Figures 2.3-2.5, the middle macrocycles in *cis*-**2c**,**d**,**f** exhibit a subsequent fold or "kink". The other macrocycles adopt approximately perpendicular orientations above and below the coordination plane.

The crystal structure of one precursor to a parachute like complex, *cis*-**1f**, could be determined. As shown in Figure 2.2, the spatial distribution of the six vinyl groups is by no means conducive for the required three fold *inter*ligand ring closing alkene metathesis. This is presumably one factor behind the modest yields in Schemes 2.2 and 2.4. In contrast, favorable or "pre-organized" conformations have been documented for hexaolefinic educts that give trigonal planar gyroscope like complexes in quite good yields.[3,7b]

2.3.2. Dynamic properties. Dynamic processes in which a macrocycle must rotate or "jump" over another moiety are not unusual.[15,32] However, the three fold variant invoked for parachute like complexes with sufficiently long methylene bridges (Figure 2.1) is to our knowledge unprecedented. In the absence of such exchange, the macrocycles above and below the coordination plane must give methylene ^{13}C NMR signals distinct from those of the macrocycle in the coordination plane.

The "jump rope" process requires that the $PtCl_2$ moiety pass through each macrocycle. Although this is accomplished by correlated rotations about the platinum-phosphorus bonds, the phosphorus-phosphorus vector, highlighted in **IX** in Figure 2.14, provides a valuable reference point for analyzing steric interactions. The two chlorine atoms are 2.88 Å from this vector (average of sixteen distances in all independent molecules in crystalline *cis*-**2c**,**d**,**f** and *cis*-**5a**,**b**; see Table 2.1). When the van der Waals radius of a chlorine atom is added (1.75 Å),[33] an effective "length" or radius of 4.63 Å is obtained.

At the same time, the $PtCl_2$ moiety has "width" or "fatness". The average chlorine-chlorine distance in *cis*-**2c**,**d**,**f** and *cis*-**5a**,**b** is 3.59 Å. When twice the van der Waals radius of a chlorine atom is added, an effective width of 7.09 Å is obtained. The activation barriers reflect the ease with which the cavities of the macrocycles can adapt to these dimensions (4.63 × 7.09 Å).

One approach to gauging the "lengths" of the macrocycles in a given complex is to calculate the distance from the center of the phosphorus-phosphorus vector to the two carbon atoms at the halfway mark of the three macrocycles. These will often, but not always, be the two carbon atoms most distant from the phosphorus-phosphorus midpoint. The six values are averaged (twelve for the cases of two independent molecules), and the van der Waals radius of an sp^3 carbon atom is subtracted. As would be expected, the

resulting values ascend in the order *cis*-**5a**,**b** and *cis*-**2c**,**d**,**f** (3.31, 4.04, 5.49, 7.09, 9.49 Å). Thus, *cis*-**2c**,**d**,**f** can easily accommodate the 4.63 Å "length" of the $PtCl_2$ moiety, whereas *cis*-**5b** requires a bit of a squeeze.

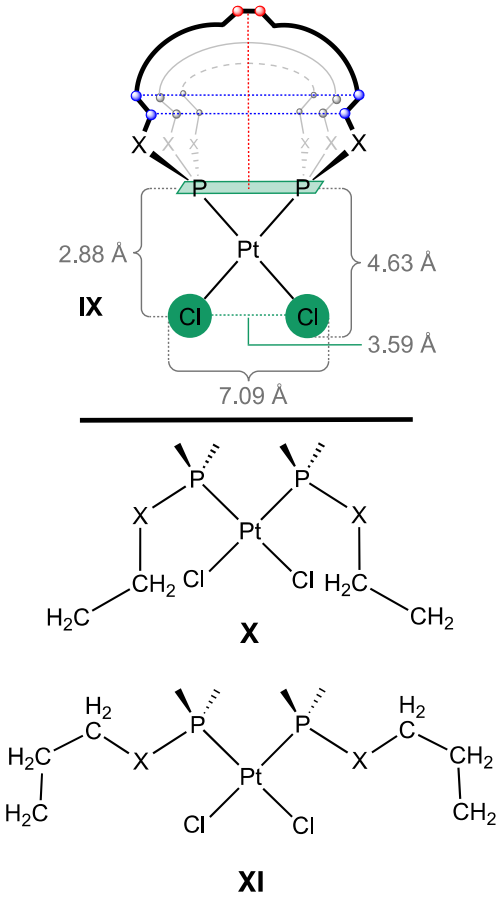

Figure 2.14. Top: spatial relationships involving the $PtCl_2$ moiety and macrocycles of *cis*-**2** (X = CH_2) and *cis*-**5** (X = O); parameters that affect the energy barriers for bridge exchange. Middle and bottom: partial macrocycle conformations corresponding to possible transition states for bridge exchange.

The effective "width" is another matter. As can be seen in Figures 2.3, 2.4, 2.7, and 2.8, the P-X-$\underline{C}H_2$ and P-X-CH_2-$\underline{C}H_2$ groups of each macrocycle will most closely

flank the $PtCl_2$ moiety during the "jump rope" process. It is a simple matter to calculate the distances between the two P-X-$\underline{C}H_2$ carbon atoms of a given macrocycle, and the two P-X-CH_2-$\underline{C}H_2$ carbon atoms (X = O or CH_2). The three values for a given complex are averaged (six for the cases of two independent molecules), and twice the van der Waals radius of a carbon atom is subtracted. This gives clearances that vary irregularly over a ca. 1 Å range for *cis*-**5a**,**b** and *cis*-**2c**,**d**,**f** (1.67, 2.21, 1.34, 1.78, 1.39 Å for P-X-$\underline{C}H_2$; 1.30, 2.31, 2.44, 1.40, 2.08 Å for P-X-CH_2-$\underline{C}H_2$). None of these are sufficient to accommodate the "width" of the $PtCl_2$ moiety (7.09 Å).

Hence, the jump rope process must incorporate conformational changes in the macrocycles that constitute significant deviations from the crystal structures. Figure 2.14 shows two partial conformations that widen the macrocycle cavity (**X** < **XI**). This is accomplished by introducing *anti* four-atom segments, e.g. P-X-CH_2-CH_2 in **X** and Pt-P-X-CH_2 and P-X-CH_2-CH_2 in **XI**. These in turn render it more difficult to "close the macrocycle" with the remaining atoms without inducing strain. Thus, the bridges of the smaller macrocycles lack sufficient degrees of freedom and the activation parameters become prohibitive. Only upon reaching *cis*-**2d**, which features nineteen membered macrocycles, does exchange become observable on the NMR time scale. The significantly negative $\Delta S^{\ddagger}$ (–27.9 eu) is consistent with highly ordered macrocycle conformations such as **X** or **XI** in the transition state. Alternative mechanisms involving the dissociation of a phosphorus atom can be excluded as all of the complexes retain $^1J_{PPt}$ values in the rapid exchange limit (e.g., *cis*-**2e**-**g** at room temperature or *cis*-**2d** at 75-100 °C).

2.3.3. Relative Isomer Stabilities. It is clear from the thermolysis experiments (Figures 2.9, 2.10, s2.5) that the gyroscope like platinum dibridgehead diphosphine complexes *trans*-**2c**,**g** are more stable than the parachute like analogs *cis*-**2c**,**g**, at least in low polarity solvents such as haloarenes. The gas phase computational data (Figure 2.12)

confirm the generality of the stability trend for all macrocycle sizes that have been synthetically accessed (*trans*-**2b**-**g** > *cis*-**2b**-**g**). Given the extreme temperatures required for equilibration (150-185 °C), it can be concluded that *cis* isomers are not intermediates in the complexation of MCl_2 by the free dibridgehead diphosphines **3** (Scheme 2.3) – a key step in their application as "container molecules".[17]

The computational data are of particular value in cases where authentic samples of both *cis* and *trans* complexes are lacking, such as with the dibridgehead diphosphite complexes *cis*-**5a**-**c**. Currently, there is no way to access suitable precursors to the *trans* isomers. As noted above, the reversal of the relative stabilities of parachute and gyroscope like complexes with the diphosphite complexes **5a**-**g** as compared to diphosphine complexes **2a**-**g** underscores the importance of electronic effects. Indeed, preliminary computational results show that with certain small ancillary ligands, parachute like diphosphine complexes can become more stable. These data, which are beyond the scope of the present study, will be presented in the future.[34]

Some issues that the computational data do *not* address deserve note. As emphasized in past studies,[3b,4b,6c] our ring closing metathesis reactions are generally under kinetic control. Thus, the ratios of constitutional isomers such as *trans*-**2** and *trans*-**2'** (Scheme 2.1), *cis*-**2** and *cis*-**2'** (Scheme 2.2), or *fac*-**12c** and *fac*-**12'c** (Scheme 2.6) reflect the ratios of the precursor cycloalkenes (prior to hydrogenation). These are always complex mixtures of *Z*/*E* isomers of undefined ratios, and should not automatically correlate to any distribution computed from the relative energies of the saturated products.

Nucleophilic substitutions of chloride ligands in both parachute and gyroscope type platinum complexes (e.g., Scheme 2.5) take place without geometric isomerization and therefore fit the rigorous definition of stereospecific reactions.[35] This leads in turn to a number of conclusions – for example, that the diphenyl complex *cis*-**6c** is not an

intermediate in the synthesis of *trans*-**6c**, and vice versa. Finally, mention should be made of related studies involving the relative stabilities of *cis*/*trans* MCl_2 (M = Pt, Pd) adducts of monophosphines as well as diphosphines capable of both *cis* and *trans* coordination.[36]

2.3.4. Conclusion. This study has established the general accessibility of square planar platinum dichloride complexes with *cis* coordinated dibridgehead diphos*phine* and diphos*phite* ligands, albeit in modest yields. When the three macrocycles in these "parachute like" species are sufficiently large, they can sequentially "jump" over the $PtCl_2$ moiety in a dynamic process that appears to be topologically unprecedented, and reminiscent of a triple axel. Isomeric *trans* dibridgehead diphos*phine* complexes, termed "gyroscope like", have been synthesized earlier and are thermodynamically more stable. Isomeric *trans* dibridgehead diphos*phite* complexes cannot presently be accessed, but computational data indicate that they are *less* stable. Results with octahedral rhenium complexes suggest that it is unlikely that parachute like complexes will be accessible with higher coordination geometries. The preceding data also eliminate certain mechanistic variants from various phenomena involving gyroscope like platinum complexes, simplifying the interpretation of their chemistry.

2.4. Experimental Section

General. Reactions were conducted under inert atmospheres using standard Schlenk techniques unless noted. DSC and TGA data were recorded with a Mettler-Toledo DSC821 instrument and treated by standard methods.[37] Solvents were treated as follows: benzene, toluene, and THF, distilled from Na/benzophenone or purified using a Glass Contour system; CH_2Cl_2, hexanes, ethyl ether, pentane, and ethyl acetate, distilled by rotary evaporation or purified using a Glass Contour system; CH_3OH, distilled from Mg; acetone, distilled from K_2CO_3; C_6H_5Cl and *o*-$C_6H_4Cl_2$, distilled under reduced pressure and degassed; C_6D_6, C_6D_5Cl, C_6D_5Br, $CDCl_3$, and CD_2Cl_2 (5 × deutero GmbH or Cambridge Isotope Laboratories), used as received. Grubbs' first generation catalyst ($(Cy_3P)_2RuCl_2$(=CHPh); Aldrich, 97%), $(Ph_3P)_3RhCl$ (Lancaster. 97%), $PtCl_2$ (ABCR, 99.9%), K_2PtCl_4 (Aldrich, 99.9%), PtO_2 (Aldrich, 99.9%), NaI (Rienst, 99%), and Ph_2Zn (Acros, 95%) were used as received.

NMR spectra were recorded on standard FT instruments at ambient probe temperatures unless noted and referenced as follows (δ, ppm): ^1H, residual internal $CHCl_3$ (7.26), C_6D_5H (7.15), $CDHCl_2$ (5.32), or C_6D_4HCl (6.96, 6.99. 7.14); $^{13}C\{^1H\}$, internal $CDCl_3$ (77.16), C_6D_6 (128.0), CD_2Cl_2 (53.5), or C_6D_5Cl (134.19, 129.26, 128.25, 125.96); $^{31}P\{^1H\}$, external H_3PO_4 (0.00). Mass spectra were recorded on a Micromass Zabspec instrument. IR spectra were recorded on ASI React-IR 1000, Thermo Scientific Nicolet IR100 FT-IR, or a Shimadzu IRAffinity-1 spectrometers. The last featured a Pike MIRacle ATR system (diamond/ ZnSe crystal). Melting points were recorded using a Stanford Research Systems MPA100 (OptiMelt) automated apparatus. Microanalyses were conducted on a Carlo Erba EA1110 instrument (in house) or by Atlantic Microlab, Inc.

Metathesis of *cis*-1b. A Schlenk flask was charged with *cis*-**1b** (0.438 g, 0.481 mmol), Grubbs' first generation catalyst (0.0274 g, 0.0329 mmol, 7.5 mol%), and CH_2Cl_2 (320 mL; the resulting solution is 0.0015 M in *cis*-**1b**), and fitted with a condenser. The solution was refluxed with stirring (12 h). The solvent was removed by oil pump vacuum, and CH_2Cl_2 was added. The sample was passed through a short pad of neutral alumina, rinsing with CH_2Cl_2. The solvent was removed from the filtrate by oil pump vacuum to give metathesized *cis*-**1b** (0.158 g, 0.191 mmol, 40%) as a light brown solid.

NMR ($CDCl_3$, δ/ppm): **^{31}P{^{1}H}** (162 MHz) 7.6 (s, 26%), 6.9 (s, 39%), 5.4 (s, 18%), 4.1 (s, 17%).

***cis*-PtCl$_2$(P((CH$_2$)$_{12}$)$_3$P) (*cis*-2b)**. A Fischer-Porter bottle was charged with metathesized *cis*-**1b** (0.150 g, 0.181 mmol), $(Ph_3P)_3RhCl$ (0.0252 g, 0.0272 mmol, 15 mol%), CH_2Cl_2 (20 mL), and H_2 (5 bar). The solution was stirred (72 h). The solvent was removed by oil pump vacuum, and CH_2Cl_2 was added. The sample was passed through a short pad of neutral alumina, rinsing with CH_2Cl_2. Two fractions were collected. The solvents were removed by oil pump vacuum. The second gave *cis*-**2b** (0.023 g, 0.028 mmol, 15%) as a light brown solid, mp (capillary) 260 °C. TGA: onset of mass loss, 109 °C (8%). Anal. Calcd. (%) for $C_{36}H_{72}Cl_2P_2Pt$ (832.89): C, 51.92; H, 8.71. Found: C, 51.22; H, 8.48.[38]

NMR ($CDCl_3$, δ/ppm): **^{1}H** (400 MHz) 2.62-2.60 (br m, 4H, PCH_2), 2.05-2.03 (br s, 4H, PCH_2), 1.72 (br s, 4H, PCH_2), 1.65-1.24 (m, 60H, remaining CH_2); **^{13}C{^{1}H}** (100 MHz)[39] 30.1 (virtual t,[41] J_{CP} = 8.4 Hz, 4C, $PCH_2CH_2CH_2$), 29.7 (virtual t,[41] J_{CP} = 5.4 Hz, 2C, $PCH_2CH_2CH_2$), 27.5 (s, 4C, CH_2), 27.1 (s, 2C, CH_2), 26.7 (s, 2C, CH_2), 26.2 (s, 2C, CH_2), 25.7 (s, 4C, CH_2), 25.2 (s, 4C, CH_2), 24.7 (s, 4C, PCH_2CH_2), 24.5 (br s, 2C, PCH_2CH_2), 24.1 (br s, 4C, PCH_2), 22.9 (br s, 2C, PCH_2); **^{31}P{^{1}H}** (162 MHz) 7.4 (s, $^{1}J_{PPt}$ = 3568 Hz[42]). **MS**:[43] 832 (**M**$^+$, 20%), 797 (**M**$^+$ – Cl, 100%), 759 (**M**$^+$ – 2Cl, 85%).

Metathesis of *cis*-1c. Grubbs' first generation catalyst (0.033 g, 0.040 mmol, 10 mol%), *cis*-**1c** (0.2000 g, 0.2009 mmol), and CH_2Cl_2 (200 mL; the resulting solution is 0.0010 M in *cis*-**1c**) were combined in a procedure analogous to that for *cis*-**1b**. An identical workup gave metathesized *cis*-**1c** (0.098 g, 0.107 mmol, 53%) as a white solid.

NMR ($CDCl_3$, δ/ppm): **^{31}P{^{1}H}** (162 MHz) 9.8 (s, 53%), 9.5 (s, 33%), 8.4 (s, 7%), 8.0 (s, 7%).

***cis*-PtCl$_2$(P((CH$_2$)$_{14}$)$_3$P) (*cis*-2c).** Metathesized *cis*-**1c** (0.0980 g, 0.108 mmol), $(Ph_3P)_3RhCl$ (0.0148 g, 0.0160 mmol, 15 mol%), toluene (20 mL), and H_2 (5 bar) were combined in a procedure analogous to that for *cis*-**2b**. An identical workup gave *cis*-**2c** (0.0740 g, 0.0807 mmol, 75%) as a light brown solid, mp (capillary) 210 °C. **DSC** ($T_i/T_e/T_p/T_c/T_f$):[37] 140.2/200.2/211.1/ 214.9/218.4 (endotherm) °C. **TGA**: onset of mass loss, 204 °C. Anal. Calcd. (%) for $C_{42}H_{84}Cl_2P_2Pt$ (917.05): C, 55.01; H, 9.23. Found: C, 52.48; H, 9.17.[38]

NMR (CD_2Cl_2, δ/ppm): **^{1}H** (400 MHz) 2.58-2.55 (br m, 4H, PCH_2), 1.84-1.78 (br m, 8H, PCH_2), 1.46-1.26 (br m, 72H, remaining CH_2); **^{13}C{^{1}H}** (100 MHz)[39] 31.0 (virtual t,[41] J_{CP} = 4.6 Hz, 2C, $PCH_2CH_2CH_2$), 30.6 (virtual t,[41] J_{CP} = 7.6 Hz, 4C, $PCH_2CH_2CH_2$), 28.7 (s, 4C, CH_2), 27.7 (s, 2C, CH_2), 27.6 (s, 2C, CH_2), 27.34 (s, 4C, CH_2), 27.25 (s, 8C, CH_2), 26.6 (s, 4C, CH_2), 25.4 (s, 4C, PCH_2CH_2), 25.2 (br s, 2C, PCH_2CH_2), 24.7 (br s, 4C, PCH_2), 23.7 (br s, 2C, PCH_2); **^{31}P{^{1}H}** (162 MHz) 5.3 (s, $^{1}J_{PPt}$ = 3543 Hz[42]). **MS**:[43] 916 (**M**$^+$, 20%), 882 (**M**$^+$ – Cl, 40%), 844 (**M**$^+$ – 2Cl, 100%).

***cis*-PtCl$_2$(P((CH$_2$)$_{16}$)$_3$P) (*cis*-2d).** Grubbs' first generation catalyst (0.0445 g, 0.0541 mmol, 12 mol%), *cis*-**1d** (0.4868 g, 0.451 mmol), and CH_2Cl_2 (750 mL; the resulting solution is 0.00060 M in *cis*-**1d**) were combined in a procedure analogous to that for the metathesis of *cis*-**1b**. After the alumina filtration step, the CH_2Cl_2 filtrate, PtO_2 (0.0236 g, 0.104 mmol) and H_2 (5 bar) were combined in a Fischer-Porter bottle. A

reaction and workup analogous to that for *cis*-**2b** gave *cis*-**2d** (0.0772 g, 0.077 mmol, 17%) as a white solid, mp (capillary) 159-161 ºC. Anal. Calcd. (%) for $C_{48}H_{96}Cl_2P_2Pt$ (1001.23): C, 57.58; H, 9.66. Found: C, 57.73; H, 9.77.

NMR ($CDCl_3$, δ/ppm): **^{1}H** (500 MHz) 2.68-1.51 (m, 12H, PCH_2), 2.01-1.88 (m, 12H, PCH_2CH_2), 1.78-1.70 (m, 12H, $PCH_2CH_2CH_2$), 1.35-1.20 (m, 60H, remaining CH_2); **^{13}C{^{1}H}** (126 MHz)[39] 31.24 (virtual t,[41] J_{CP} = 4.6 Hz, 2C, $PCH_2CH_2CH_2$), 31.16 (virtual t,[41] J_{CP} = 7.6 Hz, 4C, $PCH_2CH_2CH_2$), 29.2 (s, 4C, CH_2), 28.6 (s, 2C, CH_2), 28.4 (s, 2C, CH_2), 28.3 (s, 4C, CH_2), 27.7 (s, 4C, CH_2), 27.4 (s, 2C, CH_2), 27.0 (s, 2C, CH_2), 26.8 (s, 2C, CH_2), 26.5 (s, 4C, CH_2), 26.0 (s, 4C, CH_2), 25.8 (s, 4C, PCH_2CH_2), 24.9 (br s, 2C, PCH_2CH_2), 24.5 (br s, 4C, PCH_2), 23.8 (br s, 2C, PCH_2); **^{31}P{^{1}H}** (202 MHz) 4.35 (s, $^1J_{PPt}$ = 3550 Hz[42]). **IR** (cm^{-1}, powder film): 2930 (s), 2844 (m), 1730 (m), 1461 (m), 1265 (m), 1074 (m), 726 (m).

Metathesis of *cis*-1e. Grubbs' first generation catalyst (0.0213 g, 0.0258 mmol, 12.0 mol%), *cis*-**1e** (0.251 g, 0.215 mmol), and CH_2Cl_2 (215 mL; the resulting solution is 0.0010 M in *cis*-**1e**) were combined in a procedure analogous to that for *cis*-**1b**. An identical workup gave metathesized *cis*-**1e** (0.119 g, 0.110 mmol, 51%) as a white solid.

NMR ($CDCl_3$, δ/ppm): **^{31}P{^{1}H}** (162 MHz) 7.6 (s, 47%), 7.3 (s, 35%), 6.9 (s, 7%), 3.8 (s, 11%).

***cis*-$PtCl_2(P(CH_2)_{18})_3P$) (*cis*-2e).** Metathesized *cis*-**1e** (0.180 g, 0.167 mmol), $(Ph_3P)_3RhCl$ (0.023 g, 0.025 mmol, 15 mol%), CH_2Cl_2 (20 mL), and H_2 (5 bar) were combined in a procedure analogous to that for *cis*-**2b**. An identical workup gave *cis*-**2e** (0.033 g, 0.030 mmol, 18%) as a light brown solid, mp (capillary) 185 °C. **DSC** ($T_i/T_e/T_p/T_cT_f$):[37] 33.3/55.7/59.4/61.8/69.1 (endotherm), 133.2/155.5/166.9/168.6/169.7 (endotherm) °C. **TGA**: onset of mass loss, 169 °C. Anal. Calcd. (%) for $C_{54}H_{108}Cl_2P_2Pt$ (1085.37): C, 59.76; H, 10.03. Found: C, 59.22; H, 9.64.

NMR ($CDCl_3$, δ/ppm): **^{1}H** (400 MHz) 2.10-1.85 (m, 12H, PCH_2), 1.64-1.49 (m, 12H, PCH_2CH_2), 1.48-1.40 (m, 12H, $PCH_2CH_2CH_2$), 1.40-1.18 (m, 72H, remaining CH_2); **^{13}C{^{1}H}** (100 MHz)[39] 30.9 (virtual t,[41] $^3J_{CP}$ = 6.8 Hz, $PCH_2CH_2CH_2$), 28.9 (s, $2CH_2$), 28.6 (s, CH_2), 28.0 (s, CH_2), 27.3 (s, CH_2), 27.1 (s, CH_2), 26.5 (s, PCH_2CH_2), 24.6 (br s, PCH_2); **^{31}P{^{1}H}** (162 MHz) 4.6 (s, $^1J_{PPt}$ = 3533 Hz[42]). **MS**:[43] 1084 (**M**$^+$, 15%), 1049 ([**M** – Cl]$^+$, 80%), 1011 (unassigned, 100%).

***cis*-$PtCl_2(P((CH_2)_{20})_3P)$ (*cis*-2f).** Grubbs' first generation catalyst (0.0298 g, 0.0362 mmol, 7.5 mol%), *cis*-**1f** (0.6001 g, 0.481 mmol), and CH_2Cl_2 (450 mL; the resulting solution is 0.0011 M in *cis*-**1f**) were combined in a procedure analogous to that for the metathesis of *cis*-**1b**. After the alumina filtration step, the CH_2Cl_2 filtrate, PtO_2 (0.0232 g, 0.102 mmol), and H_2 (5 bar) were combined in a Fischer-Porter bottle. A reaction and workup analogous to that for *cis*-**2b** gave *cis*-**2f** (0.1017 g, 0.087 mmol, 18%) as a white solid, mp (capillary) 163-167 ºC. Anal. Calcd. (%) for $C_{60}H_{120}P_2Cl_2Pt$ (1169.53): C, 61.62; H, 10.34. Found C, 61.40; H, 10.29.

NMR ($CDCl_3$, δ/ppm): **^{1}H** (500 MHz) 2.08-1.85 (m, 12H, PCH_2), 1.60-1.50 (m, 12H, PCH_2CH_2), 1.45-1.37 (m, 12H, $PCH_2CH_2CH_2$), 1.36-1.17 (m, 84H, remaining CH_2); **^{13}C{^{1}H}** (126 MHz)[39] 31.2 (virtual t,[41] J_{CP} = 6.9 Hz, $PCH_2CH_2CH_2$), 29.4 (s, CH_2), 29.2 (s, CH_2), 28.9 (s, CH_2), 28.4 (s, CH_2), 27.9 (s, CH_2), 27.2 (s, CH_2), 27.1 (s, CH_2), 24.9 (br s, PCH_2CH_2), 24.6 (br s, PCH_2); **^{31}P{^{1}H}** (202 MHz) 2.84 (s, $^1J_{PPt}$ = 3540 Hz[42]). **IR** (cm^{-1}, powder film): 2916 (s), 2847 (m), 1458 (m), 718 (m).

***cis*-$PtCl_2(P((CH_2)_{22})_3P)$ (*cis*-2g).** Grubbs' first generation catalyst (0.0254 g, 0.0309 mmol, 9.4 mol%), *cis*-**1g** (0.4382 g, 0.329 mmol), and CH_2Cl_2 (450 mL; the resulting solution is 0.00073 M in *cis*-**1g)** were combined in a procedure analogous to that for the metathesis of *cis*-**1b**. After the alumina filtration step, the CH_2Cl_2 filtrate (20 mL), PtO_2 (0.0185 g, 0.0815 mmol), and H_2 (5 bar) were combined in a Fischer-Porter bottle.

A reaction and workup analogous to that for *cis*-**2b** gave *cis*-**2g** (0.0871 g, 0.0695 mmol, 21%) as a white solid, mp (capillary) 134-137 ºC. Anal. Calcd. (%) for $C_{66}H_{132}P_2Cl_2Pt$ (1253.69): C, 63.23; H, 10.61. Found C, 63.50; H, 10.73.

NMR ($CDCl_3$, δ/ppm): **^{1}H** (500 MHz) 2.08-1.85 (m, 12H, PC*H*$_2$), 1.62-1.50 (m, 12H, P CH_2CH_2), 1.44-1.37 (m, 12H, $PCH_2CH_2CH_2$), 1.36-1.20 (m, 96H, remaining C*H*$_2$); **^{13}C{^{1}H}** (126 MHz)[39] 31.1 (virtual t,[41] J_{CP} = 7.1 Hz, $PCH_2CH_2CH_2$), 29.4 (s, 2*C*H_2), 29.3 (s, *C*H_2), 28.9 (s, *C*H_2), 28.4 (s, *C*H_2), 27.9 (s, *C*H_2), 27.7 (s, *C*H_2), 27.3 (s, *C*H_2), 24.7 (apparent br m, PCH_2CH_2); **^{31}P{^{1}H}** (202 MHz) 2.27 (s, $^1J_{PPt}$ = 3530 Hz[42]). **IR** (cm^{-1}, powder film): 2916 (s), 2846 (m), 1458 (m), 718 (m).

***cis*-$PtCl_2(P(O(CH_2)_3CH=CH_2)_3)_2$ (*cis*-4a).** A Schlenk flask was charged with $PtCl_2$ (0.250 g, 0.940 mmol), toluene (10.0 mL), and $P(O(CH_2)_3CH=CH_2)_3$ (0.5920 g, 2.068 mmol).[24] The mixture was refluxed with stirring (12 h). The solvent was removed by oil pump vacuum, and CH_2Cl_2 was added. The sample was chromatographed (silica column, 70:30 v/v hexanes/ ethyl acetate). The solvent was removed from the product containing fractions by oil pump vacuum to give *cis*-**4a** (0.474 g, 0.565 mmol, 60%) as a light yellow oil. Anal. Calcd. (%) for $C_{30}H_{54}Cl_2O_6P_2Pt$ (838.68): C, 42.96; H, 6.49. Found: C, 43.57; H, 6.73.[38]

NMR ($CDCl_3$, δ/ppm): **^{1}H** (400 MHz) 5.78 (ddt, 6H, $^3J_{HHtrans}$ = 17.1 Hz, $^3J_{HHcis}$ = 10.3 Hz, $^3J_{HH}$ = 6.6 Hz, C*H*=), 5.02 (dd, 6H, $^3J_{HHtrans}$ = 17.9 Hz, $^2J_{HH}$ = 1.6 Hz, $=CH_EH_Z$), 4.99 (br d, 6H, $^3J_{HHcis}$ = 10.2 Hz, $=CH_EH_Z$), 4.18-4.93 (m, 12H, OC*H*$_2$), 2.16-2.11 (m, 12H, C*H*$_2$), 1.81-1.74 (m, 12H, C*H*$_2$); **^{13}C{^{1}H}** (100 MHz) 137.6 (s, *C*H=), 115.9 (s, =*C*H_2), 67.3 (s, O*C*H_2), 30.0 (s, *C*H_2CH=), 29.7 (virtual t,[41] J_{CP} = 3.6 Hz, OCH_2CH_2); **^{31}P{^{1}H}** (162 MHz) 69.7 (s, $^1J_{PPt}$ = 5696 Hz[42]). **MS**:[43] 803 (**M**$^+$ – Cl, 40%), 767 (**M**$^+$ – 2Cl, 8%), 343 (unassigned, 100%).

***cis*-$PtCl_2(P(O(CH_2)_4CH=CH_2)_3)_2$ (*cis*-4b).** $PtCl_2$ (0.100 g, 0.376 mmol), toluene

(5.5 mL), and $P(O(CH_2)_4CH=CH_2)_3$ (0.272 g, 0.827 mmol)[24] were combined in a procedure analogous to that for *cis*-**4a**. An identical workup gave *cis*-**4b** (0.2275 g, 0.2465 mmol, 66%) as a colorless oil. Anal. Calcd. (%) for $C_{36}H_{66}Cl_2O_6P_2Pt$ (922.84): C, 46.86; H, 7.21. Found: C, 46.94; H, 7.46.

NMR ($CDCl_3$, δ/ppm): **^{1}H** (400 MHz) 5.76 (ddt, 6H, $^3J_{HH}$*trans* = 17.0 Hz, $^3J_{HH}$*cis* = 10.2 Hz, $^3J_{HH}$ = 6.6 Hz, C*H*=), 4.99 (br d, 6H, $^3J_{HH}$*trans* = 17.6 Hz, $=CH_EH_Z$), 4.96 (br d, 6H, $^3J_{HH}$*cis* = 10.3 Hz, $=CH_EH_Z$), 4.16-4.12 (m, 12H, OCH_2), 2.09-2.02 (m, 12H, CH_2), 1.71-1.64 (m, 12H, CH_2), 1.49-1.42 (m, 12H, remaining CH_2); **^{13}C{^{1}H}** (100 MHz) 138.5 (s, *C*H=), 115.4 (s, $=CH_2$), 67.7 (s, OCH_2), 33.6 (s, CH_2), 30.0 (s, CH_2), 25.2 (s, CH_2); **^{31}P{^{1}H}** (162 MHz) 69.3 (s, $^1J_{PPt}$ = 5696 Hz[42]). **MS**:[43] 887 (M^+ – Cl, 25%), 850 (M^+ – 2Cl, <5%), 357 (100%).

***cis*-$PtCl_2(P(O(CH_2)_5CH=CH_2)_3)_2$ (*cis*-4c).** $PtCl_2$ (0.250 g, 0.940 mmol), toluene (10.0 mL), and $P(O(CH_2)_5CH=CH_2)_3$ (0.766 g, 2.068 mmol)[24] were combined in a procedure analogous to that for *cis*-**4a**. An identical workup gave *cis*-**4c** (0.900 g, 0.894 mmol, 95%) as colorless oil. Anal. Calcd. (%) for $C_{42}H_{78}Cl_2O_6P_2Pt$ (1007.00): C, 50.10; H, 7.81. Found: C, 49.78; H, 7.81.

NMR ($CDCl_3$, δ/ppm): **^{1}H** (400 MHz) 5.77 (ddt, 6H, $^3J_{HH}$*trans* = 17.1 Hz, $^3J_{HH}$*cis* = 10.3 Hz, $^3J_{HH}$ = 6.7 Hz, C*H*=), 4.98 (dd, 6H, $^3J_{HH}$*trans* = 17.2 Hz, $^2J_{HH}$ = 1.7 Hz, $=CH_EH_Z$), 4.93 (br d, 6H, $^3J_{HH}$*cis* = 10.2 Hz, $=CH_EH_Z$), 4.15-4.07 (m, 12H, OCH_2), 2.06-2.01 (m, 12H, CH_2), 1.70-1.64 (m, 12H, CH_2), 1.39-1.35 (m, 24H, remaining CH_2); **^{13}C{^{1}H}** (100 MHz) 138.9 (s, *C*H=), 115.1 (s, $=CH_2$), 67.7 (s, OCH_2), 34.0 (s, CH_2), 30.1 (s, CH_2), 28.9 (s, CH_2), 25.5 (s, CH_2); **^{31}P {^{1}H}** (162 MHz) 69.3 (s, $^1J_{PPt}$ = 5698 Hz[42]). **MS**:[43] 971 (M^+ – Cl, 100%), 371 ($[P(O(CH_2)_5CH=CH_2)_3]^+$, 100%).

Metathesis of *cis*-4a. A Schlenk flask was charged with *cis*-**4a** (0.166 g, 0.198 mmol), Grubbs' first generation catalyst (0.0163 g, 0.0198 mmol, 10 mol%), and CH_2Cl_2

(250 mL; the resulting solution is 0.00079 M in *cis*-**4a**), and fitted with a condenser. The solution was refluxed with stirring (12 h). The mixture was cooled to room temperature, and a second charge of Grubbs' first generation catalyst (0.008 g, 0.009 mmol, 5 mol%) was added. The solution was refluxed with stirring (12 h). A third cycle with 5 mol% of Grubbs' first generation catalyst was similarly conducted. The solvent was removed by oil pump vacuum, and CH_2Cl_2 (2 mL) was added. The mixture was chromatographed (silica column, 80: 20 v/v hexanes/ethyl acetate). A yellow band and then a colorless product band were collected. The solvent was removed from the latter by oil pump vacuum, and ethyl ether was added. The ether was removed by oil pump vacuum, and the cycle repeated until metathesized *cis*-**4a** (0.0450 g, 0.0596 mmol, 30%) was obtained as a white solid.

NMR ($CDCl_3$, δ/ppm): **^{1}H** (400 MHz) 5.49-5.04 (m, 6H, C*H*=), 4.51-4.02 (m, 12H, OCH_2), 2.41-1.52 (m, 24H, remaining CH_2); **^{31}P{^{1}H}** (162 MHz) 76.0 (s, 23%), 72.9 (s, 37%), 69.1 (s, 23%), 68.7 (s, 17%).

***cis*-$\overline{\text{PtCl}_2\text{(P(O(CH}_2)_8\text{O)}_3\text{P)}}$ (*cis*-5a).** A Fischer-Porter bottle was charged with metathesized *cis*-**4a** (0.045 g, 0.060 mmol), $(Ph_3P)_3RhCl$ (0.0110 g, 0.0119 mmol, 20 mol%), toluene (20 mL) and H_2 (5 bar). The solution was stirred at 70 °C (12 h). The solvent was removed by oil pump vacuum. The mixture was chromatographed (silica column, 80:20 v/v hexanes/ethyl acetate). A yellow band and then a colorless product band were collected. The solvent was removed from the latter by oil pump vacuum. Ethyl ether was added, and then removed by oil pump vacuum; hexanes were added, and then removed by oil pump vacuum. This cycle was repeated until *cis*-**5a** (0.015 g, 0.020 mmol, 33%) was obtained as a white solid, mp (capillary) 195 °C, **DSC** ($T_i/T_e/T_p/T_c/T_f$):[37] 85.8/111.0/123.6/130.4/141.4 °C (endotherm). **TGA**: onset of mass loss, 289 °C. Anal. Calcd. (%) for $C_{24}H_{48}Cl_2O_6P_2Pt$ (760.57): C, 37.90; H, 6.36. Found: C, 38.45; H, 6.27.[38]

NMR ($CDCl_3$, δ/ppm): **^{1}H** (400 MHz) 5.00-4.95 (m, 4H, OCH_2), 4.21-4.19 (m,

4H, OCH_2), 4.09-3.94 (m, 4H, OCH_2), 2.02-1.92 (m, 4H, CH_2), 1.80-1.74 (m, 4H, CH_2), 1.62-1.54 (m, 16H, CH_2), 1.40-1.21 (m, 12H, remaining CH_2); **^{13}C{^{1}H}** (100 MHz) 69.0 (s, 4C, O*C*H$_2$), 65.4 (virtual t,[41] J_{CP} = 4.6 Hz, 2C, O*C*H$_2$), 29.0 (s, 4C, *C*H$_2$), 28.1 (s, 2C, *C*H$_2$), 26.5 (s, 4C, *C*H$_2$), 24.0 (s, 4C, *C*H$_2$), 23.9 (s, 2C, *C*H$_2$), 20.8 (s, 2C, *C*H$_2$); **^{31}P{^{1}H}** (162 MHz) 68.2 (s, $^1J_{PPt}$ = 5729 Hz[42]). **MS**:[43] 759 (**M**$^+$, 20%), 723 (**M**$^+$ – Cl, 60%), 687 (**M**$^+$ – 2Cl, 100%).

Metathesis of *cis*-4b. Grubbs' first generation catalyst (0.010 g, 0.012 mmol, 10 mol%), *cis*-**4b** (0.113 g, 0.122 mmol), and CH_2Cl_2 (125 mL; the resulting solution is 0.00098 M in *cis*-**4b**) were combined in a procedure analogous to that for the metathesis of *cis*-**4a**. An identical workup gave metathesized *cis*-**4b** (0.046 g, 0.055 mmol, 45%) as a white solid.

NMR ($CDCl_3$, δ/ppm): **^{1}H** (400 MHz) 5.41-5.31 (m, 6H, C*H*=), 4.54-4.43 (m, 4H, OCH_2), 3.92-3.88 (m, 8H, OCH_2), 2.09-1.17 (m, 36H, remaining CH_2); **^{31}P{^{1}H}** (162 MHz) 68.2 (s, 22%), 68.00 (s, 46%), 67.96 (13%), 67.8 (s, 19%).

***cis*-$\overline{\mathbf{PtCl_2(P(O(CH_2)_{10}O)_3P)}}$ (*cis*-5b).** Metathesized *cis*-**4b** (0.039 g, 0.046 mmol), $(Ph_3P)_3RhCl$ (0.0064 g, 0.0069 mmol, 15 mol%), toluene (20 mL), and H_2 (5 bar) were combined in a procedure analogous to that for *cis*-**5a**. An identical workup gave *cis*-**5b** (0.017 g, 0.020 mmol, 44%) as a white solid, mp (capillary) 146 °C. DSC ($T_i/T_e/T_p/T_c/T_f$):[37] 51.2/61.4/72.1/83.8/88.0 (endotherm), 116.3/142.7/146.2/147.6 /155.1 °C (endotherm). TGA: onset of mass loss, 276 °C. Anal. Calcd. (%) for $C_{30}H_{60}Cl_2O_6P_2Pt$ (844.73): C, 42.66; H, 7.16. Found: C, 42.96; H, 7.53.

NMR ($CDCl_3$, δ/ppm): **^{1}H** (400 MHz) 4.58-4.52 (m, 4H, OCH_2), 4.13-4.04 (m, 4H, OCH_2), 4.00-3.96 (m, 4H, OCH_2), 1.81-1.68 (m, 12H, OCH$_2$CH_2), 1.48-1.34 (m, 36H, remaining CH_2); **^{13}C{^{1}H}** (100 MHz) 68.5 (s, 4C, OCH$_2$), 65.7 (br s, 2C, OCH$_2$), 29.1 (s, 4C, CH$_2$), 28.5 (s, 2C, CH$_2$), 26.9 (s, 4C, CH$_2$), 26.8 (2s, 6C, CH$_2$), 24.8 (s, 2C,

CH_2), 23.9 (s, 4C, CH_2), 22.9 (s, 2C, CH_2); **^{31}P{^{1}H}** (162 MHz) 68.1 (s, $^{1}J_{PPt}$ = 5759 Hz[42]). **MS**:[43] 810 (**M**$^{+}$ – Cl, 100%), 772 (**M**$^{+}$ – 2Cl, 40%).

Metathesis of *cis*-4c. Grubbs' first generation catalyst (0.024 g, 0.030 mmol, 10 mol%), *cis*-**4c** (0.300 g, 0.298 mmol), and CH_2Cl_2 (300 mL; the resulting solution is 0.00099 M in *cis*-**4c**) were combined in a procedure analogous to that for the metathesis of *cis*-**4a**. An identical workup gave metathesized *cis*-**4c** (0.150 g, 0.163 mmol, 55%) as colorless foam.

NMR ($CDCl_3$, δ/ppm): **^{1}H** (400 MHz) 5.38-5.23 (m, 6H, CH=), 4.45-4.39 (m, 4H, OCH_2), 4.21-4.07 (m, 8H, OCH_2), 2.26-2.06 (m, 12H, CH_2), 1.89-1.39 (m, 36H, remaining CH_2); **^{31}P{^{1}H}** (162 MHz) 67.4 (s).

***cis*-P$\overline{\text{tCl}_2(\text{P}(\text{O}(\text{CH}_2)_{12}\text{O})_3\text{P})}$ (*cis*-5c).** Metathesized *cis*-**4c** (0.0440 g, 0.0477 mmol), $(Ph_3P)_3RhCl$ (0.0083 g, 0.0095 mmol, 20 mol%), toluene (20 mL), and H_2 (5 bar) were combined in a procedure analogous to that for *cis*-**5a**. An identical workup gave *cis*-**5c** (0.016 g, 0.017 mmol, 36%) as white foam. Anal. Calcd. (%) for $C_{36}H_{72}Cl_2O_6P_2Pt$ (928.89): C, 46.55; H, 7.81. Found: C, 47.23; H, 7.97.[38]

NMR ($CDCl_3$, δ/ppm): **^{1}H** (400 MHz) 4.33-4.30 (m, 4H, OCH_2), 4.17-4.14 (m, 8H, OCH_2), 1.75-1.58 (m, 12H, CH_2), 1.42-1.34 (m, 48H, remaining CH_2; **^{13}C{^{1}H}** (100 MHz) 68.0 (s, 4C, O*C*H_2), 67.8 (virtual t,[41] J_{CP} = 2.6 Hz, 2C, O*C*H_2), 30.1 (virtual t,[41] J_{CP} = 3.1 Hz, 2C, *C*H_2), 29.7 (virtual t,[41] J_{CP} = 3.1 Hz, 4C, *C*H_2), 27.3 (s, 2C, *C*H_2), 27.1 (s, 2C, *C*H_2), 26.8 (s, 4C, *C*H_2), 26.7 (s, 4C, *C*H_2), 26.3 (s, 2C, *C*H_2), 26.1 (s, 4C, *C*H_2), 24.7 (s, 2C, *C*H_2), 24.3 (s, 4C, *C*H_2); **^{31}P{^{1}H}** (162 MHz) 68.3 (s, $^{1}J_{PPt}$ = 5721 Hz[42]). **MS**:[43] 894 (**M**$^{+}$ – Cl, 100%), 856 (**M**$^{+}$ – 2Cl, 45%).

***cis*-P$\overline{\text{tPh}_2(\text{P}((\text{CH}_2)_{14})_3\text{P})}$ (*cis*-6c).** A Schlenk flask was charged with *cis*-**2c** (0.0502 g, 0.0545 mmol) and Ph_2Zn (0.0375 g, 0.171 mmol), and THF (5 mL) was added with stirring. After 18 h, CH_3OH (several drops) was added. The sample was exposed to

air. After 1 h, the solvent was removed by oil pump vacuum, and benzene was added. The suspension was filtered through a pipette filled with silica, which was rinsed with benzene. The solvent was removed from the combined filtrate by oil pump vacuum to give *cis*-**6c** (0.0381 g, 0.0379 mol, 70%) as a white solid, dec. pt. (capillary) 160 °C. Anal. Calcd. (%) for $C_{54}H_{94}P_2Pt$ (1000.36): C, 64.84; H, 9.47. Found: C, 61.87; H, 9.42.[38]

NMR ($CDCl_3$, δ/ppm): **^{1}H** (400 MHz) 7.34 (m, 4H, *o*-Ph),[44] 6.83 (t, $^3J_{HH}$ = 6.9 Hz, 4H, *m*-Ph), 6.63 (t, $^3J_{HH}$ = 6.8 Hz, 2H, *p*-Ph), 2.12-2.04 (m, 4H, PCH_2), 1.90 (br, 4H, PCH_2), 1.47-1.24 (m, 4H/72H, PCH_2/remaining CH_2; **^{13}C{^{1}H}** (100 MHz)[39,45] 136.4 (s, 4C, *o*-Ph), 126.8 (s, 4C, *m*-Ph), 120.7 (s, 2C, *p*-Ph), 30.8 (virtual t,[41] $^3J_{CP}$ = 4.3 Hz, 2C, $PCH_2CH_2CH_2$), 30.5 (virtual t,[41] $^3J_{CP}$ = 7.0 Hz, 4C, $PCH_2CH_2CH_2$), 28.5 (s, 6C, CH_2), 27.4 (s, 4C, CH_2), 27.3 (s, 4C, CH_2), 27.2 (s, 6C, CH_2), 27.0 (s, 6C, CH_2), 26.3 (s, 6C, PCH_2CH_2), 25.0 (s, 4C, PCH_2), 22.5 (br s, 2C, PCH_2); **^{31}P{^{1}H}** (162 MHz) 1.0 (s, $^1J_{PPt}$ = 1779 Hz[42]). **MS**:[43] 920 (**M**$^+$ – C_6H_5, 25%), 844 (**M**$^+$ – $2C_6H_5$, 100%).

***cis*-$\overline{\text{PtPh}_2(\text{P}((\text{CH}_2)_{16})_3\text{P})}$ (*cis*-6d).** THF (5 mL), Ph_2Zn (0.0404 g, 0.184 mmol), and *cis*-**2d** (0.0621 g, 0.0620 mmol), were combined in a procedure analogous to that for *cis*-**6c**. An identical workup gave *cis*-**6d** (0.0458 g, 0.0422 mol, 68%) as a white solid, mp (capillary) 153 °C. Anal. Calcd. (%) for $C_{60}H_{106}P_2Pt$ (1084.54): C, 66.45; H, 9.85. Found: C, 64.70; H, 10.01.[38]

NMR ($CDCl_3$, δ/ppm): **^{1}H** (500 MHz) 7.33 (m, 4H, *o*-Ph),[44] 6.89 (t, $^3J_{HH}$ = 6.9 Hz, 4H, *m*-Ph), 6.68 (t, $^3J_{HH}$ = 6.8 Hz, 2H, *p*-Ph), 2.04-1.87 (m, 4H, PCH_2), 1.73 (br, 4H, PCH_2), 1.61-1.10 (m, 4H/84H, PCH_2/remaining CH_2; **^{13}C{^{1}H}** (126 MHz)[39,45] 136.4 (s, 4C, *o*-Ph), 126.7 (s, 4C, *m*-Ph), 120.6 (s, 2C, *p*-Ph), 31.3 (virtual t,[41] $^3J_{CP}$ = 4.3 Hz, 2C, $PCH_2CH_2CH_2$), 31.2 (virtual t,[41] $^3J_{CP}$ = 7.0 Hz, 4C, $PCH_2CH_2CH_2$), 29.2 (s, 4C, CH_2), 28.7 (s, 2C, CH_2), 28.33 (s, 2C, CH_2), 28.27 (s, 4C, CH_2), 27.9 (s, 4C, CH_2), 27.5 (s, 2C, CH_2), 27.0 (s, 2C, CH_2), 26.9 (s, 2C, CH_2), 26.8 (s, 4C, CH_2), 26.5 (s, 4C, CH_2), 25.4 (s,

6C, *C*H_2), 23.6 (s, 4C, P*C*H_2), 22.5 (br s, 2C, P*C*H_2); **^{31}P{^{1}H}** (202 MHz) –0.68 (s, $^1J_{PPt}$ = 1778 Hz[42]). **IR** (cm^{-1}, powder film): 3043 (w), 2920 (s), 2850 (m), 1568 (w), 1458 (m), 1261 (m), 1091 (m), 1055 (m), 1020 (m), 800 (m).

***cis*-PtI$_2$(P(O(CH$_2$)$_{10}$O)$_3$P) (*cis*-7b).** An NMR tube was charged with *cis*-**5b** (0.0101 g, 0.0118 mmol), NaI (0.0071g, 0.047 mmol) and THF/acetone (0.6 mL, 50:50 v/v). After 17 h, a ^{31}P{^{1}H} NMR spectrum showed >99% conversion. The solvent was removed by oil pump vacuum, and benzene was added. The suspension was filtered through glass fibers. The solvent was removed from the filtrate by oil pump vacuum to give a yellow oil. Hexanes were added and then removed by oil pump vacuum. Pentane was added and then removed by oil pump vacuum to give *cis*-**7b** (0.0119 g, 0.0116 mmol, 98%) as a yellow solid, mp (capillary) 147 °C. Anal. Calcd. (%) for $C_{30}H_{60}I_2O_6P_2Pt$ (1027.63): C, 35.06; H, 5.88. Found: C, 37.56; H, 6.24.[38]

NMR ($CDCl_3$, δ/ppm):[46] **^{1}H** (400 MHz) 4.47-4.38 (m, 4H, OC*H*$_2$), 4.15-4.07 (m, 4H, OC*H*$_2$), 3.99-3.94 (m, 4H, OC*H*$_2$), 1.84-1.71 (m, 12H, OCH$_2$C*H*$_2$), 1.40-1.23 (m, 36H, remaining C*H*$_2$); **^{13}C{^{1}H}** (100 MHz) 69.4 (s, 4C, O*C*H$_2$), 66.2 (d, $^2J_{CP}$ = 9.8 Hz, 2C, O*C*H$_2$), 29.2 (d, 4C, $^3J_{CP}$ = 5.8 Hz OCH$_2$*C*H$_2$), 28.6 (d, 2C, $^3J_{CP}$ = 7.7 Hz, OCH$_2$*C*H$_2$), 27.25 (s, 4C, *C*H$_2$), 27.22 (s, 4C, *C*H$_2$), 25.3 (s, 2C, *C*H$_2$), 25.1 (s, 2C, *C*H$_2$), 24.2 (s, 4C, *C*H$_2$), 23.3 (s, 2C, *C*H$_2$); **^{31}P{^{1}H}** (162 MHz) 72.6 (s, $^1J_{PPt}$ = 5517 Hz[42]). **MS**:[43] 901 (**M**$^+$ – I, 100%), 772 (**M**$^+$ – 2I, 50%).

***fac*-ReCl(CO)$_3$(P((CH$_2$)$_6$CH=CH$_2$)$_3$)$_2$ (*fac*-10c).** A Schlenk flask was charged with $ReCl(CO)_5$ (0.500 g, 1.38 mmol),[47] THF (15 mL), and P((CH$_2$)$_6$CH=CH$_2$)$_3$ (1.011 g, 2.773 mmol),[14] and fitted with a condenser. The yellow solution was stirred at 60 °C and turned orange as gas evolved. After 21 h, the solution was cooled, and the solvent was removed by rotary evaporation and oil pump vacuum. The residue was chromatographed (alumina column, 3 × 15 cm; 4:1 and then 2:1 v/v hexanes/CH_2Cl_2). The solvent was

removed from the major yellow band by oil pump vacuum to give *fac*-**10c** (0.953 g, 0.921 mmol, 67%) as a colorless viscous oil. Anal. Calcd. (%) for $C_{51}H_{90}ClO_3P_2Re$ (1034.87): C, 59.19; H, 8.77. Found C, 59.05; H, 8.76.

NMR (C_6D_6, δ/ppm):[46] **^{1}H** (300 MHz) 5.78 (ddt, 6H, $^3J_{HHtrans}$ = 16.8 Hz, $^3J_{HHcis}$ = 10.2 Hz, $^3J_{HH}$ = 6.6 Hz, C*H*=), 5.05 (br d, $^3J_{HHtrans}$ = 17.3 Hz, 6H, =CH_EH_Z), 5.00 (br d, $^3J_{HHcis}$ = 11.1 Hz, 6H, =CH_EH_Z), 2.14-1.82 (br m, 12H/12H, CH_2CH=CH_2/PCH_2), 1.72-1.50 (br m, 12H, PCH_2CH_2), 1.42-1.22 (br m, 36H, remaining CH_2); **^{13}C{^{1}H}** (100 MHz) 192.3/ 192.1/191.8/191.6/191.3 (apparent s/s/s/s/m, unassigned $^2J_{CP}$, 3CO), 138.9 (s, *C*H=), 114.7 (s, =*C*H_2), 34.0 (s, *C*H_2), 31.5 (virtual t,[41] $^3J_{CP}$ = 6.0 Hz, $PCH_2CH_2CH_2$), 29.11 (s, *C*H_2), 29.06 (s, *C*H_2), 26.5 (virtual t,[41] $^1J_{CP}$ = 12.9 Hz, P*C*H_2), 24.0 (s, PCH_2CH_2); **^{31}P{^{1}H}** (121 MHz) –16.6 (s). **IR** (cm^{-1}, oil film): 2019 (s, ν_{CO}), 1930 (s, ν_{CO}), 1884 (s, ν_{CO}), 1640 (m, $\nu_{C=C}$). **MS**:[43] 1034[48] (**M**$^+$, 5%), 1007 (**M**$^+$ – CO, 45%), 1000 (**M**$^+$ – Cl, 100%).

***fac*-ReBr(CO)$_3$(P((CH$_2$)$_6$CH=CH$_2$)$_3$)$_2$ (*fac*-11c).** THF (15 mL), $ReBr(CO)_5$ (0.500 g, 1.23 mmol),[47] and $P((CH_2)_6CH=CH_2)_3$ (0.912 g, 2.50 mmol)[14] were combined in a procedure analogous to that for *fac*-**10c**, except that the solution was stirred at 80 °C. A similar workup (alumina column, 3 × 15 cm; hexanes and then 4:1 v/v hexanes/CH_2Cl_2) gave *fac*-**11c** (0.575 g, 0.533 mmol, 43%) as yellow viscous oil. Anal. Calcd. (%) for $C_{51}H_{90}BrO_3P_2Re$ (1079.31): C, 56.75; H, 8.40. Found C, 56.28; H 8.53.

NMR (C_6D_6, δ/ppm):[46] **^{1}H** (300 MHz) 5.78 (ddt, 6H, $^3J_{HHtrans}$ = 16.8 Hz, $^3J_{HHcis}$ = 10.2 Hz, $^3J_{HH}$ = 6.6 Hz, C*H*=), 5.05 (br d, $^3J_{HHtrans}$ = 16.6 Hz, 6H, =CH_EH_Z), 5.00 (br d, $^3J_{HHcis}$ = 11.1 Hz, 6H, =CH_EH_Z), 2.12-1.80 (br m, 12H/12H, CH_2CH=CH_2/PCH_2), 1.67-1.47 (br m, 12H, PCH_2CH_2), 1.40-1.18 (br m, 36H, remaining CH_2); **^{13}C{^{1}H}** (75 MHz) 191.5/191.2/ 190.9/190.6/190.3 (apparent s/s/s/m/s, unassigned $^2J_{CP}$, 3CO), 138.9 (s, *C*H=), 114.8 (s, =*C*H_2), 34.1 (s, *C*H_2), 31.4 (virtual t,[41] $^3J_{CP}$ = 5.8 Hz, $PCH_2CH_2CH_2$),

29.10 (s, CH_2), 29.08 (s, CH_2), 27.0 (virtual t,[41] $^1J_{CP}$ = 13.3 Hz, PCH_2), 24.2 (s, PCH$_2$$CH_2$); **^{31}P{^{1}H}** (121 MHz) –22.4 (s). **IR** (cm^{-1}, oil film): 2023 (s, ν_{CO}), 1934 (s, ν_{CO}), 1888 (s, ν_{CO}), 1640 (m, $\nu_{C=C}$). **MS**:[43] 1078[49] (**M**$^+$, 8%), 1050[49] (**M**$^+$ – CO, 50%), 999[49] (**M**$^+$ – Br, 100%).

Metathesis of *fac*-10c. A three necked flask was charged with *fac*-**10c** (0.795 g, 0.768 mmol) and C_6H_5Cl (700 mL; the resulting solution is 0.0011 M in *fac*-**10c**), and fitted with a condenser. Grubbs' first generation catalyst (0.031 g, 0.038 mmol, 5 mol%) was added. Then N_2 was sparged through the solution with stirring. After 1 d, the solution was filtered through alumina, which was rinsed with CH_2Cl_2. The solvent was removed from the combined filtrates by oil pump vacuum to give metathesized *fac*-**10c** (0.558 g, 0.587 mmol, 76%) as a yellow viscous oil.

NMR (C_6D_6, δ/ppm): **^{1}H** (300 MHz) 5.67-5.20 (br m, 6H, C*H*=), 2.45-1.86 (br m, 12H, CH_2CH=CH), 1.84-1.60 (br m, 12H, PCH_2), 1.59-1.16 (br m, 60H, remaining CH_2); **^{31}P{^{1}H}** (121 MHz) –14.7 (s, 10%), –15.1 (s, 26%), –15.3 (s, 39%), –15.5 (s, 25%). **MS**:[43] 1846[50] (2**M**$^+$ – 2CO, 15%), 1836[50] (2**M**$^+$ – CO – Cl, 50%), 1815[50] (2**M**$^+$ – 3CO, 100%), 1786[50] (2**M**$^+$ – 4CO, 25%), 1774[50] (2**M**$^+$ – 2CO – 2Cl, 30%), 1747[50] (2**M**$^+$ – 3CO – 2Cl, 5%), 922 (**M**$^+$ – CO, 5%), 894 (**M**$^+$ – 2CO, 5%).

Metathesis of *fac*-11c. Grubbs' first generation catalyst (0.017 g, 0.021 mmol, 5 mol%), *fac*-**11c** (0.450 g, 0.417 mmol), and C_6H_5Cl (400 mL; the resulting solution is 0.0010 M in *fac*-**11c**) were combined in a procedure analogous to that for the metathesis of *fac*-**10c**. An identical workup gave metathesized *fac*-**11c** (0.329 g, 0.331 mmol, 79%) as a yellow viscous oil.

NMR (C_6D_6, δ/ppm): **^{1}H** (300 MHz) 5.60-5.18 (br m, 6H, C*H*=), 2.31-1.87 (br m, 12H/12H, CH_2CH=CH/PCH_2), 1.80-1.01 (br m, 48H, remaining CH_2); **^{31}P{^{1}H}** (121 MHz) –20.3 (s, 22%), –21.0 (s, 29%), –21.1 (s, 29%), –21.3 (s, 20%). **MS**:[43] 995[51] (**M**$^+$,

35%), 967[52] (**M**$^+$ – CO, 100%), 916 (**M**$^+$ – Br, 95%).

***fac*-ReCl(CO)$_3$(P(CH$_2$)$_{13}$CH$_2$)((CH$_2$)$_{14}$)(P(CH$_2$)$_{13}$CH$_2$) (*fac*-12'c).** A Schlenk flask was charged with metathesized *fac*-**10c** (0.558 g, 0.587 mmol; the entire quantity prepared above), THF (10 mL), and PtO_2 (0.013 g, 0.057 mmol), connected to a H_2 balloon, and partially evacuated. Then H_2 was introduced (1 bar), and the suspension was stirred. After 1 d, the solvent was removed by oil pump vacuum. The residue was chromatographed (alumina column, 3 × 20 cm, 1:1 v/v hexanes/CH_2Cl_2). The solvent was removed from the product containing fractions by rotary evaporation and oil pump vacuum to give *fac*-**12'c** (0.283 g, 0.296 mmol, 50%; 39% from *fac*-**10c**) as a white solid, mp (capillary) 76 °C, **DSC** (T_i/T_e/T_p/T_c/T_f):[37] 36.57/36.87/41.14/45.42 /46.10 °C (endotherm); 146.37/167.04/186.96/205.24/220.99 °C (exotherm). **TGA**: onset of mass loss, 279 °C. Anal. Calcd (%) for $C_{45}H_{84}ClO_3P_2Re$ (956.75): C, 56.49; H 8.85. Found C, 56.21; H 8.50.

NMR (C_6D_6, δ/ppm):[46] **^{1}H** (300 MHz) 2.29-1.89 (br m, 12H, PC*H*$_2$), 1.88-1.62 (br m, 12H, PCH$_2$C*H*$_2$), 1.60-1.18 (br m, 60H, remaining C*H*$_2$); **^{13}C{^{1}H}** (75 MHz) 192.1/191.6/191.3 (apparent s/s/m, unassigned $^2J_{CP}$, 3CO), 31.2 (virtual t,[41] $^3J_{CP}$ = 6.4 Hz), PCH$_2$CH$_2$*C*H$_2$), 29.1 (virtual t,[41] $^3J_{CP}$ = 5.4 Hz, PCH$_2$CH$_2$*C*H$_2$), 27.6 (s, *C*H$_2$), 27.5 (virtual t,[41] $^1J_{CP}$ = 18.6 Hz, P*C*H$_2$),[53] 27.4 (s, *C*H$_2$), 27.1 (s, *C*H$_2$), 26.9 (virtual t,[41] $^1J_{CP}$ = 18.2 Hz, P*C*H$_2$),[53] 26.8 (s, *C*H$_2$), 26.2 (s, *C*H$_2$), 26.1 (s, *C*H$_2$), 26.0 (s, *C*H$_2$), 24.2 (s, *C*H$_2$), 22.6 (s, PCH$_2$*C*H$_2$), 22.4 (s, PCH$_2$*C*H$_2$); **^{31}P{^{1}H}** (121 MHz) –15.7 (s). **IR** (cm^{-1}, powder film): 2019 (m, ν_{CO}), 1930 (s, ν_{CO}), 1880 (s, ν_{CO}). **MS**:[43] 957 (**M**$^+$, 30%), 929 (**M**$^+$ – CO, 70%), 922 (**M**$^+$ – Cl, 100%).

***fac*-ReBr(CO)$_3$(P(CH$_2$)$_{13}$CH$_2$)((CH$_2$)$_{14}$)(P(CH$_2$)$_{13}$CH$_2$) (*fac*-13'c).** Metathesized *fac*-**11c** (0.329 g, 0.331 mmol; the entire quantity prepared above), THF (15 mL), and PtO_2 (0.020 g, 0.088 mmol) were combined in a procedure analogous to that for *fac*-

12'c.[54] A similar workup (alumina column, 3 × 20 cm, 2:1 v/v hexanes/CH_2Cl_2) gave *fac*-**13'c** (0.062 g, 0.062 mmol, 19%; 15% from *fac*-**11c**) as a white solid, mp (capillary) 66 °C. **DSC** ($T_i/T_e/T_p/T_c/\ T_f$):[37] 146.26/170.84/191.10/241.88/242.08 °C (exotherm); 242.24/247.99/263.74/282.72/289.73 °C (exotherm, minor). **TGA**: onset of mass loss, 289 °C. Anal. Calcd (%) for $C_{45}H_{84}BrO_3P_2Re$ (1001.21): C 53.98; H 8.46. Found C, 53.87; H 8.33.

NMR (C_6D_6, δ/ppm):[46] **^{1}H** (300 MHz) 2.25-1.82 (br m, 12H, PCH_2), 1.80-1.59 (br m, 12H, PCH_2CH_2), 1.58-1.05 (br m, 60H, remaining CH_2); **^{13}C{^{1}H}** (100 MHz) 191.4/191.2/ 191.0/190.8/190.5 (apparent s/s/s/s/m, unassigned $^2J_{CP}$, 3CO), 31.1 (virtual t,[41] $^3J_{CP}$ = 6.4 Hz, $PCH_2CH_2CH_2$), 29.0 (br m, $PCH_2CH_2CH_2$), 27.6 (s, CH_2), 27.5 (virtual t,[41] $^1J_{CP}$ = 13.9 Hz, PCH_2),[53] 27.4 (s, CH_2), 27.1 (s, CH_2), 26.8 (d, $^3J_{CP}$ = 3.5 Hz, CH_2), 26.2 (s, CH_2), 26.1 (s, CH_2), 26.03 (s, CH_2), 25.95 (virtual t,[41] $^1J_{CP}$ = 13.9 Hz, PCH_2),[53] 24.3 (s, CH_2), 22.6 (s, PCH_2CH_2), 22.4 (s, PCH_2CH_2); **^{31}P{^{1}H}** (121 MHz) –21.4 (s). **IR** (cm^{-1}, powder film): 2019 (m, ν_{CO}), 1934 (s, ν_{CO}), 1888 (s, ν_{CO}). **MS**:[43] 1001[52] (**M**$^+$, 15%), 972 (**M**$^+$ – CO, 70%), 944 (**M**$^+$ – 2CO, 35%), 921[49] (**M**$^+$ – Br, 100%).

Thermolyses of Platinum Complexes. The following are representative and additional experiments are described in the APPENDIX A. **A.** An NMR tube was charged with *cis*-**2c** (0.0071 g, 0.0078 mmol) and *o*-$C_6H_4Cl_2$ (0.7 mL) and kept at 185 °C. The tube was periodically cooled and $^{31}P\{^1H\}$ NMR spectra were recorded (Figure 2.9; δ/ppm: 6.46 (s, $^1J_{PPt}$ = 2395 Hz,[42] *trans*-**2c**), 4.04 (s, $^1J_{PPt}$ = 3540 Hz,[42] *cis*-**2c**)). The *trans*-**2c**/*cis*-**2c** ratios were 5:95 (1 d), 72:28 (3 d), 87:13 (4 d), 89:11 (5 d), and 89:11 (6 d). **B.** An NMR tube was charged with *cis*-**2g** (0.0081 g, 0.0065 mmol) and C_6D_5Br (0.7 mL) and kept at 150 °C. The tube was periodically cooled and $^{31}P\{^1H\}$ NMR spectra were recorded (Figure 2.10; δ/ppm: 5.32 (s, $^1J_{PPt}$ = 2388 Hz,[42] *trans*-**2g**), 3.21 (s, oligomer), 2.87 (s, $^1J_{PPt}$ = 3530 Hz,[42] *cis*-**2g**)). The *trans*-**2g**/*cis*-**2g**/oligomer ratios were 74:7:19 (1

d) and 65:6:29 (2 d). **C.** An NMR tube was charged with *cis*-**2c** (0.0085 g, 0.0093 mmol) and C_6D_5Br (0.7 mL) and kept at 150 °C. The tube was periodically cooled and $^{31}P\{^1H\}$ NMR spectra were recorded (Figure s2.5; δ/ppm: 7.21 (s, $^1J_{PPt}$ = 2395 Hz,[42] *trans*-**2c**), 5.25 (s, oligomer), 4.59 (s, $^1J_{PPt}$ = 3540 Hz,[42] *cis*-**2c**), 2.94 (s, $^1J_{PPt}$ = 2344 Hz,[42] *trans*-$\overline{PtBr_2(P((CH_2)_{14})_3P)}$[4b,25]). The *trans*-**2g**/*cis*-**2g**/oligomer/*trans*-$\overline{PtBr_2(P((CH_2)_{14})_3P)}$ ratios were 16:78:6:<1 (1 d), 22:62:16: <1 (2 d), and 22:<1:48:30 (3 d).

Thermolyses of Rhenium Complexes. The following is representative and additional experiments are described in the APPENDIX A. **A.** A flask was charged with *fac*-**10c** (0.700 g, 0.649 mmol) and C_6H_5Cl (30 mL) and heated to 140 °C. The reaction was monitored by $^{31}P\{^1H\}$ NMR. After 21 h, conversion was complete. The solvent was removed by oil pump vacuum. The residue was chromatographed (alumina column, 3 × 20 cm, 1:1 v/v hexanes/CH_2Cl_2). The solvent was removed from the product-containing fractions by rotary evaporation and oil pump vacuum to give previously reported *mer,trans*-**11c** (0.625 g, 0.580 mmol, 89%)[6a,b] as a yellow viscous oil.

NMR (C_6D_6, δ/ppm): **^{1}H** (300 MHz) 5.77 (ddt, $^3J_{HHtrans}$ = 16.9 Hz, $^3J_{HHcis}$ = 10.2 Hz, $^3J_{HH}$ = 6.7 Hz, 6H, C*H*=), 5.04 (br d, $^3J_{HHtrans}$ = 17.1 Hz, 6H, =CH_EH_Z), 4.99 (br d, $^3J_{HHcis}$ = 10.3 Hz, 6H, =CH_EH_Z), 2.11-2.00 (br m, 12H, CH_2CH=CH_2), 1.99-1.91 (br m, 12H, PCH_2), 1.69-1.51 (br m, 12H, PCH_2CH_2), 1.49-1.20 (br m, 36H, remaining CH_2); **^{31}P{^{1}H}** (121 MHz) −13.2 (s). **IR** (cm^{-1}, oil film): 2026 (m, ν_{CO}), 1999 (m, ν_{CO}), 1934 (s, ν_{CO}), 1888 (s, ν_{CO}), 1640 (m, $\nu_{C=C}$).

Crystallography. **A.** A CH_2Cl_2 solution of *cis*-**1f** was allowed to slowly concentrate. After 9 d, colorless plates were collected and data obtained as outlined in Table A-1. Cell parameters were obtained from 45 data frames using a 1° scan and refined with 32664 reflections. Integrated intensity information for each reflection was obtained by reduction of the data frames with the program APEX3.[A10] Lorentz and polarization

corrections were applied. Data were scaled, and absorption corrections were applied using the program SADABS.[A11] No reflections were observed for 2θ >100. The structure was solved by direct methods using SHELXTL (SHELXS) and refined (weighted least squares refinement on F^2) using SHELXTL.[A12] Non-hydrogen atoms were refined with anisotropic thermal parameters. Hydrogen atoms were placed in idealized positions and refined using a riding model. Some terminal carbon atoms exhibited elongated thermal ellipsoids, suggesting disorder. For C31-C33, the disorder could be modeled between two positions (occupancy ratio of 52:48); appropriate restraints were used to keep the metrical parameters meaningful. The absence of additional symmetry or voids was confirmed using PLATON (ADDSYM).[A13] **B.** A CH_2Cl_2 solution of *cis*-**2c** was layered with pentane. After 14 d, colorless needles were collected and data were obtained as outlined in Table A-1. The structure was solved as in A (10 frames, 10° scan, 10162 reflections) with some minor differences in the software employed.[A12,A14] Scattering factors were taken from literature.[A15] **C.** A THF solution of *cis*-**2d** was allowed to slowly concentrate. After 7 d, colorless plates were collected and data were obtained as outlined in Table A-1. The structure was solved as in A (45 frames, 1° scan, 18089 reflections) but with newer software for some steps (e.g., Olex2[A16]). Two independent molecules were present in the unit cell. **D.** A THF solution of *cis*-**2f** was allowed to slowly concentrate. After 10 d, colorless plates were collected and data were obtained as outlined in Table A-1. The structure was solved as in C (45 frames, 1° scan, 64213 reflections). Two independent molecules were present in the unit cell. Some of the carbon atoms showed unusual thermal ellipsoids. Efforts to model the disorder were unsuccessful. Appropriate restraints were placed to keep the metrical parameters meaningful. **E.** A CH_2Cl_2 solution of *cis*-**6c** was layered with hexanes. After 14 d, colorless needles were collected and the structure solved as in B (10 frames, 10° scan, 11632 reflections). **F**. A CH_2Cl_2 solution of *cis*-**5a** was

layered with hexanes and stored at 4 °C. After 2 d, colorless needles were collected and the structure solved as in B (10 frames, 10° scan, 13085 reflections). Two independent molecules were present in the unit cell. **G**. A CH_2Cl_2 solution of *cis*-**5b** was layered with hexanes and stored at 4 °C. After 2 d, colorless needles were collected and the structure solved as in B (10 frames, 10° scan, 2894 reflections). Some carbon atoms in one of the methylene chains were disordered, but this could not be resolved. The structure exhibited a two-fold symmetry axis that passed through the platinum atom and bisected the Cl-Pt-Cl angle.

2.5. References

(1) Review: "Multifold Ring Closing Olefin Metatheses in Syntheses of Organometallic Molecules with Unusual Connectivities", Fiedler, T.; Gladysz, J. A. in *Olefin Metathesis – Theory and Practice*, Grela, K., Ed.; John Wiley & Sons: Hoboken, New Jersey, 2014, 311-328.

(2) Representative examples since the coverage in reference 1: (a) Wu, Q.; Rauscher, P. M.; Lang, X.; Wojtecki, R. J.; de Pablo, J. J.; Hore, M. J. A.; Rowan, S. J. *Science*, **2017**, *358*, 1434-1439. (b) Danon, J. J.; Krüger, A.; Leigh, D. A.; Lemonnier, J.-F.; Stephens, A. J.; Vitorica-Yrezabel, I. J.; Woltering, S. L. *Science* **2017**, *355*, 159-162. (c) Ogasawara, M.; Tseng, Y.-Y.; Liu, Q.; Chang, N.; Yang, X.; Takahashi, T.; Kamikawa, K. *Organometallics* **2017**, *36*, 1430-1435 and earlier papers by this group cited therein. (d) Masuda, T.; Arase, J.; Inagaki, Y.; Kawahata, M.; Yamaguchi, K.; Ohhara, T.; Nakao, A.; Momma, H.; Kwon, E.; Setaka, W. *Cryst. Growth Des.* **2016**, *16*, 4392-4401 and earlier papers by this group cited therein. (e) Gil-Ramírez, G.; Hoekman, S.; Kitching, M. O.; Leigh, D. A.; Vitorica-Yrezabal, I. J.; Zhang, G. *J. Am. Chem. Soc.* **2016**, *138*, 13159-13162. (f) Cain, M. F.; Forrest, W. P., Jr.; Peryshkov, D. V.; Schrock, R. R.; Müller, P. *J. Am. Chem. Soc.* **2013**, *135*, 15338-15341.

(3) (a) Shima, T.; Hampel, F.; Gladysz, J. A. *Angew. Chem., Int. Ed.* **2004**, *43*, 5537-5540; *Angew. Chem.* **2004**, *116*, 5653-5656. (b) Lang, G. M.; Shima, T.; Wang, L.; Cluff, K. J.; Hampel, F.; Blumel, J.; Gladysz, J. A. *J. Am. Chem. Soc.* **2016**, *138*, 7649-7663. (c) Lang, G. M.; Skaper, D.; Hampel, F.; Gladysz, J. A. *Dalton Trans.* **2016**, *45*, 16190-16204. (d) Steigleder, E.; Shima, T.; Lang, G. M.; Ehnbom, A.; Hampel, F.; Gladysz, J. A. *Organometallics* **2017**, *36*, 2891-2901.

(4) (a) Nawara, A. J.; Shima, T.; Hampel, F.; Gladysz, J. A. *J. Am. Chem. Soc.* **2006**, *128*, 4962-4963. (b) Nawara-Hultzsch, A. J.; Stollenz, M.; Barbasiewicz, M.;

Szafert, S.; Lis, T.; Hampel, F.; Bhuvanesh, N.; Gladysz, J. A. *Chem. Eur. J.* **2014**, *20*, 4617-4637. (c) Joshi, H.; Kharel, S.; Bhuvanesh, N.; Gladysz, J. A. *Organometallics*, submitted.

(5) (a) Wang, L.; Hampel, F.; Gladysz, J. A. *Angew. Chem., Int. Ed.* **2006**, *45*, 4372-4375; *Angew. Chem.* **2006**, *118*, 4479-4482. (b) Wang, L.; Shima, T.; Hampel, F.; Gladysz, J. A. *Chem. Commun.* **2006**, 4075-4077.

(6) (a) Hess, G. D.; Hampel, F.; Gladysz, J. A. *Organometallics* **2007**, *26*, 5129-5131. (b) Hess, G. D.; Fiedler, T.; Hampel, F.; Gladysz, J. A. *Inorg. Chem.* **2017**, 56, 7454-7469. (c) Fiedler, T.; Bhuvanesh, N.; Hampel, F.; Reibenspies, J. H.; Gladysz, J. A. *Dalton Trans.* **2016**, *45*, 7131-7147.

(7) See also (a) Zeits, P. D.; Rachiero, G. P.; Hampel, F.; Reibenspies, J. H.; Gladysz, J. A. *Organometallics* **2012**, *31*, 2854-2877. (b) Lang, G. M.; Bhuvanesh, N.; Reibenspies, J. H.; Gladysz, J. A. *Organometallics* **2016**, *35*, 2873-2889.

(8) (a) Setaka, W.; Yamaguchi, K. *J. Am. Chem. Soc.* **2013**, *135*, 14560-14563 and earlier work cited therein. (b) Setaka, W.; Inoue, K.; Higa, S.; Yoshigai, S.; Kono, H.; Yamaguchi, K. *J. Org. Chem.* **2014**, *79*, 8288-8295. (c) Setaka, W.; Higa, S.; Yamaguchi, K. *Org. Biomol. Chem.* **2014**, *12*, 3354-3357. (d) Shionari, H.; Inagaki, Y.; Yamaguchi, K.; Setaka, W. *Org. Biomol. Chem*. **2015**, *13*, 10511-10516. (e) Nishiyama, Y.; Inagaki, Y.; Yamguchi, K.; Setaka, W. *J. Org. Chem.* **2015**, *80*, 9959-9966.

(9) In exploratory efforts, the reaction mixture derived from *trans*-**1b** (*m* = 5) was analyzed by $^{31}P\{^{1}H\}$ NMR. A multitude of signals were present, but chromatography gave a yellowish oil of moderate purity with a $^{31}P\{^{1}H\}$ NMR signal very close to that of *trans*-**2c** (δ/ppm $CDCl_3$: 7.1 vs. 7.9, s; $^{1}J_{PPt}$ (satellite) 2393 vs. 2398 Hz). The sample decomposed with repeated chromatography.

(10) Kottas, G. S.; Clarke, L. I.; Horinek, D.; Michl, J. *Chem. Rev.* **2005**, *105*,

1281-1376.

(11) For additional relevant platinum complexes, see Taher, D.; Nawara-Hultzsch, A. J.; Bhuvanesh, N.; Hampel, F.; Gladysz, J. A. *J. Organomet. Chem.* **2016**, *821*, 136-141.

(12) (a) Khuong, T.-A. V.; Nuñez, J. E.; Godinez, C. E.; Garcia-Garibay, M. A. *Acc. Chem. Res.* **2006**, *39*, 413-422. (b) Nuñez, J. E.; Natarajan, A.; Saeed, K. I.; Garcia-Garibay, M. A. *Org. Lett.* **2007**, *9*, 3559-3561.

(13) (a) Prack, E.; O'Keefe, C. A.; Moore, J. K.; Lai, A.; Lough, A. J.; Macdonald, P. M.; Conradi, M. S.; Schurko, R. W.; Fekl, U. *J. Am. Chem. Soc.* **2015**, *137*, 13464-13467. (b) Li, W.; He, C.-T.; Zeng, Y.; Ji, C.-M.; Du, Z.-Y.; Zhang, W.-X.; Chen, X.-M. *J. Am. Chem. Soc.* **2017**, *139*, 8086-8089.

(14) Nawara-Hultzsch, A. J.; Skopek, K.; Shima, T.; Barbasiewicz, M.; Hess, G. D.; Skaper, D.; Gladysz, J. A. *Z. Naturforsch.* **2010**, *65b*, 414-424.

(15) (a) Marshall, J. A. *Acc. Chem. Res.* **1980** *13*, 213-218. (b) Chang, M. H.; Dougherty, D. A. *J. Am. Chem. Soc.* **1983**, *105*, 4102-4103. (c) Marshall, J. A.; Audia, V. H.; Jenson, T. M.; Guida, W. C. *Tetrahedron* **1986**, *42*, 1703-1709. (d) Kanomata, N.; Ochiai, Y. *Tetrahedron Lett.* **2001**, *42*, 1045-1048. (e) Ciogli, A.; Cort, A. D.; Gasparrini, F.; Lunazzi, L.; Mandolini, L.; Mazzanti, A.; Pasquini, C.; Pierini, M.; Schiaffino, L.; Mihan, F. Y. *J. Org. Chem.* **2008**, *73*, 6108-6118. (f) Castillo, A.; Greer, A. *Struct. Chem.* **2009**, *20*, 399-407. (g) Romuald, C.; Ardá, A.; Clavel, C.; Jiménez-Barbero, J.; Coutrot, F. *Chem. Sci.* **2012**, *3*, 1851-1857.

(16) Estrada, A. L.; Jia, T.; Bhuvanesh, N.; Blümel, J.; Gladysz, J. A. *Eur. J. Inorg. Chem.* **2015**, *2015*, 5318-5321.

(17) Kharel, S.; Joshi, H.; Bierschenk, S.; Stollenz, M.; Taher, D.; Bhuvanesh, N.; Gladysz, J. A. *J. Am. Chem. Soc.* **2017**, *139*, 2172-2175.

(18) Stollenz, M.; Barbasiewicz, M.; Nawara-Hultzsch, A. J.; Fiedler, T.; Laddusaw, R. M.; Bhuvanesh, N.; Gladysz, J. A. *Angew. Chem., Int. Ed*. **2011**, *50*, 6647-6651; *Angew. Chem.* **2011**, *123*, 6777-6781

(19) Skopek, K.; Barbasiewicz, M.; Hampel, F.; Gladysz, J. A. *Inorg. Chem.* **2008**, *47*, 3474-3476.

(20) Grim, S. O.; Keiter, R. L.; McFarlane, W. *Inorg. Chem.* **1967**, *6*, 1133-1137.

(21) (a) Skopek, K. Doctoral thesis, Universität Erlangen-Nürnberg, 2008. (b) A reviewer has noted that Grubbs' catalyst can contain ruthenium hydride impurities that can effect C=C isomerizations of terminal alkenes. See for example Chase, P. A.; Lutz, M.; Spek, A. L.; van Klink, G. P. M.; van Koten, G. *J. Mol. Cat. A* **2006**, *254*, 2-19.

(22) Crispini, A.; Harrison, K. N.; Orpen, A. G.; Pringle, P. G.; Wheatcroft, J. R. *J. Chem. Soc., Dalton Trans.* **1996**, 1069-1076.

(23) (a) Ahmad, N.; Ainscough, E. W.; James, T. A.; Robinson, S. D. *J. Chem. Soc., Dalton Trans.* **1973**, 1148-1150. (b) van der Vlugt, J. I.; Ackerstaff, J.; Dijkstra, T. W.; Mills, A. M.; Kooijman, H.; Spek, A. L.; Meetsma, A.; Abbenhuis, H. C. L.; Vogt, D. *Adv. Synth. Catal.* **2004**, *346*, 399-412.

(24) Skopek, K.; Gladysz, J. A *J. Organomet. Chem.* **2008**, *693*, 857-866.

(25) Another logical product would be the mixed bromide/chloride complex *trans*-$\overline{\text{PtBrCl(P((CH}_2)_{14})_3\text{P)}}$, and it could be questioned whether this might correspond to the ^{31}P NMR signal assigned to oligomer. In this context, the palladium analog has been characterized,[4b] and is easily eluted on a silica gel column. In contrast, the presumedly oligomeric product remains at the origin.

(26) Budzelaar, P. H. M., *gNMR: NMR Simulation Program*, Version 5.0.6.0, Adept Scientific: Luton, U.K. 2006.

(27) (a) Boag, N. M.; Kasez, H. D. Technetium and Rhenium. In *Comprehensive*

Organometallic Chemistry, Wilkinson, G.; Stone, F. G. A.; Abel, E. W. Eds; Pergamon: Oxford, 1982. Vol. 4, pp 173-176. (b) Bauer, E. B.; Hampel, F.; Gladysz, J. A. *Adv. Synth. Catal.* **2004**, *346*, 812-822.

(28) (a) Jung, J. H.; Ono, Y.; Shinkai, S. *Chem. Lett*. **2000**, *29*, 636-637. (b) Aoki, K.; Kudo, M.; Tamaoki, N. *Org. Lett.* **2004**, *6*, 4009-4012. (c) Thalladi, V. R.; Nüsse, M.; Boese, R. *J. Am. Chem. Soc.* **2000**, *122*, 9227-9236.

(29) Alder, R. W.; Butts, C. P.; Orpen, A. G.; Read, D.; Oliva, J. M. *J. Chem. Soc., Perkin Trans. 2*, **2001**, 282-287, and references therein.

(30) (a) Bauer, I.; Gruner, M.; Goutal, S.; Habicher, W. D. *Chem. Eur. J.* **2004**, *10*, 4011-4016. (b) Earlier papers in this series have been reviewed: Bauer, I.; Habicher, W. D. *Collect. Czech. Chem. Commun.* **2004**, *69*, 1195-1230.

(31) (a) Stollenz, M.; Bhuvanesh, N.; Reibenspies, J. H.; Gladysz, J. A. *Organometallics* **2011**, *30*, 6510-6513. (b) Stollenz, M.; Taher, D.; Bhuvanesh, N.; Reibenspies, J. H.; Baranová, Z.; Gladysz, J. A. *Chem. Commun.* **2015**, *51*, 16053-16056.

(32) Lewanzik, N.; Oeser, T.; Blümel, J.; Gladysz, J. A. *J. Mol. Catal. A*. **2006**, *254*, 20-28.

(33) (a) Bondi, A. *J. Phys. Chem*. **1964**, *68*, 441-451. (b) Mantina, M.; Chamberlin, A. C.; Valero, R.; Cramer, C. J.; Truhlar, D. G. *J. Phys. Chem. A* **2009**, *113*, 5806-5812.

(34) Ehnbom, A.; Gladysz, J. A. manuscript in preparation.

(35) (a) Eliel, E. N.; Wilen, S. H. *Stereochemistry of Organic Compounds*; Wiley: New York, 1994; pp 837-838 and 1208. (b) Ward, R. S. Selectivity versus specificity. *Chemistry in Britain* 1991, 803-804.

(36) (a) Holt, M. S.; Nelson, J. H. *Inorg. Chem.* **1986**, *25*, 1316-1320. (b) Canac, Y.; Debono, N.; Lepetit, C.; Duhayon, C.; Chauvin, R. *Inorg. Chem.* **2011**, *50*, 10810-10819. (c) Jarvis, A. G.; Schnal, P. E.; Bajwa, S. E.; Whitwood, A. C.; Zhang, X.; Cheung,

M. S.; Lin, Z.; Fairlamb, I. J. S. *Chem. Eur. J.* **2013**, *19*, 6034-6043.

(37) Cammenga, H. K.; Epple, M. *Angew. Chem., Int. Ed. Engl.* **1995**, 34, 1171-1187; *Angew. Chem.* **1995**, 107, 1284-1301. The T_e values best represent the temperature of phase transition or endotherm. DSC measurements were generally not continued above the temperature of initial mass loss (TGA).

(38) This microanalysis poorly or marginally agrees with the empirical formula, but is nonetheless reported as the best obtained to date. The NMR spectra indicate high purities ($\geq$ 98%). See also Gabbaï, F. P.; Chirik, P. J.; Fogg, D. E.; Meyer, K.; Mindiola, D. J.; Schafer, L. L.; You, S.-L. *Organometallics* **2016**, *35*, 3255-3256.

(39) The P$CH_2CH_2CH_2$ ^{1}H and ^{13}C NMR signals of *cis*-**1g** and *cis*-**2d**,**g** were assigned by ^{1}H,^{1}H COSY, ^{1}H,^{13}C{^{1}H} COSY, ^{13}C{^{13}C} COSY, and ^{1}H,^{13}C{^{1}H} HMBC experiments. Representative spectra have been given for related compounds in earlier papers.[6c,40] The corresponding signals of *cis*-**1f** and *cis*-**2b**,**c**,**e**,**f** were assigned analogously.

(40) Lang, G. M.; Skaper, D.; Shima, T.; Otto, M.; Wang, L.; Gladysz, J. A. *Aust. J. Chem.* **2015**, *68*, 1342-1351.

(41) The *J* values given for virtual triplets represent the *apparent* couplings between adjacent peaks, and not the mathematically rigorously coupling constants. See Hersh, W. H. *J. Chem. Educ.* **1997**, *74*, 1485-1488.

(42) This coupling represents a satellite (d, ^{195}Pt = 33.8%), and is not reflected in the peak multiplicity given.

(43) FAB, 3-NBA, *m/z* (relative intensity, %); the most intense peak of the isotope envelope is given.

(44) The *ortho* proton signal was assigned by analogy to that of *trans*-**6c** (two downfield signals due to restricted Pt-C_{ipso} rotation, δ 7.38 and 7.08, 2d, $^3J_{HH}$ = 7.0-7.2

Hz).[4b] The chemical shifts and multiplicities of the *meta* and *para* proton signals are also in close agreement.

(45) The signal for the *ipso* phenyl carbon atom was not observed.

(46) The P$CH_2CH_2CH_2$ ^{1}H and ^{13}C NMR signals of *cis*-**7b** and *fac*-**10c** were made by ^{1}H,^{1}H COSY and ^{1}H,^{13}C{^{1}H} COSY experiments. The corresponding signals of *fac*-**11c**, *fac*-**12'c**, and *fac*-**13'c** were assigned analogously.

(47) Schmidt, S. P.; Trogler, W. C.; Basolo, F.; Urbancic, M. A.; Shapley, J. R. *Inorg. Synth.* **1985**, *23*, 41-46.

(48) The exact mass of the most intense [**M**]$^+$ peak should be 1034.56. It is presumed that the instrument, which provides masses to the nearest whole integer, rounded the value down, and thus it does not represent the ion [**M** − H]$^+$. All peak assignments were checked versus the theoretical isotope envelope pattern.

(49) The situation with this ion is similar to that described in footnote 48.

(50) These dirhenium peaks deviate by as many as ± 3 mass units from that expected for the ion given. However, the isotope envelopes are otherwise in good agreement with those calculated.

(51) The situation with this ion is similar to that described in footnote 48 (calculated exact mass of most intense [**M**]$^+$ peak = 994.42; the instrument is presumed to have rounded the value up, such that it does not represent the ion [**M** + H]$^+$).

(52) The situation with this ion is similar to that described in footnote 51.

(53) One peak of this triplet is obscured; the chemical shift and coupling constant are extrapolated from the two that are visible.

(54) This reaction was carried out with a Fischer-Porter bottle and H_2 (5 bar), instead of a balloon pressure of H_2 (1 bar).

(55) Macrae, C. F.; Bruno, I. J.; Chisholm, J. A.; Edgington, P. R.; McCabe, P.;

Pidcock, E.; Rodriguez-Monge, L.; Taylor, R.; van de Streek, J.; Wood, P. A. *J. Appl. Cryst.* **2008**, *41*, 466-470.

(56) Lichtenberger, D. L.; Gladysz, J. A. *Organometallics* **2014**, *33*, 835-835.

Table 2.1. Summary of crystallographic data for *cis*-**1f,2c,d,f,6c,5a,b**.

	cis-**1f**	*cis*-**2c**	*cis*-**2d**[a]
empirical formula	$C_{66}H_{126}Cl_2P_2Pt$	$C_{42}H_{84}Cl_2P_2Pt$	$C_{48}H_{96}Cl_2P_2Pt$
formula weight	1247.59	917.02	1001.17
temperature [K]	100.0	173(2)	110.0
diffractometer	Bruker Venture	Nonius Kappa CCD	Bruker Quest X-ray
wavelength [Å]	1.54178	0.71073	0.71073
crystal system	monoclinic	monoclinic	triclinic
space group	P_12_1/c_1	$P2_1/c$	P-1
unit cell dimensions:			
a [Å]	24.469(2)	15.8988(3)	14.0147(19)
b [Å]	13.8800(12)	13.9099(4)	18.709(3)
c [Å]	20.2636(18)	20.4188(6)	20.052(3)
α [°]	90	90	80.5030(10)
β [°]	95.492(5)	93.141(2)	87.9950(10)
γ [°]	90	90	85.6440(10)
V [Å^3]	6850.6(11)	4508.8(2)	5169.5(12)
Z	4	4	4
ρ_{calc} [Mg/m^{-3}]	1.210	1.351	1.286
μ [mm^{-1}]	5.235	3.328	2.908
F(000)	2656	1912	2104
crystal size [mm^3]	0.21 × 0.108 × 0.037	0.30 × 0.15 × 0.10	0.372 × 0.366 × 0.076
Θ limit [°]	3.629 to 49.998	2.22 to 27.45	2.223 to 25.00
index range (h, k, l)	−24, 24; −13, 13; −20, 19	−20, 20; −17, 15; −26, 26	−16, 16; −21, 22; 0, 23
reflections collected	32664	18048	18089
independent reflections	6880	10243	18089
R(int)	0.0685	0.0420	0.0653
completeness to Θ	98.0	99.5	99.9
max. and min. transmission	0.8303 and 0.3770	0.7320 and 0.4351	0.262 and 0.158
data/restraints/parameters	6880/136/668	10243/0/424	18089/1338/956
goodness-of-fit on F^2	1.127	1.020	1.063

Table 2.1 continued.

	cis-**1f**	*cis*-**2c**	*cis*-**2d**[a]
R indices (final) [$I > 2\sigma(I)$]			
R_1	0.0550	0.0436	0.0452
wR_1	0.1128	0.0947	0.1035
R indices (all data)			
R_2	0.0712	0.0849	0.0514
wR_2	0.1260	0.1099	0.1076
largest diff. peak and hole [eÅ^{-3}]	1.530 and −0.692	1.101 and −1.428	1.666 and −1.722

Table 2.1 continued**.**

	cis-**2f**[a]	*cis*-**6c**	*cis*-**5a**[a]	*cis*-**5b**
empirical formula	$C_{60}H_{120}Cl_2P_2Pt$	$C_{54}H_{94}P_2Pt$	$C_{24}H_{48}Cl_2O_6P_2Pt$	$C_{30}H_{60}Cl_2O_6P_2Pt$
formula weight	1169.48	1000.32	760.55	844.71
temperature [K]	110.0	173(2)	173(2)	173(2)
diffractometer	Bruker Quest X-ray	Nonius Kappa CCD	Nonius Kappa CCD	Nonius Kappa CCD
wavelength [Å]	0.71073	0.71073	0.71073	0.71073
crystal system	triclinic	triclinic	triclinic	trigonal
space group	*P*-1	*P*-1	*P*-1	*R*-3c
unit cell dimensions:				
a [Å]	13.8635(12)	13.1005(1)	10.5573(2)	27.3660(7)
b [Å]	18.4284(16)	13.3774(2)	16.0058(3)	27.3660(7)
c [Å]	25.106(2)	15.5372(2)	17.6476(9)	26.3180(8)
α [°]	83.861(2)	77.946(1)	94.620(9)	90
β [°]	88.110(2)	79.853(1)	91.338(8)	90
γ [°]	86.673(2)	82.140(1)	97.183(9)	120
V [Å^3]	6364.3(9)	2607.05(6)	2947.35(17)	17068.9(8)
Z	4	2	4	18
ρ_{calc} [Mg/m^{-3}]	1.221	1.274	1.714	1.479
μ [mm^{-1}]	2.372	2.785	5.086	3.960
F(000)	2488	1052	1528	7740

Table 2.1 continued**.**

	cis-**2f**[a]	*cis*-**6c**	*cis*-**5a**[a]	*cis*-**5b**
crystal size [mm^3]	0.286 × 0.087 × 0.017	0.20 × 0.15 × 0.15	0.25 × 0.15 × 0.15	0.35 × 0.25 × 0.25
Θ limit [°]	2.168 to 18.962	2.24 to 27.52	2.30 to 27.49	2.31 to 25.06
index range (h, k, l)	−12, 12; −16, 16; −22, 22	−15, 17; −17, 17; −20, 20	−13, 13; −20, 20; −22, 22	−32, 32; −32, 31; −31, 28
reflections collected	64213	22639	25666	6654
independent reflections	10049	11958	13515	2664
R(int)	0.0710	0.0197	0.0192	0.1292
completeness to Θ	98.5	99.6	99.8	78.9
max. and min. transmission	0.4243 and 0.3060	0.6801 and 0.6058	0.5159 and 0.3629	0.4376 and 0.3378
data/restraints/parameters	10049/1702/1171	11958/0/514	13515/0/632	2664/1/186
goodness-of-fit on F^2	1.175	1.024	1.020	1.050
R indices (final) [$I > 2\sigma(I)$]				
R_1	0.0506	0.0258	0.0251	0.0608
wR_1	0.0966	0.0592	0.0576	0.15464
R indices (all data)				
R_2	0.0671	0.0319	0.0357	0.1032
wR_2	0.1062	0.0618	0.0617	0.1813
largest diff. peak and hole [$eÅ^{-3}$]	1.394 and −1.002	1.226 and −1.138	1.390 and −1.249	1.752 and −0.939

[a]There are two independent molecules in the unit cell. The empirical formula is for one of the two molecules, and the Z values represent the total number of molecules of both types.

Table 2.2. Key crystallographic bond lengths [Å] and angles [°] for *cis*-**1f,2c,d,f**.

	cis-**1f**	*cis*-**2c**	*cis*-**2d**[a]	*cis*-**2d**[a]	*cis*-**2f**[a]
Pt-P	2.256(2) 2.263(2)	2.2507(14) 2.2563(14)	2.2506(18) 2.248(2)	2.258(2) 2.2492(19)	2.245(3) 2.243(3)
Pt-X[c]	2.352(2) 2.354(2)	2.3661(14) 2.3689(14)	2.351(2) 2.774(19)	2.360(2) 2.371(2)	2.347(3) 2.365(3)
P-Pt-P	100.27(9)	104.37(5)	104.59(7)	104.70(7)	104.66(11)
P-Pt-X	83.94(9) 90.72(8) 168.69(8) 174.59(8)	83.23(5) 84.98(5) 170.65(5) 172.35(5)	83.42(7) 84.17(7) 171.22(7) 171.97(7)	83.66(7) 84.23(7) 171.07(7) 171.61(7)	83.52(10) 84.08(11) 171.22(10) 171.66(11)
X-Pt-X	84.94(9)	87.42(6)	87.82(7)	87.42(7)	87.77(10)

	cis-**2f**[a]	*cis*-**6c**	*cis*-**5a**[a]	*cis*-**5a**[a]	*cis*-**5b**[b]
Pt-P	2.250(3) 2.231(3)	2.3188(6) 2.3204(6)	2.2138(7) 2.2248(8)	2.2167(7) 2.2191(8)	2.209(3)
Pt-X[c]	2.345(3) 2.373(3)	2.056(3) 2.070(3)	2.3509(7) 2.3548(7)[d]	2.3455(7) 2.3492(7)[d]	2.352(3)[d]
P-Pt-P	104.29(11)	105.00(2)	100.11(3)	99.37(3)	91.07(16)
P-Pt-X	83.17(11) 84.13(11) 171.36(11) 172.23(11)	85.66(8) 86.10(7) 168.08(8) 168.45(7)	82.84(3) 88.73(3) 170.85(3) 176.87(3)	83.99(3) 89.38(3) 171.15(3) 175.77(3)	91.17(13) 172.7(1)
X-Pt-X	88.51(11)	83.61(10)	88.29(3)	87.21(3)	87.5(2)

[a]Values for the two independent molecules in the unit cell. [b]A C_2 symmetry axis renders the Pt-P and Pt-X bond lengths and other parameters equivalent. [c]Distances from platinum to the ligating atoms of the non-phosphine ligands. [d]The phosphorus-oxygen and oxygen-carbon bond lengths in *cis*-**5a**,**b** fall into the ranges 1.557(2)-1.593(2) Å and 1.432(17)-1.475(4) Å.

3. SYNTHESES, STRUCTURES, AND THERMAL PROPERTIES OF GYROSCOPE LIKE COMPLEXES CONSISTING OF $PtCl_2$ ROTATORS ENCASED IN MACROCYCLIC DIBRIDGEHEAD DIPHOSPHINES $P((CH_2)_n)_3P$ WITH EXTENDED METHYLENE CHAINS (n = 20/22/30), AND ISOMERS THEREOF

3.1. Introduction

The design and synthesis of sterically protected molecular rotors is under intense study in a number of laboratories.[1,2] In many cases, these are envisioned as components of various types of molecular devices.[3] In previous efforts, we have reported ring closing alkene metatheses of platinum bis(phosphine) dichloride complexes of the formula *trans*-$PtCl_2(P((CH_2)_mCH{=}CH_2)_3)_2$ (*trans*-**1**)[4] with Grubbs' first generation catalyst, and subsequent hydrogenations.[5] When m is six to eight, gyroscope like platinum complexes of the formula *trans*-$PtCl_2(P((CH_2)_n)_3P)$ (*trans*-**2**; n = **c**/14, **d**/16, **e**/18) can be isolated, where n is the number of carbon atoms in the methylene chains ($n = 2m + 2$).[5] As shown in Scheme 3.1, these feature cage like, triply *trans* spanning dibridgehead diphosphine ligands.

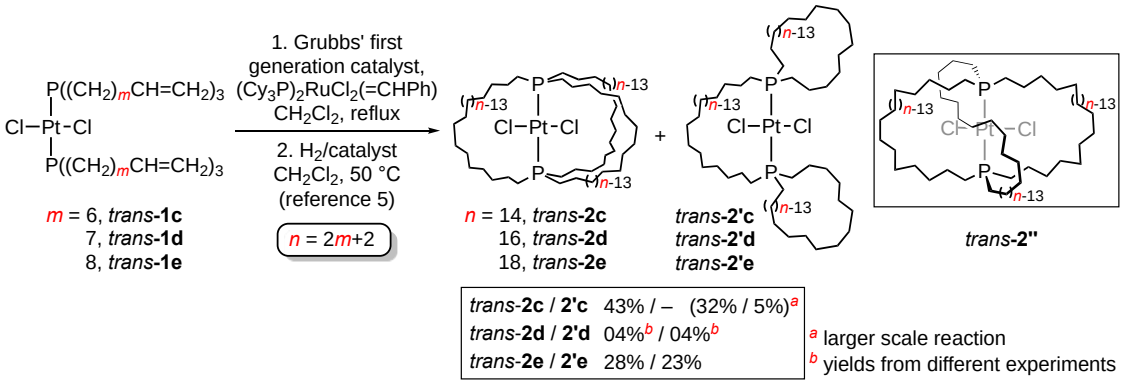

Scheme 3.1. Three fold ring closing metatheses of *trans*-**1c-e**; syntheses of gyroscope like complexes *trans*-**2c-e**.

In some cases, the yields of *trans*-**2** are modest. However, trigonal bipyramidal $Fe(CO)_3$ adducts of the same dibridgehead diphosphines (as well as homologs with fewer methylene groups) can be similarly accessed in higher yields, as rationalized elsewhere.[6] Palladium analogs of *trans*-**2** have also been described.[5] With all MCl_2 adducts, rotation is fast on the NMR time scale, even at –100 °C.

In all of the above reactions, varying amounts of isomeric monoplatinum coproducts, *trans*-$PtCl_2((H_2C)_nP((CH_2)_n)P(CH_2)_n))$ (*trans*-**2'a-c**), have also been isolated.[5b] Whereas *trans*-**2a-c** are derived from three fold *inter*ligand alkene metathesis, *trans*-**2'a-c** are derived from combinations of *intra*ligand (two fold) and *inter*ligand (single fold) metathesis. The latter cyclization mode has also been seen with other metal fragments. However, except for a few octahedral systems with certain values of n,[7] it is always a minor pathway. DFT calculations (gas phase) suggest that *trans*-**2** is more stable than *trans*-**2'** for $n < 16$, but *trans*-**2'** is more stable for $n \geq 20$.[8,9]

We have sought to fully explore the topological space associated with the preceding compounds, as well as the free diphosphine ligands, and have systematically targeted various types of stereoisomers that may be isolable.[8,10] One of these, *trans*-**2"** in Scheme 3.1, is also derived from three fold interligand alkene metathesis, but two of the methylene chains "cross", unlike the disposition in *trans*-**2**. A *di*metallic adduct of a bridgehead diphosphine, as well as a free dibridgehead diphosphine dioxide, with crossed methylene chains have in fact been isolated.[10,11]

Another variable is the *cis*/*trans* sense at platinum. First consider the educts **1**. Only *trans*-**1b-g**, which lack permanent dipole moments, are obtained when the precursors are reacted in the nonpolar solvent benzene.[4] In contrast, *cis*-**1b-g**, which are shown in Scheme 3.2 and have dipole moments, dominate when syntheses are carried out in the polar solvent water.[4,8] Related phenomena have been observed with other bis(phosphine)

platinum dichloride complexes.[12] In any event, *cis*-**1b-g** undergo three fold interligand alkene metathesis followed by hydrogenation to give *cis*-**2b-g** (Scheme 3.2).[8] For reasons detailed elsewhere, such complexes are often referred to as parachute like[8] – a counterpart to the gyroscope like attribute of *trans*-**2**. When kept in halobenzene solutions at 150-185 °C, *cis*-**2c**,**g** isomerize to *trans*-**2c**,**g**.[8] DFT calculations indicate the gas phase stability trend *trans* > *cis* for **2a-g**.[8]

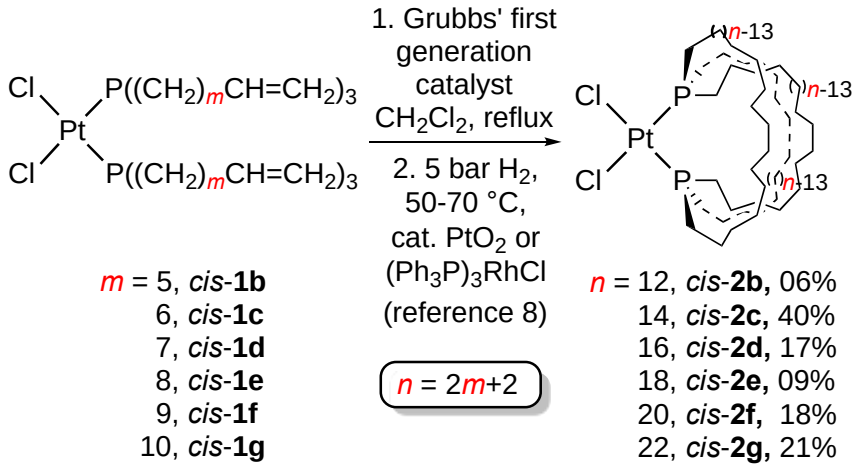

Scheme 3.2. Three fold ring closing metatheses of *cis*-**1b-g**; syntheses of parachute like complex *cis*-**2b-g**.

In this study, we sought to extend the syntheses of gyroscope like complexes *trans*-**2** in Scheme 3.1 to higher values of *n*. Questions to be addressed included the following: (1) Might additional types of products, such as *trans*-**2"**, form? (2) Do *trans*-**2**/*trans*-**2'** selectivities vary? (3) Is the stability order *trans*-**2** > *cis*-**2** maintained? Additional motivation was provided by earlier observations that reactions of *trans*-**2c,e** and excesses of appropriate nucleophiles liberate the dibridgehead diphosphines **3c**,**e** as shown in Scheme 3.3.[13-15] These can serve as "container molecules" for the selective transport of $PtCl_2$ and $PdCl_2$ away from $NiCl_2$.[15] It was thought that diphosphines with larger

macrocycles might exhibit complementary selectivities, as well as other interesting chemistry.

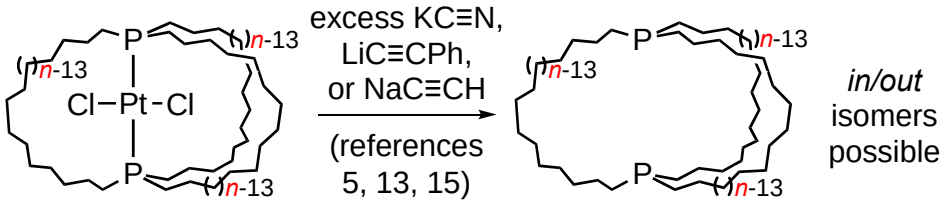

n = 14, *trans*-**2c**
18, *trans*-**2e**

n = 14, **3c** (66-91%)
18, **3e** (85%)

Scheme 3.3. Syntheses of dibridgehead diphosphines **3c**,**e**.

3.2. Results

3.2.1. Syntheses of Title Compounds. The alkene containing phosphines $P((CH_2)_mCH{=}CH_2)_3$ were prepared from PCl_3 and Grignard reagents $MgBr(CH_2)_mCH{=}CH_2)_3$ as described earlier (m = 9)[4,8] or by applying analogous protocols to Grignard reagents with longer methylene chains (m = 10, 14; experimental section). As shown in Scheme 3.4, $PtCl_2$ and the phosphines (2.0 equiv) were combined in the nonpolar solvent toluene. Workups gave the new platinum complexes *trans*-$PtCl_2(P((CH_2)_mCH{=}CH_2)_3)_2$ (*trans*-**1f**,**g**,**k**) as yellow oils or solids in 63-42% yields.

Complexes *trans*-**1f**,**g**,**k** and all other homogeneous new species below were characterized by IR and NMR (^{1}H, ^{13}C{^{1}H}, ^{31}P{^{1}H}) spectroscopy. Satisfactory microanalyses were also obtained. The $^1J_{PPt}$ values (2382-2375 Hz) were characteristic of *trans* stereoisomers,[16] and much lower than those of *cis*-**1a-g** (3511-3518 Hz).[8] Other spectroscopic properties were similar to those of the lower homologs in Scheme 3.1

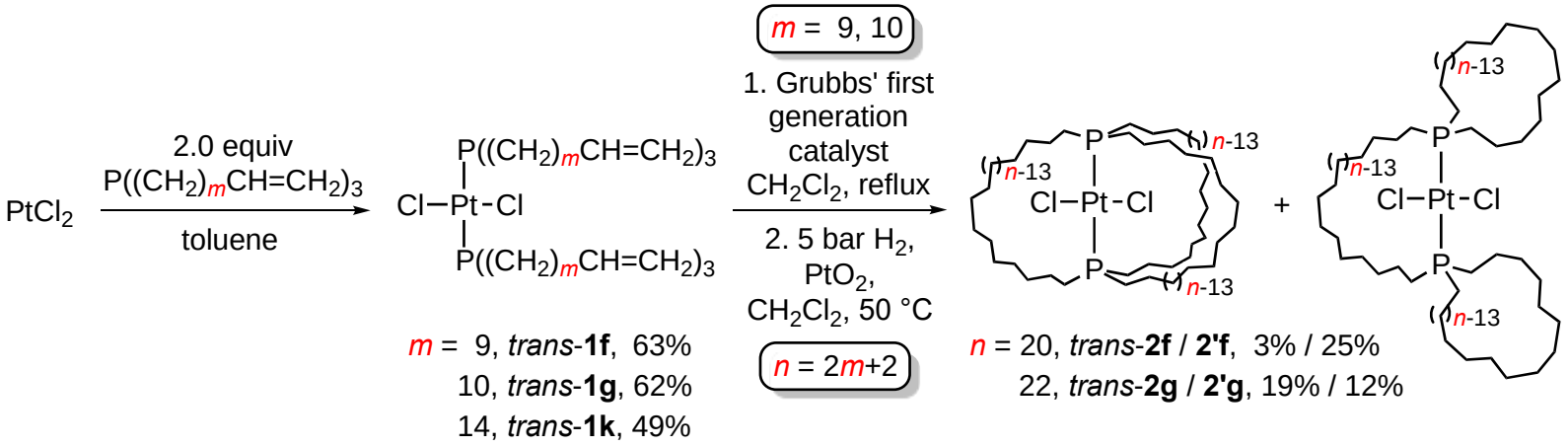

Scheme 3.4. Syntheses of title complexes with n = 20 and 22.

As shown in Scheme 3.4, dilute CH_2Cl_2 solutions of the two complexes with shorter methylene chains, *trans*-**1f**,**g** (ca. 0.00057 M), and Grubbs' first generation catalyst (12.4 mol%) were refluxed. The crude reaction mixtures were filtered through alumina and then treated with H_2 (5 bar) and PtO_2 (5 mol%) at 50 °C. In each case, two monoplatinum products could be isolated by silica gel column chromatography, *trans*-**2f**,**g** and *trans*-**2'f**,**g**. These paralleled those obtained in the earlier work in Scheme 3.1. However, with *trans*-**2f** and *trans*-**2'f**, the latter dominated (25% vs. 3%). This represents the first time a complex derived from *intra*ligand *and inter*ligand metathesis has preferentially formed from a non-octahedral educt.

Careful efforts to detect other monoplatinum products were unsuccessful. Thus, the low mass balance was presumed to reflect the formation of oligomers and polymers, which would be retained on the column. The structures of *trans*-**2'f**,**g** were evidenced by a diagnostic pattern of ^{13}C NMR signals (two sets of *n*/2 signals in a ca. 2:1 area ratio), and supported by the crystal structures of their *cis* isomers below. Readers are referred to earlier papers for analyses of additional NMR properties.[5,8]

An analogous reaction sequence for the complex with the longest methylene chain, *trans*-**2k**, is presented in Scheme 3.5. However, analogous products were not obtained. Rather, a single monoplatinum complex could be isolated in 39% yield. It exhibited a much larger $^1J_{PPt}$ value (3530 vs. 2389-2307 Hz), suggesting a *cis* coordination geometry and the parachute like complex *cis*-**2k**, as proven by additional experiments below. This result was reproduced by two coworkers several times (although in one case a minor coproduct was detected).

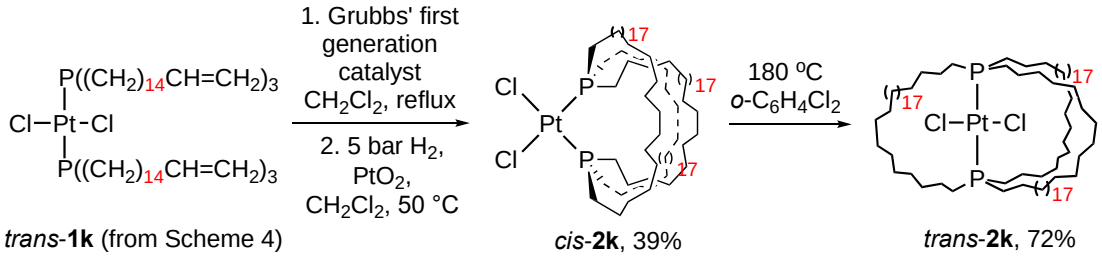

Scheme 3.5. Syntheses of title complexes with n = 30.

Given the thermodynamic relationships established below, this requires a species on the *trans*-**1k** to *cis*-**2k** reaction coordinate that is more stable as a *cis* isomer (in CH_2Cl_2), and an accessible mechanism for isomerization. Thus, a $^{31}P\{^1H\}$ NMR spectrum of the soluble crude metathesis product prior to hydrogenation was recorded ($CDCl_3$). As usual, numerous signals were observed, with some presumably reflecting a distribution of *E*/*Z* C=C isomers. These included two prominent singlets at 1.5 and 2.5 ppm, and a cluster near 5.5 ppm. Based upon chemical shift trends,[17] the last group can be confidently be assigned to *trans* P-Pt-P isomers, and the first singlet to a *cis* P-Pt-P isomer.

When analogous experiments were conducted, but $^{31}P\{^1H\}$ NMR spectra recorded prior to complete metathesis, there were additional signals in the 1.5 ppm region, consistent with the presence of *cis*-**1k**. However, in none of these spectra were any platinum satellites ($^1J_{PPt}$) resolved. When *trans*-**1k** was subjected to the initial conditions in Scheme 3.5, but in the absence of Grubbs' catalyst, it was recovered unchanged.

3.2.2. Thermal Equilibrations. In order to provide context for the first step in Scheme 3.5, various thermolyses were carried out, with the goal of effecting equilibrations. First, an *o*-$C_6H_4Cl_2$ (*ortho*-dichlorobenzene) solution of *cis*-**2k** was kept at 180 °C and monitored by $^{31}P\{^1H\}$ NMR. Clean isomerization to gyroscope like *trans*-**2k**

– the product initially expected in Scheme 3.5 – was observed. Workup after 48 h gave *trans*-**2k** in 72% yield ($^1J_{PPt}$ = 2364 Hz). This result is in line with analogous isomerizations of *cis*-**2c**,**g** (Scheme 3.2) to *trans*-**2c**,**g** reported earlier, as well as extensive gas phase DFT calculations.[8]

Next, room temperature CH_2Cl_2 solutions of the educts *trans*-**1f**,**g** were monitored by $^{31}P\{^1H\}$ NMR for several months. As shown in Scheme 3.6 (top) and Figures 3.1 and 3.2, 40-60% conversions to *cis*-**1f**,**g**[4,8] (very) gradually occurred. An analogous experiment with *trans*-**1g** in toluene gave only a 9% conversion to cis-**1g**. When this sample was kept at 100 °C for 2 d, no further reaction occurred. Hence, it is concluded that the isomerization of *trans*-**1g** is thermodynamically unfavorable in the less polar medium toluene, but favorable in the more polar medium CH_2Cl_2. The isomerization of *trans*-**1f** appears slightly unfavorable in CH_2Cl_2, suggesting a modest dependence of the equilibrium upon the methylene chain length.

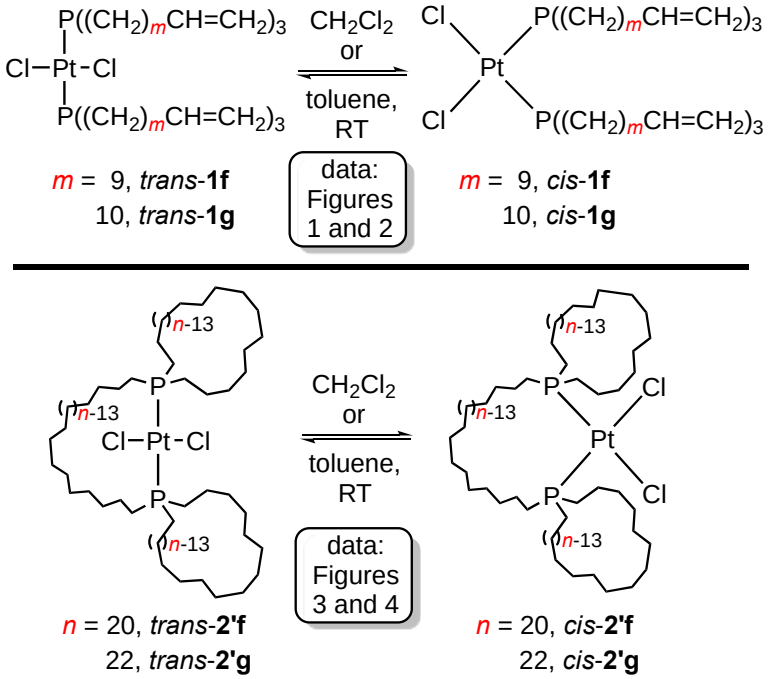

Scheme 3.6. Additional thermal isomerizations.

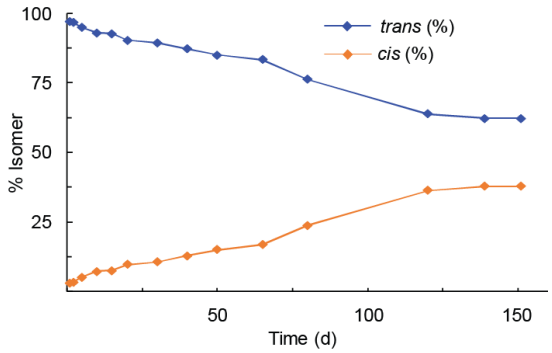

Figure 3.1. Isomerization of *trans*-**1f** (♦) to *cis*-**1f** (♦) in CH_2Cl_2 at RT (62:38 after 151 d).

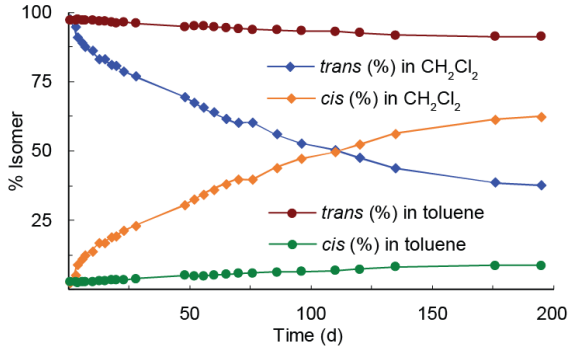

Figure 3.2. Isomerization of *trans*-**1g** (♦ or ●) to *cis*-**1g** (♦ or ●) in CH_2Cl_2 or toluene at RT (39:61 or 91:09 after 195 d).

Analogous experiments were conducted with CH_2Cl_2 and toluene solutions of *trans*-**2'f**,**g**. As shown in Scheme 3.6 (bottom) and Figures 3.3 and 3.4, 58-56% conversions to *cis*-**2'f**,**g** were observed in CH_2Cl_2, but only a 7% conversion to *cis*-**2'f** in toluene. When the last sample was kept at 100 °C for 2 d, no further reaction occurred. The toluene was replaced by *o*-$C_6H_4Cl_2$ and the sample kept at 150 °C for 2 d. Again, no further reaction occurred. Hence, toluene and *o*-$C_6H_4Cl_2$ are insufficiently polar to drive the equilibrium towards the *cis* isomers. These results are in line with gas phase DFT

calculations reported earlier.[8]

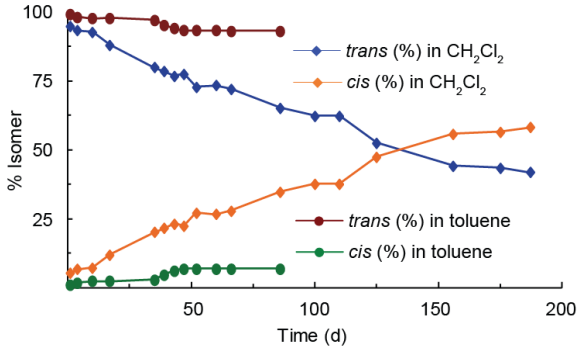

Figure 3.3. Isomerization of *trans*-**2'f** (♦ or ●) to *cis*-**2'f** (♦ or ●) in CH_2Cl_2 or toluene at RT (42:58 or 93:07 after 187 d or 86 d).

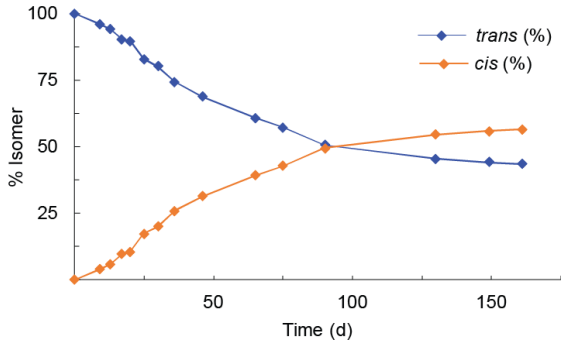

Figure 3.4. Isomerization of *trans*-**2'g** (♦) to *cis*-**2'g** (♦) in CH_2Cl_2 at RT (44:56 after 161 d).

3.2.3. Crystal Structures. In view of the potential for interesting structural features, efforts were made to crystallize all of the cyclic compounds in Schemes 3.4-3.6. Crystals of a THF solvate of gyroscope like *trans*-**2g**, and two complexes representing the alternative ring closing metathesis mode, *cis*-**2'f**,**g**, were grown as described in the experimental section. X-ray data were collected, and the structures solved, as summarized in Table 3.1 and the experimental section. The molecular structures are depicted in Figures

3.5 and 3.6. Key bond lengths and angles are given in Table 3.2.

Complex *trans*-**2g** represents the gyroscope like complex with the largest macrocycles (twenty five membered) that has been structurally characterized to date. The THF molecule is sandwiched between two macrocycles, as opposed to occupying the cavity of only one. The structure illustrates two limiting modes by which increasingly larger macrocycles can fill space. The left most macrocycle in either view can be considered "horizontally extended" with an "all anti" $(CH_2)_9$ segment emanating from each phosphorus atom (torsion angle range 180.0(4)° to 169.7(4)°); average 176.5°). The ninth methylene group then initiates a *gauche* C-C-C-C linkage (torsion angles 65.2(6)° and 60.6(6)°), several of which are necessary for closing any carbocyclic ring. The other macrocycles extend somewhat in the (vertical) direction of the P-Pt-P axis, as reflected by two Pt-P-C-C linkages with *anti* conformations (torsion angles 178.3(3)° and 179.2(3)°). This leads to particularly spacious macrocycle cavities, as seen in the space filling representation in the toc graphic.

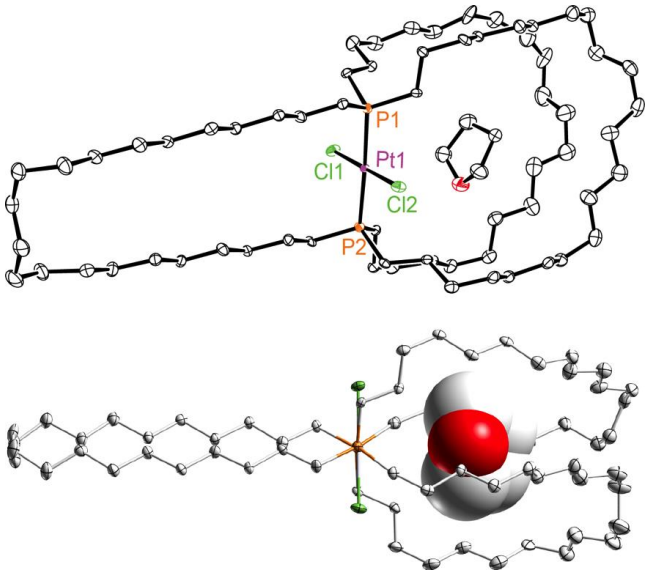

Figure 3.5. Thermal ellipsoid plot (50% probability) of *trans*-**2g·THF** (top) and view along P-Pt-P axis (bottom).

As is evident from Figure 3.6, *cis*-**2'f**,**g** adopt quite similar solid state conformations, with several homologous *gauche*/*anti* sequences. Furthermore, both crystallize in the space group $P2_1/c$ with $Z = 4$. Accordingly, the unit cell dimensions are similar, with the volume of the former slightly smaller (6246.7 vs. 6798.9 $Å^3$). The greatest difference is found in the lengths of the *a* axes (24.5316(12) vs. 26.533(3) Å), the directions of which nearly coincide with the long dimensions of the roughly elliptical macrocycles in Figure 3.6.

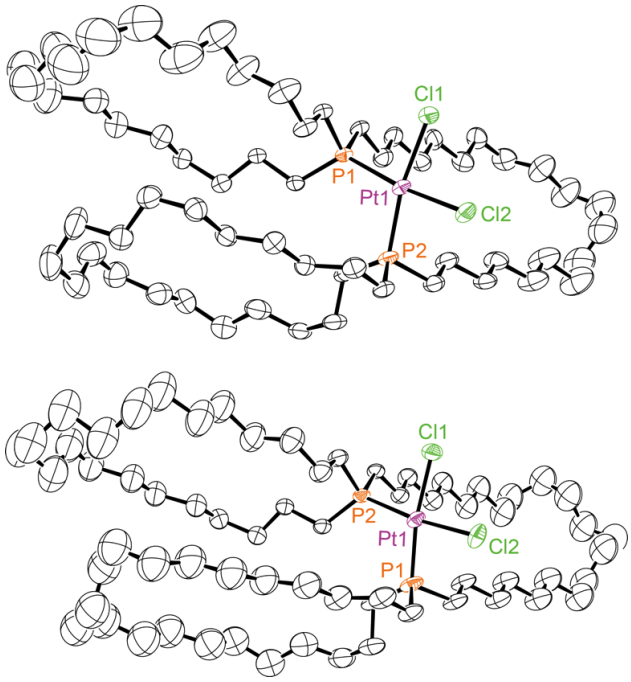

Figure 3.6. Thermal ellipsoid plots (50% probability) of *cis*-**2'f** (top) and *cis*-**2'g** (bottom).

The bond lengths and angles in Table 3.2 fall within standard ranges. However, the platinum-phosphorus bonds that are *trans* to phosphorus atoms are distinctly longer than those that are *trans* to chlorine atoms (2.3199(11)-2.3100(11) Å vs. 2.263(4)-

2.2468(15) Å), and the platinum-chlorine bonds that are *trans* to phosphorus atoms are distinctly longer than those that are *trans* to chlorine atoms (2.3717(16)-2.359(4) Å vs. 2.3125(11)-2.3099(11) Å). These trends follow logically from the *trans* influence, and are paralleled in other series of related complexes.[18]

3.3. Discussion

The results in Schemes 3.4 and 3.5 establish that an upper limit has not yet been reached with respect to macrocycle sizes in gyroscope like complexes accessed by three fold intramolecular alkene metatheses. Extensions beyond the thirty three membered rings in *trans*-**2k** would seemingly only require α,ω-haloalkene building blocks $X(CH_2)_mCH=CH_2$ with $m \geq 14$, for which viable synthetic routes exist.[19] This also augurs well for the availability of increasingly larger dibridgehead diphosphines of the type **3** (Scheme 3.3).

However, the initial formation of the parachute like complex *cis*-**2k** is a proverbial "elephant in the room" with respect to future extensions. On a positive note, there seems to be a beneficial effect upon yield relative to those of *trans*-**2f**,**g** in Scheme 3.4, and the subsequent thermal isomerization to *trans*-**2k** is spectroscopically quantitative. Importantly, the isomerizations of the model compounds in Scheme 3.6 and Figures 3.1-3.4 show that *cis* isomers are generally favored in CH_2Cl_2, the solvent for the metatheses and hydrogenations in Schemes 3.4 and 3.5. However, equilibrations require months at room temperature, and should not be appreciably accelerated under the reflux conditions of the metatheses.

The detection of some *cis* adducts among the crude metathesis products, as well as the apparent *trans*/*cis* isomerization of the educt **1k**, supports the possibility of a catalyzed isomerization. Indeed, the interconversion of *cis*/*trans* isomers of platinum(II) complexes is known to be catalyzed by both phosphines and anions,[20] either of which can be supplied

by Grubbs' first generation catalyst. This scenario poses the question as to why analogous phenomena are not seen with the reactions in Scheme 3.1, which in several cases were carefully scrutinized for *cis* products. Although it represents an extrapolation from only two points, the data for *trans*-**1f**,**g** (Figures 3.1 and 3.2) seem to indicate that in CH_2Cl_2, *trans*-**1** becomes progressively more favored as the methylene chains are shortened.

Grubbs' catalyst has often been applied in toluene,[21] and occasionally in haloarenes.[7,8,22] Thus, another test of the preceding interpretation would be to conduct analogous metatheses in these less polar solvents. This might enable a direct route from *trans*-**1k** to *trans*-**2k**. However, in preliminary experiments, the metathesis in Scheme 3.5 was much slower in toluene, even at higher catalyst loadings (conversion still incomplete after 7 d).

Another open question is whether it will prove possible, with increasing methylene chain lengths, to access additional types of isomers, such as the topologically novel species *trans*-**2"** in Scheme 3.1. As noted above, such chain crossing has now been documented in derivatives of dibridgehead diphosphines **3** that lack P-M-P linkages.[10,11] All that seemingly would be needed are methylene bridges that are sufficiently long to accommodate both a svelte Cl-Pt-Cl moiety and a methylene chain. Towards this end, the macrocycle size in *trans*-**2g** already seems adequate (see toc graphic).

However, there are additional considerations. On the reaction coordinate to gyroscope like complexes *trans*-**2**, the final ring closing step involves the bicyclic intermediate **I** with *syn* $(CH_2)_mCH{=}CH_2$ chains (Figure 3.7). In contrast, the final ring closing step en route to *trans*-**2"** requires the bicyclic intermediate **II**, with "mismatched" *anti* $(CH_2)_mCH{=}CH_2$ chains. This insight suggests a more sophisticated synthetic approach, inspired by an earlier synthesis of a related diphosphine complex **III** (n = 14) which features two *anti* pentafluorophenyl groups.[23] The optimum precursor to *trans*-**2"**

would be **IV**, in which the aryl groups of **III** have been replaced by $(CH_2)_mCH{=}CH_2$ moieties. A subsequent reaction with Grubbs' catalyst is certain to give oligomer, but some amount of *trans*-**2"** would (after hydrogenation) logically be anticipated. The challenge is to realize a viable route to **IV**, possibly from an analog of **III** with appropriate *anti* P-X groups.

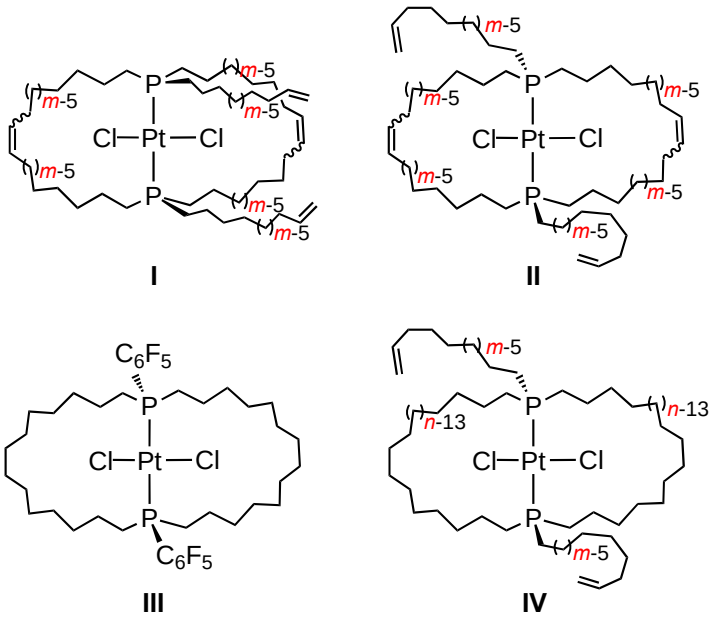

Figure 3.7. Additional relevant structures.

In summary, this study has greatly expanded the range of *m*/*n* dimensions available to the types of platinum complexes in Schemes 3.1 and 3.2. The new monophosphine ligands $P((CH_2)_mCH{=}CH_2)_3$ can also likely be applied to other metals and coordination geometries to yield numerous new gyroscope like complexes, with enhanced possibilities for topologically novel coproducts. These and related themes will be the subject of future studies from this laboratory.

3.4. Experimental Section

General. All reactions except hydrogenations were conducted under inert atmospheres using standard Schlenk techniques. Chemicals were treated as follows: hexanes, CH_2Cl_2, toluene, and THF, dried and degassed using a Glass Contour solvent purification system; *o*-$C_6H_4Cl_2$, distilled under reduced pressure and degassed; $CDCl_3$ (Cambridge Isotope Laboratories), magnesium turnings (Aldrich, 98%), anhydrous $PtCl_2$ (ABCR, 99.9%), PCl_3 (Merck, 99%), NH_4Cl (Mallinckrodt Chemicals, 99.9%), Grubbs' first generation catalyst ($(Cy_3P)_2RuCl_2$(=CHPh); Aldrich, 97%), PtO_2 (Aldrich, 99.9%), 16-bromo-1-hexadecene (Amadis Chemical, 95%), SiO_2 (Silicycle), and neutral Al_2O_3 (Macherey-Nagel), used as received.

NMR spectra were recorded on a Varian NMRS 500 MHz instrument at ambient probe temperatures and referenced as follows (δ, ppm): ^1H, residual internal $CHCl_3$ (7.26); $^{13}C\{^1H\}$, internal $CDCl_3$ (77.16); $^{31}P\{^1H\}$, external H_3PO_4 (0.00). IR spectra were recorded on a Shimadzu IRAffinity-1 spectrometer with a Pike MIRacle ATR system (diamond/ZnSe crystal). Melting points were recorded using a Stanford Research Systems MPA100 (OptiMelt) automated apparatus. Microanalyses were conducted by Atlantic Microlab, Inc.

$P((CH_2)_{10}CH=CH_2)_3$. A round bottom flask was charged with $Br(CH_2)_{10}CH=CH_2$ (5.014 g, 20.3 mmol)[24] and degassed (3 × freeze-pump-thaw). THF (25 mL) was added, the mixture was cooled to 0 °C, and magnesium turnings (0.984 g, 40.5 mmol) were added with stirring. After 1 h, the cooling bath was removed. The mixture was stirred overnight and then filtered (glass frit). The filtrate was cooled to 0 °C. A solution of PCl_3 (0.49 mL, 5.6 mmol) in THF (10 mL) was added dropwise via syringe over 5 min. After 1 h, the cooling bath was removed. The mixture was stirred overnight an again cooled to 0 °C. Aqueous NH_4Cl (20 mL) was added dropwise over 5 min. After

1 h, the cooling bath was removed. The mixture was stirred for 2 h and the colorless aqueous phase removed via syringe. The solvent was removed from the organic phase by rotary evaporation, and CH_2Cl_2 (10 mL) was added. The solution was filtered under a nitrogen atmosphere through a short pad of silica gel (5 × 3 cm), which was washed with CH_2Cl_2 (100 mL). The solvent was removed by oil pump vacuum to give $P((CH_2)_{10}CH{=}CH_2)_3$ (2.036 g, 3.82 mmol, 68%) as a greenish yellow oil.

NMR ($CDCl_3$, δ/ppm): **^{1}H** (500 MHz) 5.80 (ddt, 3H, $^3J_{HH\textit{trans}}$ = 17.0 Hz, $^3J_{HH\textit{cis}}$ = 10.1 Hz, $^3J_{HH}$ = 6.8 Hz, C*H*=), 4.98 (br d, 3H, $^3J_{HH\textit{trans}}$ = 17.1 Hz, $=CH_EH_Z$), 4.92 (br d, 3H, $^3J_{HH\textit{cis}}$ = 10.2 Hz, $=CH_EH_Z$), 2.07-1.99 (m, 6H, $CH_2CH{=}$), 1.45-1.21 (m, 54H, remaining CH_2); **^{13}C{^{1}H}**[25] (126 MHz) 139.0 (s, *C*H=), 114.0 (s, $=CH_2$), 33.8 (s, $CH_2CH{=}$), 31.4 (d, $^3J_{CP}$ = 10.6 Hz, $PCH_2CH_2CH_2$), 29.53 (s, CH_2), 29.48 (s, CH_2), 29.4 (s, CH_2), 29.3 (s, CH_2), 29.1 (s, CH_2), 28.9 (s, CH_2), 27.2 (d, $^2J_{CP}$ = 12.4 Hz, PCH_2CH_2), 25.8 (d, $^1J_{CP}$ = 12.6 Hz, PCH_2); **^{31}P{^{1}H}** (202 MHz) –31.0 (s).

$P((CH_2)_{14}CH{=}CH_2)_3$. THF (30 mL), $Br(CH_2)_{14}CH{=}CH_2$ (7.085 g, 23.3 mmol), magnesium turnings (1.162 g, 48.4 mmol), a solution of PCl_3 (0.56 mL, 6.46 mmol) in THF (10 mL), and aqueous NH_4Cl (20 mL) were combined in a procedure analogous to that given for $P((CH_2)_{10}CH{=}CH_2)_3$. An identical workup gave $P((CH_2)_{14}CH{=}CH_2)_3$ (2.090 g, 4.13 mmol, 64%) as a greenish yellow oil.

NMR ($CDCl_3$, δ/ppm): **^{1}H** (500 MHz) 5.83 (ddt, 3H, $^3J_{HH\textit{trans}}$ = 17.0 Hz, $^3J_{HH\textit{cis}}$ = 10.3 Hz, $^3J_{HH}$ = 6.7 Hz, C*H*=), 5.00 (br d, 3H, $^3J_{HH\textit{trans}}$ = 17.0 Hz, $=CH_EH_Z$), 4.94 (br d, 3H, $^3J_{HH\textit{cis}}$ = 10.8 Hz, $=CH_EH_Z$), 2.09-2.01 (m, 6H, $CH_2CH{=}$), 1.46-1.20 (m, 78H, remaining CH_2); **^{13}C{^{1}H}**[25] (126 MHz) 139.2 (s, *C*H=), 114.1 (s, $=CH_2$), 33.8 (s, $CH_2CH{=}$), 31.5 (d, $^3J_{CP}$ = 10.3 Hz, $PCH_2CH_2CH_2$), 29.70 (s, CH_2), 29.69 (s, 2 × CH_2), 29.64 (s, CH_2), 29.58 (s, CH_2), 29.5 (s, CH_2), 29.41 (s, CH_2), 29.37 (s, CH_2), 29.17 (s, CH_2), 29.0 (s, CH_2), 27.2 (d, $^2J_{CP}$ = 11.6 Hz, PCH_2CH_2), 25.9 (d, $^1J_{CP}$ = 12.6 Hz, PCH_2);

$^{31}P\{^{1}H\}$ (202 MHz) −25.7 (s).

***trans*-$PtCl_2(P((CH_2)_9CH{=}CH_2)_3)_2$** (*trans*-**1f**). A Schlenk flask was charged with $P((CH_2)_9CH{=}CH_2)_3$ (1.596 g, 3.25 mmol),[4] toluene (10 mL), and $PtCl_2$ (0.433 g, 1.63 mmol) with stirring. After 48 h, the mixture was concentrated to ca. 2 mL and placed at the top of a silica column (3.5 × 20 cm), which was eluted with hexanes/CH_2Cl_2 (90:10 to 80:20 v/v) and then CH_2Cl_2. The solvent was removed from the product fractions by oil pump vacuum to give *trans*-**1f** (0.821 g, 1.02 mmol, 63%) as a pale yellow oil. Anal. Calcd (%) for $C_{66}H_{126}Cl_2P_2Pt$ (1247.67): C, 63.54; H, 10.18; found C, 63.80; H, 10.34.

NMR ($CDCl_3$, δ/ppm): **^{1}H** (500 MHz) 5.80 (ddt, 6H, $^{3}J_{HH\mathit{trans}}$ = 17.0 Hz, $^{3}J_{HH\mathit{cis}}$= 10.2 Hz, $^{3}J_{HH}$ = 6.7 Hz, C*H*=), 4.99 (br d, 6H, $^{3}J_{HH\mathit{trans}}$= 17.1 Hz, $=CH_EH_Z$), 4.92 (br d, 6H, $^{3}J_{HH\mathit{cis}}$ = 10.3 Hz, $=CH_EH_Z$), 2.09-1.98 (m, 12H, $CH_2CH=$), 1.87-1.77 (br m, 12H, PCH_2), 1.60-1.51 (br m, 12H, PCH_2CH_2), 1.45-1.21 (m, 72H, remaining CH_2); **$^{13}C\{^{1}H\}$**[25] (126 MHz) 139.2 (s, *C*H=), 114.1 (s, $=CH_2$), 33.8 (s, $CH_2CH=$), 31.2 (virtual t,[27] $^{3}J_{CP}$ = 6.48 Hz, $PCH_2CH_2CH_2$), 29.5 (s, 2 × CH_2), 29.22 (s, CH_2), 29.15 (s, CH_2), 28.9 (s, CH_2), 23.7 (s, PCH_2CH_2), 20.4 (virtual t,[27] $^{1}J_{CP}$ = 16.3 Hz, PCH_2); **$^{31}P\{^{1}H\}$** (202 MHz) 5.09 (s, J_{PPt} = 2375 Hz[28]). **IR** (cm^{-1}, powder film): 2924 (s), 2855 (m), 1458 (m), 718 (m).

***trans*-$PtCl_2(P((CH_2)_{10}CH{=}CH_2)_3)_2$** (*trans*-**1g**). Toluene (10 mL), $P((CH_2)_{10}CH{=}CH_2)_3$ (1.529 g, 2.87 mmol), and $PtCl_2$ (0.382 g, 1.44 mmol) were combined in a procedure analogous to that for *trans*-**1f**. An identical workup gave *trans*-**1g** (1.186 g, 0.891 mmol, 62%) as a pale yellow oil. Anal. Calcd (%) for $C_{72}H_{138}Cl_2P_2Pt$ (1331.83): C, 64.93; H, 10.44; found C, 65.21; H, 10.54.

NMR ($CDCl_3$, δ/ppm): **^{1}H** (500 MHz) 5.79 (ddt, 6H, $^{3}J_{HH\mathit{trans}}$ = 17.0 Hz, $^{3}J_{HH\mathit{cis}}$ = 10.1 Hz, $^{3}J_{HH}$ = 6.67 Hz, C*H*=), 4.98 (br d, 6H, $^{3}J_{HH\mathit{trans}}$ = 17.1 Hz, $=CH_EH_Z$), 4.91 (br d, 6H, $^{3}J_{HH\mathit{cis}}$ = 10.3 Hz, $=CH_EH_Z$), 2.06-1.99 (m, 12H, $CH_2CH=$), 1.87-1.77 (br m,

12H, PCH_2), 1.59-1.50 (br m, 12H, PCH_2CH_2), 1.45-1.33 (m, 24H, 2 × CH_2), 1.32-1.20 (m, 60H, remaining CH_2); **^{13}C{^{1}H}**[25] (126 MHz) 139.1 (s, *C*H=), 114.1 (s, =*C*H_2), 33.8 (s, *C*H_2CH=), 31.2 (virtual t,[27] $^3J_{CP}$ = 6.5 Hz, PCH_2CH_2*C*H_2), 29.6 (s, *C*H_2), 29.5 (s, 2 × *C*H_2), 29.22 (s, *C*H_2), 29.17 (s, *C*H_2), 28.9 (s, *C*H_2), 23.6 (s, PCH_2*C*H_2), 20.4 (virtual t,[27] $^3J_{CP}$ = 16.1 Hz, P*C*H_2); **^{31}P{^{1}H}** (202 MHz) 4.69 (s, $^1J_{PPt}$ = 2382 Hz[28]). **IR** (cm^{-1}, powder film): 2924 (s), 2847 (m), 1458 (m), 718 (m).

***trans*-PtCl$_2$(P((CH$_2$)$_{14}$CH=CH$_2$)$_3$)$_2$** (*trans*-**1k**). Toluene (10 mL), P((CH_2)$_{14}$CH=CH_2)$_3$ (1.614 g, 2.30 mmol), and PtCl$_2$ (0.3061 g, 1.151 mmol) were combined in a procedure analogous to that for *trans*-**1f**. An identical workup gave *trans*-**1k** (0.941 g, 0.564 mmol, 49%) as a light yellow solid, mp (capillary) 57 °C. Anal. Calcd (%) for $C_{96}H_{186}Cl_2P_2Pt$ (1668.48): C, 69.11; H, 11.24; found C, 69.12; H, 11.41.

NMR ($CDCl_3$, δ/ppm): **^{1}H** (500 MHz) 5.82 (ddt, 6H, $^3J_{HH\textit{trans}}$ = 17.0 Hz, $^3J_{HH\textit{cis}}$ = 10.1 Hz, $^3J_{HH}$ = 6.6 Hz, C*H*=), 5.00 (br d, 6H, $^3J_{HH\textit{trans}}$ = 17.1 Hz, =CH$_E$*H*$_Z$), 4.93 (br d, 6H, $^3J_{HH\textit{cis}}$ = 10.9 Hz, =C*H*$_E$H$_Z$), 2.09-2.01 (m, 12H, C*H*$_2$CH=), 1.88-1.80 (m, 12H, PC*H*$_2$), 1.61-1.52 (m, 12H, PCH_2C*H*$_2$), 1.45-1.35 (m, 24H, C*H*$_2$), 1.34-1.20 (m, 108H, remaining C*H*$_2$); **^{13}C{^{1}H}**[25] (126 MHz) 139.2 (s, *C*H=), 114.1 (s, =*C*H_2), 33.8 (s, *C*H_2CH=), 31.2 (virtual t,[27] $^3J_{CP}$ = 6.5 Hz, PCH_2CH_2*C*H_2), 29.71 (s, 2 × *C*H_2), 29.74 (s, 2 × *C*H_2), 29.67 (s, *C*H_2), 29.58 (s, *C*H_2), 29.56 (s, *C*H_2), 29.3 (s, *C*H_2), 29.2 (s, *C*H_2), 27.0 (s, *C*H_2), 23.7 (s, PCH_2*C*H_2), 20.4 (virtual t,[27] $^1J_{CP}$ = 16.1 Hz, P*C*H_2); **^{31}P{^{1}H}** (202 MHz) 4.69 (s, J_{PPt} = 2379 Hz[28]). **IR** (cm^{-1}, powder film): 2916 (s), 2850 (m), 1465 (m), 911 (m), 717 (m).

***trans*-PtCl$_2$(P(CH$_2$)$_{20}$)$_3$P)** (*trans*-**2f**) and ***trans*-PtCl$_2$((H$_2$C)$_{20}$P((CH$_2$)$_{20}$)P(C-H$_2$)$_{20}$))** (*trans*-**2'f**). A Schlenk flask was charged with *trans*-**1f** (0.545 g, 0.437 mmol), Grubbs' first generation catalyst (0.0444 g, 0.054 mmol, 12.4 mol%), and CH_2Cl_2 (750 mL; the resulting solution is 0.00058 M in *trans*-**1f**), and fitted with a condenser. The

solution was refluxed with stirring (48 h). The solvent was removed by oil pump vacuum, and CH_2Cl_2 was added. The sample was passed through a short pad of neutral alumina, rinsing with CH_2Cl_2. A Fischer-Porter bottle was charged with the filtrate (reduced to 20 mL), PtO_2 (0.200 g, 0.022 mmol), and H_2 (5 bar). The mixture was kept at 50 °C (venting H_2 to maintain 5 bar) and stirred (48 h). The solvent was removed by oil pump vacuum. The residue was placed at the top of a silica column (3.5 × 26 cm), which was eluted with hexanes (1000 mL) and then hexanes/CH_2Cl_2 (10:1 to 6:1 v/v). The solvent was removed from the product fractions by rotary evaporation to give *trans*-**2f** (0.0175 g, 0.015 mmol, 3%) and *trans*-**2'f** (0.1263 g, 0.108 mmol, 25%) as a pale yellow waxy oils that solidified after 48-72 h.

Data for *trans*-**2f**. mp 47 ºC (capillary). Anal. Calcd (%) for $C_{60}H_{120}Cl_2P_2Pt$ (1169.55): C, 61.62; H, 10.34; found C, 61.40; H, 10.40.

NMR ($CDCl_3$, δ/ppm): **^{1}H** (500 MHz) 1.90-1.75 (m, 12H, PCH_2), 1.70-1.58 (m, 12H, PCH_2CH_2), 1.50-1.38 (m, 12H, $PCH_2CH_2CH_2$), 1.38-1.19 (m, 84H, remaining CH_2); **^{13}C{^{1}H}**[25] (126 MHz) 30.9 (virtual t,[27] $^3J_{CP}$ = 6.8 Hz, $PCH_2CH_2CH_2$), 28.9 (s, CH_2), 28.71 (s, CH_2), 28.66 (s, CH_2), 28.46 (s, CH_2), 28.45 (s, CH_2), 28.1 (s, CH_2), 28.0 (s, CH_2), 23.6 (s, PCH_2CH_2), 20.6 (virtual t,[27] $^1J_{CP}$ = 16.2 Hz, PCH_2); **^{31}P{^{1}H}** (202 MHz) 5.06 (s, $^1J_{PPt}$ = 2307 Hz[28]). **IR** (cm^{-1}, powder film): 2916 (s), 2847 (m), 1458 (m), 718 (m).

Data for *trans*-**2'f**. mp 66 ºC (capillary). Anal. Calcd (%) for $C_{60}H_{120}Cl_2P_2Pt$ (1169.55): C, 61.62; H, 10.34; found C, 61.89; H, 10.46.

NMR ($CDCl_3$, δ/ppm): **^{1}H** (500 MHz) 2.06-1.89 (m, 6H, PCH_2), 1.88-1.53 (m, 24H, $PCH_2CH_2CH_2$), 1.52-1.21 (m, 90H, remaining CH_2); **^{13}C{^{1}H}**[25] (126 MHz) 31.2 (virtual t,[27] $^3J_{CP}$ = 6.8 Hz, $PCH_2CH_2CH_2$), 30.7 (virtual t,[27] $^3J_{CP}$ = 6.3 Hz, $2PCH_2CH_2CH_2$), 29.24 (s, CH_2), 29.17 (s, CH_2), 28.9 (s, $2CH_2$), 28.8 (s, CH_2), 28.5 (s,

2 × 2CH_2), 28.3 (s, CH_2/ 2CH_2), 28.1 (s, 2CH_2), 28.01 (s, 2CH_2), 27.97 (s, CH_2), 27.6 (s, 2CH_2), 27.4 (s, CH_2), 27.3 (s, CH_2), 24.5 (s, PCH_2CH_2), 23.0 (s, $2PCH_2CH_2$), 22.2 (virtual t,[27] $^1J_{CP}$ = 16.4 Hz, PCH_2), 19.3 (virtual t,[27] $^1J_{CP}$ = 16.3 Hz, $2PCH_2$); **$^{31}P\{^1H\}$** (202 MHz) 4.93 (s, $^1J_{PPt}$ = 2375 Hz[28]). **IR** (cm^{-1}, powder film): 2916 (s), 2844 (m), 1459 (m), 716 (m).

***trans*-P$\overbrace{PtCl_2(P(CH_2)_{22})_3P}$)** (*trans*-**2g**) and ***trans*-P$\overbrace{PtCl_2((H_2C)_{22}P((CH_2)_{22})P(C-H_2)_{22})}$)** (*trans*-**2'g**). Grubbs' first generation catalyst (0.0427 g, 0.052 mmol, 12.4 mol%), *trans*-**1g** (0.557 g, 0.418 mmol), CH_2Cl_2 (750 mL; the resulting solution is 0.00056 M in *trans*-**1g**), PtO_2 (0.200 g, 0.022 mmol), and H_2 (5 bar) were combined in a procedure analogous to that given for *trans*-**2f** and *trans*-**2'f**. An identical workup gave *trans*-**2g** (0.1015 g, 0.081 mmol, 19%) and *trans*-**2'g** (0.0652 g, 0.052 mmol, 12%) as a pale yellow waxy oils that solidified after 48-72 h.

Data for *trans*-**2g**. mp 47 ºC (capillary). Anal. Calcd (%) for $C_{66}H_{132}Cl_2P_2Pt$ (1253.71): C, 63.23; H, 10.61; found C, 63.53; H, 10.77.

NMR ($CDCl_3$, δ/ppm): **^1H** (500 MHz) 1.88-1.80 (br m, 12H, PCH_2), 1.63-1.55 (br m, 12H, PCH_2CH_2), 1.45-1.39 (br m, 12H, $PCH_2CH_2CH_2$), 1.36-1.24 (br m, 96H, remaining CH_2); **$^{13}C\{^1H\}$**[25] (126 MHz) 31.1 (virtual t,[27] $^3J_{CP}$ = 6.6 Hz, $PCH_2CH_2CH_2$), 29.2 (s, CH_2), 29.0 (s, CH_2), 28.91 (s, CH_2), 28.88 (s, CH_2), 28.7 (s, CH_2), 28.4 (s, CH_2), 28.3 (s, CH_2), 28.1 (s, CH_2), 23.7 (s, PCH_2CH_2), 20.6 (virtual t,[27] $^1J_{CP}$ = 16.2 Hz, PCH_2); **$^{31}P\{^1H\}$** (202 MHz) 4.85 (s, $^1J_{PPt}$ = 2389 Hz[28]). **IR** (cm^{-1}, powder film): 2916 (s), 2847 (m), 1458 (m), 718 (m).

Data for *trans*-**2'g**. mp 53 ºC (capillary). Anal. Calcd (%) for $C_{66}H_{132}Cl_2P_2Pt$ (1253.71): C, 63.23; H, 10.61; found C, 63.46; H, 10.78.

NMR ($CDCl_3$, δ/ppm): **^1H** (500 MHz) 2.01-1.90 (m, 6H, PCH_2), 1.82-1.75 (m, 6H, PCH_2), 1.68-1.54 (m, 12H, PCH_2CH_2), 1.47-1.37 (m, 12H, $PCH_2CH_2CH_2$), 1.30-

1.22 (m, 96H, remaining CH_2); **^{13}C{^{1}H}**[25] (126 MHz) 31.2 (virtual t,[27] $^3J_{CP}$ = 6.76 Hz, $PCH_2CH_2CH_2$), 30.8 (virtual t,[27] $^3J_{CP}$ = 6.76 Hz, $2PCH_2CH_2CH_2$), 29.31 (s, CH_2), 29.25 (s, CH_2), 29.2 (s, CH_2), 29.1 (s, $2CH_2$), 28.91 (s, CH_2), 28.86 (s, $2CH_2$), 28.64 (s, 2 × $2CH_2$), 28.63 (s, $2CH_2$), 28.48 (s, CH_2), 28.45 (s, $2CH_2$), 28.1 (s, $2CH_2$), 28.0 (s, CH_2), 27.91 (s, CH_2), 27.88 (s, $2CH_2$), 27.5 (s, CH_2), 24.3 (s, PCH_2CH_2), 23.0 (s, $2PCH_2CH_2$), 22.0 (virtual t,[27] $^1J_{CP}$ = 16.6 Hz, PCH_2), 19.4 (virtual t,[27] $^1J_{CP}$ = 16.6 Hz, $2PCH_2$); **^{31}P{^{1}H}** (202 MHz) 4.85 (s, $^1J_{PPt}$ = 2369 Hz[28]). **IR** (cm^{-1}, powder film): 2916 (s), 2847 (m), 1458 (m), 718 (m).

***cis*-P$\overline{\text{tCl}_2(\text{P}(\text{CH}_2)_{30})_3\text{P}}$) (*cis*-2k).** Grubbs' first generation catalyst (0.0138 g, 0.017 mmol, 8.9 mol%), *trans*-**1k** (0.3125 g, 0.187 mmol), CH_2Cl_2 (600 mL; the resulting solution is 0.00031 M in *trans*-**1k**), PtO_2 (0.0164 g, 0.072 mmol), and H_2 (5 bar) were combined in a procedure analogous to that given for *trans*-**2f**. An identical workup gave *cis*-**2k** (0.1159 g, 0.073 mmol, 39%) as a white solid, mp (capillary) 153.6 °C. Anal. Calcd (%) for $C_{90}H_{180}Cl_2P_2Pt$ (1590.36): C, 67.97; H, 11.41; found C, 67.88; H, 11.53.

NMR ($CDCl_3$, δ/ppm): **^{1}H** (500 MHz) 2.05-2.91 (m, 12H, PCH_2), 1.60-1.50 (m, 12H, PCH_2CH_2), 1.46-1.37 (m, 12H, $PCH_2CH_2CH_2$), 1.34-1.21 (m, 144H, remaining CH_2); **^{13}C{^{1}H}**[25] (126 MHz) 31.2 (virtual t,[27] $^3J_{CP}$ = 7.1 Hz, 4C, $PCH_2CH_2CH_2$), 29.70 (s, CH_2), 29.65 (s, CH_2), 29.6 (s, 2 × CH_2), 29.5 (s, CH_2), 29.4 (s, CH_2), 29.3 (s, CH_2), 29.0 (s, CH_2), 28.8 (s, CH_2), 28.6 (s, CH_2), 28.4 (s, CH_2), 28.2 (s, CH_2), 24.8 (br s, PCH_2CH_2), 24.6 (br s, PCH_2); **^{31}P{^{1}H}** (202 MHz) 1.8 (s, $^1J_{PPt}$ = 3530 Hz[28]). **IR** (cm^{-1}, powder film): 2916 (s), 2850 (m), 1465 (m), 717 (m).

***trans*-P$\overline{\text{tCl}_2(\text{P}(\text{CH}_2)_{30})_3\text{P}}$) (*trans*-2k).** A Schlenk flask was charged with *cis*-**1k** (0.0685 g, 0.043 mmol) and *o*-$C_6H_4Cl_2$ (10 mL) and heated to 180 °C. The isomerization was monitored by $^{31}P\{^1H\}$ NMR. After 48 h, conversion was complete. The solvent was removed by oil pump vacuum. The residue was chromatographed (silica column, 3 × 20

cm, 6:1 v/v hexanes/CH_2Cl_2). The solvent was removed from the product fractions by rotary evaporation and oil pump vacuum to give *trans*-**2k** as a pale yellow waxy oil, which solidified after 24 h (0.0495 g, 0.031 mmol, 72%), mp (capillary) 46 °C. Anal. Calcd (%) for $C_{90}H_{180}Cl_2P_2Pt$ (1590.36): C, 67.97; H, 11.41; found C, 67.83; H, 11.58.

NMR ($CDCl_3$, δ/ppm): **^{1}H** (500 MHz) 1.89-1.80 (m, 12H, PCH_2), 1.62-1.53 (m, 12H, PCH_2CH_2), 1.46-1.39 (m, 12H, $PCH_2CH_2CH_2$), 1.36-1.23 (m, 144H, remaining CH_2); **^{13}C{^{1}H}**[25] (126 MHz) 31.2 (virtual t,[27] $^3J_{CP}$ = 6.8 Hz, $PCH_2CH_2CH_2$), 29.6 (s, 2 × CH_2), 29.54 (s, CH_2), 29.48 (s, CH_2), 29.34 (s, CH_2), 29.28 (s, CH_2), 29.2 (s, CH_2), 29.1 (s, CH_2), 29.0 (s, CH_2), 28.8 (s, CH_2), 28.72 (s, CH_2), 28.65 (s, CH_2), 23.7 (s, PCH_2CH_2), 20.5 (virtual t,[27] $^1J_{CP}$ = 16.2 Hz, PCH_2); **^{31}P{^{1}H}** (202 MHz) 4.73 (s, $^1J_{PPt}$ = 2364 Hz[28]). **IR** (cm^{-1}, powder film): 2916 (s), 2847 (m), 1458 (m), 718 (m).

Equilibration Experiments. The following are representative. **A** (Figure 3.2). An NMR tube was charged with *trans*-**1g** (0.0065 g, 0.0049 mmol) and CH_2Cl_2 (0.7 mL). $^{31}P\{^1H\}$ NMR spectra were periodically recorded (after 195 d, δ/ppm): 4.99 (s, $^1J_{PPt}$ = 2382 Hz,[28] *trans*-**1g**, 39%), 0.96 (s, $^1J_{PPt}$ = 3515 Hz,[28] *cis*-**1g**, 61%). **B** (Figure 3.2). An NMR tube was charged with *trans*-**1g** (0.0064 g, 0.0048 mmol) and toluene (0.7 mL). $^{31}P\{^1H\}$ NMR spectra were periodically recorded (after 195 d, δ/ppm): 5.21 (s, $^1J_{PPt}$ = 2385 Hz,[28] *trans*-**1g**, 91%), 1.18 (s, $^1J_{PPt}$ = 3518 Hz,[28] *cis*-**1g**, 9%). The tube was kept at 100 °C for 2 d. The sample was cooled and $^{31}P\{^1H\}$ NMR spectra were recorded (δ/ppm): 5.21 (s, $^1J_{PPt}$ = 2380 Hz,[28] *trans*-**1g**, 91%), 1.18 (s, $^1J_{PPt}$ = 3513 Hz,[28] *cis*-**1g**, 9%). **C** (Figure 3.3). An NMR tube was charged with *trans*-**2'f** (0.0059 g, 0.0050 mmol) and toluene (0.7 mL). $^{31}P\{^1H\}$ NMR spectra were periodically recorded (after 86 d, δ/ppm): 4.93 (s, $^1J_{PPt}$ = 2374 Hz,[28] *trans*-**2'f**, 93%), 1.33 (s, $^1J_{PPt}$ = 3515 Hz,[28] *cis*-**2'f**, 7%). The tube was kept at 100 °C for 2 d. The sample was cooled and $^{31}P\{^1H\}$ NMR spectra were recorded (δ/ppm): 5.20 (s, $^1J_{PPt}$ = 2380 Hz,[28] *trans*-**2'f**, 93%), 1.17 (s, $^1J_{PPt}$ = 3513 Hz,[28]

cis-**2'f**, 7%). The solvent was removed by rotary evaporation and *o*-$C_6H_4Cl_2$ (0.7 mL) was added. The tube was kept at 150 °C for 2 d. The sample was cooled and $^{31}P\{^1H\}$ NMR spectra was recorded (δ/ppm): 5.27 (s, $^1J_{PPt}$ = 2380 Hz,[28] *trans*-**2'f**, 93%), 1.33 (s, $^1J_{PPt}$ = 3514 Hz,[28] *cis*-**2'f**, 7%).

Crystallography. A. A THF solution of *trans*-**2g** was allowed to slowly concentrate. After 7 d, colorless blocks were obtained. Data were collected as outlined in Table B-1. Cell parameters were obtained from 45 frames using a 1° scan and refined with 164010 reflections. Integrated intensity information for each reflection was obtained by reduction of the data frames with the program APEX3.[29] Lorentz and polarization corrections were applied. Data were scaled, and absorption corrections were applied using the program SADABS.[30] The space group was determined from systematic reflection conditions and statistical tests. The structure was refined (weighted least squares refinement on F^2) to convergence,[31,32] which revealed a THF molecule for each *trans*-**2g** molecule. Olex2[32] was employed for the final data presentation. Non-hydrogen atoms were refined with anisotropic thermal parameters. Hydrogen atoms were fixed in idealized positions using a riding model. Some carbon atoms exhibited elongated thermal ellipsoids, suggesting disorder. For C57-C60, the disorder could be modeled between two positions (occupancy ratio of 61:39); appropriate restraints were used to keep the metrical parameters meaningful. The absence of additional symmetry or voids was confirmed using PLATON (ADDSYM).[33] **B**. A CH_2Cl_2 solution of *trans*-**2'f** was allowed to slowly concentrate. After 16 d, colorless thin plates were obtained. Data were collected (64049 reflections) and the structure was solved as in A. **C**. A THF solution of *trans*-**2'g** was allowed to slowly concentrate. After 15 d, colorless plates were obtained. Data were collected (123992 reflections) and the structure was solved as in A.

3.5. References

(1) (a) Khuong, T.-A. V.; Nuñez, J. E.; Godinez, C. E.; Garcia-Garibay, M. A. *Acc. Chem. Res.* **2006**, *39*, 413-422. (b) Nuñez, J. E.; Natarajan, A.; Khan, S. I.; Garcia-Garibay, M. A. *Org. Lett.* **2007**, *9*, 3559-3561. (c) Vogelsberg, C. S.; Garcia-Garibay, M. A. *Chem. Soc. Rev.* **2012**, *41*, 1892-1910. (d) Pérez-Estrada, S.; Rodríguez-Molina, B.; Xiao, L.; Santillan, R.; Jiménez-Osés, G.; Houk, K. N.; Garcia-Garibay, M. A. *J. Am. Chem. Soc*. **2015**, *137*, 2175-2178. (e) Acros-Ramos, R. Rodriguez-Molina, B.; Gonzalez-Rodriguez, E.; Ramirez-Montes, P. I.; Ochoa, M. E.; Santillan, R.; Farfán, N.; Garcia-Garibay, M. A. *RSC Adv.* **2015**, *5*, 55201-55208. (f) Jiang, X.; O'Brien, Z. J.; Yang, S.; Lai, L. H.; Buenaflor, J.; Tan, C.; Khan, S.; Houk, K. N.; Garcia-Garibay, M. A. *J. Am. Chem. Soc.* **2016**, *138*, 4650-4656. (g) Catalano, L.; Perez-Estrada, S.; Wang, H.-H.; Ayitou, A. J.-L.; Khan, S. I.; Terraneo, G.; Metrangolo, P.; Brown, S.; Garcia-Garibay, M. A. *J. Am. Chem. Soc.* **2017**, *139*, 843-848.

(2) (a) Setaka, W.; Yamaguchi, K. *J. Am. Chem. Soc.* **2013**, *135*, 14560-14563 and earlier work cited therein. (b) Setaka, W.; Inoue, K.; Higa, S.; Yoshigai, S.; Kono, H.; Yamaguchi, K. *J. Org. Chem.* **2014**, *79*, 8288-8295. (c) Setaka, W.; Higa, S.; Yamaguchi, K. *Org. Biomol. Chem.* **2014**, *12*, 3354-3357. (d) Shionari, H.; Inagaki, Y.; Yamaguchi, K.; Setaka, W. *Org. Biomol. Chem*. **2015**, *13*, 10511-10516. (e) Nishiyama, Y.; Inagaki, Y.; Yamguchi, K.; Setaka, W. *J. Org. Chem.* **2015**, *80*, 9959-9966. (f) Masuda, T.; Arase, J.; Inagaki, Y.; Kawahata, M.; Yamaguchi, K.; Ohhara, T.; Nakao, A.; Momma, H.; Kwon, E.; Setaka, W. *Cryst. Growth Des.* **2016** *16*, 4392-4401.

(3) Kottas, G. S.; Clarke, L. I.; Horinek, D.; Michl, J. *Chem. Rev.* **2005**, *105*, 1281-1376.

(4) Nawara-Hultzsch, A. J.; Skopek, K.; Shima, T.; Barbasiewicz, M.; Hess, G. D.; Skaper, D.; Gladysz, J. A. *Z. Naturforsch.* **2010**, *65b*, 414-424.

(5) (a) Nawara, A. J.; Shima, T.; Hampel, F.; Gladysz, J. A. *J. Am. Chem. Soc.* **2006**, *128*, 4962-4963. (b) Nawara-Hultzsch, A. J.; Stollenz, M.; Barbasiewicz, M.; Szafert, S.; Lis, T.; Hampel, F.; Bhuvanesh, N.; Gladysz, J. A. *Chem. Eur. J.* **2014**, *20*, 4617-4637.

(6) (a) Shima, T.; Hampel, F.; Gladysz, J. A. *Angew. Chem., Int. Ed.* **2004**, *43*, 5537-5540; *Angew. Chem.* **2004**, *116*, 5653-5656. (b) Lang, G. M.; Shima, T.; Wang, L.; Cluff, K. J.; Skopek, K.; Hampel, F.; Blümel, J.; Gladysz, J. A. *J. Am. Chem. Soc.* **2016**, *138*, 7649-7663. (c) Lang, G. M.; Skaper, D.; Hampel, F.; Gladysz, J. A. *Dalton Trans.* **2016**, *45*, 16190-16204.

(7) (a) Fiedler, T.; Bhuvanesh, N.; Hampel, F.; Reibenspies, J. H.; Gladysz, J. A. *Dalton Trans.* **2016**, *45*, 7131-7147. (b) Hess, G. D.; Fiedler, T.; Hampel, F.; Gladysz, J. A. *Inorg. Chem*. **2017**, 56, 7454-7469.

(8) Joshi, H.; Kharel, S.; Ehnbom, A.; Skopek, K.; Hess, G. D.; Fiedler, T.; Hampel, F.; Bhuvanesh, N.; Gladysz, J. A. *J. Am. Chem. Soc.* **2018**, *140*, in press. DOI: 10.1021/jacs.8b02846.

(9) See also Steigleder, E.; Shima, T.; Lang, G. M.; Ehnbom, A.; Hampel, F.; Gladysz, J. A. *Organometallics* **2017**, *36*, 2891-2901.

(10) Stollenz, M.; Taher, D.; Bhuvanesh, N.; Reibenspies, J. H.; Baranová, Z.; Gladysz, J. A. *Chem. Commun.* **2015**, *51*, 16053-16056.

(11) Kharel, S.; Jia, T.; Bhuvanesh, N.; Reibenspies, J. H.; Blümel, J.; Gladysz, J. A. C*hem. Asian J.* **2018**, accepted.

(12) Hartley, F. R. *Organometal. Chem. Rev. A.* **1970**, *6*, 119-137.

(13) Stollenz, M.; Barbasiewicz, M.; Nawara-Hultzsch, A. J.; Fiedler, T.; Laddusaw, R. M.; Bhuvanesh, N.; Gladysz, J. A. *Angew. Chem., Int. Ed*. **2011**, *50*, 6647-6651; *Angew. Chem.* **2011**, *123*, 6777-6781.

(14) See also Estrada, A. L.; Jia, T.; Bhuvanesh, N.; Blümel, J.; Gladysz, J. A. *Eur. J. Inorg. Chem.* **2015**, *2015*, 5318-5321.

(15) Kharel, S.; Joshi, H.; Bierschenk, S.; Stollenz, M.; Taher, D.; Bhuvanesh, N.; Gladysz, J. A. *J. Am. Chem. Soc.* **2017**, *139*, 2172-2175.

(16) Grim, S. O.; Keiter, R. L.; McFarlane, W. *Inorg. Chem.* **1967**, *6*, 1133-1137.

(17) Relevant $^{31}P\{^{1}H\}$ NMR data ($CDCl_3$) for isolated complexes from this work and reference 8 are as follows: *trans*/*cis*-**1f**, 5.1/0.97; *trans*/*cis*-**1g**, 4.7/0.92; *trans*-**1k**, 4.7; *trans*/*cis*-**2f**, 5.1/2.8; *trans*/*cis*-**2g**, 4.9/2.3; *trans*/*cis*-**2k**, 4.7/1.8.

(18) (a) Rigamonti, L.; Forni, A. Manassero, M.; Manassero, C.; Pasini, A. *Inorg. Chem.* **2010**, *49*, 123-135, and earlier work cited therein. (b) For analogous bond length trends in a complex with both *cis* and *trans* $PtCl_2(PArMe_2)_2$ units, see Table 1 of Drahoš, B.; Rohlik, Z.; Kotek, J.; Císařová, I.; Hermann, P. *Dalton Trans.* **2009**, *48*, 4942-4953.

(19) (a) Balachander, N.; Sukenik, C. N. *Langmuir* **1990**, *6*, 1621-1627. (b) Effenberger, F.; Heid, S. *Synthesis* **1995**, 1126-1130.

(20) (a) Louw, W. J. *Inorg. Chem.* **1977**, *16*, 2147-2160. (b) Cooper, M. K.; Downes, J. M. *Inorg. Chem.* **1978**, *17*, 880-884. (c) Anderson, G. K.; Cross, R. J. *Chem. Soc. Rev.* **1980**, *9*, 185-215.

(21) Sanford, M. S.; Love, J. A.; Grubbs, R. H. *J. Am. Chem. Soc.* **2001**, *123*, 6543-6554.

(22) (a) Marvey, B. B.; Segakweng, C. K.; Vosloo, M. H. C. *Int. J. Mol. Sci*. **2008**, *9*, 615-625. (b) Martinez, A.; Gutiérrez, S.; Tienkopatchev, M. A. *Nat. Sci.* **2013**, *5*, 857-864 (DOI: org./10.4236/ns.2013.57103).

(23) Shima, T.; Bauer, E. B.; Hampel, F.; Gladysz, J. A. *Dalton Trans*. **2004**, *33*, 1012-1028.

(24) Roux, M.-C.; Paugam, R.; Rousseau, G. *J. Org. Chem.* **2001**, *66*, 4304-4310.

(25) The P$CH_2CH_2CH_2$ ^{1}H and ^{13}C NMR signal assignments of the free phosphines were confirmed by ^{1}H,^{1}H COSY and ^{1}H,^{13}C{^{1}H} COSY experiments. The corresponding signals in the platinum complexes were assigned by analogy to those of closely related complexes reported earlier.[5b] Representative 2D NMR spectra that provide the basis for these assignments have been published.[7a,26]

(26) Lang, G. M.; Skaper, D.; Shima, T.; Otto, M.; Wang, L.; Gladysz, J. A. *Aust. J. Chem.* **2015**, *68*, 1342-1351.

(27) The *J* values given for virtual triplets represent the *apparent* couplings between adjacent peaks, and not the mathematically rigorously coupling constants. See Hersh, W. H. *J. Chem. Educ.* **1997**, *74*, 1485-1488.

(28) This coupling represents a satellite (d, ^{195}Pt = 33.8%), and is not reflected in the peak multiplicity given.

(29) *APEX3*, Bruker AXS Inc., Madison, WI, USA, 2012.

(30) Sheldrick, G. M. *SADABS*, Bruker AXS Inc., Madison, WI, USA, 2001.

(31) (a) Sheldrick, G. M. *Acta Cryst.* **2008**, *A64*, 112-122. (b) Sheldrick, G. M. *Acta Cryst.* **2015**, *A71*, 3-8. (c) Sheldrick, G. M. *Acta Cryst.* **2015**, *C71*, 3-8.

(32) Dolomanov, O. V.; Bourhis, L. J.; Gildea, R. J.; Howard, J. A. K.; Puschmann, H. *J. Appl. Cryst.* **2009***, 42*, 339-341.

(33) Spek, A. L. *J. Appl. Cryst.* **2003**, *36*, 7-13.

Table 3.1. Summary of crystallographic data for *trans*-**2g**·THF, *cis*-**2'f**,**2'g**.

	trans-**2g**·THF	*cis*-**2'f**	*cis*-**2'g**
empirical formula	$C_{70}H_{140}Cl_2OP_2Pt$	$C_{60}H_{120}Cl_2P_2Pt$	$C_{66}H_{132}Cl_2P_2Pt$
formula weight	1325.74	1169.48	1253.64
temperature [K]	100	100	100
diffractometer	Bruker Quest X-ray	Bruker Venture X-ray	Bruker Venture X-ray
wavelength [Å]	0.71073	1.54178	1.54178
crystal system	monoclinic	monoclinic	monoclinic
space group	*C*2/*c*	$P2_1/c$	$P2_1/c$
unit cell dimensions:			
a [Å]	31.5078(19)	24.5316(12)	26.553(3)
b [Å]	9.1437(5)	14.6896(7)	14.4341(19)
c [Å]	50.793(3)	18.6506(8)	18.775(2)
α [°]	90	90	90
β [°]	98.675(4)	111.651(2)	109.127(6)
γ [°]	90	90	90
V [Å^3]	14466.1(14)	6246.7(5)	6798.9(14)
Z	8	4	4
ρ_{calc} [Mg/m^3]	1.217	1.244	1.225
μ [mm^{-1}]	2.096	5.706	5.275
F(000)	5680	2488	2680
crystal size [mm^3]	0.446 × 0.314 × 0.165	0.875 × 0.38 × 0.038	0.408 × 0.186 × 0.036
Θ limit [°]	2.321 to 23.990	3.579 to 70.270	3.523 to 65.380
index range (*h*, *k*, *l*)	−35, 35; −10, 10; −57, 57	−29, 26; −17, 17; −22, 22	−31, 31; −16, 16; −22, 22
reflections collected	164010	64049	123992
independent reflections	11239	11722	11189
R(int)	0.0569	0.0657	0.0915
completeness to θ	99 (23.990)	98.8 (67.679)	95.9(65.380)
max. and min. transmission	0.3299 and 0.2060	0.2833 and 0.0441	0.4433 and 0.2394
data/restraints/parameters	11239/149/722	11722/299/586	11189/1059/640
goodness-of-fit on F^2	1.243	1.090	1.264
R indices (final) [$I > 2\sigma(I)$]			
R_1	0.0389	0.0600	0.1265
wR_1	0.0701	0.1295	0.2770

Table 3.1 continued.

	trans-**2g**·THF	*cis*-**2'f**	*cis*-**2'g**
R indices (all data)			
R_2	0.0466	0.0766	0.1521
wR_2	0.0721	0.1431	0.2918
largest diff. peak and hole [eÅ^{-3}]	0.835 and −1.538	2.145 and −1.295	3.639 and −2.450

Table 3.2. Key crystallographic bond lengths [Å] and angles [°] for *trans*-**2g**·THF, *cis*-**2'f**,**2'g**.

	trans-**2g**·THF	*cis*-**2'f**	*cis*-**2'g**
Pt-P	2.3100(11)	2.2576(15)	2.251(4)
	2.3199(11)	2.2468(15)	2.263(4)
Pt-Cl	2.3099(11)	2.3717(16)	2.367(4)
	2.3125(11)	2.3590(16)	2.359(4)
P-Pt-P	177.06(4)	103.90(6)	104.35(14)
P-Pt-Cl	93.97(4)	84.93(6)	83.59(16)
	86.29(4)	84.16(6)	84.31(13)
	85.91(4)	171.62(6)	170.67(15)
	93.86(4)	169.94(6)	172.03(14)
Cl-Pt-Cl	179.59(5)	87.25(6)	87.81(15)

4. HOMEOMORPHIC ISOMERIZATION AS A DESIGN ELEMENT IN CONTAINER MOLECULES; BINDING, DISPLACEMENT, AND SELECTIVE TRANSPORT OF MCl_2 SPECIES (M = Pt, Pd, Ni)*

4.1. Introduction

A variety of types of "container molecules" have been developed.[1] By definition, they are capable of encapsulating suitable guest molecules, often with objectives such as sequestration or transport/release.[1f] The nature of the container/guest interaction can vary widely, ranging from modest van der Waals forces[1a-e,j] to much stronger covalent bonds.[1h] One means of acquiring transport data involves triphasic U-tube experiments, as illustrated in Figure 4.1.[2] The container molecule is commonly localized in a lower liquid phase, and the guest molecule equilibrates from an orthogonal liquid phase in one arm to the same phase in the other.

We have described the syntheses and a limited range of reactions of the *in*/*out* isomers of the dibridgehead diphosphine $P((CH_2)_{14})_3P$ (**1**),[3,4] which feature thirty-membered macrocycles. These molecules have a fascinating ability to turn themselves inside out, which has been termed homeomorphism.[5] As shown in Scheme 4.1, this rapidly interconverts *in*,*in*-**1** (more stable) and *out*,*out*-**1** (less stable). Phosphorus inversion, which would initially give *in*,*out*-**1**, only occurs at much higher temperatures.

Since the lone pairs are directed in an *exo* sense in *out*,*out*-**1**, and an *endo* sense in *in*,*in*-**1**, we thought that such diphosphines might be used to scavenge suitable Lewis acids and possibly transport them as payloads to an orthogonal phase. Hence, a proof of principle was sought. Accordingly, in this section, we report that CH_2Cl_2 solutions of *in*-

*Reproduced with permission from Kharel, S.; Joshi, H.; Bierschenk, S.; Stollenz, M.; Taher, D.; Bhuvanesh, N.; Gladysz, J. A. *J. Am. Chem. Soc.* **2017**, *139*, 2172-2175.

-,*in/out,out*-**1** can transport MCl_2 fragments between aqueous phases in U-tubes, and with appreciable selectivities ($PdCl_2$ > $PtCl_2$).

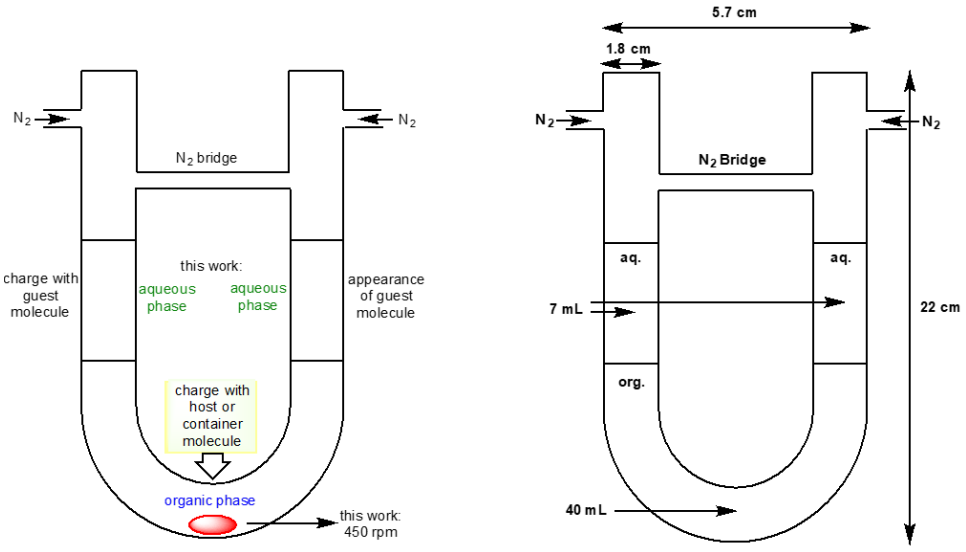

Figure 4.1. U-tube apparatus commonly used to assay guest transport in host/guest chemistry (left), metrical parameters of the apparatus used in this work (right).

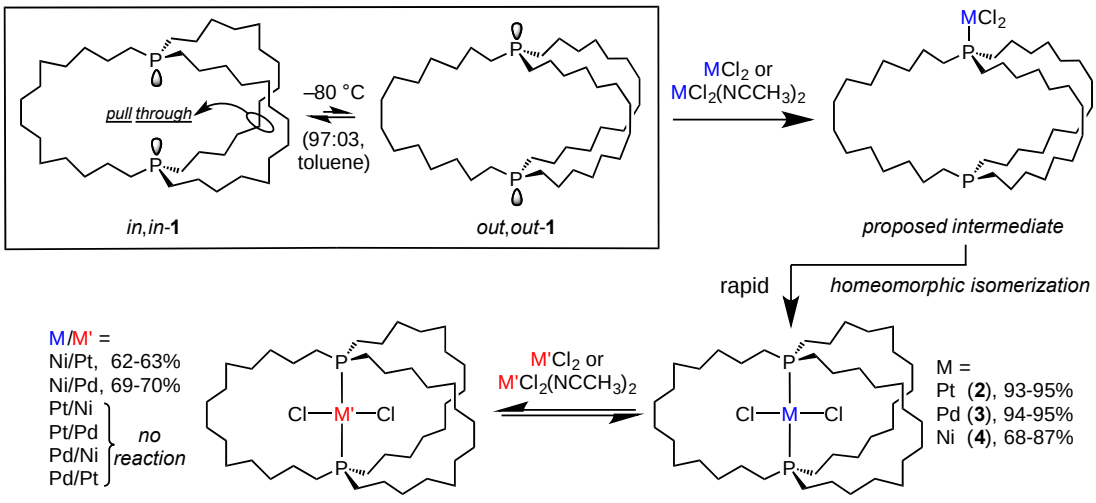

Scheme 4.1. Dibridgehead diphosphine **1**: *in*,*in* and *out*,*out* isomers and proposed mode of MCl_2 binding.

4.2. Results and Discussion

In an initial set of experiments, basic binding properties of *in*,*in*/*out*,*out*-**1** were established. As shown in Scheme 4.1, CH_2Cl_2 solutions were treated with $PtCl_2$, $PdCl_2$, or $NiCl_2$ (all insoluble in CH_2Cl_2). Workups gave the corresponding 1:1 adducts *trans*-$\overline{MCl_2(P((CH_2)_{14})_3P)}$ (M = Pt/**2**, Pd/**3**, Ni/**4**) in 93%, 94%, and 68% yields, respectively. The generation of **2** by this route has already been reported.[6] In the case of **3**, this represents a new synthesis of an independently prepared complex.[6] In the case of **4**, this represents a new complex. High yields of **2**-**4** were also obtained when the soluble complexes $MCl_2(NCCH_3)_2$ were used in place of MCl_2. All of these adducts gave distinct ^{31}P NMR chemical shifts, and the new complex **4** was fully characterized as described in the Supporting Information (SI). The crystal structure was also determined. As shown in Figure 4.2, the "filled container" has a roughly ovoid shape.

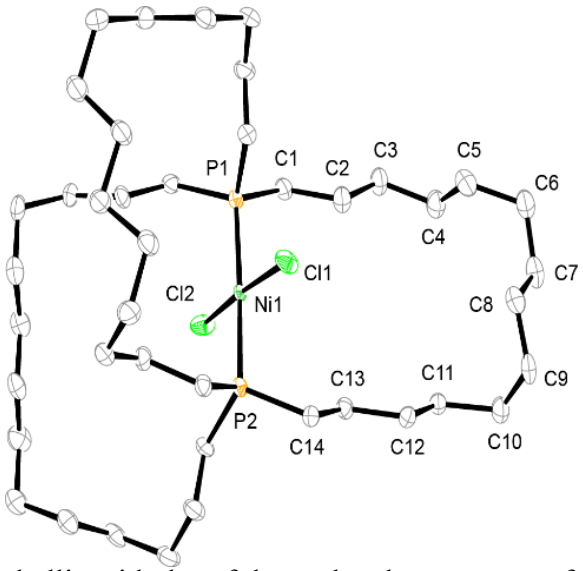

Figure 4.2. Thermal ellipsoid plot of the molecular structure of **4** (50% probability level).

To set the stage for transport experiments, equilibrations involving the MCl_2 moieties were attempted. First, the nickel complex **4** was treated either with $PtCl_2$ or $PdCl_2$ (1.2 equiv, CH_2Cl_2, heterogeneous, 5 d), or $PtCl_2(NCCH_3)_2$ or $PdCl_2(NCCH_3)_2$ (1.2 equiv, THF, homogeneous, 2 d). Workups gave the platinum and palladium complexes **2** and **3** in 62-63% and 69-70% yields, respectively. Analogous experiments were conducted with all other possible combinations of nickel, palladium, and platinum reactants. However, the $PtCl_2$ and $PdCl_2$ moieties in **2** and **3** could not be replaced by any other MCl_2 source. Identical results were obtained when $PdCl_2/PtCl_2$ exchange was attempted in CH_3CN at 70 °C (6 d). Hence, the binding enthalpy of $NiCl_2$ to *in*,*in*-**1** is lower than those of $PdCl_2$ or $PtCl_2$, but the relative affinities of the last two fragments remain unknown.

Next, attention was turned to the U-tube experiments represented in Figure 4.3. Thus, 0.246 mmol of *in,in*/*out,out*-**1** was dissolved in CH_2Cl_2 (40 mL), and 0.361 mmol of a $PtCl_2$ source, K_2PtCl_4, was dissolved in water (7.0 mL). The former solution was added to the U-tube (bottom), and the latter was added to the charging arm. The receiving arm was loaded with an aqueous solution of KCl (3.68 mmol in 7.0 mL) to regenerate K_2PtCl_4 from the transported $PtCl_2$. Since this represents only a five-fold excess above the 0.722 mmol needed for complete conversion and a 50:50 equilibrium distribution, there is only a modest "driving force" for transport. Furthermore, the *in*,*in*/*out*,*out*-**1** would be expected to retain an equilibrium quantity of $PtCl_2$ in the CH_2Cl_2 phase.

The CH_2Cl_2 phase was stirred (450 rpm, all experiments) and the slow disappearance/appearance of the K_2PtCl_4 in the charging/receiving arms was monitored by UV-visible spectroscopy. As shown in Figure 4.4 (top), after one day there was a drop of concentration in the charging arm roughly equal to the amount of *in*,*in*/*out*,*out*-**1** in the CH_2Cl_2 phase. This suggested the saturation of the host molecules with $PtCl_2$ to give **2**.

Subsequently, slow $PtCl_2$ transport to the receiving arm began, with equal concentrations of K_2PtCl_4 realized after 8-11 days. However, the low values suggested that the *in,in*/*out,out*-**1** remained saturated with $PtCl_2$ in the CH_2Cl_2 phase.

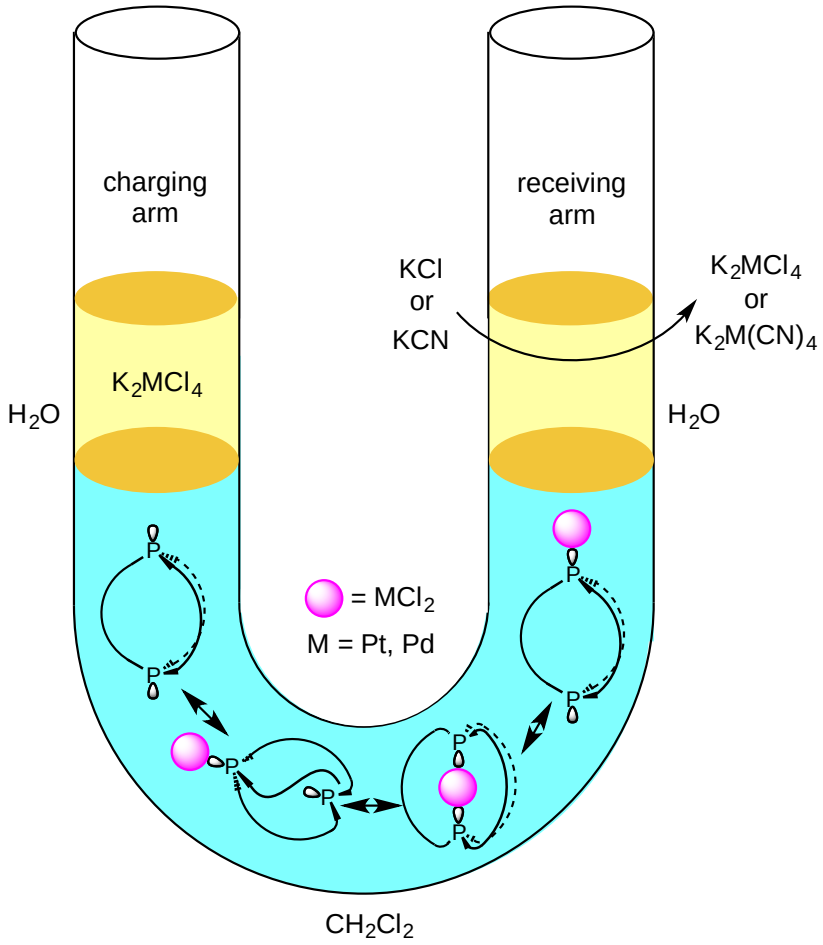

Figure 4.3. Transport of MCl_2 from aqueous K_2MCl_2 to aqueous KCl or KCN via CH_2Cl_2 solutions of *in*,*in*/*out*,*out*-**1.**

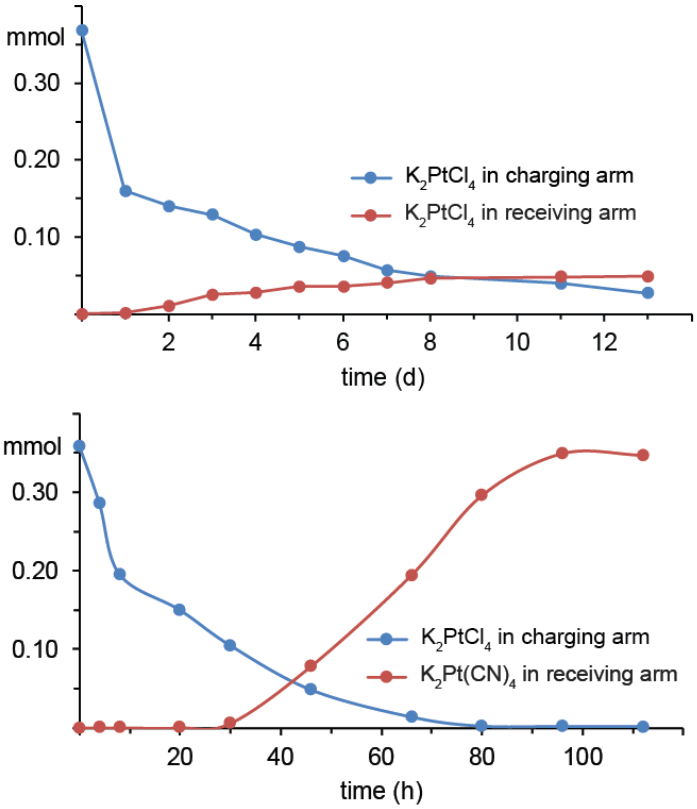

Figure 4.4. Data for Figure 4.3. Top: disappearance of K_2PtCl_4 from the charging arm (•; 0.361 mmol) and appearance of K_2PtCl_4 in the receiving arm (•; 3.68 mmol KCl) using *in*,*in*/*out*,*out*-**1** (0.246 mmol) in the CH_2Cl_2 phase. Bottom: disappearance of K_2PtCl_4 from the charging arm (•; 0.357 mmol) and appearance of $K_2Pt(CN)_4$ in the receiving arm (•; 3.59 mmol KCN) using *in*,*in*/*out*,*out*-**1** (0.245 mmol) in the CH_2Cl_2 phase.

To support this hypothesis, an aqueous solution of K_2PtCl_4 (0.150 mmol in 3.5 mL) was layered onto a CH_2Cl_2 solution of *in*,*in*/*out*,*out*-**1** (0.101 mmol in 20 mL) in an "I tube" (see Figure 4.5). As can be seen in Figure 4.6, the K_2PtCl_4 concentration decreased on the same time scale as in the transport experiment in Figure 4.4. The data indicate that after 1 and 7 d, >76% and >99% of the *in*,*in*/ *out*,*out*-**1** has been converted to **2**, as verified by ^{31}P NMR spectra of aliquots. The expected amount of K_2PtCl_4 (0.049 mmol) remained in the aqueous phase.

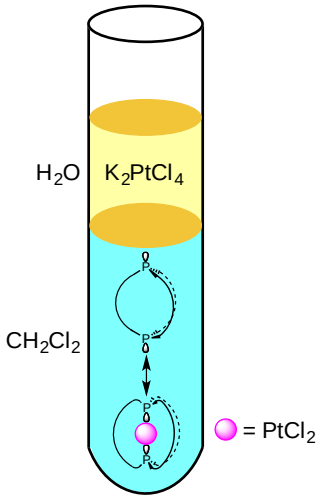

Figure 4.5. I-tube experiment for probing biphasic equilibria.

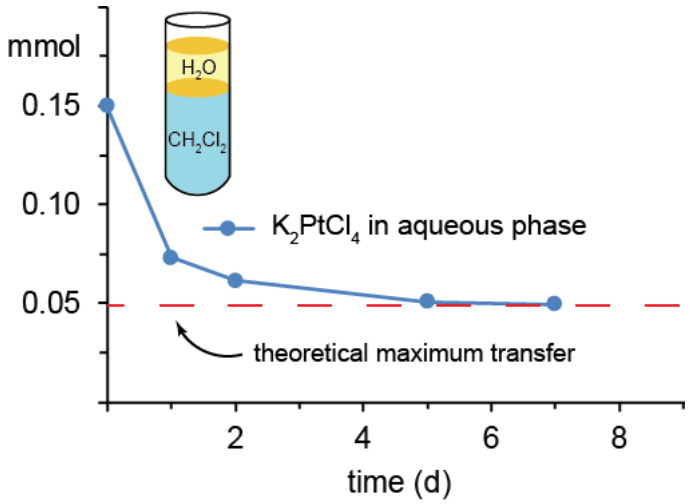

Figure 4.6. Equilibration of $PtCl_2$ between an aqueous solution of K_2PtCl_4 (•; 0.150 mmol, 3.5 mL) and a CH_2Cl_2 solution of *in*,*in*/*out*,*out*-**1** (0.101 mmol, 20 mL) in an "I-tube".

The slow time scale in Figure 4.4 (top) is typical of U-tube experiments.[2] Nonetheless, in the interest of accelerating $PtCl_2$ transport, a stronger driving force was sought. When K_2PtCl_4 and KCN (4.0 equiv) are combined in water, complete conversion to the tetracyanide complex $K_2Pt(CN)_4$ rapidly occurs.[7] The formation constants (log ß$_4$,

$ß_4$ = $[MX_4^{2-}]/[M][X^-]^4$: $PtCl_4^{2-}$, 16; $PtCN_4^{2-}$, 41)[8] indicate a much higher thermodynamic stability for the latter. Thus, the preceding experiment was repeated, but with the receiving arm charged with an aqueous KCN solution (3.59 mmol in 7.0 mL). As shown in Figure 4.4 (bottom), over 24 h there was a similar drop in concentration of K_2PtCl_4 in the charging arm. But now transport was faster, with an equal concentration of platinum in the two arms after 43 h. With additional time, all of the platinum was carried from the charging to the receiving arm. No color or detectable amount of **2** (^{31}P NMR) remained in the CH_2Cl_2 phase.

Next, experiments analogous to those in Figure 4.4 were conducted with the palladium salt K_2PdCl_4 in the charging arm. Although minor differences were evident, transport rates were very close to those obtained with K_2PtCl_4, both with KCl and KCN in the receiving arm (Figure 4.7). However, similar experiments with K_2NiCl_4[9] did not give any $NiCl_2$ transport, even though the viability of the required intermediate **4** has been unambiguously demonstrated (Scheme 4.1, Figure 4.2). The reason appears to involve the facile aquation of $NiCl_2$ to give the very stable blue complex $NiCl_2{\cdot}6H_2O$ (*trans*-$NiCl_2(H_2O)_4{\cdot}2H_2O$).[10]

We wondered whether *in,in*/*out,out*-**1** might be able to selectively transport one of several MCl_2 species. Thus, the experiments in Figures 4.4 and 4.6 were repeated, but with 50:50 K_2PtCl_4/ K_2PdCl_4 mixtures. That conducted with KCN in the receiving arm gave the more striking results, and is presented in Figure 4.8 (see Figure 4.9 for that with KCl in the receiving arm). After an initial drop in both the K_2PdCl_4 and K_2PtCl_4 concentrations in the charging arm (10 h), the former was much more rapidly consumed, reaching parity with $K_2Pd(CN)_4$ in the receiving arm after 50 h (0.015 mmol) and drop-

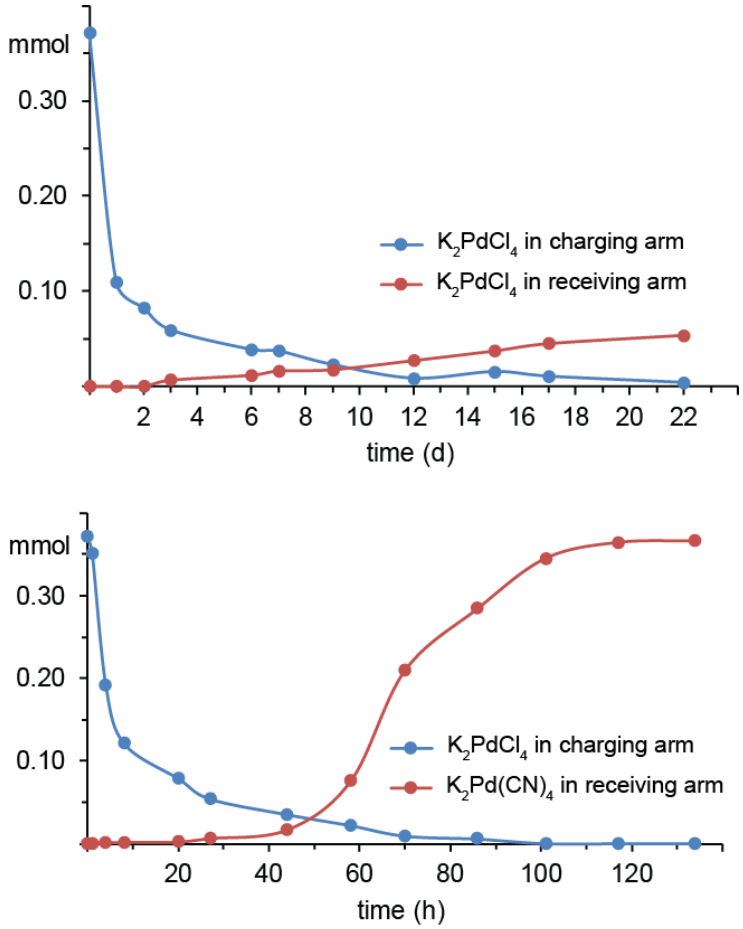

Figure 4.7. Additional data for Figure 4.3. Top: disappearance of K_2PdCl_4 from the charging arm (•; 0.371 mmol) and appearance of K_2PdCl_4 in the receiving arm (•; 3.66 mmol KCl) using *in*,*in*/*out*,*out*-**1** (0.244 mmol) in the CH_2Cl_2 phase. Bottom: disappearance of K_2PdCl_4 from the charging arm (•; 0.371 mmol) and appearance of $K_2Pd(CN)_4$ in the receiving arm (•; 3.70 mmol KCN) using *in*,*in*/*out*,*out*-**1** (0.244 mmol) in the CH_2Cl_2 phase.

-ping to <0.003 mmol after 120 h. In contrast, appreciable amounts of K_2PtCl_4 remained in the charging arm after 50-120 h (0.069-0.020 mmol). These trends were mirrored by the $K_2Pd(CN)_4$ and $K_2Pt(CN)_4$ quantities in the receiving arm, with the former greatly dominating at 75-150 h (0.054-0.158 mmol). At 254 h, nearly all of the K_2PdCl_4 and K_2-$PtCl_4$ had been transferred to the receiving arm (98% and 96%). Thus, $PdCl_2$ transport is

favored kinetically, in line with the rate trends observed for many substitution reactions.[11]

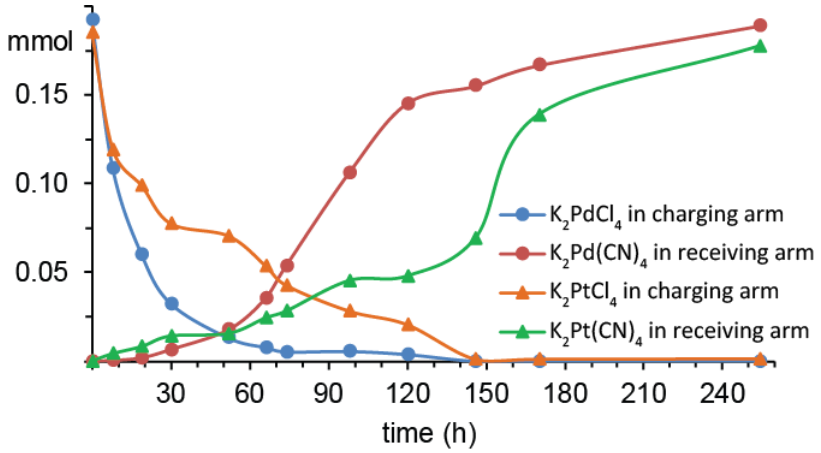

Figure 4.8. Additional data for Figure 4.3. Disappearance of K_2PtCl_4 (▲, 0.185 mmol) and K_2PdCl_4 (•, 0.192 mmol) from the charging arm and appearance of $K_2Pt(CN)_4$ (▲) and $K_2Pd(CN)_4$ (•) in the receiving arm (3.67 mmol KCN) using *in*,*in*/*out*,*out*-**1** (0.243 mmol) in the CH_2Cl_2 phase.

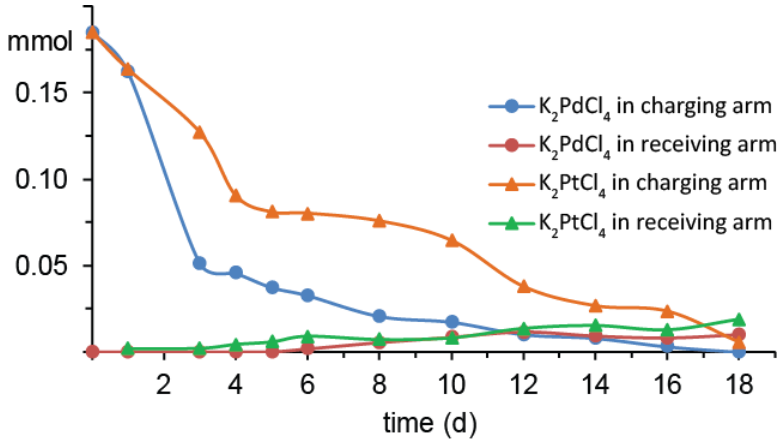

Figure 4.9. Additional data for Figure 3. Disappearance of K_2PtCl_4 (▲; 0.185 mmol) and K_2PdCl_4 (•; 0.185 mmol) from the charging arm and appearance of K_2PtCl_4 (▲) and K_2PdCl_4 (•) in the receiving arm (3.69 mmol KCl) using *in*,*in*/*out*,*out*-**1** (0.246 mmol) in the CH_2Cl_2 phase.

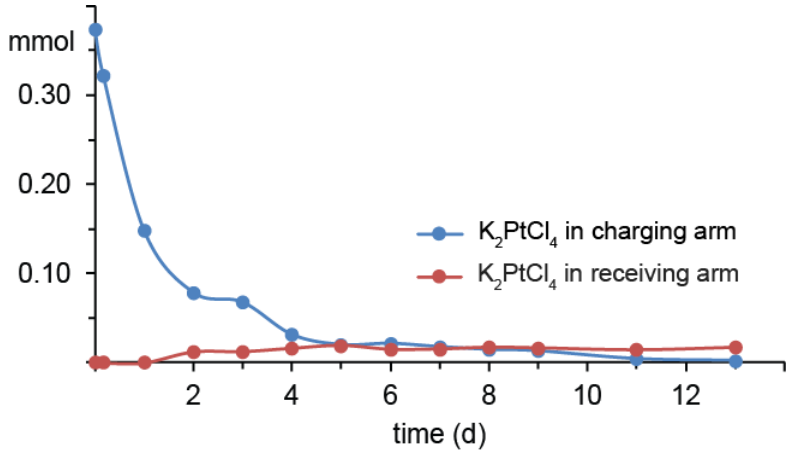

Figure 4.10. Additional data for Figure 3. Disappearance of K_2PtCl_4 from the charging arm (•; 0.374 mmol) and appearance of K_2PtCl_4 in the receiving arm (•; 3.72 mmol KCl) using *in*,*in*/*out*,*out*-**5** (0.241 mmol) in the CH_2Cl_2 phase.

A final issue concerns the breadth of phosphorus donor ligands that are effective for MCl_2 transport. Can homologs of *in*,*in*/*out*,*out*-**1**, or even acyclic diphosphines or simple monophosphines, behave similarly? First, a dibridgehead diphosphine with four additional carbon atoms in each methylene chain, *in*,*in*/*out*,*out*-$P((CH_2)_{18})_3P$ (*in*,*in*/*out*,*out*-**5**), was similarly synthesized as described in the experimental section. The types of experiments with K_2PtCl_4 in Figure 4.4 were repeated. That conducted with KCN in the receiving arm gave the more striking results, and is presented in Figure 4.11 (see Figure 4.10 for that with KCl in the receiving arm). Importantly, the time scale and extent of $PtCl_2$ transport are very close to that with *in*,*in*/*out*,*out*-**1**.

U-tube experiments were conducted with 1,2-bis(dimethylphosphino)ethane (DMPE) and $(n\text{-Oct})_3P$. As shown in Figures B-3 and B-5 (Appendix B), no transport was observed after 12 d when KCl was used in the receiving arm, although DMPE did extract an equivalent of $PtCl_2$ into the CH_2Cl_2 phase. When KCN was used in the receiving arm, very low levels of transport could be detected (DMPE, 8% after 12 d; $(n\text{-Oct})_3P$, 7% after

12 d (Figures B-4 and B-6 (Appendix B))). In both cases, significant quantities of $PtCl_2$ were extracted into the CH_2Cl_2 phases. Finally, when the amounts of *in*, *in*/*out*,*out*-**1** in the CH_2Cl_2 phases in Figure 4.4 were decreased, the transport rates also decreased.

As a concluding perspective, we note that container molecules span a diverse range of architectures. Major classes include assemblies derived from hydrogen bonded subunits,[1a-d] and Platonic or Archimedean solids composed of metal-based corners and organic linkers.[1g,i,j] In both cases, encapsulation is achieved by partial disassembly and reassembly. The new host systems reported herein do not require disassembly, but rather incorporate guests by an uncommon dynamic process, homeomorphism.[3,5] Our data clearly establish the viability of guest transport, together with some thermodynamic ($PtCl_2/PdCl_2 > NiCl_2$) and kinetic ($PdCl_2 > PtCl_2$) selectiveity trends.

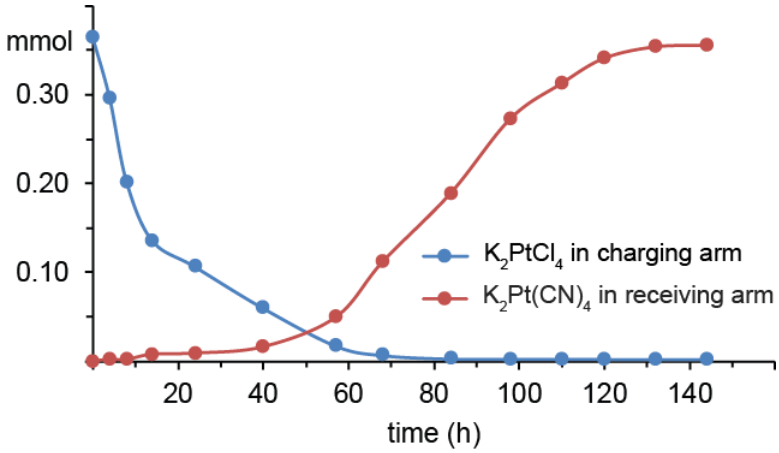

Figure 4.11. Additional data for Figure 3.3. Disappearance of K_2PtCl_4 from the charging arm (•; 0.365 mmol) and appearance of $K_2Pt(CN)_4$ in the receiving arm (•; 3.67 mmol KCN) using *in*,*in*/*out*,*out*-**5** (0.249 mmol) in the CH_2Cl_2 phase.

Although the experiments in Figures 4.3-4.11 operate on the time scales of hours or days, this is an artificial distinction as faster rates would be attained at higher

temperatures with less volatile solvents. Indeed, container molecules based upon non-covalent bonding are likely to be entropically destabilized at higher temperatures, but the dibridgehead diphosphines *in*,*in*/*out*,*out*-**1** and -**5** are thermally robust. Since potential real world applications for binding and transport of metallic species can involve extreme conditions, this class of compounds has exceptional promise. Additional relevant properties and extensions of these concepts will be disclosed in future publications.

4.3. Experimental Section

General. Reactions were conducted under nitrogen or argon using standard techniques. Chemicals were treated as follows: hexanes, CH_2Cl_2, toluene, and THF, dried and degassed us-ing a Glass Contour solvent purification system; K_2PdCl_4 (Acros), K_2PtCl_4 (Aldrich), $K_2M(CN)_4$ (M = Pt/Pd/Ni; 3 × Strem), $PtCl_2$ (Aldrich), $PdCl_2$ (Pressure Chemical), anhydrous $NiCl_2$, $NiCl_2 \cdot 6H_2O$ (2 × Aldrich), KCl (Aldrich), KCN (Alfa Aesar), 1,2-bis(dimethylphosphino)ethane (DMPE; Aldrich), (n-Oct)$_3$P (Aldrich), $CDCl_3$, C_6D_6 (2 × Cambridge Isotope Laboratories), and SiO_2 (Silicycle, 40-63 μm. 230-400 mesh), used as purchased; K_2NiCl_4,[12] $PtCl_2(NCCH_3)_2$,[13] $PdCl_2(NCCH_3)_2$,[14] $NiCl_2(NCCH_3)_2$,[15] P((CH$_2$)$_{14}$)$_3$P (**1**),[16] and *trans*-P$\overline{\text{tCl}_2(\text{P}((\text{CH}_2)_{18})_3\text{P})}$,[17] prepared by literature procedures.

NMR spectra were recorded on a Varian NMRS 500 MHz instrument at ambient probe temperatures and referenced as follows (δ, ppm): ^{1}H, residual internal $CHCl_3$ (7.26) or C_6D_5H (7.16); $^{13}C\{^1H\}$, internal $CDCl_3$ (77.16) or C_6D_6 (128.0); $^{31}P\{^1H\}$, external H_3PO_4 (0.00). IR spectra were recorded on a Shimadzu IRAffinity-1 spectrometer with a Pike MIRacle ATR system (diamond/ZnSe crystal). Mass spectra were obtained on an Applied Biosystem STR Voyager (APCI) instrument. UV-visible spectra were recorded on a Shimadzu UV 1800 spectrometer. Melting points were recorded using a Stanford Research Systems MPA100 (OptiMelt) automated apparatus. Microanalyses were conducted by Atlantic Microlab, Inc.

***trans*-P$\overline{\text{tCl}_2(\text{P}((\text{CH}_2)_{14})_3\text{P})}$ (2). A.** A round bottom flask was charged with *in*,*in*/*out*,*out*-**1** (0.0635 g, 0.097 mmol), $PtCl_2$ (0.0306 g, 0.115 mmol), and CH_2Cl_2 (7 mL) in a glove box. The mixture was stirred for 24 h and chromatographed (SiO_2 column, 1 × 5 cm, 4:1 v/v hexanes/CH_2Cl_2). The solvent was removed from the product containing fractions by rotary evaporation to give **2** (0.0825 g, 0.090 mmol, 93%) as a yellow

powder.[17] **B.** A round bottom flask was charged with *in*,*in*/*out*,*out*-**1** (0.0629 g, 0.096 mmol), $PtCl_2(NCCH_3)_2$ (0.0400 g, 0.115 mmol), and THF (7 mL) in a glove box. The mixture was stirred for 6 h and chromatographed (SiO_2 column, 1 × 5 cm, 4:1 v/v hexanes/CH_2Cl_2). The solvent was removed from the product containing fractions by rotary evaporation to give **2** (0.0835 g, 0.091 mmol, 95%) as a yellow powder.[17]

***trans*-$\overline{PdCl_2(P((CH_2)_{14})_3P)}$ (3). A.** A round bottom flask was charged with *in*,*in*/*out*,*out* -**1** (0.0668 g, 0.102 mmol), $PdCl_2$ (0.0216 g, 0.122 mmol), and CH_2Cl_2 (7 mL) in a glove box. The mixture was stirred for 24 h and chromatographed (SiO_2 column, 1 × 5 cm, 4:1 v/v hexanes/ CH_2Cl_2). The solvent was removed from the product containing fractions by rotary evaporation to give **3** (0.0795 g, 0.096 mmol, 94%) as a yellow powder.[17] **B.** A round bottom flask was charged with *in*,*in*/*out*,*out*-**1** (0.0740 g, 0.113 mmol), $PdCl_2(NCCH_3)_2$ (0.0311 g, 0.120 mmol), and THF (7 mL) in a glove box. The mixture was stirred for 6 h and chromatographed (SiO_2 column, 1 × 5 cm, 4:1 v/v hexanes/CH_2Cl_2). The solvent was removed from the product containing fractions by rotary evaporation to give **3** (0.0886 g, 0.107 mmol, 95%) as a yellow powder.[17]

***trans*-$\overline{NiCl_2(P((CH_2)_{14})_3P)}$ (4). A.** A round bottom flask was charged with a solution of *in*,*in*/*out*,*out*-**1** (0.0812 g, 0.124 mmol) in CH_2Cl_2 (30 mL) in a glove box, and anhydrous $NiCl_2$ (0.0196 g, 0.151 mmol) was added. The mixture was stirred for 48 h, turning first pink (4 h) and then red, and then chromatographed (SiO_2 column, 2 × 7 cm, CH_2Cl_2). The solvent was removed from the product containing fractions by rotary evaporation to give **4** (0.0662 g, 0.084 mmol, 68%) as a red solid. **B.** A round bottom flask was charged with a solution of *in*,*in*/*out*,*out*-**1** (0.0576 g, 0.088 mmol) in THF (20 mL) in a glove box, and $NiCl_2(NCCH_3)_2$ (0.0276 g, 0.130 mmol) was added. The mixture was stirred for 14 h, turning first pink (1 min) and then deep red, and then chromatographed (SiO_2 column, 2 × 7 cm, CH_2Cl_2). The solvent was removed from the product containing

fractions by rotary evaporation to give **4** (0.0604 g, 0.077 mmol, 87%) as a red solid, mp (capillary) 179-181 °C. Anal. calcd (%) for $C_{42}H_{84}P_2NiCl_2$ (780.66): C 64.62, H 10.85; found C 64.07, H 10.73.

Data from route B. **NMR** ($CDCl_3$, δ/ppm): **^{1}H** (500 MHz) 1.93-1.79 (br m, 12H, PC*H*$_2$), 1.56-1.43 (br m, 24H, C*H*$_2$), 1.43-1.36 (br m, 24H, C*H*$_2$), 1.36-1.29 (br m, 24H, C*H*$_2$); **^{13}C{^{1}H}** (126 MHz)[18] 30.15 (s, $PCH_2CH_2CH_2$), 27.74 (s, CH_2), 27.00 (s, CH_2), 26.72 (s, CH_2), 26.61 (s, CH_2), 23.36 (s, PCH_2CH_2), 21.35 (virtual t, J_{CP} = 15.3 Hz, P*C*H$_2$); **^{31}P{^{1}H}** (202 MHz) −0.92 (br s). **IR** (cm^{-1}, powder film): 2924 (m), 1258 (s), 1088 (w), 1011 (w), 964 (w), 795 (w), 702 (m).

in,*in*/*out*,*out*-**P((CH$_2$)$_{18}$)$_3$P** (*in*,*in*/*out*,*out*-**5**)**.** A Schlenk flask was charged with *trans*-$\overline{PtCl_2(P((CH_2)_{18})_3P)}$ (0.2529 g, 0.233 mmol), KCN (0.2319 g, 3.561 mmol; 15 equiv), THF (15 mL), and degassed water (0.5 mL). The mixture was stirred. After 24 h, the mixture was filtered. The filter cake was washed with THF (2 × 5 mL). The solvent was removed from the filtrate by oil pump vacuum, and CH_2Cl_2 (25 mL) was added to the solid residue. The sample was filtered through a pad of celite (1.5 × 1 cm). The filter cake was washed with CH_2Cl_2 (2 × 10 mL). The solvent was removed from the filtrate by oil pump vacuum to give *in*,*in*/*out*,*out*-**5** (0.1622 g, 0.198 mmol, 85%) as a white solid, mp (capillary) 54-57 °C. Anal. calcd (%) for $C_{54}H_{108}P_2$ (819.38): C 79.15, H 13.29; found C 79.16, H 13.48.

NMR (C_6D_6, δ/ppm): **^{1}H** (500 MHz) 1.60-1.52 (br m, 12H, C*H*$_2$), 1.49-1.40 (br m, 24H, C*H*$_2$), 1.40-1.29 (br m, 72H, C*H*$_2$); **^{13}C{^{1}H}** (126 MHz) 32.09 (d, J_{CP} = 10.5 Hz, CH_2), 30.34 (s, CH_2), 30.32 (s, CH_2), 30.29 (s, CH_2), 30.24 (s, CH_2), 30.13 (s, CH_2), 29.95 (s, CH_2), 28.42 (d, J_{CP} = 13.6 Hz, CH_2), 26.76 (d, J_{CP} = 13.0 Hz, CH_2); **^{31}P{^{1}H}** (202 MHz) –32.8 (s). **IR** (cm^{-1}, powder film): 2916 (s), 2847 (s), 1466 (s), 1442 (s), 725 (s). **MS** (APCI$^+$, m/z): calcd for MH^+ (isotope envelope) 819.8/820.8/821.8 100:58:17;

found: 819.6/ 820.6/821.6 100:58:17.

Addition of *in*,*in*/*out*,*out*-1 and $NiCl_2 \cdot 6H_2O$. A Schlenk flask was charged with a solution of *in*,*in*/*out*,*out*-**1** (0.0653 g, 0.099 mmol) in CH_2Cl_2 (20 mL). Then a blue solution of $NiCl_2 \cdot 6H_2O$ (*trans*-$NiCl_2(H_2O)_4 \cdot 2H_2O$; 0.0288 g, 0.121 mmol) in water (3.5 mL) was added. The biphasic mixture was stirred for 2 d. No reaction occurred, as indicated by a $^{31}P\{^1H\}$ NMR spectrum of the colorless organic phase.

Addition of 2 and KCN. A Schlenk flask was charged with **2** (0.4356 g, 0.475 mmol), KCN (0.4674 g, 7.177 mmol, 15 equiv), THF (20 mL) and degassed water (0.5 mL). The mixture was stirred for 24 h and filtered to remove a yellow precipitate. The solvent was removed from the filtrate by oil pump vacuum to give *in*,*in*/*out*,*out*-**1** (0.2692 g, 0.411 mmol, 87%) as a white solid.[17] A $^{13}C\{^1H\}$ NMR spectrum of the yellow precipitate showed signals (D_2O, δ/ppm) for $K_2Pt(CN)_4$ (126.5; lit[19] 126.5) and KCN (166.8). The precipitate was dissolved in water (5 mL) and the solution allowed to slowly concentrate. After 7 d, colorless thin plates were obtained, as verified by X-ray crystallography.[20]

Addition of 2 and $PdCl_2$. A round bottom flask was charged with **2** (0.0916 g, 0.099 mmol), $PdCl_2$ (0.0213 g, 0.120 mmol), and CH_2Cl_2 (7 mL) in a glove box. The mixture was stirred for 6 d. No reaction occurred, as assayed by $^{31}P\{^1H\}$ NMR.

Addition of 2 and $NiCl_2$. A round bottom flask was charged with **2** (0.0880 g, 0.096 mmol), $NiCl_2$ (0.0149 g, 0.115 mmol), and CH_2Cl_2 (7 mL) in a glove box. The mixture was stirred for 6 d. No reaction occurred, as assayed by $^{31}P\{^1H\}$ NMR.

Addition of 3 and $PtCl_2$. A round bottom flask was charged with **3** (0.0845 g, 0.102 mmol), $PtCl_2$ (0.0327 g, 0.123 mmol), and CH_2Cl_2 (7 mL) in a glove box. The mixture was stirred for 6 d. No reaction occurred, as assayed by $^{31}P\{^1H\}$ NMR.

Addition of 3 and $NiCl_2$. A round bottom flask was charged with **3** (0.0837 g,

0.101 mmol), $NiCl_2$ (0.0158 g, 0.122 mmol), and CH_2Cl_2 (7 mL) in a glove box. The mixture was stirred for 6 d. No reaction occurred, as assayed by $^{31}P\{^1H\}$ NMR.

Addition of 4 and $PtCl_2$. A round bottom flask was charged with **4** (0.0801 g, 0.102 mmol), $PtCl_2$ (0.0327 g, 0.123 mmol), and CH_2Cl_2 (7 mL) in a glove box. The red mixture was stirred for 5 d, turning yellow. The sample was placed on top of a column (SiO_2, 1 × 5 cm), which was rinsed with CH_2Cl_2. The solvent was removed from the rinses by rotary evaporation to give **2** (0.0577 g, 0.063 mmol 62%) as a yellow powder.[17]

Addition of 4 and $PdCl_2$. A round bottom flask was charged with **4** (0.0816 g, 0.104 mmol), $PdCl_2$ (0.0219 g, 0.124 mmol), and CH_2Cl_2 (7 mL) in a glove box. The red mixture was stirred for 5 d, turning yellow. The sample was placed on top of a column (SiO_2, 1 × 5 cm), which was rinsed with CH_2Cl_2. The solvent was removed from the rinses by rotary evaporation to give **3** (0.0589 g, 0.071 mmol, 69%) as a yellow powder.[17]

Addition of 2 and $PdCl_2(NCCH_3)_2$. A round bottom flask was charged with **2** (0.0898 g, 0.098 mmol) and a solution of $PdCl_2(NCCH_3)_2$ (0.0306 g, 0.118 mmol) in THF (7 mL) in a glove box. The mixture was stirred for 6 d. No reaction occurred, as assayed by $^{31}P\{^1H\}$ NMR.

Addition of 2 and $NiCl_2(NCCH_3)_2$. A round bottom flask was charged with **2** (0.0898 g, 0.098 mmol) and a solution of $NiCl_2(NCCH_3)_2$ (0.0249 g, 0.118 mmol) in THF (7 mL) in a glove box. The mixture was stirred for 6 d. No reaction occurred, as assayed by $^{31}P\{^1H\}$ NMR.

Addition of 3 and $PtCl_2(NCCH_3)_2$. A round bottom flask was charged with **3** (0.0927 g, 0.112 mmol) and a solution of $PtCl_2(NCCH_3)_2$ (0.0463 g, 0.133 mmol) in THF (7 mL) in a glove box. The mixture was stirred for 6 d. No reaction occurred, as assayed by $^{31}P\{^1H\}$ NMR.

Addition of 3 and $NiCl_2(NCCH_3)_2$. A round bottom flask was charged with **3**

(0.0845 g, 0.102 mmol) and a solution of $NiCl_2(NCCH_3)_2$ (0.0265 g, 0.125 mmol) in THF (7 mL) in a glove box. The mixture was stirred for 6 d. No reaction occurred, as assayed by $^{31}P\{^1H\}$ NMR.

Addition of 4 and $PtCl_2(NCCH_3)_2$. A round bottom flask was charged with **4** (0.0816 g, 0.104 mmol) and a solution of $PtCl_2(NCCH_3)_2$ (0.0456 g, 0.131 mmol) in THF (7 mL) in a glove box. The red mixture was stirred for 2 d, turning yellow. The sample was placed on top of a column (SiO_2, 1 × 5 cm), which was rinsed with CH_2Cl_2. The solvent was removed from the rinses by rotary evaporation to give **2** (0.0605 g, 0.066 mmol, 63%) as a yellow powder.[17]

Addition of 4 and $PdCl_2(NCCH_3)_2$. A round bottom flask was charged with **4** (0.0824 g, 0.105 mmol) and a solution of $PdCl_2(NCCH_3)_2$ (0.0332 g, 0.128 mmol) in THF (7 mL) in a glove box. The red mixture was stirred for 2 d, turning yellow. The sample was placed on top of a column (SiO_2, 1 × 5 cm), which was rinsed with CH_2Cl_2. The solvent was removed from the rinses by rotary evaporation to give **3** (0.0613 g, 0.074 mmol, 70%) as a yellow powder.[17]

U-Tube Transport Experiments (Single Component); General Aspects. A glass U-tube (Figure 4.1) was charged with a solution of **1** (1.0 equiv) in CH_2Cl_2 (40 mL). The charging arm of the tube was filled with an aqueous solution of K_2MCl_4 (0.051-0.053 M; 1.5 equiv, M = Pt, Pd, Ni). The receiving arm was charged with an aqueous solution of KCl or KCN ((2.0-2.5 M; 15 equiv). The organic phase was stirred (450 rpm). The diffusion of MCl_2 into the receiving arm was monitored by UV-visible spectroscopy. Samples of the two arms were taken with a micropipette (0.25 mL) at different time intervals and diluted into quartz crystal cells (10 mm path length). A series of aqueous solutions of K_2MCl_4 or $K_2M(CN)_4$ (known concentrations) were prepared and used to calibrate the UV-visible response at the λ_{max} of each species (K_2PtCl_4, 391 nm; K_2PdCl_4,

305 nm; $K_2Pt(CN)_4$, 279 nm; $K_2Pd(CN)_4$, 240 nm). All gave linear fits across the concentrations employed which allowed the Beer-Lambert law to be applied for calculations.

Specific quantities employed for individual experiments: **A** (Figure 4.4, top), **1**/K_2PtCl_4/ KCl = (0.1611 g, 0.246 mmol)/(0.1498 g, 0.361 mmol)/(0.2743 g, 3.679 mmol). **B** (Figure 4.4, bottom), **1**/K_2PtCl_4/KCN = (0.1605 g, 0.245 mmol)/(0.1482 g, 0.357 mmol)/(0.234 g, 3.587 mmol). **C** (Figure 4.7, top), **1**/K_2PdCl_4/KCl = (0.1600 g, 0.244 mmol)/(0.1212 g, 0.371 mmol)/ (0.2728 g, 3.659 mmol). **D** (Figure 4.7, bottom), **1**/K_2PdCl_4/KCN = (0.1601 g, 0.244 mmol)/ (0.1210 g, 0.371 mmol)/(0.2410 g, 3.701 mmol). **E** (Figure B-3, Appendix), DMPE/K_2PtCl_4/KCl = (0.0554 g, 0.368 mmol)/(0.1545 g, 0.372 mmol)/ (0.1830 g, 2.455 mmol). **F** (Figure B-4, Appendix), DMPE/K_2PtCl_4 /KCN = (0.0368 g, 0.245 mmol)/(0.1527 g, 0.368 mmol)/(0.2401 g, 3.687 mmol). **G** (Figure B-5, Appendix), (*n*-Oct)$_3$P/K_2PtCl_4/KCl = (0.0914 g, 0.247 mmol)/(0.1647 g, 0.379 mmol)/(0.2815 g, 3.776 mmol). **H** (Figure B-6, Appendix), (*n*-Oct)$_3$P/K_2PtCl_4/KCN = (0.0914 g, 0.247 mmol)/(0.1546 g, 0.372 mmol)/(0.2364 g, 3.630 mmol). **I** (Figure 4.10), **5**/K_2PtCl_4/KCl = (0.1974 g, 0.241 mmol)/(0.1552 g, 0.374 mmol)/(0.2773 g, 3.72 mmol). **J** (Figure 4.11), **5**/K_2PtCl_4/KCN = (0.2040 g, 0.249 mmol)/ (0.1515 g, 0.365 mmol)/(0.2389 g, 3.67 mmol).

U-Tube Transport Experiments (Double Component); General Aspects. The apparatus described in the single component experiment was charged with a solution of **1** (1.0 equiv) in CH_2Cl_2 (40 mL). The charging arm was filled with an aqueous solution of K_2PtCl_4 and K_2PdCl_4 (2 × 0.026 M; 0.75 equiv); the receiving arm was charged with an aqueous solution of KCl or KCN ((2.0-2.5 M; 15 equiv). The organic phase was stirred (450 rpm). The samples were analyzed as described for the single component transport experiments above at an absolute or local λ_{max} for each species (K_2PtCl_4, 215 nm;

K_2PdCl_4, 317 nm; $K_2Pt(CN)_4$, 279 nm; $K_2Pd(CN)_4$, 216 nm).

Specific quantities employed for individual experiments: **A** (Figure 4.9). **1**/K_2PtCl_4/K_2PdCl_4/KCl = (0.1612 g, 0.246 mmol)/(0.768 g, 0.185 mmol)/(0.6039 g, 0.185 mmol)/(0.2752 g, 3.691 mmol). **B** (Figure 4.8). **1**/K_2PtCl_4/K_2PdCl_4/KCN = (0.1592 g, 0.243 mmol)/(0.0768 g, 0.185 mmol)/(0.0627 g, 0.192 mmol)/(0.239 g, 3.672 mmol).

I-Tube Experiment. A Schlenk tube was charged with a solution of **1** (0.0662 g, 0.101 mmol) in CH_2Cl_2 (20 mL). A solution of K_2PtCl_4 (0.0623 g, 0.150 mmol) in water (3.5 mL) was carefully layered on top of the CH_2Cl_2 phase. The mixture was then stirred. Samples were taken from the aqueous layer with a micropipette (0.25 mL) at different time intervals and assayed by UV-visible spectroscopy.

Crystallography. Two methods provided crystals with identical unit cell dimensions. **A**. A 4:1 v/v CH_2Cl_2/Et_2O solution of **4** was allowed to slowly concentrate. After 3 d at room temperature, thin red plates were obtained. **B**. Diethyl ether vapor was allowed to slowly diffuse into a CH_2Cl_2 solution of **4** (ca. 0.036 mmol in 5 mL) at 4 °C (3 d) and then –35 °C. This gave red blocks of **4**.

Data were collected as outlined in Table 4.1. Cell parameters were obtained from 180 frames using a 0.5° scan and refined with 6518 reflections. Lorentz, polarization, and absorption corrections were applied.[21] The space group was determined from systematic reflection conditions and statistical tests. The structure was refined (weighted least squares refinement on F^2) to convergence.[22,23] X−seed[24] was employed for the final data presentation. Non−hydrogen atoms were refined with anisotropic thermal parameters. Hydrogen atoms were fixed in idealized positions using a riding model.

4.4. References

(1) Most of the following citations are taken from a special issue of *Chem. Soc. Rev*. entitled "Molecular Containers" (Guest Editors: Ballester, P.; Fujita, M.; Rebek, J.): (a) Ajami, D.; Liu, L.; Rebek, J. *Chem. Soc. Rev.* **2015**, *44*, 490-499. (b) Jordan, J. H.; Gibb, B. C. *Chem. Soc. Rev.* **2015**, *44*, 547-585. (c) Hermann, K.; Ruan, Y.; Hardin, A. M.; Hadad, C. M.; Badjić, J. D. *Chem. Soc. Rev.* **2015**, *44*, 500-514. (d) Kobayashi, K.; Yamanaka, M. *Chem. Soc. Rev.* **2015**, *44*, 449-466. (e) Assaf, K. I.; Nau, W. M. *Chem. Soc. Rev.* **2015**, *44*, 394-418. (f) Kim, D. S.; Sessler, J. L. *Chem. Soc. Rev.* **2015**, *44*, 532-546. (g) Zarra, S.; Wood, D. M.; Roberts, D. A.; Nitschke, J. R. *Chem. Soc. Rev.* **2015**, *44*, 419-432. (h) Rebilly, J.-N.; Colasson, B.; Bistri, O.; Over, D.; Reinaud, O. *Chem. Soc. Rev.* **2015**, *44*, 467-489. (i) Breiner, B.; Clegg, J. K.; Nitschke, J. R. *Chem. Sci.* **2011**, *2*, 51-56. (j) Leenders, S. H. A. M.; Becker, R.; Kumpulainen, T.; de Bruin, B.; Sawada, T.; Kato, T.; Fujita, M.; Reek, J. N. H. *Chem. Eur. J.* **2016**, *22*, 15468-15474 and earlier work of these authors cited therein.

(2) (a) Newcomb, M.; Toner, J. L.; Helgeson, R. C.; Cram, D. J. *J. Am. Chem. Soc.* **1979**, *101*, 4941-4947. (b) Ameerunisha, S.; Srinivas, B.; Zacharias, P. S. *Bull. Chem. Soc. Jpn.* **1994**, *67*, 263-266. (c) Govender, T.; Hariprakasha, H. K.; Kruger, H. G.; Marchand, A. P. *Tetrahedron: Asymmetry* **2003**, *14*, 1553-1557. (d) Verkuijl, B. J. V.; Minnaard, A. J.; de Vries, J. G.; Feringa, B. L. *J. Org. Chem.* **2009**, *74*, 6526-6533. (e) Urban, C.; Schmuck, C. *Chem. Eur. J.* **2010**, *16*, 9502-9510.

(3) Stollenz, M.; Barbasiewicz, M.; Nawara-Hultzsch, A. J.; Fiedler, T.; Laddusaw, R. M.; Bhuvanesh, N.; Gladysz, J. A. *Angew. Chem., Int. Ed*. **2011**, *50*, 6647-6651; *Angew. Chem.* **2011**, *123*, 6777-6781.

(4) (a) Stollenz, M.; Bhuvanesh, N.; Reibenspies, J. H.; Gladysz, J. A. *Organometallics* **2011**, *30*, 6510-6513. (b) Stollenz, M.; Taher, D.; Bhuvanesh, N.;

Reibenspies, J. H.; Baranová, Z.; Gladysz, J. A. *Chem. Commun.* **2015**, *51*, 16053-16056.

(5) Park, C. H.; Simmons, H. E. *J. Am. Chem. Soc.* **1968**, *90*, 2429-2431.

(6) (a) Nawara, A. J.; Shima, T.; Hampel, F.; Gladysz, J. A. *J. Am. Chem. Soc.* **2006**, *128*, 4962-4963. (b) Nawara-Hultzsch, A. J.; Stollenz, M.; Barbasiewicz, M.; Szafert, S.; Lis, T.; Hampel, F.; Bhuvanesh, N.; Gladysz, J. A. *Chem. Eur. J.* **2014**, *20*, 4617-4637.

(7) Brown, C.; Heaton, B. T.; Sabounchei, J. *J. Organomet. Chem.* **1977**, *142*, 413-421.

(8) Livingstone, S. E. The Chemistry of Ruthenium, Rhodium, Palladium, Osmium, Iridium and Platinum. In *Pergamon Texts in Inorganic Chemistry*; Pergamon Press: UK, **1973**; Vol. 25, p 1339.

(9) Durand, B.; Paris, J. M.; Behrman, E. C.; Huang, A.; Wold, A. *Inorg. Synth.* **1980**, *20,* 50-53.

(10) (a) Mizuno, J. *J. Phys. Soc. Jpn.* **1961**, *16*, 1574-1580. (b) Although $NiCl_2 \cdot 6H_2O$ and diphosphines can react under homogeneous conditions in protic solvents to give $(L)_2Ni(Cl)_2$ species, no reactions occur on the time scale of days (dppe, *in,in*/*out,out*-**1**) under biphasic conditions that mimic those in the U-tube experiments. See Van Hecke, G. R.; Horrocks, D. W., Jr. *Inorg. Chem.* **1966**, *5*, 1968-1974.

(11) (a) Basolo, F. *Adv. Chem. Ser.* **1965**, *49*, 81-106. (b) Hynes, M. J.; Brannick, P. F. *Proc. R. Ir. Acad. B.* **1977**, *77*, 479-493.

(12) Durand, B.; Paris, J. M.; Behrman, E. C.; Huang, A.; Wold, A. *Inorg. Synth.* **1980**, *20,* 50-53.

(13) Muñoz, M. P.; Méndez, M.; Nevado, C.; Cárdenas D. J.; Echavarren, A. M. *Synthesis* **2003**, *18*, 2898-2902.

(14) Andrews, M. A.; Chang, T. C. T.; Cheng, C. W. F.; Emge, T. J.; Kelly, K. P.;

Koetzle, T. F. *J. Am. Chem. Soc.* **1984**, *106*, 5913-5920.

(15) Hathaway, B. J.; Holah, D. G. *J. Chem. Soc*. **1964**, 2400-2408.

(16) Nawara, A. J.; Shima, T.; Hampel, F.; Gladysz, J. A. *J. Am. Chem. Soc.* **2006**, *128*, 4962-4963.

(17) The identity and spectroscopic purity of this previously reported compound was confirmed by $^{31}P\{^{1}H\}$ and ^{1}H NMR ($CDCl_3$). Nawara-Hultzsch, A. J.; Stollenz, M.; Barbasiewicz, M.; Szafert, S.; Lis, T.; Hampel, F.; Bhuvanesh, N.; Gladysz, J. A. *Chem. Eur. J.* **2014**, *20*, 4617-4637.

(18) The ^{13}C NMR assignments were made by analogy to those of related complexes in reference 17, which were established by 2D NMR experiments.

(19) Brown, C.; Heaton, B. T.; Sabounchei, J. *J. Organomet. Chem.* **1977**, *142*, 413-421.

(20) Mühle, C.; Nuss, J.; Jansen, M. *Z. Kristallogr., New Cryst. Struct.* **2009**, *224*, 9–10.

(21) (a) "Collect" data collection software, Nonius, B. V., **1998**. (b) "Scalepack" data processing software: Otwinowski, Z.; Minor, W. in *Methods in Enzymology* **1997**, *276* (Macromolecular Crystallography, Part A), 307-326.

(22) (a) Sheldrick, G. M. *Acta Cryst.* **2008**, *A64*, 112-122. (b) Sheldrick, G. M. *Acta Cryst.* **2015**, *A71*, 3-8. (c) Sheldrick, G. M. *Acta Cryst.* **2015**, *C71*, 3-8.

(23) Dolomanov, O. V.; Bourhis, L. J.; Gildea, R. J.; Howard, J. A. K.; Puschmann, H. *J. Appl. Cryst.* **2009***, 42*, 339-341.

(24) Barbour, L. J. *J. Supramol. Chem.* **2001***, 1,* 189-191.

Table 4.1. Summary of crystallographic data for **4.**

empirical formula	$C_{42}H_{84}Cl_2NiP_2$
formula weight	780.64
Diffractometer	Bruker Gadds X-ray (three-circle)
Temperature [K]	110.15
Wavelength [Å]	1.54178
crystal system	monoclinic
space group	$P2_1/n$
unit cell dimensions :	
a [Å]	16.1660(6)
b [Å]	13.7100(5)
c [Å]	19.9425(7)
α [°]	90
β [°]	92.391(2)
γ [°]	90
V [Å^3]	4416.1(3)
Z	4
ρ_{calcd} [Mg/m^3]	1.174
μ [mm^{-1}]	2.611
F(000)	1712
crystal size [mm^3]	0.15 × 0.03 × 0.01
θ limit [°]	3.450 to 60.000
index ranges [h, k, l]	−17, 18; −15, 15; −22, 22
reflections collected	40048
independent reflections	6518
R(int)	0.0809
completeness to θ	99.3 (60.00)
max. and min. transmission	0.7522 and 0.5495
data/restraints/parameters	6518/0/424
goodness-of-fit on F^2	1.041
R indices (final) [$I > 2\sigma(I)$]	
R_1	0.0564
wR_2	0.1318
R indices (all data)	
R_1	0.0694
wR_2	0.1380
Largest diff. peak and hole [eÅ^{-3}]	0.958 and −0.528

5. A NON-TEMPLATED ROUTE TO MACROCYCLIC DIBRIDGEHEAD DIPHOSPHORUS COMPOUNDS: CRYSTALLOGRAPHIC CHARACTERIZATION OF A "CROSSED CHAIN" VARIANT OF *in*/*out* STEREOISOMERS*

5.1. Introduction

In principle, most macrocyclic bicyclic molecules – or more economically expressed, macro*bi*cycles – with pyramidal or tetrahedral bridgehead atoms can exhibit *in*/*out* stereoisomerism.[1] This refers to the directional sense of the bridgehead lone pair or substituent with respect to the bicyclic framework. However, this duality is seldom exploited. Thus, only recently have *in*/*out* isomers begun to evolve from curiosities to task specific substances that can (for example) serve as container molecules and separate homologous platinum and palladium complexes from those of the base metal nickel.[2]

Our interest in *in*/*out* isomerism was in part prompted by the unexpected discovery of facile routes to aliphatic dibridgehead diphosphines of the formula $P((CH_2)_n)_3P$ (**1**; n = 14, **c**; 18, **e**).[2-5] As depicted in Scheme 5.1, these were first stitched together in metal coordination spheres via threefold intramolecular ring closing alkene metatheses of *trans* phosphine ligands $P(CH_2)_mCH{=}CH_2)_3$ ($n = 2m + 2$) followed by hydrogenations.[3,4a] Reactions with excesses of appropriate nucleophiles then afforded the demetalated diphosphines in good yields.[2-5] Interestingly, the "largest" such diphosphine previously synthesized consisted of one $(CH_2)_3$ and two $(CH_2)_4$ bridges.[6]

Macrobicyclic dibridgehead diphosphines such as **1c**,**e** are capable of homeomorphism,[7] a dynamic process that was defined fifty years ago but remains unfami-

*Reproduced with permission from Kharel, S.; Jia, T.; Bhuvanesh, N.; Reibenspies, J. H.; Blümel, J.; Gladysz, J. A. *Chem. Asian J.* **2018**. accepted. DOI: 10.1002/asia.201800739R1.

-liar to many chemists. As exemplified with **1c** and adducts thereof in Scheme 5.2, one bridge is threaded through the other two, effectively turning the molecules inside out.

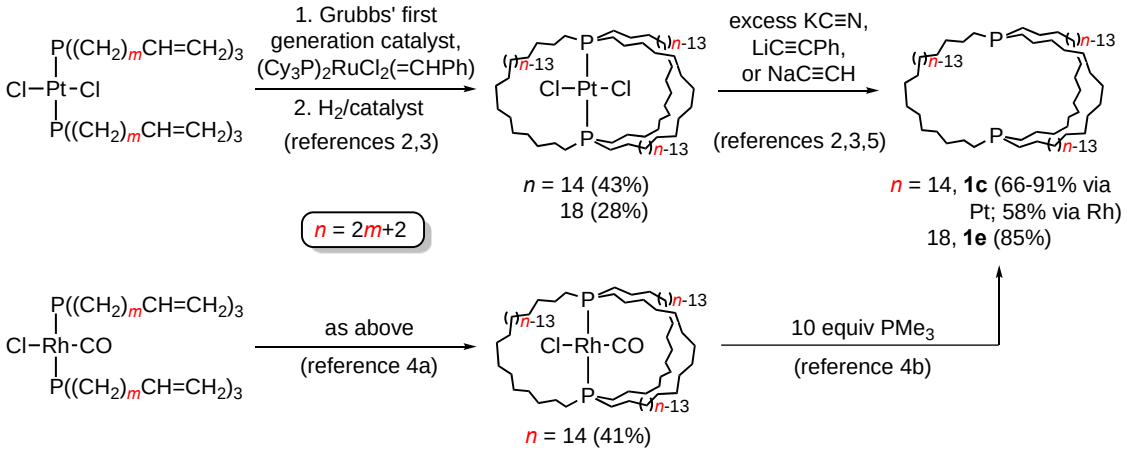

Scheme 5.1. Syntheses of gyroscope like platinum and rhodium complexes and dibridgehead diphosphines derived therefrom.

For many dibridgehead diphosphines, there would also be a parallel pathway involving pyramidal inversion at both phosphorus atoms. However, this would require on the order of 30 kcal/mol,[8] which is far too high for processes that are rapid below room temperature. In any case, this enables the direct equilibration of *in*,*in* and *out*,*out* isomers. Analogous *in*,*out* and *out*,*in* isomers can similarly equilibrate, but these will be degenerate when the top and bottom hemispheres of the molecule are identical. Surprisingly, homeomorphic isomerization has been explicitly demonstrated only for a handful of molecules.[1,9]

In previous efforts, we have sought to probe the expanded manifold of relationships between *in*/*out* isomers depicted in Scheme 5.3,[5,10] in which the bridgeheads are generalized as X-E. A "half turn" denotes that only one of the two X-E units rotates by 180°; two such turns are required to complete a homeomorphic isomerization. Of

particular relevance to certain results below are the intermediates with "crossed" or "intertwined" chains (**II**, **IV**, **VI**). Do any represent energy minima, and if so could the minima be made deep enough to permit isolation? Indeed, we could ultimately show that adducts of dibridgehead diphosphines and appropriately designed Lewis acids adopt "crossed chain" structures both in solution and the solid state (*vide infra*).[10b]

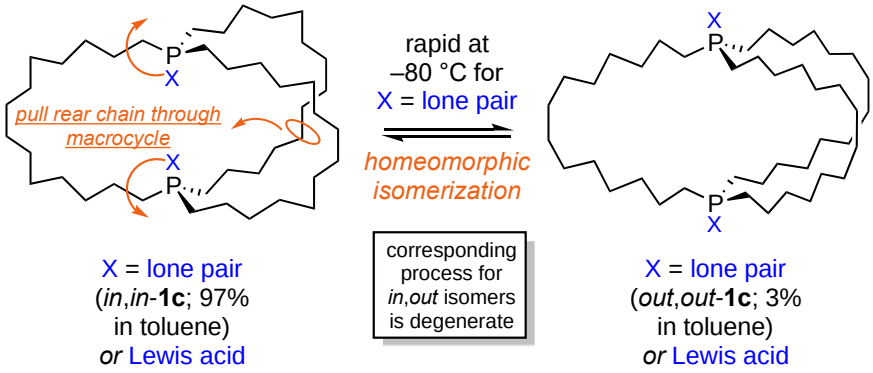

Scheme 5.2. Homeomorphic isomerization of the dibridgehead diphosphine **1c** or Lewis acid adducts thereof.

With regard to further developing the chemistry of **1c**,**e** and related diphosphorus compounds, one problem has been the requirement for stoichiometric quantities of precious metals in the syntheses in Scheme 5.1. Interestingly, the analogous trigonal bipyramidal $Fe(CO)_3$ complexes undergo metathesis and hydrogenation in significantly higher overall yields.[11] However, it has proved problematic to detach the dibridgehead diphosphine ligands from the $Fe(CO)_3$ moieties. So far, oxidative methods that give the corresponding dibridgehead diphosphine dioxides $(O{=})P((CH_2)_n)_3P(=O)$ (**2**) have shown the most promise, but purification issues remain.[12]

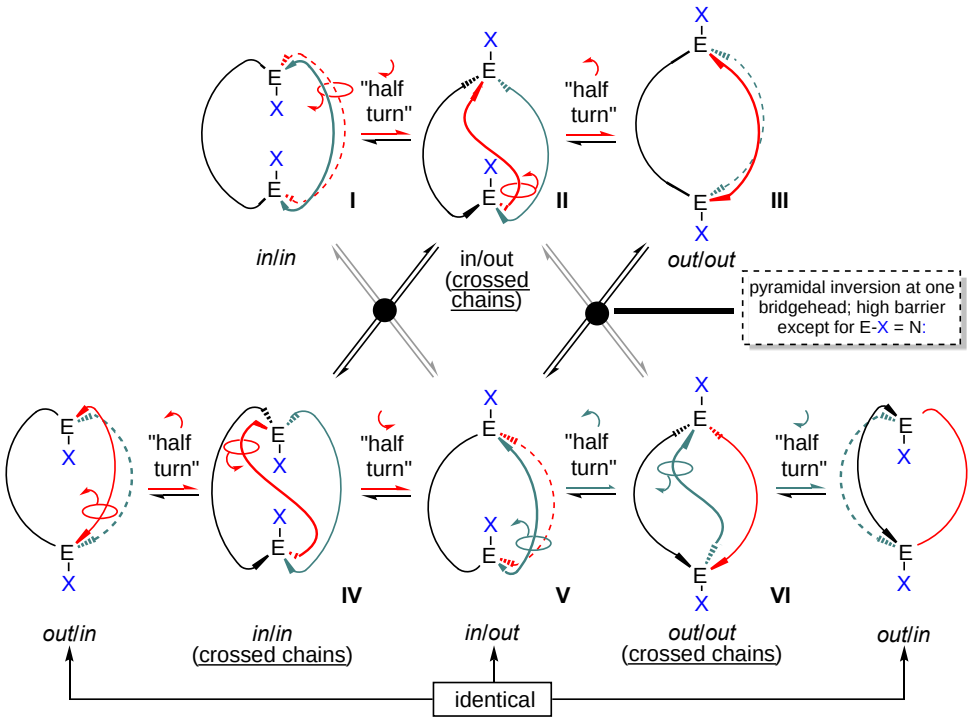

Scheme 5.3. Relationships between the traditional *in*/*out* isomers **I**, **III**, and **V** and "crossed chain" variants **II**, **IV**, and **VI** (X = lone pair or Lewis acid).

Hence, it has been of interest to investigate routes to **1** or **2** or Lewis acid adducts thereof that do not require metal templates. As shown in Scheme 5.4, we subjected the phosphine borane $(H_3B)P((CH_2)_6CH{=}CH_2)_3$ to an alkene metathesis/hydrogenation sequence analogous to those in Scheme 5.1.[5] However, only very low yields of the target compound $(H_3B)P((CH_2)_{14})_3P(BH_3)$ (**1c**·$2BH_3$) were obtained. Not unexpectedly, oligomeric and polymeric products dominated.

In this section, we describe a new metal free strategy based upon dialkylphosphonate building blocks that leads to dibridgehead diphosphine dioxides – and presumably, after reduction, the analogous dibridgehead diphosphines. The two phosphorus atoms are first linked in an alkylation step by a methylene chain, and subsequent metathesis/hydrogenation steps install the second and third methylene chains.

While this methodology is superior to the metal free route in Scheme 5.4, it still falls short of the platinum and rhodium mediated syntheses in Scheme 5.1. Nonetheless, there is unexpected novelty, as one of the diphosphine dioxides crystallizes with "crossed chains", as described below. This further substantiates their viability as energy minima in sequences such as Scheme 5.3.

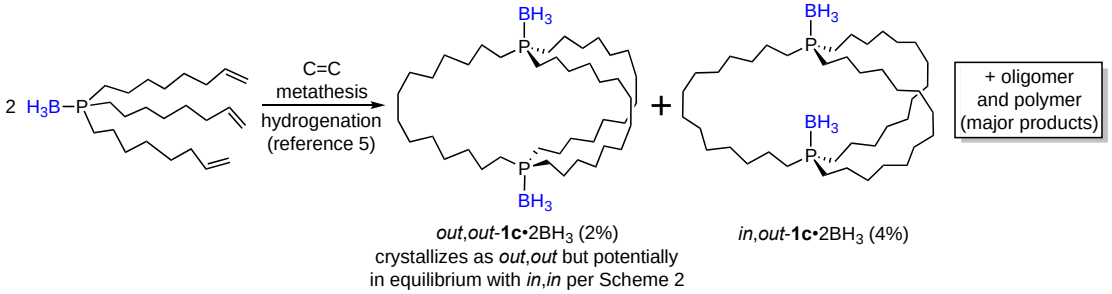

Scheme 5.4. A phosphine borane precursor to bis(BH_3) adducts of the dibridgehead diphosphine **1c**.

5.2. Results

5.2.1. Substrates for alkene metathesis. The compound (O=)PH(OCH_2CH_3)$_2$, commonly termed both diethyl phosphonate and diethyl phosphite, reacts with Grignard reagents RMgX to give secondary or dialkylphosphine oxides, (O=)PHR_2.[13] For both the starting material and product, the tautomeric structures with trivalent phosphorus atoms, HO-PX'_2, are much less stable.[14] Thus, the commercially available α,ω-olefinic alkyl bromides Br(CH_2)$_m$CH=CH_2 (*m* = **a**/4, **b**/5, **c**/6) were converted to the corresponding Grignard reagents BrMg(CH_2)$_m$CH=CH_2. As shown in Scheme 5.5, these were added in 3.2-4.9 fold excesses to (O=)PH(OCH_2CH_3)$_2$. Presumably one equiv of the Grignard reagent is quenched by an acidic (O=)PH or H-OP proton of the reactant.

Workups gave the corresponding dialkylphosphine oxides

(O=)PH($(CH_2)_m$CH=$CH_2)_2$ (**2a-c**) as white solids in 77-81% yields. These new compounds and all others below were characterized by NMR (^{1}H, ^{13}C, ^{31}P) and IR spectroscopy, and in most cases microanalyses, as summarized in the experimental section. All features were routine, and representative spectra for each compound type are provided in the Supporting Information (SI). The PH ^{1}H NMR signals were doublets that were strongly coupled to phosphorus ($^1J_{HP}$ = 445-436 Hz, δ/ppm 6.62-6.83, $CDCl_3$). The ^{13}C{^{1}H} NMR spectra showed three phosphorus coupled doublets for the P$\underline{C}H_2\underline{C}H_2\underline{C}H_2$ signals ($^1J_{CP} > {}^3J_{CP} > {}^2J_{CP}$). Assignments (experimental section) were confirmed by ^{1}H,^{1}H COSY, ^{1}H,^{13}C{^{1}H} COSY, and ^{1}H,^{13}C{^{1}H} HMBC experiments.

It has been previously shown that secondary phosphine oxides (O=)PH$(R)_2$ can be deprotonated with suitable bases, and that the conjugate bases are readily alkylated.[15] Thus, **2a-c** were treated with NaH and then different α,ω-dibromides Br$(CH_2)_n$Br (0.49-0.32 equiv) as shown in Scheme 5.5 (*n* = **a'**/8, **b'**/10, **c'**/12, **d'**/14). Workups gave the bis(trialkylphosphine oxides) $(H_2C{=}CH(CH_2)_m)_2P(=O)(CH_2)_n(O=)P((CH_2)_m CH{=}CH_2)_2$ (**3ab', 3bc', 3cd', 3ca')** as white solids in 79-84% yields based upon the dibromide. The ^{31}P{^{1}H} NMR signals were downfield of those of the precursors **2a-c** (δ/ppm 48.6-48.9 vs. 34.4-35.0, $CDCl_3$). The ^{13}C{^{1}H} NMR spectra showed six phosphorus coupled doublets (P$\underline{C}H_2\underline{C}H_2\underline{C}H_2$), three of which were approximately twice as intense as the others. These and other signals were assigned as described above.

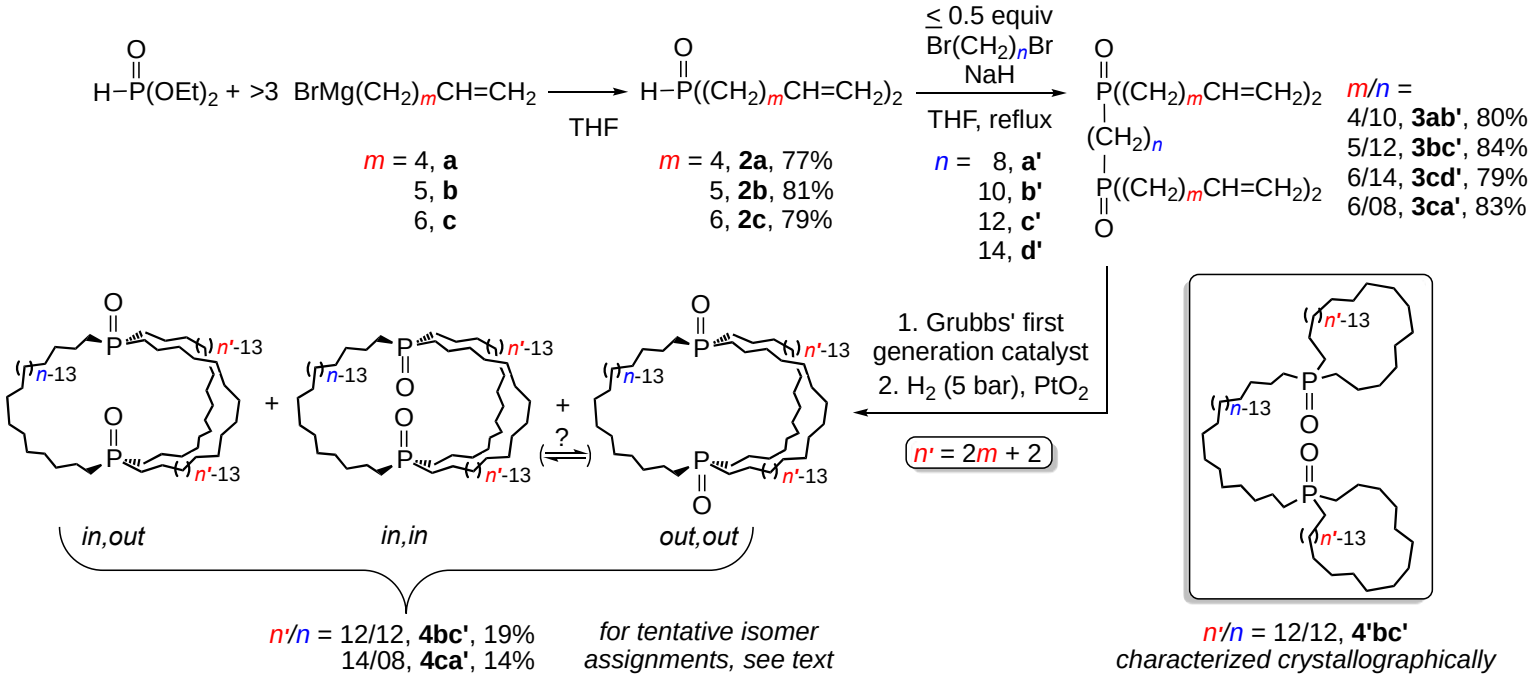

Scheme 5.5. Title reaction sequence.

5.2.2. Alkene metatheses. The stage was now set to probe whether dibridgehead diphosphorus compounds could be accessed more efficiently by alkene metathesis when one phosphorus-phosphorus linkage had first been installed (rendering the initial step intramolecular), as opposed to the "all at once" strategy in Scheme 5.4 (initial step intermolecular). Two substrates were selected for emphasis. The first, **3bc'**, would, after the hydrogenation step, afford a dibridgehead diphosphine dioxide with three identical bridges ($(CH_2)_{12}$). The second, **3ca'**, would afford a diphosphine dioxide in which one linkage was shorter than the other two ($(CH_2)_8$ vs. $(CH_2)_{14}$).

Accordingly, a CH_2Cl_2 solution of **3bc'** (0.00105 M) and Grubbs' first generation catalyst (10 mol%) was heated to reflux (48 h). As shown in Scheme 5.5, the crude product was hydrogenated (5 bar H_2, cat. PtO_2) and then chromatographed on a silica column to give the target compound (O=)P($(CH_2)_{12}$)$_3$P(=O) (**4bc'**) as a light brown solid in 19% yield. One other easily identified phosphine oxide eluted, (O=)PCy_3 derived from Grubbs' catalyst. Trace amounts of other products were noted, one of which could be crystallized as described below. Per extensive experience with the types of alkene metatheses in Scheme 5.1, oligomers were presumed to be retained on the column.

The $^{31}P\{^1H\}$ NMR spectrum of **4bc'** showed two closely spaced signals at (δ/ppm) 50.9 and 51.3 in a 70:30 area ratio. Several $^{13}C\{^1H\}$ NMR signals were similarly doubled, such as the P$\underline{C}H_2\underline{C}H_2\underline{C}H_2$ peaks at (major/minor) 27.5/28.1 ($^1J_{CP}$ = 64.6/64.6 Hz), 21.4/21.6 ($^2J_{CP}$ = 3.4/3.8 Hz), and 30.6/30.7 ($^3J_{CP}$ = 14.1/12.2 Hz). Given the unequal ratios, the sample must contain two isomers. The *in*,*in* and *out*,*out* isomers (see Scheme 5.5) would each give one ^{31}P NMR signal, provided that homeomorphic isomerization were slow on the NMR time scale; the *in*,*out* isomer would give one signal if (degenerate) homeomorphic isomerization were fast.

To probe the latter possibility, a $^{31}P\{^1H\}$ NMR spectrum was recorded at –90 °C

(CD_2Cl_2). However, there was no decoalescence or change in the signal ratio. In the case of the *in*,*out*-**1c**, a diphosphine with fourteen methylene groups in each bridge (cf. Scheme 5.2), one signal was observed at room temperature, but two (50:50) at –73 °C. The decoalescence data gave a $\Delta G^{\ddagger}_{200K}$ value of 8.5 kcal/mol.[5] It seems probable that a homeomorphic isomerization involveing larger bridgehead groups ((O=)P vs. :P) and shorter methylene bridges would have a signifycantly higher barrier and a more readily observed decoalescence. Thus, **4bc'** is tentatively assigned as a mixture of *in*,*in* and *out*,*out* isomers.

When an analogous sequence and workup was carried out with **3ca'**, the target compound (O=)P(CH_2)$_8$((CH_2)$_{14}$)$_2$P(=O) (**4ca'**) was isolated as a light brown solid in 14% yield. This sample also exhibited two closely spaced $^{31}P\{^1H\}$ NMR signals at (δ/ppm) 50.11 and 49.95 (relative integrals again 70:30). More than one set of ^{13}C NMR signals were again observed, as listed in the experimental section. By analogy to **4bc'**, the tendency would be to assign this sample as a mixture of *in*,*in*-**4ca'** and *out*,*out*-**4ca'**. However, the following section reveals a "twist".

5.2.3. Crystallography. Crystals of the dibridgehead diphosphine dioxides were sought. When $CHCl_3$ solutions of **4ca′** were allowed to slowly concentrate, colorless plates were obtained. X-ray data were acquired for two different crystals grown some years apart. The structures were solved as outlined in Table 5.1 and the experimental section. Interestingly, two distinct forms of **4ca'** were obtained, as shown in Figure 5.1. Key metrical parameters are given in Table 5.2. The bond lengths and angles were quite similar. However, the phosphorus-phosphorus distance was somewhat greater in the second structure (bottom; 12.15 vs. 11.54 Å), which also exhibited a C_2 symmetry axis that exchanged the (O=)P moieties.

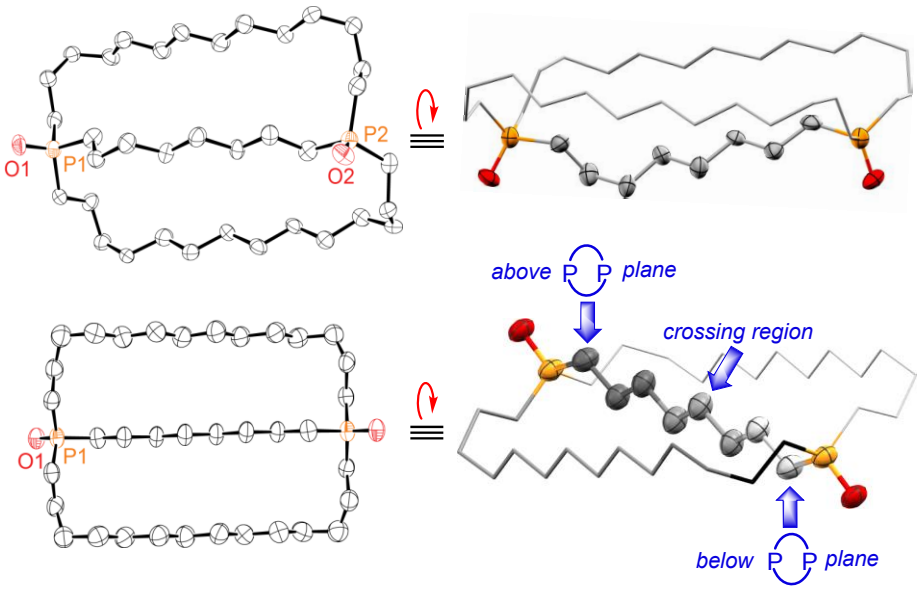

Figure 5.1. Thermal ellipsoid plots (50% probability) obtained from different crystals of **4ca'** (left), and alternative representations (right). Top, traditional *out*,*out* isomer; bottom, "crossed chain" *out*,*out* isomer.

The first structure in Figure 5.1 (top) is a traditional *out*,*out* isomer. This is somewhat obscured by the shorter $(CH_2)_8$ chain, which ratchets the phosphorus atoms closer together and pivots the (O=)P moieties into roughly parallel orientations. The second (bottom) is also best termed an *out*,*out* isomer. However, in addition there is a "crossed chain" feature. Note that with respect to the macrocycle defined by the two longer $(CH_2)_{14}$ bridges (i.e., $\overline{P(CH_2)_{14}P(CH_2)_{14}}$ in bottom right structure), the shorter $(CH_2)_8$ bridge connects a P-C linkage that extends above the macrocycle plane (left side) to a P-C linkage that extends below the macrocycle plane (right side). As shown in Scheme 5.6, this type of structure is formally derived by conformationally contorting a traditional *in*,*out* isomer (**VII** → **VIII**, analogous to **V** → **VI** in Scheme 5.3). This represents an altogether new type of isolable *in*/*out* isomer, namely a "crossed chain" *out*,*out* species.[10b]

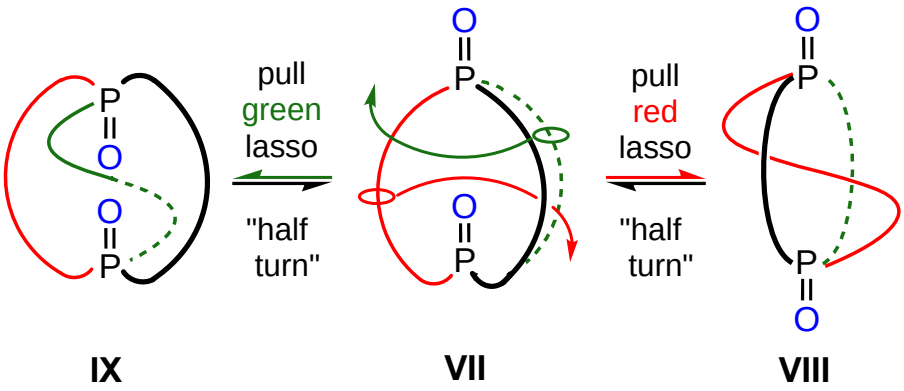

Scheme 5.6. Conversion of a traditional *in*,*out* dibridgehead diphosphine dioxide (**VII**) to a "crossed chain" *out*,*out* isomer (**VIII**; Figure 5.1, bottom), or a "crossed chain" *in*,*in* isomer (**IX**; not observed).

Crystals of **4bc'** were similarly sought, but without success. However, a minor byproduct crystallized from a trailing chromatography fraction, and X-ray data gave the structure shown in Figure 5.2. This diphosphine dioxide, which features two remotely situated thirteen membered rings, is derived from the metathesis of $(CH_2)_5CH{=}CH_2$ moieties on the same as opposed to different phosphorus atoms. In previous papers,[3b,16,17] we have designated such isomers by a prime following the Arabic numeral (i.e., **4'bc'**). This structure also exhibits a C_2 symmetry axis that exchanges the (O=)P moieties. In the course of carrying out the preceding chemistry, crystals of **3ab'** and **3bc'** were also obtained.

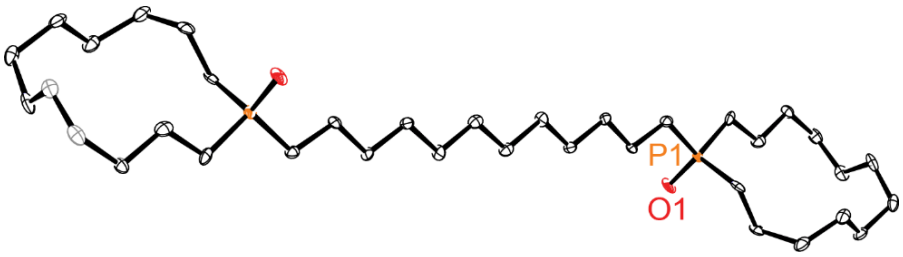

Figure 5.2. Thermal ellipsoid plot (50% probability) of **4'bc'**.

The structures were similarly solved and are depicted in Figure 5.3, and data are summarized in the SI. The P-C and P-O bond lengths and C-P-O and C-P-C bond angles all fall into typical and narrow ranges (average values with standard deviations in parentheses: 1.807(12) Å, 1.149(7) Å, 113.1(5)°, 105.5(12)°), similar to those of *out*,*out*-**4ca'** and "crossed chain" *out*,*out*-**4ca'** (Table 5.2). The spatial arrangements of the four vinyl groups in **3ab'** and **3bc'** are not conducive to intramolecular alkene metathesis (Figure 5.3), consistent with the modest yields of the title molecules. In contrast, there is evidence for favorable or "pre-organized" conformations with hexaolefinic bis(phosphine) $Fe(CO)_3$ complexes analogous to the platinum and rhodium educts in Scheme 5.1.[11a] These give much higher overall yields of gyroscope like products (50-70%).

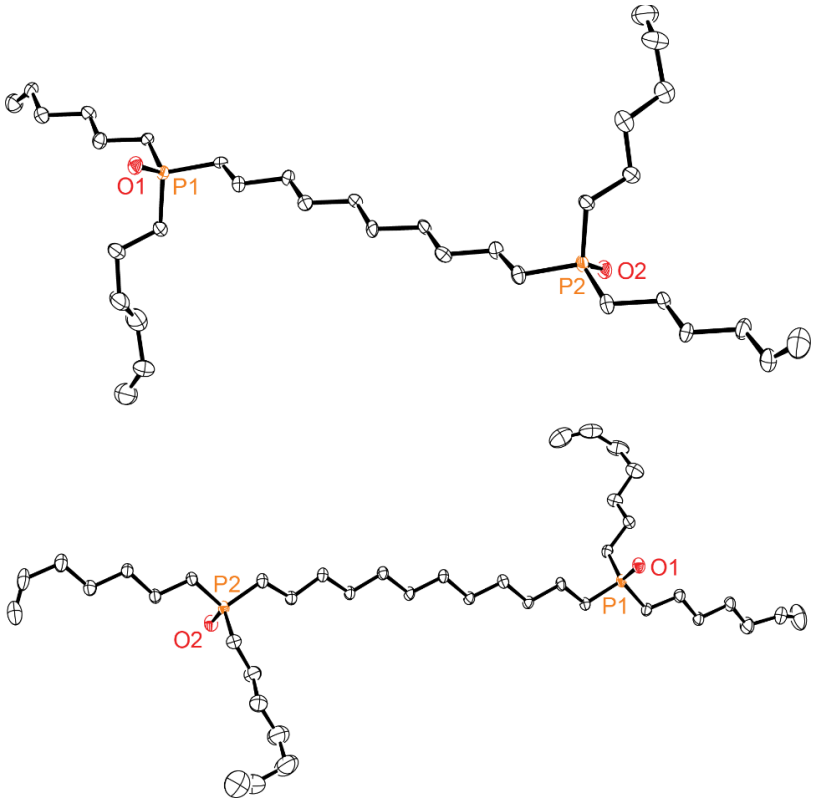

Figure 5.3. Thermal ellipsoid plot (50% probability) of **3ab'** (top) and **3bc'** (bottom).

5.3. Discussion

This study represents another chapter in the evaluation of alkene metathesis based strategies for syntheses of dibridgehead diphosphorus compounds. In contrast to the three fold ring closing metatheses in Scheme 5.1, the new approach (Scheme 5.5) lacks a metal template. This methodology does constitute a distinct improvement over the very low yielding template-less route in Scheme 5.4. This is due to the initial introduction of a phosphorus-phosphorus linkage that renders subsequent alkene metathesis steps intramolecular. However, the route is not competitive with Scheme 5.1, despite eliminating the need for a precious metal. Screening reactions with the other tetraalkenes in Scheme 5.5 (e.g., **3cd'**) indicated similarly modest yields. Also, although dibridgehead diphosphine dioxides represent very interesting and potentially useful molecules, an additional reduction step is required if dibridgehead diphosphines are the ultimate goal.

In this context, several macrocyclic dibridgehead diphosphine dioxides have been reported.[18-20] However, all are based upon tri*aryl*phosphorus units, which confer added rigidity. For example, the tris(alkynyl) triarylphosphine oxide **5** (Scheme 5.7, top) could be oxidatively coupled to a tris(1,3-diyne) and then hydrogenated a mixture of to *out*,*out*-**6** and *in*,*out*-**6**.[19] Stereochemical assignments were verified crystallographically. Whereas *out*,*out*-**6** exhibited a single ^{31}P NMR signal, *in*,*out*-**6** exhibited two, indicating a high energy barrier for homeomorphic isomerization.

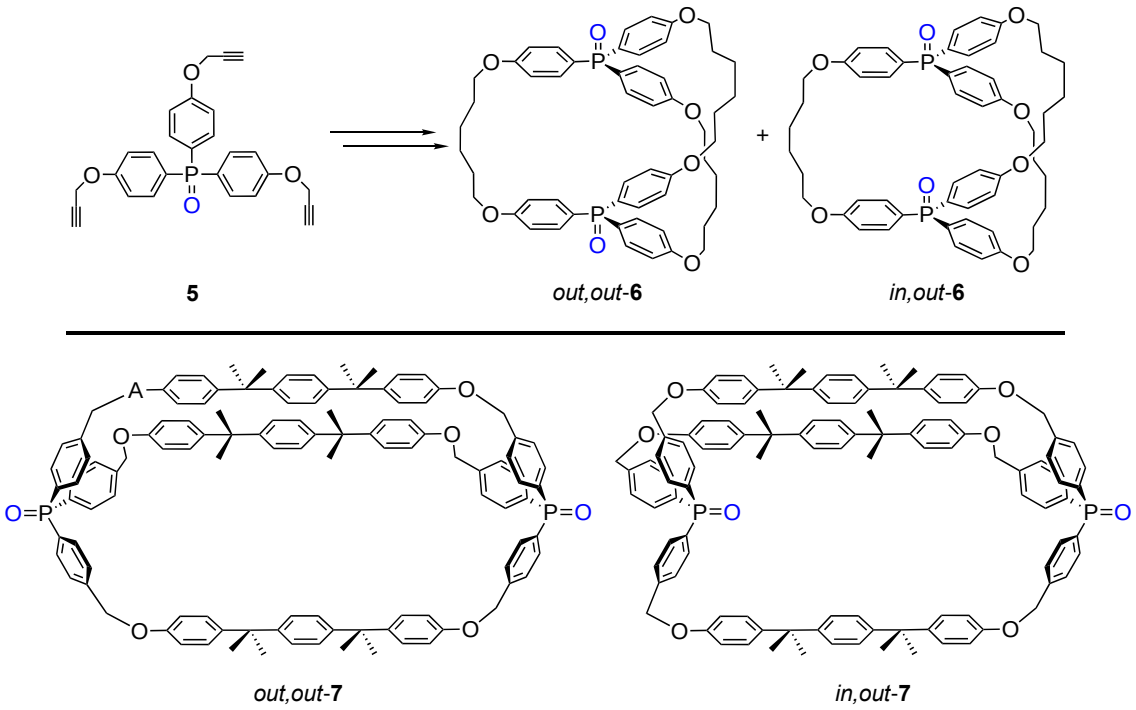

Scheme 5.7. Previously characterized macrocyclic dibridgehead diphosphine dioxides.

The larger macrocycles *out*,*out*-**7** and *in*,*out*-**7** (Scheme 5.7, bottom) were prepared by Williamson ether syntheses in surprisingly high yields (61% combined, final macrocyclization step),[20] likely aided by the quaternary centers and Thorpe-Ingold effect.[21] Now the *in*,*out* isomer exhibited one ^{31}P NMR signal, indicative of a low barrier for homeomorphic isomerization. Reductions gave the analogous dibridgehead diphosphines and phosphine/BH_3 adducts,[20b] and related dibridgehead diphosphites and diphosphates were also prepared.[18,22]

The crystal structures of **4ca'** expand the range of molecular topologies that can be realized with *in*/*out* isomers. That of *out*,*out*-**4ca'** appears unusual due to the large deviation of the (O=)P vectors from colinearity, imposed by the shorter methylene chain. However, comparable phenomena have been observed with related carbocycles.[1] In contrast, "crossed chain" *out*,*out*-**4ca'** is virtually unprecedented. The likelihood of

"crossed chain" species on the reaction coordinates for homeomorphic isomerizations has been recognized in the literature,[1,9a,18] but usually in the context of transition states as opposed to ground states.[9a] Our inability to isolate "crossed chain" *out*,*out*-**4ca'** in pure form has hampered a more definitive characterization. If it represents a global energy minimum, then one ^{31}P NMR signal is expected at all temperatures. In contrast, if the progenitor *in*,*out*-**4ca'** is lower in energy (see **VII**, Scheme 5.6), two signals should be found at sufficiently low temperatures. For the sake of completeness, it should be noted that *in*,*out*-**4ca'** can also equilibrate with "crossed chain" *in*,*in*-**4ca'**, per the green lasso in **VII**.

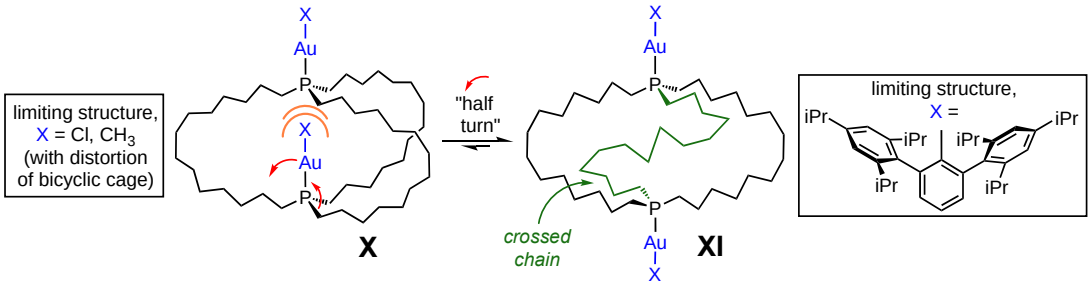

Scheme 5.8. Chain crossing in gold Lewis acid adducts of dibridgehead diphosphines.

To our knowledge, there is only a single precedent for "crossed chain" *out*,*out*-**4ca'**. In earlier work, we prepared a variety of AuX adducts of dibridgehead diphosphines in which the sizes of the gold substituents X were systematically increased.[10] All of the AuX moieties were easily accommodated by the *out*,*out* diphosphines. This was not the case with the *in*,*out* diphosphines. As depicted in Scheme 5.8, when the *in* bridgehead substituent became sufficiently large, it "flipped" to the *out* position ("half turn") with concomitant crossing of one chain through the macrocycle defined by the other two (**X** →

XI). This required phenyl groups substituted with very bulky *ortho* substituents. Importantly, two sets of ^{13}C NMR signals were observed (ca. 2:1 area ratio), which requires **XI** (as opposed to **X**) to be the ground state in solution.

Since the crystal structures in Figure 5.1 represent conformers of different isomers of **4ca'**, they are not polymorphs. Nonetheless, the volumes of the unit cells can be compared. After normalizing for *Z* (4 and 1, respectively), one obtains 904.9(4) $Å^3$ and 923.3(13) $Å^3$. These correspond to densities of 1.099 and 1.067 Mg/m^3, respectively. With polymorphs, it is generally found that the denser modification is the thermodynamically more stable crystal,[23] as would typically be assayed by DSC data. Towards related ends, we are engaged in an extensive computational study of the gas phase stabilities of a variety of dibridgehead diphosphorus compounds. We had (incorrectly) thought it more likely that the "crossed chain" species would be denser due to the "occupancy" of the cavity associated with the macrocycle defined by the other two chains.

In summary, this study has explored another alkene metathesis based route to dibridgehead diphosphorus compounds. While the methodology is superior to that involving phosphine boranes in Scheme 5.4, it does not attain the efficiency of those involving precious metals in Scheme 5.1. Nonetheless, a very rare "crossed chain" variant of an *in*/*out* isomer could be characterized. Additional approaches to these target molecules, as well as a variety of unusual phenomena and applications, will be detailed in future reports.

5.4. Experimental Section

General. Reactions (except hydrogenations) were conducted under inert atmospheres using standard Schlenk techniques. Solvents were treated as follows: THF, CH_2Cl_2, hexanes, and diethyl ether, distilled by rotary evaporation or purified using a Glass Contour system; CH_3OH, pentane, $CDCl_3$ (Cambridge Isotope Laboratories), used as received. Mg turnings (Aldrich, 99.9%), $Br(CH_2)_8Br$ (TCI, 97%), $Br(CH_2)_nCH=CH_2$ (n = 4, 5; Matrix Scientific, 95%), $Br(CH_2)_{10}Br$ (Aldrich, 97%), $Br(CH_2)_{12}Br$ (Aldrich, 98%), NaH (Aldrich, 60% w/w dispersion in (solid) mineral oil), $(O=)PH(OCH_2CH_3)_2$ (Aldrich, 98%), Grubbs' first generation catalyst $(Cy_3P)_2Cl_2Ru=CHPh$ (Aldrich, 97%), and PtO_2 (Aldrich, 99.9%) were used as received; $Br(CH_2)_6CH=CH_2$[24] and $Br(CH_2)_{14}Br$[25] were prepared by literature procedures.

NMR spectra were recorded on a Varian NMRS 500 MHz instrument at ambient probe temperatures and referenced as follows (δ, ppm): ^1H, residual internal $CHCl_3$ (7.26) or C_6D_5H (7.15); $^{13}C\{^1H\}$, internal $CDCl_3$ (77.16) or C_6D_6 (128.0); $^{31}P\{^1H\}$, external H_3PO_4 (0.00). IR spectra were recorded on a Shimadzu IRAffinity-1 spectrometer with a Pike MIRacle ATR system (diamond/ZnSe crystal). Microanalyses were conducted by Atlantic Microlab.

$(O=)PH((CH_2)_4CH=CH_2)_2$ (2a). A Schlenk flask was charged with $Br(CH_2)_4CH=CH_2$ (6.201 g, 38.03 mmol) and THF (50.0 mL) and cooled to 0 °C. Then Mg turnings (1.092 g, 44.9 mmol) were added in portions with stirring (ca. 2 min). After 6 h, the cooling bath was removed. After 14 h, the mixture was filtered under nitrogen. The filtrate was cooled to 0 °C and $(O=)PH(OCH_2CH_3)_2$ (1.081 g, 7.83 mmol) in THF (30 mL) was added dropwise with stirring (ca. 15 min). The cooling bath was removed. After 3 h, the flask was cooled to 0 °C and aqueous HCl (0.10 M, 20 mL) was added dropwise over 5 min. After 1 h, the organic phase was separated. The aqueous phase was

extracted with THF (3 × 10 mL). The combined organic phases were dried (Na_2SO_4). The solvents were removed by rotary evaporation to give a colorless oil. Hexane was added, and the sample was cooled to –35 °C. After 4-10 h, the white solid was rapidly collected by filtration, as it melted with warming. The sample was dried by oil pump vacuum to give **2a** (1.292 g, 6.03 mmol, 77%) as a colorless liquid.

NMR ($CDCl_3$, δ/ppm): **^{1}H** (500 MHz) 6.72 (d, 1H, $^1J_{HP}$ = 445 Hz, P*H*), 5.63 (ddt, 2H, $^3J_{HH\textit{trans}}$ = 16.8 Hz, $^3J_{HH\textit{cis}}$ = 10.2 Hz, $^3J_{HH}$ = 6.8 Hz, C*H*=), 4.82 (br d, 2H, $^3J_{HH\textit{trans}}$ = 16.0 Hz, = CH_EH_Z), 4.86 (br d, 2H, $^3J_{HH\textit{cis}}$ = 9.6 Hz, = CH_EH_Z), 2.02-1.88 (m, 4H, CH_2CH=), 1.75-1.57 (m, 4H, PCH_2), 1.55-1.41 (m, 8H, remaining CH_2); **^{13}C{^{1}H}** (126 MHz) 137.5 (s, *C*H=), 114.7 (s, =*C*H_2), 32.8 (s, *C*H_2CH=), 29.4 (d, $^3J_{CP}$ = 13.7 Hz, P(CH_2)$_2$*C*H_2), 27.7 (d, $^1J_{CP}$ = 65.1 Hz, P*C*H_2), 20.8 (d, $^2J_{CP}$ = 3.8 Hz, PCH_2*C*H_2); **^{31}P{^{1}H}** (202 MHz) 34.4 (s). **IR** (cm^{-1}, powder film): 2914 (s), 2849 (m), 1641 (w), 1154 (s), 990 (m), 914 (s).

(O=)PH((CH$_2$)$_5$CH=CH$_2$)$_2$ (2b). The bromide Br(CH_2)$_5$CH=CH_2 (5.851 g, 33.0 mmol), THF (50.0 mL), Mg turnings (0.9752 g, 40.1 mmol), (O=)PH(OCH_2CH_3)$_2$ (1.080 g, 7.82 mmol) in THF (30 mL), and HCl (0.10 M, 20 mL) were combined in a procedure analogous to that for **2a**. An identical workup gave **2b** (1.535 g, 6.33 mmol, 81%) as a white solid, mp (capillary) 48-51 °C. Anal. calcd (%) for $C_{14}H_{27}OP$ (242.34): C, 69.39; H, 11.23; found C, 67.05; H, 11.07.[26]

NMR ($CDCl_3$, δ/ppm): **^{1}H** (500 MHz) 6.83 (d, 1H, $^1J_{HP}$ = 442.5 Hz, P*H*), 5.76 (ddt, 2H, $^3J_{HH\textit{trans}}$ = 16.8 Hz, $^3J_{HH\textit{cis}}$ = 10.2 Hz, $^3J_{HH}$ = 6.8 Hz, C*H*=), 4.97 (br d, 2H, $^3J_{HH\textit{trans}}$ = 16.0 Hz, = CH_EH_Z), 4.94 (br d, 2H, $^3J_{HH\textit{cis}}$ = 9.6 Hz, = CH_EH_Z), 2.07-1.99 (m, 4H, CH_2CH=), 1.86-1.69 (m, 4H, PCH_2), 1.66-1.55 (m, 4H, PCH_2C*H*$_2$), 1.46-1.35 (m, 8H, remaining CH_2); **^{13}C{^{1}H}** (126 MHz) 138.5 (s, *C*H=), 114.6 (s, =*C*H_2), 33.3 (s, *C*H_2CH=), 30.0 (d, $^3J_{CP}$ = 13.8 Hz, P(CH_2)$_2$*C*H_2), 28.3 (s, *C*H_2CH_2CH=), 28.1 (d, $^1J_{CP}$

= 64.9 Hz, P*C*H_2), 21.6 (d, $^2J_{CP}$ = 3.8 Hz, PCH$_2$*C*H$_2$); **^{31}P{^{1}H}** (202 MHz) 34.8 (s). **IR** (cm^{-1}, powder film): 2914 (s), 2849 (m), 1641 (w), 1154 (s), 990 (m), 914 (s).

(O=)PH((CH$_2$)$_6$CH=CH$_2$)$_2$ (2c). The bromide Br(CH$_2$)$_6$CH=CH$_2$ (9.640 g, 50.4 mmol), THF (50.0 mL), Mg turnings (1.431 g, 58.9 mmol), (O=)PH(OCH$_2$CH$_3$)$_2$ (2.176 g, 15.8 mmol) in THF (90 mL), and HCl (0.10 M, 20 mL) were combined in a procedure analogous to that for **2a**. An identical workup gave **2c** (3.348 g, 12.4 mmol, 79%) as a white solid, mp (capillary) 62-64 °C. Anal. calcd (%) for C$_{16}$H$_{31}$OP (270.40): C, 71.07; H, 11.56; found C, 70.46; H, 11.47.

NMR (CDCl$_3$, δ/ppm): **^{1}H** (500 MHz) 6.62 (d, 1H, $^1J_{HP}$ = 435.6 Hz), 5.78 (ddt, 2H, $^3J_{HH\textit{trans}}$ = 16.9 Hz, $^3J_{HH\textit{cis}}$ = 10.2 Hz, $^3J_{HH}$ = 6.7 Hz, C*H*=), 4.98 (br d, 2H, $^3J_{HH\textit{trans}}$ = 16.0 Hz, =CH$_E$*H*$_Z$), 4.95 (br d, 2H, $^3J_{HH\textit{cis}}$ = 9.6 Hz, = CH$_E$*H*$_Z$), 2.07-1.99 (m, 4H, C*H*$_2$CH=), 2.00-1.89 (m, 4H, PC*H*$_2$), 1.89-1.80 (m, 4H, PCH$_2$C*H*$_2$), 1.76-1.72 (m, 4H, PCH$_2$CH$_2$C*H*$_2$), 1.72-1.2 (br m, 8H, remaining C*H*$_2$); **^{13}C{^{1}H}** (126 MHz) 138.8 (s, *C*H=), 114.4 (s, =*C*H$_2$), 33.6 (s, *C*H$_2$CH=), 30.5 (d, $^3J_{CP}$ = 13.8 Hz, P(CH$_2$)$_2$*C*H$_2$), 28.5 (double intensity s, P(CH$_2$)$_3$(*C*H$_2$)$_2$), 28.3 (d, $^1J_{CP}$ = 65.1 Hz, P*C*H$_2$), 21.7 (d, $^2J_{CP}$ = 3.8 Hz, PCH$_2$*C*H$_2$); **^{31}P{^{1}H}** (202 MHz) 35.0 (s). **IR** (cm^{-1}, powder film): 2913 (s), 2849 (m), 1641 (w), 1154 (s), 990 (m), 914 (s).

(H$_2$C=CH(CH$_2$)$_4$)$_2$P(=O)(CH$_2$)$_{10}$(O=)P((CH$_2$)$_4$CH=CH$_2$)$_2$ (3ab'). A Schlenk flask was charged with **2a** (0.220 g, 1.03 mmol), NaH (60% w/w dispersion in mineral oil; 0.131 g, 3.28 mmol), and THF (20.0 mL), and fitted with a condenser. The mixture was heated to 65 °C. After 10 min, Br(CH$_2$)$_{10}$Br (0.150 g, 0.500 mmol) was added dropwise. The solution was refluxed overnight. The solvent was removed by rotary evaporation, and water (10 mL) and diethyl ether (10 mL) were added. The organic phase was separated, and the aqueous phase was extracted with diethyl ether (2 × 10 mL). The combined organic phases were dried (Na$_2$SO$_4$). The solvent was removed by rotary evaporation to give a

colorless viscous oil. Pentane was added, and the sample was cooled to –35 °C. After 4-10 h, the white solid was collected by filtration and dried by oil pump vacuum to give **3ab'** (0.227 g, 0.401 mmol, 80%), mp (capillary) 59-61 °C.

NMR ($CDCl_3$, δ/ppm): **^{1}H** (500 MHz) 5.75 (ddt, 4H, $^3J_{HH\textit{trans}}$ = 16.8 Hz, $^3J_{HH\textit{cis}}$ = 10.3 Hz, $^3J_{HH}$ = 6.8 Hz, C*H*=), 4.98 (br d, 4H, $^3J_{HH\textit{trans}}$ = 17.4 Hz, =CH_EH_Z), 4.93 (br d, 4H, $^3J_{HH\textit{cis}}$ = 10.4 Hz, =CH_EH_Z), 2.10-1.01 (m, 8H, C*H*=), 1.68-1.59 (m, 12H, PCH_2), 1.57-1.43 (m, 20H, CH_2), 1.39-1.30 (br m, 4H, CH_2), 1.29-1.21 (br m, 8H, remaining CH_2); **^{13}C{^{1}H}** (126 MHz) 138.0 (s, 4*C*H=), 114.9 (s, 4 =*C*H_2), 33.1 (s, 4*C*H_2CH=), 31.1 (d, $^3J_{CP}$ = 13.7 Hz, P$(CH_2)_2C$H$_2(CH_2)_4C$H$_2(CH_2)_2$P), 30.2 (d, $^3J_{CP}$ = 13.7 Hz, 4P$(CH_2)_2C$H$_2(CH_2)_3$CH=), 29.2 and 29.0 (2s, P$(CH_2)_3(C$H$_2)_4(CH_2)_3$P), 27.9 (d, $^1J_{CP}$ = 64.9 Hz, P*C*H$_2(CH_2)_6C$H$_2$P), 27.7 (d, $^1J_{CP}$ = 64.9 Hz, 4P*C*H$_2(CH_2)_5$CH=), 21.6 (d, $^2J_{CP}$ = 3.7 Hz, PCH$_2C$H$_2(CH_2)_6C$H$_2$CH$_2$P), 21.1 (d, $^2J_{CP}$ = 3.7 Hz, 4PCH$_2C$H$_2(CH_2)_4$CH=); **^{31}P{^{1}H}** (202 MHz) 48.8 (s). **IR** (cm^{-1}, powder film): 2920 (s), 2850 (m), 1641 (w), 1155 (s), 991 (m), 908 (s).

$(H_2C$=CH$(CH_2)_5)_2$P(=O)$(CH_2)_{12}$(O=)P$((CH_2)_5$CH=CH$_2)_2$ (3bc'). Compound **2b** (0.251 g, 1.04 mmol), NaH (60% w/w dispersion in mineral oil; 0.132 g, 3.31 mmol), THF (20.0 mL), and Br$(CH_2)_{12}$Br (0.163 g, 0.497 mmol) were combined in a procedure analogous to that for **3ab'**. An identical workup gave **3bc'** (0.271 g, 0.416 mmol, 84%) as a white solid, mp (capillary) 59-61 °C. Anal. calcd (%) for $C_{40}H_{76}O_2P_2$ (650.99): C, 73.80; H, 11.77; found C, 73.93; H, 11.93.

NMR ($CDCl_3$, δ/ppm): **^{1}H** (500 MHz) 5.76 (ddt, 4H, $^3J_{HH\textit{trans}}$ = 16.8 Hz, $^3J_{HH\textit{cis}}$ = 10.3 Hz, $^3J_{HH}$ = 6.8 Hz, C*H*=), 4.96 (br d, 4H, $^3J_{HH\textit{trans}}$ = 17.4 Hz, =CH_EH_Z), 4.93 (br d, 4H, $^3J_{HH\textit{cis}}$ = 10.4 Hz, =CH_EH_Z), 2.08-1.97 (m, 8H, C*H*=), 1.69-1.58 (m, 12H, PCH_2), 1.58-1.48 (m, 12H, PCH$_2$CH_2), 1.45-1.19 (br m, 32H, remaining CH_2); **^{13}C{^{1}H}** (126 MHz) 138.6 (s, 4*C*H=), 114.5 (s, 4 =*C*H_2), 33.5 (s, 4*C*H_2CH=), 31.2 (d, $^3J_{CP}$ = 13.8 Hz,

P(CH_2)$_2$*C*H$_2$(CH_2)$_6$*C*H$_2$(CH_2)$_2$P), 30.6 (d, $^3J_{CP}$ = 13.9 Hz, 4P(CH_2)$_2$*C*H$_2$(CH_2)$_3$CH=), 29.5 (s, 4P(CH_2)$_3$*C*H$_2$CH$_2$CH=), 29.3, 29.1, and 28.4 (3s, P(CH_2)$_3$(*C*H$_2$)$_6$(CH_2)$_3$P), 27.94 (d, $^1J_{CP}$ = 64.7 Hz, P*C*H$_2$(CH_2)$_{10}$*C*H$_2$P), 27.91 (d, $^1J_{CP}$ = 64.7 Hz, 4P*C*H$_2$(CH_2)$_5$CH=), 21.7 (d, $^2J_{CP}$ = 3.7 Hz, PCH$_2$*C*H$_2$(CH_2)$_8$*C*H$_2$CH$_2$P), 21.6 (d, $^2J_{CP}$ = 3.7 Hz, 4PCH$_2$*C*H$_2$(CH_2)$_4$CH=); **^{31}P{^{1}H}** (202 MHz) 48.9 (s). **IR** (cm^{-1}, powder film): 2920 (s), 2850 (m), 1641 (w), 1155 (s), 991 (m), 908 (s).

(H$_2$C=CH(CH_2)$_6$)$_2$P(=O)(CH_2)$_{14}$(O=)P((CH_2)$_6$CH=CH$_2$)$_2$ (3cd'). Compound **2c** (0.314 g, 1.16 mmol), NaH (60% w/w dispersion in mineral oil; 0.131 g, 3.28 mmol), THF (40.0 mL), and Br(CH_2)$_{14}$Br (0.180 g, 0.547 mmol) were combined in a procedure analogous to that for **3ab'**. A similar workup (all water and diethyl ether quantities doubled) gave **3cd'** (0.3176 g, 0.432 mmol, 79%) as a white solid, mp (capillary) 58-60 °C. Anal. calcd (%) for $C_{46}H_{88}O_2P_2$ (735.16): C, 75.15; H, 12.07; found C, 74.40; H, 12.29.[26]

NMR ($CDCl_3$, δ/ppm): **^{1}H** (500 MHz) 5.79 (ddt, 4H, $^3J_{HH\textit{trans}}$ = 16.9 Hz, $^3J_{HH\textit{cis}}$ = 10.3 Hz, $^3J_{HH}$ = 6.8 Hz, C*H*=), 4.98 (br d, 4H, $^3J_{HH\textit{trans}}$ = 17.2 Hz, =CH$_E$*H*$_Z$), 4.93 (br d, 4H, $^3J_{HH\textit{cis}}$ = 10.2 Hz, =C*H*$_E$H$_Z$), 2.09-1.99 (m, 8H, C*H*=), 1.69-1.60 (m, 12H, PC*H*$_2$), 1.59-1.50 (m, 12H, PCH$_2$C*H*$_2$), 1.42-1.23 (br m, 44H, remaining C*H*$_2$); **^{13}C{^{1}H}** (126 MHz) 138.8 (s, 4*C*H=), 114.3 (s, 4 =*C*H$_2$), 33.6 (s, 4*C*H$_2$CH=), 31.2 (d, $^3J_{CP}$ = 14.2 Hz, P(CH_2)$_2$*C*H$_2$(CH_2)$_8$*C*H$_2$(CH_2)$_2$P), 31.0 (d, $^3J_{CP}$ = 14.2 Hz, 4P(CH_2)$_2$*C*H$_2$(CH_2)$_3$CH=), 29.58, 29.6, 29.4, and 29.1 (4s, P(CH_2)$_3$(*C*H$_2$)$_8$(CH_2)$_3$P), 28.59 and 28.57 (2s, 4P(CH_2)$_3$(*C*H$_2$)$_2$CH$_2$CH=), 27.96 (d, $^1J_{CP}$ = 64.7 Hz, P*C*H$_2$(CH_2)$_{12}$*C*H$_2$P), 27.95 (d, $^1J_{CP}$ = 64.7 Hz, 4P*C*H$_2$(CH_2)$_5$CH=), 21.69 (d, $^2J_{CP}$ = 3.7 Hz, PCH$_2$*C*H$_2$(CH_2)$_{10}$*C*H$_2$CH$_2$P), 21.66 (d, $^2J_{CP}$ = 3.7 Hz, 4PCH$_2$*C*H$_2$(CH_2)$_4$CH=); **^{31}P{^{1}H}** (202 MHz) 48.7 (s). **IR** (cm^{-1}, powder film): 2916 (s), 2850 (m), 1641 (w), 1157 (s), 991 (m), 901 (s).

$(H_2C{=}CH(CH_2)_6)_2P(=O)(CH_2)_8(O=)P((CH_2)_6CH{=}CH_2)_2$ (3ca'). Compound **2c** (0.686 g, 2.54 mmol), NaH (60% w/w dispersion in mineral oil; 0.236 g, 5.90 mmol), THF (40.0 mL), and $Br(CH_2)_8Br$ (0.222 g, 0.816 mmol) were combined in a procedure analogous to that for **3ab'**. A similar workup (all water and diethyl ether quantities doubled) gave **3ca'** (0.441 g, 0.677 mmol, 83%) as a white solid, mp (capillary) 57-59 °C. Anal. calcd (%) for $C_{40}H_{76}O_2P_2$ (650.99): C, 73.80; H, 11.77; found C, 73.59; H, 11.79.

NMR ($CDCl_3$, δ/ppm): **^{1}H** (500 MHz) 5.79 (ddt, 4H, $^3J_{HH\textit{trans}}$ = 16.9 Hz, $^3J_{HH\textit{cis}}$ = 10.3 Hz, $^3J_{HH}$ = 6.8 Hz, C*H*=), 4.98 (br d, 4H, $^3J_{HH\textit{trans}}$ = 17.2 Hz, $=CH_EH_Z$), 4.93 (br d, 4H, $^3J_{HH\textit{cis}}$ = 10.2 Hz, $=CH_EH_Z$), 2.07-1.99 (m, 8H, C*H*=), 1.67-1.59 (m, 12H, PCH_2), 1.58-1.49 (m, 12H, PCH_2CH_2), 1.41-1.35 (m, 16H, CH_2), 1.35-1.26 (br m, 16H, CH_2); **^{13}C{^{1}H}** (126 MHz) 138.8 (s, 4*C*H=), 114.3 (s, 4 $=CH_2$), 33.6 (s, $4CH_2CH{=}$), 31.1 (d, $^3J_{CP}$ = 14.2 Hz, $P(CH_2)_2CH_2(CH_2)_2CH_2(CH_2)_2P$), 30.9 (d, $^3J_{CP}$ = 14.2 Hz, $4P(CH_2)_2CH_2(CH_2)_3CH{=}$), 28.9 (s, $P(CH_2)_3(CH_2)_2(CH_2)_3P$), 28.57 and 28.56 (2s, $4P(CH_2)_3(CH_2)_2CH_2CH{=}$), 28.0 (d, $^1J_{CP}$ = 64.7 Hz, $4PCH_2(CH_2)_5CH{=}$ and $PCH_2(CH_2)_6CH_2P$), 21.7 (d, $^2J_{CP}$ = 3.5 Hz, $4PCH_2CH_2(CH_2)_4CH{=}$), 21.6 (d, $^2J_{CP}$ = 3.5 Hz, $PCH_2CH_2(CH_2)_4CH_2CH_2P$); **^{31}P{^{1}H}** (202 MHz) 48.6 (s). **IR** (cm^{-1}, powder film): 2926 (s), 2855 (m), 1638 (w), 1144 (s), 991 (m), 905 (s).

$(O=)P((CH_2)_{12})_3P(=O)$ (4bc'). A Schlenk flask was charged with **3bc'** (0.513 g, 0.788 mmol), Grubbs' first generation catalyst (0.0632 g, 0.077 mmol, 9.8 mol%), and CH_2Cl_2 (750 mL), and fitted with a condenser. The solution (0.00105 M in **3bc'**) was refluxed with stirring (48 h), concentrated to ca. 20 mL by rotary evaporation, and transferred to a Fischer-Porter bottle. Then PtO_2 (0.1004 g, 0.442 mmol) and H_2 (5 bar) were added. The mixture was stirred (48 h). The solvent was removed by rotary evaporation, and CH_2Cl_2 was added. The sample was chromatographed on silica (3.5 × 14 cm column), which was eluted with CH_3OH/CH_2Cl_2 (1:50 v/v). The solvents were

removed from the main product containing fraction to give **4bc'** (0.0916 g, 0.153 mmol, 19%) as a light brown solid, mp (capillary) 67-69 °C. Other fractions containing smaller amounts of other products were saved for crystallizations described below (R_f, TLC, 95:5 v/v CH_2Cl_2/CH_3OH): **4bc'**, 0.20; **4'bc'**, 0.18).

NMR ($CDCl_3$, δ/ppm): **^{1}H** (500 MHz) 1.76-1.63 (m, 12H, PCH_2), 1.61-1.50 (m, 12H, PCH_2CH_2), 1.47-1.37 (m, 12H, $P(CH_2)_2CH_2$), 1.36-1.23 (br m, 36H, remaining CH_2); **^{13}C{^{1}H}** (126 MHz) 30.2 (minor, d, $^3J_{CP}$ = 11.4 Hz, $P(CH_2)_2CH_2$), 30.1 (major, d, $^3J_{CP}$ = 13.8 Hz, $P(CH_2)_2CH_2$), 28.7 (major, s, CH_2), 28.3 (major, s, CH_2), 28.21 (minor s, CH_2), 28.1 (minor, s, CH_2), 28. (minor, CH_2), 27.9 (major, s, CH_2), 27.1 (major + minor, d, $^1J_{CP}$ = 64.4 Hz, $2PCH_2$), 21.5 (minor, d, $^2J_{CP}$ = 3.5 Hz, PCH_2CH_2), 21.0 (major, d, $^2J_{CP}$ = 3.6 Hz, PCH_2CH_2); **^{31}P{^{1}H}** (202 MHz) 51.3 (s, 30%), 50.90 (s, 70%). **IR** (cm^{-1}, powder film): 2914 (s), 2851 (m), 1655 (s), 1255 (w), 1145 (m), 990 (s).

(O=)P(CH$_2$)$_8$((CH$_2$)$_{14}$)$_2$P(=O) (4ca'). Compound **4ca'** (0.477 g, 0.732 mmol), Grubbs' first generation catalyst (0.0643 g, 0.078 mmol, 10.7 mol%), CH_2Cl_2 (750 mL; the resulting solution is 0.00098 M in **4ca'**), PtO_2 (0.1002 g, 0.441 mmol), and H_2 (5 bar) were combined in a procedure analogous to that for **4bc'**. An identical workup gave **4ca'** (0.0629 g, 0.105 mmol, 14%) as a light brown solid, mp (capillary) 67-69 °C.

NMR ($CDCl_3$, δ/ppm):[27] **^{1}H** (500 MHz) 1.74-1.61 (m, 12H, PCH_2), 1.60-1.50 (m, 12H, PCH_2CH_2), 1.441.36 (m, 12H, $P(CH_2)_2CH_2$), 1.33-1.25 (br m, 36H, remaining CH_2); **^{13}C{^{1}H}** (126 MHz) 30.7 (minor, d, $^3J_{CP}$ = 12.2 Hz, $P(CH_2)_2CH_2$), 30.6 (major, d, $^3J_{CP}$ = 14.1 Hz, $P(CH_2)_2CH_2$), 29.25 (s, $3CH_2$), 29.01 (minor, s, CH_2), 29.03 (minor, s, CH_2), 28.9 (major, s, CH_2), 28.8 (minor, s, CH_2), 28.7 (minor, s, CH_2), 28.5 (major, s, CH_2), 28.1 (minor, d, $^1J_{CP}$ = 64.6 Hz, PCH_2), 27.5 (major, d, $^1J_{CP}$ = 64.6 Hz, PCH_2), 21.6 (minor, d, $^2J_{CP}$ = 3.8 Hz, PCH_2CH_2), 21.4 (major, d, $^2J_{CP}$ = 3.4 Hz, PCH_2CH_2); **^{31}P{^{1}H}** (202 MHz) 50.11 (s, 70%), 49.95 (s, 30%). **IR** (cm^{-1}, powder film): 2918 (s), 2849 (m),

1728 (s), 1260 (w), 1145 (m), 991 (s).

Crystallography. **A.** A CH_2Cl_2 solution of **3ab'** was layered with pentane. After 7 d, colorless needles were collected and data obtained as outlined in Table 5.1. Cell parameters were obtained from 180 data frames using a 0.5° scan and refined with 9519 reflections. Integrated intensity information for each reflection was obtained by reduction of the data frames with the program APEX2.[28] Lorentz and polarization corrections were applied. Data were scaled, and absorption corrections were applied using the program SADABS.[29] The structure was solved by direct methods using SHELXTL (SHELXS) and refined (weighted least squares refinement on F^2) using SHELXTL.[30] Non-hydrogen atoms were refined with anisotropic thermal parameters. Hydrogen atoms were placed in idealized positions and refined using a riding model. **B.** A CH_2Cl_2 solution of **3bc'**was layered with hexane. After 5 d, colorless blocks were collected and data obtained as outlined in Table 5.1. The structure was solved as in A (45 frames, 1° scan, 29802 reflections), but using APEX3[31] in place of APEX2 and SADABS. The elongated thermal ellipsoids on C25 and C26 suggested that these two atoms were disordered, and refinement gave an occupancy ratio of 63:37. **C.** A CH_2Cl_2 solution of one of the minor product fractions obtained upon chromatographic purification of **4bc'** was layered with hexane. After 2 d, colorless needles were collected and data obtained as outlined in Table 5.1. The structure (**4bc'**) was solved as in A (12866 reflections). **D.** A $CHCl_3$ solution of **4ca'** was allowed to slowly concentrate. After 2 d, colorless plates were collected and data obtained as outlined in Table 5.1. The structure was solved as in A (2100 frames, 0.5° scan, 20742 reflections) but using SAINT[32] in place of APEX2. **E.** A second $CHCl_3$ solution of **4ca'** was allowed to slowly concentrate. After 1 d, colorless plates were collected and data obtained as outlined in Table 5.1. The structure – different from that in D – was solved as in A (7297 reflections).

5.5. References

(1) Alder, R. W.; East, S. P. *Chem. Rev.* **1996**, *96*, 2097-2011.

(2) Kharel, S.; Joshi, H.; Bierschenk, S.; Stollenz, M.; Taher, D.; Bhuvanesh, N.; Gladysz, J. A. *J. Am. Chem. Soc.* **2017**, *139*, 2172-2175.

(3) (a) Nawara, A. J.; Shima, T.; Hampel, F.; Gladysz, J. A. *J. Am. Chem. Soc.* **2006**, *128*, 4962-4963. (b) Nawara-Hultzsch, A. J.; Stollenz, M.; Barbasiewicz, M.; Szafert, S.; Lis, T.; Hampel, F.; Bhuvanesh, N.; Gladysz, J. A. *Chem. Eur. J.* **2014**, *20*, 4617-4637.

(4) (a) Wang, L.; Shima, T. Hampel, F.; Gladysz, J. A. *Chem. Commun.* **2006**, 4075-4077. (b) Estrada, A. L.; Jia, T.; Bhuvanesh, N.; Blümel, J.; Gladysz, J. A. *Eur. J. Inorg. Chem.* **2015**, *2015*, 5318-5321.

(5) Stollenz, M.; Barbasiewicz, M.; Nawara-Hultzsch, A. J.; Fiedler, T.; Laddusaw, R. M.; Bhuvanesh, N.; Gladysz, J. A. *Angew. Chem., Int. Ed*. **2011**, *50*, 6647–6651; *Angew. Chem.* **2011**, *123*, 6777-6781.

(6) Alder, R. W.; Butts, C. P.; Orpen, A. G.; Read, D.; Oliva, J. M. *J. Chem. Soc., Perkin Trans. 2* **2001**, 282-287, and references therein. The conjugate acid of the analog with three $(CH_2)_4$ bridges has been reported, but attempted deprotonations afford deep-seated rearrangements.

(7) Park, C. H.; Simmons, H. E. *J. Am. Chem. Soc.* **1968**, *90*, 2429-2431.

(8) Baechler, R. D.; Mislow, K. *J. Am. Chem. Soc.* **1970**, *92*, 3090-3093.

(9) (a) Haines, A. H.; Karntiang, P. *J. Chem. Soc. Perkin Trans. 1* **1979**, 2577-2587. (b) Wareham, R. S.; Kilburn, J. D.; Turner, D. L.; Rees, N. H.; Holmes, D. S. *Angew. Chem., Int. Ed. Engl.* **1995**, *34*, 2660-2662; *Angew. Chem.* **1995**, *107*, 2902-2904. (c) Saunders, M.; Krause, N. *J. Am. Chem. Soc.* **1990**, *112*, 1791-1795. (d) Alder, R. W.; Heilbronner, E.; Honegger, E.; McEwan, A. B.; Moss, R. E.; Olefirowicz, E.; Petillo, P.

A.; Sessions, R. B.; Weisman, G. R.; White, J. M.; Yang, Z.-Z. *J. Am. Chem. Soc.* **1993**, *115*, 6580-6591.

(10) (a) Stollenz, M.; Bhuvanesh, N.; Reibenspies, J. H.; Gladysz, J. A. *Organometallics* **2011**, *30*, 6510-6513. (b) Stollenz, M.; Taher, D.; Bhuvanesh, N.; Reibenspies, J. H.; Baranová, Z.; Gladysz, J. A. *Chem. Commun.* **2015**, *51*, 16053-16056.

(11) (a) Lang, G. M.; Shima, T.; Wang, L.; Cluff, K. J.; Skopek, K.; Hampel, F.; Blümel, J.; Gladysz, J. A. *J. Am. Chem. Soc*. **2016**, *138*, 7649-7663. (b) Lang, G. M.; Skaper, D.; Hampel, F.; Gladysz, J. A. *Dalton Trans.* **2016**, *45*, 16190-16204.

(12) Hilliard, C. R. Diphosphine Dioxide Cages and Hydrogen Peroxide Adducts of Phosphine Oxides: Syntheses and Applications in Surface Science. Doctoral dissertation, Texas A&M University, Texas, USA, 2013.

(13) (a) Williams, R. H.; Hamilton, L. A. *J. Am. Chem. Soc.* **1952**, *74*, 5418-5420. (b) Williams, R. H.; Hamilton, L. A. *J. Am. Chem. Soc.* **1955**, *77*, 3411-3412. (c) Miller, R. C.; Bradley, J. S.; Hamilton, L. A. *J. Am. Chem. Soc.* **1956**, *78*, 5299-5303. (d) Hunt, B. B.; Saunders, B. C. *J. Chem. Soc.* **1957**, 2413-2414. (e) Hays, H. R. *J. Org. Chem.* **1968**, *33*, 3690-3694.

(14) (a) Pietro, W. J.; Hehre, W. J. *J. Am. Chem. Soc.* **1982**, *104*, 3594-3595. (b) Kenttämaa, H. I.; Cooks, R. G. *J. Am. Chem. Soc.* **1985**, *107*, 1881-1886.

(15) (a) Tsvetkov, E. N.; Bondarenko, N. A.; Malakhova, I. G.; Kabachnik, M. I. *Synthesis* **1986**, 198-208. (b) Kendall, A. J.; Seidenkranz, D. T.; Tyler, D. R. *Organometallics* **2017**, *36*, 2412-2417.

(16) (a) Fiedler, T.; Bhuvanesh, N.; Hampel, F.; Reibenspies, J. H.; Gladysz, J. A. *Dalton Trans.* **2016**, *45*, 7131-7147. (b) Hess, G. D.; Fiedler, T.; Hampel, F.; Gladysz, J. A. *Inorg. Chem.* **2017**, *56*, 7454-7469.

(17) (a) Joshi, H.; Kharel, S.; Ehnbom, A.; Skopek, K.; Hess, G. D.; Fiedler, T.;

Hampel, F.; Bhuvanesh, N.; Gladysz, J. A. *J. Am. Chem. Soc.* **2018**, *140*, in press. DOI: 10.1021/jacs.8b02846. (b) Steigleder, E.; Shima, T.; Lang, G. M.; Ehnbom, A.; Hampel, F.; Gladysz, J. A. *Organometallics* **2017**, *36*, 2891-2901. (c) Fiedler, T.; Chen, L.; Wagner, N. D.; Russell, D. R.; Gladysz, J. A. *Organometallics* **2016**, *35*, 2071-2075.

(18) Bauer, I.; Habicher, W. D. *Collect. Czech. Chem. Commun.* **2004**, *69*, 1195-1230.

(19) Friedrichsen, B. P.; Powell, D. R.; Whitlock, H. W. *J. Am. Chem. Soc.* **1990**, *112*, 8931-8941.

(20) (a) Däbritz, F.; Jäger, A.; Bauer, I. *Eur. J. Org. Chem.* **2008**, 5571-5576. (b) Däbritz, F.; Theumer, G.; Gruner, M.; Bauer, I. *Tetrahedron* **2009**, *65*, 2995-3002.

(21) Jung, M. E.; Piizzi, G. *Chem. Rev.* **2005**, *105*, 1735-1766.

(22) Zong, J.; Mague, J. T.; Kraml, C. M.; Pascal, R. A. Jr. *Org. Lett.* **2013**, *15*, 2179-2181.

(23) Burger, A.; Ramberger, R. *Mikrochimica Acta* **1979**, *72*, 259-271.

(24) (a) Roux, M.-C.; Paugam, R.; Rousseau, G. *J. Org. Chem.* **2001**, *66*, 4304-4310. (b) Appel, R. *Angew. Chem., Int. Ed. Engl.* **1975**, *14*, 801-811; *Angew. Chem.* **1975**, *87*, 863-874.

(25) Nguyen, T. B.; Castanet, A.-S.; Nguyen, T.-H.; Nguyen, K. P. P.; Bardeau, J.-F.; Gibaud, A.; Mortier, J. *Tetrahedron* **2006**, *62*, 647-651.

(26) This microanalysis poorly or marginally agrees with the empirical formula, but is nonetheless reported as the best obtained to date. The NMR spectra indicate high purities ($\geq$ 98%). See also Gabbaï, F. P.; Chirik, P. J.; Fogg, D. E.; Meyer, K.; Mindiola, D. J.; Schafer, L. L.; You, S.-L. **2016**, *35*, 3255-3256.

(27) For this compound, the ^{13}C NMR signals labeled minor can refer to the $(CH_2)_8$ chain (lowered intensity compared to the signals for the two $(CH_2)_{14}$ chains), or

the minor component by ^{31}P NMR.

(28) *APEX2*, Bruker AXS Inc., Madison, WI, USA, 2012.

(29) Sheldrick, G. M. *SADABS*, Bruker AXS Inc., Madison, WI, USA, 2001.

(30) (a) Sheldrick, G. M. *Acta Cryst.* **2008**, *A64*, 112-122. (b) Sheldrick, G. M. *Acta Cryst.* **2015**, *A71*, 3-8. (c) Sheldrick, G. M. *Acta Cryst.* **2015**, *C71*, 3-8.

(31) *APEX3*, Bruker AXS Inc., Madison, WI, USA, 2012.

(32) *SAINT*, Bruker AXS Inc., Madison, WI, USA, 2012.

Table 5.1. Summary of crystallographic data for the isomers of **4ca'**.

	out,*out*-**4ca'**	"crossed chain" *out*,*out*-**4ca'**
empirical formula	$C_{36}H_{72}O_2P_2$	$C_{36}H_{72}O_2P_2$
formula weight	598.88	598.88
temperature [K]	110(2)	110(2)
diffractometer	Bruker Gadds X-ray	Bruker Gadds X-ray
wavelength [Å]	1.54178	1.54178
crystal system	monoclinic	triclinic
space group	$P2_1/c$	P-1
unit cell dimensions:		
a [Å]	21.448(6)	5.639(5)
b [Å]	5.7115(17)	11.995(9)
c [Å]	30.969(8)	14.560(11)
α [°]	90	100.25(4)
β [°]	107.440(13)	96.86(4)
γ [°]	90	102.74(4)
V [Å^3]	3619.4(17)	932.3(13)
Z	4	1
ρ_{calc} [Mg/m^3]	1.099	1.067
μ [mm^{-1}]	1.288	1.250
F(000)	1336	334
crystal size [mm^3]	0.10 × 0.01 × 0.01	0.08 × 0.08 × 0.03
Θ limit [°]	2.16 to 64.04	3.127 to 59.985
index range (h, k, l)	–24, 24; –24, 6; –35, 32	–6, 6; –13, 12; –15, 16
reflections collected	20742	7297
independent reflections	5695	2596
R(int)	0.3090	0.0817
completeness to Θ	94.6	93.2
max. and min. transmission	0.7524 and 0.5155	0.7522 and 0.6150
data/restraints/parameters	5695/0/362	2596/0/182
goodness-of-fit on F^2	1.011	0.954
R indices (final) [$I > 2\sigma(I)$]		
R_1	0.1024	0.0802
wR_1	0.1908	0.2032
R indices (all data)		
R_2	0.2216	0.1187
wR_2	0.2291	0.2375
largest diff. peak and hole [eÅ^{-3}]	0.467 and –0.467	0.521 and –0.350

Table 5.2. Key crystallographic distances [Å] and angles [°] for the isomers of **4ca'**

	out,*out*-**4ca'**	"crossed chain" *out*,*out*-**4ca'**[a]
P-O	1.493(5) 1.505(5)	1.496(3)
P-C	1.786(7) 1.789(7) 1.814(7) 1.779(7) 1.779(7) 1.796(7)	1.809(5) 1.791(5) 1.807(5)
P-P	11.540	12.152
C-P-O	110.2(3) 113.7(3) 112.3(3) 110.6(3) 113.8(3) 112.8(4)	113.4(2) 112.8(2) 110.9(2)
C-P-C	106.9(4) 106.1(3) 107.2(4) 106.5(3) 106.4(3) 106.4(4)	107.2(2) 106.2(2) 105.8(2)

[a]There are fewer values for the "crossed chain" isomer due to the C_2 symmetry axis.

Table 5.3. Summary of crystallographic data for other structurally characterized compounds.

	3ab'	**3bc'**	**4'bc'**
empirical formula	$C_{34}H_{64}O_2P_2$	$C_{40}H_{76}O_2P_2$	$C_{36}H_{72}O_2P_2$
formula weight	566.79	650.94	598.87
temperature [K]	110(2)	150.0	296(2)
diffractometer	Bruker Gadds X-ray	Bruker Venture X-ray	Bruker Gadds X-ray
wavelength [Å]	1.54178	1.54178	1.54178
crystal system	monoclinic	monoclinic	monoclinic
space group	P_21	C_12_1	P_12_1/c_1
unit cell dimensions:			
a [Å]	5.1106(9)	36.634(2)	21.021(3)
b [Å]	32.060(4)	5.0635(3)	5.0517(7)
c [Å]	10.7574(17)	24.2310(12)	17.302(2)
α [°]	90	90	90
β [°]	97.043(10)	112.966(2)	107.507(7)
γ [°]	90	90	90
V [Å^3]	1749.2(5)	4138.5(4)	1752.2(4)
Z	2	4	2
ρ_{calc} [Mg/m^3]	1.076	1.045	1.135
μ [mm^{-1}]	1.311	1.161	1.330
F(000)	628	1448	668
crystal size [mm^3]	0.47 × 0.02 × 0.01	0.207 × 0.09 × 0.029	0.098 × 0.022 × 0.005
Θ limit [°]	2.76 to 49.99	2.596 to 70.273	2.204 to 49.968
index range (h, k, l)	–5, 4; –31, 30; –10, 9	–44, 44; –5, 6; –28, 29	–20, 20; –4, 4; –16, 16
reflections collected	9519	29802	12866
independent reflections	3054	7623	1754
R(int)	0.0456	0.0745	0.1732
completeness to Θ	96.8	99.6	55.6
max. and min. transmission	0.9870 and 0.5778	0.7533 and 0.5832	0.7519 and 0.5344
data/restraints/parameters	3054/1/344	7623/69/417	1754/16/181
goodness-of-fit on F^2	1.070	1.127	1.068
R indices (final) [$I > 2\sigma(I)$]			
R_1	0.0434	0.0630	0.0698
wR_1	0.1133	0.1252	0.1613
R indices (all data)			
R_2	0.0496	0.0761	0.1101
wR_2	0.1190	0.1237	0.1775
largest diff. peak and hole [eÅ^{-3}]	0.397 and –0.244	0.365 and –0.392	0.276 and −0.588

Table 5.4. Key crystallographic bond lengths [Å] and angles [°] for other structurally characterized compounds.

	3ab'	**3bc'**	**4'bc'**[a]
P-O	1.498(4) 1.490(4)	1.488(4) 1.486(4)	1.501(4)
P-C	1.778(5) 1.811(5) 1.826(5) 1.802(6) 1.819(5) 1.826(5)	1.807(4) 1.811(4) 1.809(4) 1.807(4) 1.808(4) 1.813(4)	1.800(6) 1.794(6) 1.801(5)
C-P-O	112.9(2) 113.2(2) 112.6(2) 113.2(2) 112.2(2) 113.8(2)	113.56(19) 113.4(2) 113.0(2) 113.4(2) 113.7(2) 112.4(2)	113.4(2) 112.9(2) 113.4(2)
C-P-C	105.6(2) 106.9(2) 104.9(2) 106.1(2) 107.3(3) 103.4(2)	104.6(2) 104.6(2) 106.8(2) 103.9(2) 107.8(2) 104.8(2)	105.0(3) 105.9(3) 105.5(3)

[a]There are fewer values for this diphosphine dioxide due to the C_2 symmetry axis.

6. SUMMARY AND CONCLUSION

Section 1 has described the literature precedent of both *cis* and *trans* coordinated platinum complexes. The work in this dissertation focused on expanding the compound scope and accessing their utility.

Section 2 has provided a general synthetic route towards *cis* coordinated square planar platinum dichloride complexes bearing dibridgehead diphosphine ligands termed "parachute like". In addition, similar complexes with diphos*phite* ligands were also synthesized. The macrocycles on these complexes varied in size and could jump over the platinum chloride moiety when sufficiently large. This rare topological isomerism known as "jump rope" isomerism is reminiscent of a triple axel. Thermal equilibrations and DFT calculations suggested that these "parachute like" complexes are less stable than their isomeric form that has chlorine atoms *trans* at the platinum. The diphosphite analogs of these complexes, however, were more stable in their *cis* geometry than *trans* form, as suggested by DFT calculations.

Section 3 has expanded the size of *trans* platinum gyroscope complexes by increasing the number of atoms in the macrocycle. Gyroscopes bearing 33 membered macrocycles have been synthesized. Thermal equilibrations also showed that the compounds obtained from *inter*ligand ring closing metathesis reactions are thermodynamically more stable in their *trans* platinum dichloride form as opposed to *cis*. The same applied for bisphosphine platinum dichloride complexes. The possibilities for topologically novel compounds are endless if new monophosphine ligands $P((CH_2)_mCH=CH_2)_3$ are applied to other metals and coordination geometries.

The container molecules described in section 4 were efficient in transporting metal dichlorides, and even distinguished one metal from the other, indicative of bearing a great

potential. These systems incorporated guests by an uncommon dynamic process, homeomorphism and did not require disassembly as many other container molecules in this field do. Thermodynamic selectivity of guest transport was obtained from several U-tube transport experiments and found to be $PtCl_2/PdCl_2 > NiCl_2$, while kinetic selectivity was $PdCl_2 > PtCl_2$.

The study in section 5 has explored a low-yielding, yet viable synthesis of dibridgehead diphosphorus compounds via alkene metathesis. Though its efficiency still falls behind the schemes involving precious metals, the methodology is superior to that involving phosphine boranes. A very rare "crossed chain" variant of an *in*/*out* isomer was characterized crystallographically. This isomer was not interconvertible to the *out/out* variant *via* homeomorphic isomerism, but rather required cleavage of P-C bond, thus, rendering the process unfeasible. The crystal structure of the product obtained from *intra*ligand ring closing metathesis reactions was also characterized via X-ray crystallography. This type of ring closing pathway was found to be rare as compared to the complexes involving precious metals.

The studies in this dissertation have greatly expanded the scope of the platinum-based gyroscopes and provided detailed structural and dynamic properties providing relevant insight for related complexes. Future studies should focus on synthesizing larger empty diphosphine cages and utilizing them to capture small molecules. This application can potentially be helpful in the field of drug delivery. Another project should focus on study of radioactive metal capture using diphosphine dioxide cages. There is enough literature precedent that phosphine oxides can be used to capture lanthanides, however, the cage molecules presented in this dissertation could have an added benefit of cage effect, hence selectivity.

APPENDIX A

A-1. Additional NMR data for section 2.

***cis*-$PtCl_2(P((CH_2)_9CH=CH_2)_3)_2$ (*cis*-1f).** Degassed distilled water (10 mL), K_2PtCl_4 (0.2998 g, 0.7223 mmol), and $P((CH_2)_9CH=CH_2)_3$ (0.7092 g, 1.445 mmol)[A1] were combined in a procedure analogous to that for *cis*-**1b**.[A1] An identical workup gave *trans*-**1f** (0.1472 g, 0.118 mmol, 16%)[A2] as a yellow oil and *cis*-**1f** (0.4629 g, 0.371 mmol, 51%) as a white solid, mp (capillary) 46-47 ºC. Data for the latter follow. Anal. Calcd. (%) for $C_{66}H_{126}P_2Cl_2Pt$ (1247.64): C, 63.54; H, 10.18. Found C, 63.25; H, 10.33.

NMR ($CDCl_3$, δ/ppm): **^{1}H** (500 MHz) 5.77 (ddt, 6H, $^3J_{HH\textit{trans}}$ = 17.1 Hz, $^3J_{HH\textit{cis}}$ = 10.2 Hz, $^3J_{HH}$ = 6.4 Hz, C*H*=), 4.95 (br d, 6H, $^3J_{HH\textit{trans}}$= 17.2 Hz, $=CH_EH_Z$), 4.89 (br d, 6H, $^3J_{HH\textit{cis}}$ = 10.3 Hz, $=CH_EH_Z$), 2.06-1.97 (m, 12H, $CH_2CH=$), 1.97-1.88 (m, 12H, PCH_2), 1.57-1.46 (m, 12H, PCH_2CH_2), 1.42-1.20 (m, 72H, remaining CH_2); **^{13}C{^{1}H}** (126 MHz)[A3] 138.9 (s, *C*H=), 114.0 (s, $=CH_2$), 33.6 (s, $CH_2CH=$), 30.9 (virtual t,[A4] J_{CP} = 6.5 Hz, $PCH_2CH_2CH_2$), 29.3 (s, $2CH_2$), 29.1 (s, CH_2), 29.0 (s, CH_2), 28.8 (s, CH_2), 24.6 (br s, PCH_2CH_2), 24.3 (br s, PCH_2); **^{31}P{^{1}H}** (202 MHz) 0.97 (s, J_{PPt} = 3516 Hz[A5]). **IR** (cm^{-1}, powder film): 2915 (s), 2849 (m), 1641 (m), 1466 (m), 909 (s), 716 (m).

***cis*-$PtCl_2(P((CH_2)_{10}CH=CH_2)_3)_2$ (*cis*-1g).** Degassed distilled water (10 mL), K_2PtCl_4 (0.3001 g, 0.7230 mmol), and $P((CH_2)_{10}CH=CH_2)_3$ (0.7701 g, 1.445 mmol)[A2] were combined in a procedure analogous to that for *cis*-**1b**.[A1] An identical workup gave *trans*-**1g** (0.2144 g, 0.161 mmol, 22%)[A2] as a yellow oil and *cis*-**1g** (0.4248 g, 0.319 mmol, 44%) as a white solid, mp (capillary) 42-43 ºC. Data for the latter follow. Anal. Calcd. (%) for $C_{72}H_{138}P_2Cl_2Pt$ (1331.80): C, 64.93; H, 10.44. Found C, 64.65; H, 10.45.

NMR ($CDCl_3$, δ/ppm): **^{1}H** (500 MHz) 5.80 (ddt, 6H, $^3J_{HH\textit{trans}}$ = 17.1 Hz, $^3J_{HH\textit{cis}}$ = 10.2 Hz, $^3J_{HH}$ = 6.7 Hz, C*H*=), 4.98 (br d, 6H, $^3J_{HH\textit{trans}}$ = 16.9 Hz, $=CH_EH_Z$), 4.92 (br

d, 6H, $^{3}J_{HHcis}$ = 10.2 Hz, =CH_EH$_Z$), 2.09-1.99 (m, 12H, CH_2CH=), 1.99-1.89 (m, 12H, PCH_2), 1.57-1.47 (m, 12H, PCH$_2$CH_2), 1.44-1.20 (m, 84H, remaining CH_2); **^{13}C{^{1}H}** (126 MHz)[A3] 139.1 (s, *C*H=), 114.1 (s, =CH$_2$), 33.8 (s, *C*H$_2$CH=), 31.1 (virtual t,[A4] J_{CP} = 7.0 Hz, PCH$_2$CH$_2$*C*H$_2$), 29.6 (s, *C*H$_2$), 29.53 (s, *C*H$_2$), 29.50 (s, *C*H$_2$), 29.3 (s, *C*H$_2$), 29.1 (s, *C*H$_2$), 28.9 (s, *C*H$_2$), 24.7 (br s, PCH$_2$*C*H$_2$), 24.5 (br s, P*C*H$_2$); **^{31}P{^{1}H}** (202 MHz) 0.92 (s, J_{PPt} = 3518 Hz[A5]). **IR** (cm^{-1}, powder film): 2915 (s), 2844 (m), 1466 (m), 906 (s), 716 (m).

A-2. Calculation, limiting $\Delta G^{\ddagger}$ value, methylene bridge exchange for *cis*-2c.

Applicable equations include the following:[A6]

$$\Delta G^{\ddagger}_{T\,coal}\ (\text{kcal/mol}) = (0.004575)T_{coal}[10.319 + \log (T_{coal}/k_A)] \quad (1)$$

$$k_A = p_B/\tau_c;$$

$$\tau_c = X/2\pi\delta\nu;$$

All $(CH_2)_{14}$ positions of *cis*-**2c** are equally populated, so the values of p_B and p_A are each 0.50. Per the 25 °C spectrum in Figure s1 (see asterisked peaks):

$$\delta\nu = \nu_A - \nu_B = 0.38\ \text{ppm} = 47.88\ \text{Hz}.$$

A lower limit for T_{coal} (120 °C, 393.15K) is available from the 120 °C spectrum in Figure s1.

Table 6.1 in reference A6 gives X = 1.4142 Hz·K^{-1} for $p_A - p_B = 0$.

This in turn gives the following values: τ_c = 0.004701 K^{-1} and k_A = 106.3637 K

These terms are substituted into the preceding equations, with equation (1) becoming:

$$\Delta G^{\ddagger}_{393K}\ (\text{kcal/mol}) \geq (0.004575)(393)[10.319 + \log (393/106.3637)]$$

$$\Delta G^{\ddagger}_{393K} \geq 19.6\ \text{kcal/mol}$$

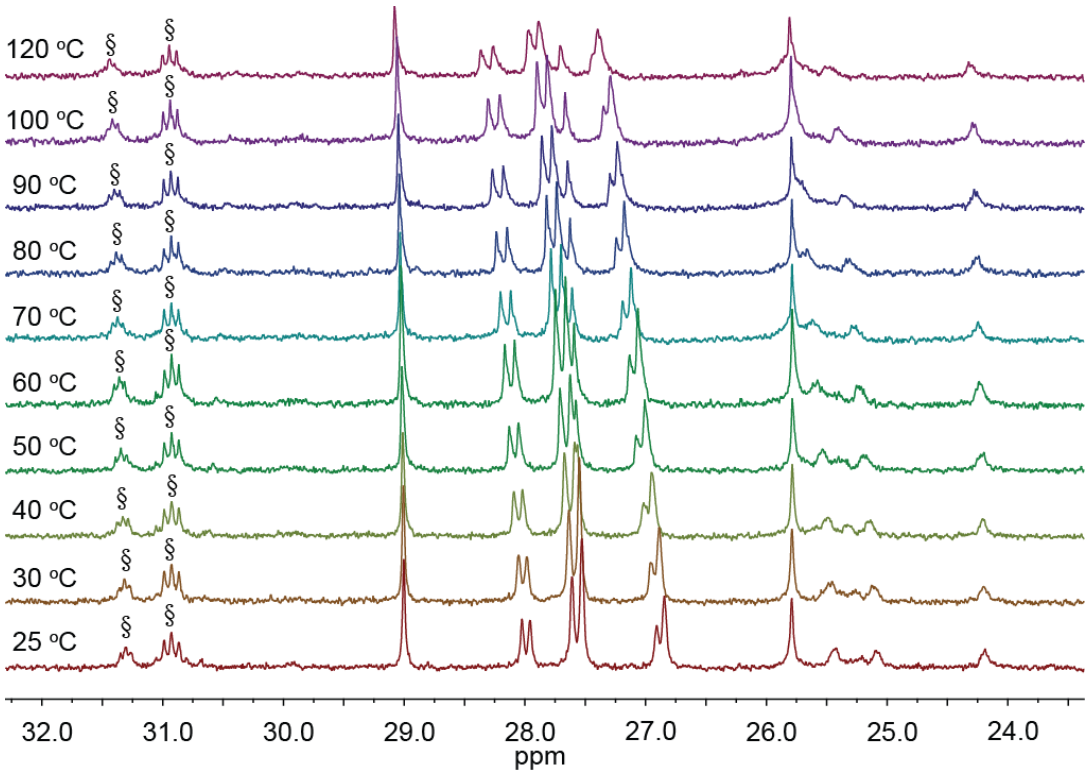

Figure A-1. $^{13}C\{^{1}H\}$ NMR spectra of *cis*-**2c** (126 MHz, C_6D_5Br) as a function of temperature. The signals used for the $\Delta G^{\ddagger}$ calculation are denoted with a §.

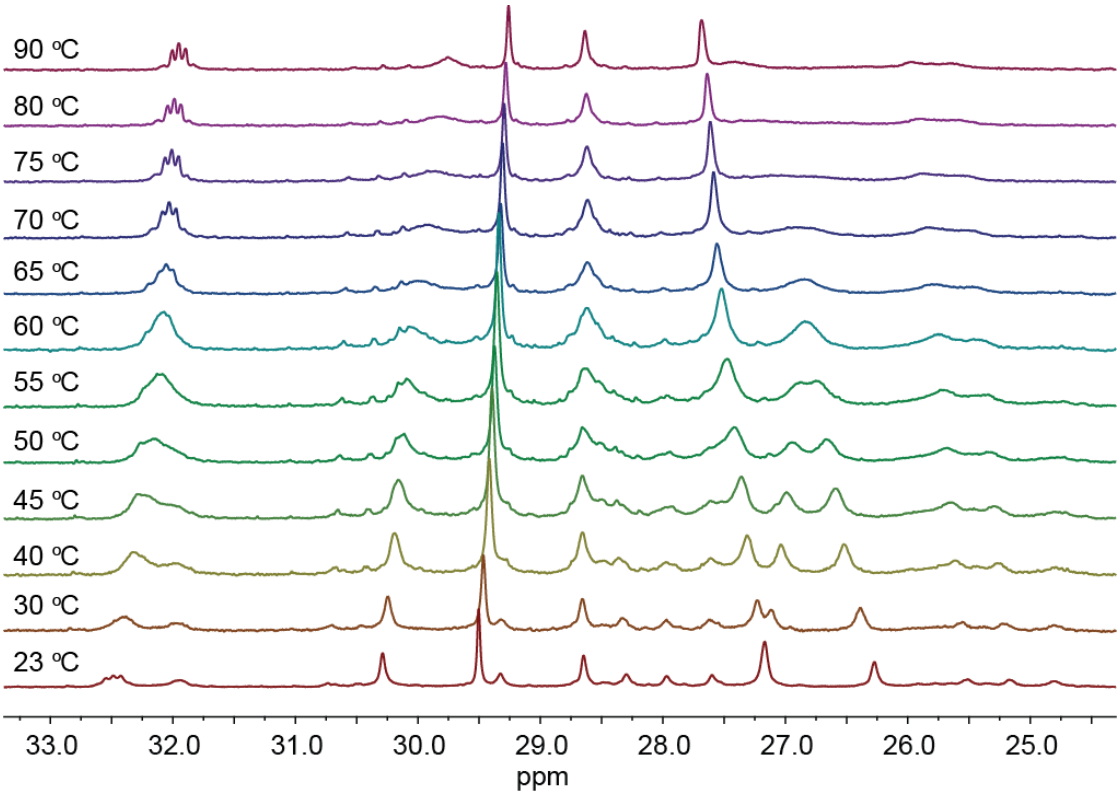

Figure A-2. $^{13}C\{^{1}H\}$ NMR spectra of *cis*-**2d** (126 MHz, C_6D_5Br, methylene signals only) as a function of temperature. The partial spectra in Figure 11 were taken from these traces.

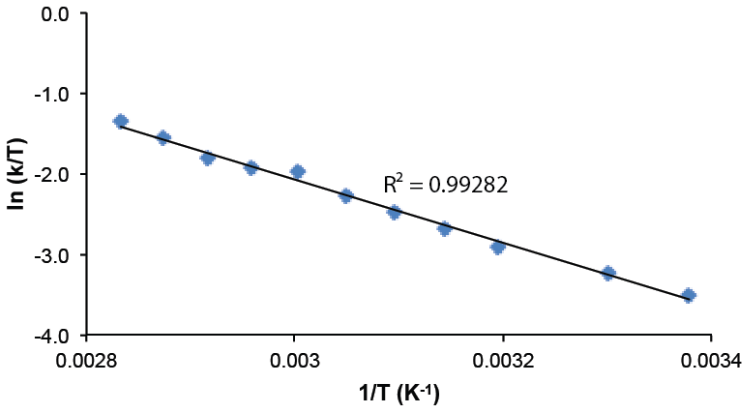

Figure A-3. Eyring plot using rate constants derived from Figure 11 for the "jump rope" bridge exchange in *cis*-**2d**.

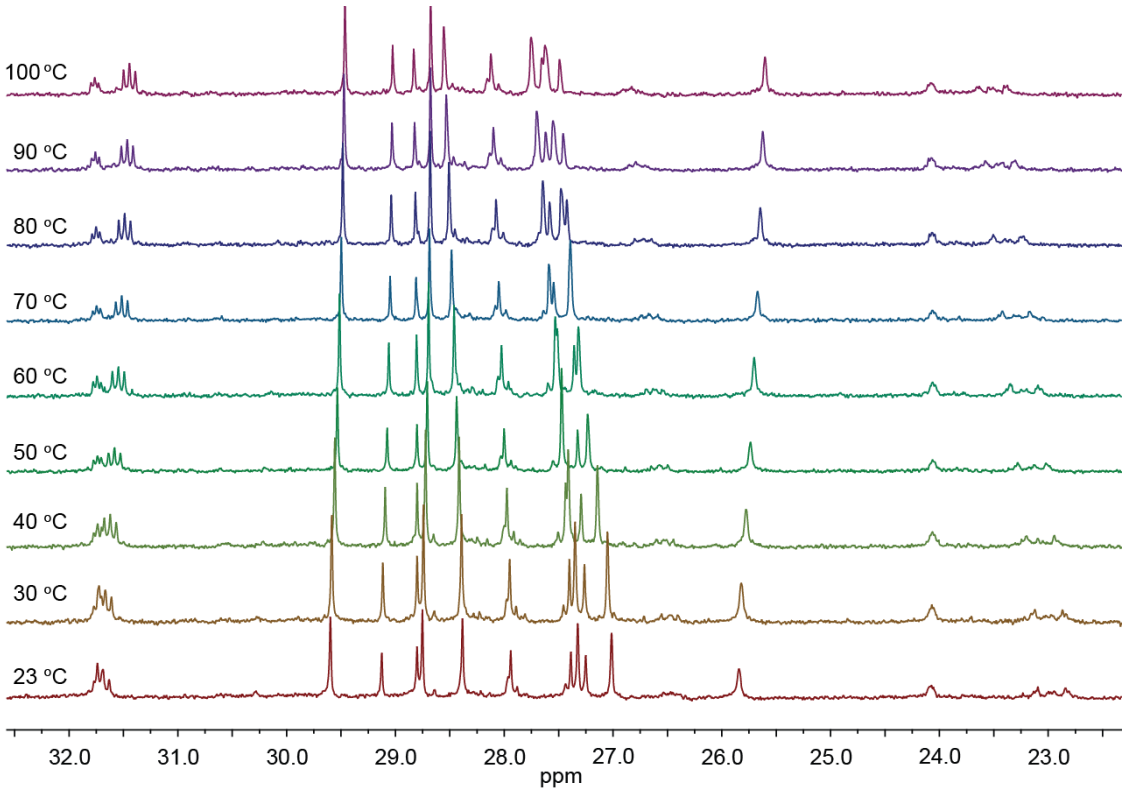

Figure A-4. Partial $^{13}C\{^{1}H\}$ NMR spectra of *cis*-**6d** (C_6D_5Br) as a function of temperature.

A-3. Thermolyses of Platinum Complexes (continued from section 2). D. An NMR tube was charged with *trans*-**2c** (0.0074 g, 0.0081 mmol) and C_6D_5Br (0.7 mL) and heated to 150 °C. After 2 d, the sample was cooled. $^{31}P\{^{1}H\}$ NMR (δ/ppm): 7.21 (s, $^{1}J_{PPt}$ = 2395 Hz,[s5] 100%; *trans*-**2c**). **E.** A NMR tube was charged with *trans*-**2c** (0.0050 g, 0.0055 mmol) and *o*-$C_6H_4Cl_2$ (0.5 mL), and heated at 180 °C. After 14 h, the sample was cooled. $^{31}P\{^{1}H\}$ NMR (δ/ppm), 5.9 (s, $^{1}J_{PPt}$ = 2426 Hz,[A5] 92%, *trans*-**2c**), 4.5 (s, 8%). **F.** An NMR tube was charged with *trans*-**2g** (0.0068 g, 0.0054 mmol) and C_6D_5Br (0.7 mL) and heated to 150 °C. After 2 d, the sample was cooled. $^{31}P\{^{1}H\}$ NMR (δ/ppm): 5.32 (s, $^{1}J_{PPt}$ = 2388 Hz,[A5] 100%; *trans*-**2g**). **G.** An NMR tube was charged with *cis*-**5b** (0.0016 g, 0.0019 mmol) and *o*-$C_6H_4Cl_2$ (0.7 mL) and heated to 110 °C. After 1 d, the

sample was cooled. $^{31}P\{^{1}H\}$ NMR (δ/ppm): 66.2 (s, $^{1}J_{PPt}$ = 5759 Hz,[A5] 100%; *cis*-**5b**). The tube was heated to 185 °C. After 2 d, the sample was cooled. The $^{31}P\{^{1}H\}$ NMR spectrum was unchanged.

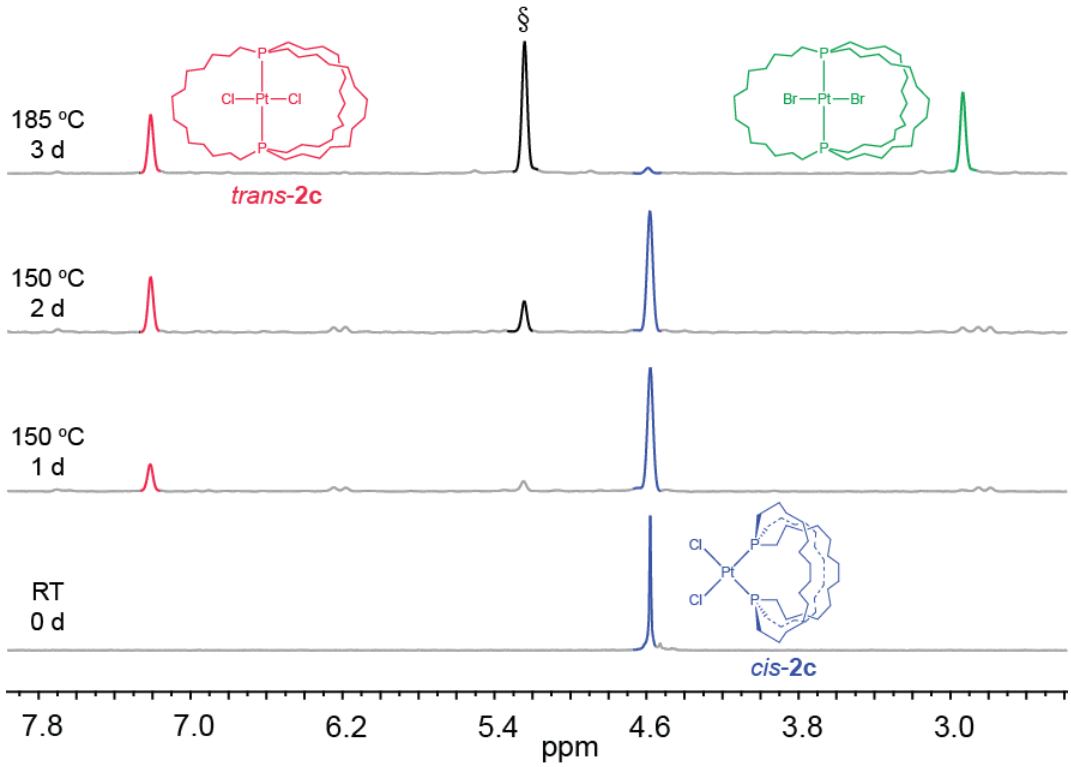

Figure A-5. Thermolysis of *cis*-**2c** in C_6D_5Br at 150 °C (2 d) and then 185 °C (1 d); $^{31}P\{^{1}H\}$ NMR data (§ denotes an unidentified substance believed to be oligomer).

A-4. Thermolysis of Rhenium Complexes (continued from section 2). B (*fac*-12'c). An NMR tube was charged with *fac*-**12'c** (0.050 g, 0.052 mmol) and C_6D_5Cl (0.7 mL) and heated to 130 °C. The reaction was monitored by $^{31}P\{^{1}H\}$ NMR. After 6 h, conversion was complete. The sample was filtered through alumina, which was rinsed with THF. The solvent was removed from the combined filtrates by oil pump vacuum to give previously reported *mer,trans*-**12'c** (0.009 g, 0.009 mmol, 17%)[A7] as a sticky white gum.

NMR (C_6D_5Cl, δ/ppm): **^{1}H** NMR (300 MHz) 2.13-1.60 (br m, 12H/12H, PCH_2/PCH_2CH_2), 1.58-1.03 (br m, 60H, remaining CH_2); **^{31}P{^{1}H}** (121 MHz) −7.2 (s). **IR** (cm^{-1}, oil film): 2013 (w, ν_{CO}), 1994 (w, ν_{CO}), 1927 (s, ν_{CO}), 1880 (s, ν_{CO}).

C (*fac*-13'c). An NMR tube was charged with *fac*-**13'c** (0.050 g, 0.050 mmol) and C_6D_5Cl (0.7 mL) and heated to 140 °C. The reaction was monitored by $^{31}P\{^1H\}$ NMR. After 2 d, conversion was complete. The sample was filtered through alumina, which was rinsed with THF. The solvent was removed from the combined filtrates by oil pump vacuum to give *mer, trans*-**13'c** (0.011 g, 0.011 mmol, 22%) as a sticky white gum.

NMR (C_6D_5Cl, δ/ppm): **^{1}H** (300 MHz) 2.25-1.88 (br m, 12H, PCH_2), 1.85-1.55 (br m, 12H, PCH_2CH_2), 1.54-1.03 (br m, 60H, remaining CH_2); **^{31}P{^{1}H}** (121 MHz) −12.2 (s). **IR** (cm^{-1}, oil film): 2023 (w, ν_{CO}), 1934 (s, ν_{CO}), 1888 (s, ν_{CO}). **MS**:[A8] 1000 (**M**$^+$, 5%), 972 (**M**$^+$ – CO, 70%), 944 (**M**$^+$ – 2CO, 35%), 921[A9] (**M**$^+$ – Br, 40%), 684 ($OP((CH_2)_{14})_3PO^+$, 100%), 668 ($P((CH_2)_{14})_3PO^+$, 60%), 652 ($P((CH_2)_{14})_3P^+$, 35%).

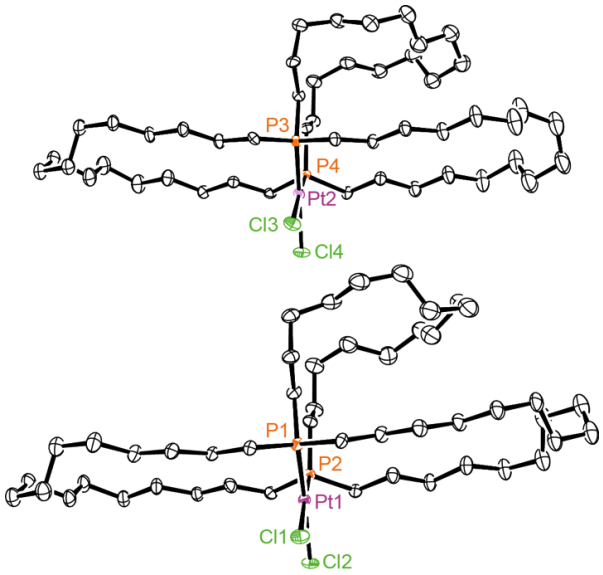

Figure A-6. Thermal ellipsoid plots (50% probability) for the two independent molecules of *cis*-**2d** in the unit cell.

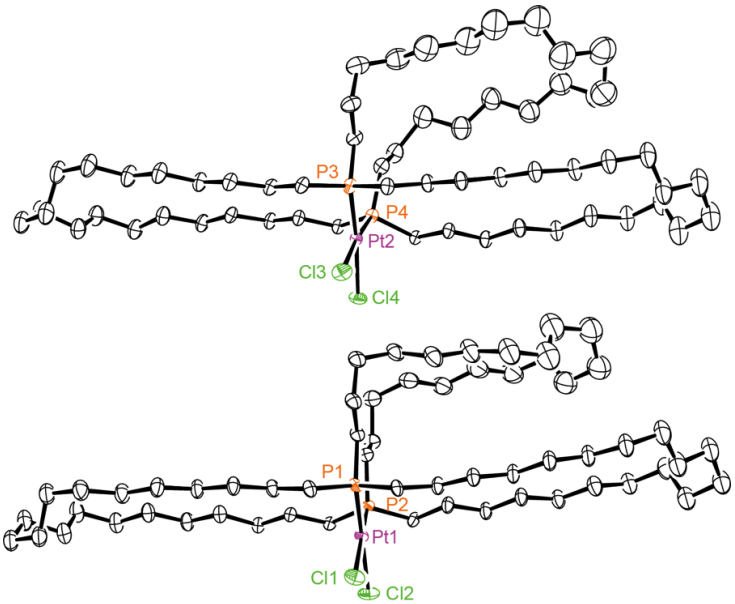

Figure A-7. Thermal ellipsoid plots (50% probability) for the two independent molecules of *cis*-**2f** in the unit cell.

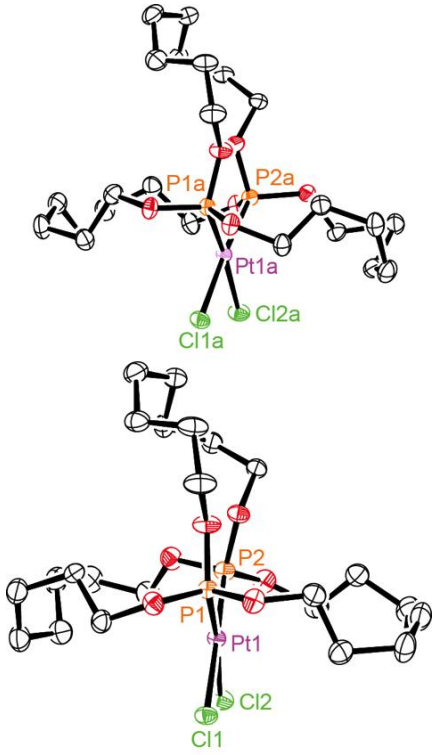

Figure A-8. Thermal ellipsoid plots (50% probability) for the two independent molecules of *cis*-**5a** in the unit cell.

A-5. DFT and molecular dynamics experiments from section 2. Computations were performed with the Gaussian09 program package, employing the ultrafine grid (99,590) to enhance accuracy.[A17] The gas phase geometries were optimized using DFT and the frequencies were analyzed to confirm that the structures were local minima. The B3LYP[A18-A20] functional was employed with an all-electron 6-311+G(d)[A21] basis set on all atoms except the transition metals, which were treated using an effective core potential (ECP), SDD.[A22] The heavier elements bromine and iodine used other ECPs.[A22,A23] Dispersion corrections were implemented using the D3 version of Grimme's dispersion function with Becke-Johnson damping (referred to as GD3BJ).[A24] A sample input file for a platinum complex with chloride ligands is given after the reference section.

Each structure output from the DFT calculations was subjected to molecular

dynamics computations, specifically simulated annealing, in order to sample the conformational space and identify the lowest energy conformer. This used the Materials Studio program package[A25] with the Forcite component.[A26] The lowest energy conformation was subsequently optimized by DFT as described above to obtain accurate energetics. The structure of each calculated species is disclosed in an xyz formatted text file (Supporting Information File 1) that can be opened with a variety of programs, e.g. Mercury.[A27]

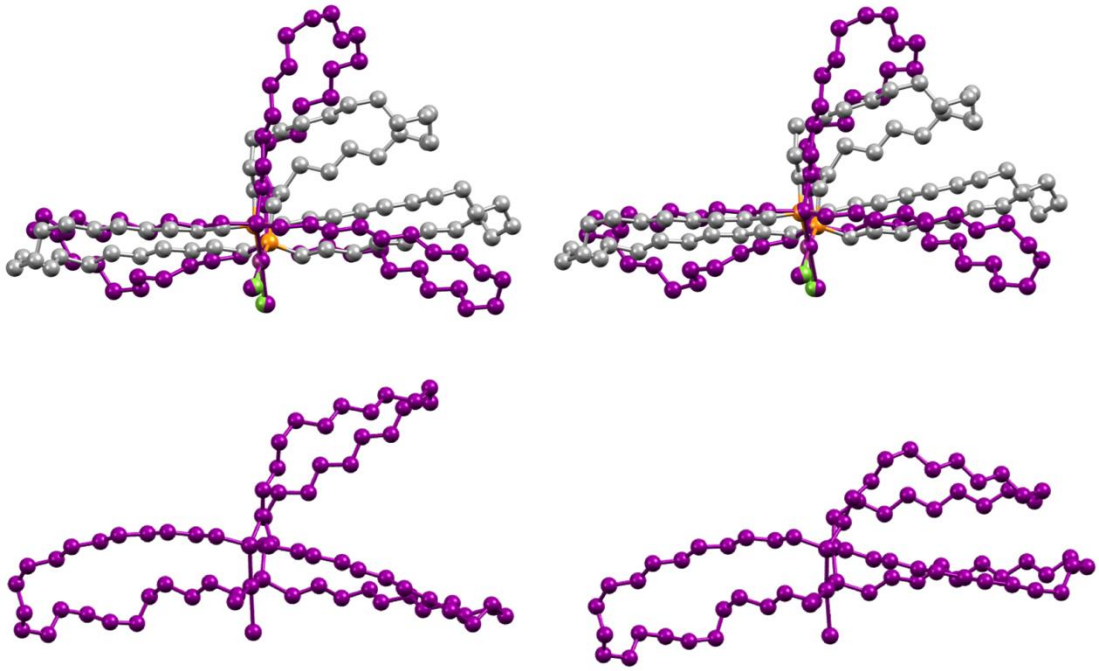

Figure A-9. Comparison of DFT results (purple atoms) using functionals uncorrected (left) and corrected for dispersion (right). top: *cis*-**2d**, superimposed over the crystal structure (one of two independent molecules); bottom: *cis*-**2f**.

A-6. Additional references for section 2.

(A1) Nawara-Hultzsch, A. J.; Skopek, K.; Shima, T.; Barbasiewicz, M.; Hess, G. D.; Skaper, D.; Gladysz, J. A. *Z. Naturforsch.* **2010**, *65b*, 414-424.

(A2) Kharel, S.; Joshi, H.; Bhuvanesh, N.; Gladysz, J. A. submitted to

Organometallics.

(A3) The P$CH_2CH_2CH_2$ ^{1}H and ^{13}C NMR signals of *cis*-**1g** and *cis*-**2d**,**g** were assigned by ^{1}H,^{1}H COSY, ^{1}H,^{13}C{^{1}H} COSY, ^{13}C{^{13}C} COSY, and ^{1}H,^{13}C{^{1}H} HMBC experiments. The corresponding signals of *cis*-**1f** and *cis*-**2b**,**c**,**e**,**f** were assigned analogously.

(A4) The *J* values given for virtual triplets represent the *apparent* couplings between adjacent peaks, and not the mathematically rigorously coupling constants. See Hersh, W. H. *J. Chem. Educ.* **1997**, *74*, 1485-1488.

(A5) This coupling represents a satellite (d, ^{195}Pt = 33.8%), and is not reflected in the peak multiplicity given.

(A6) Sandström, J. *Dynamic NMR Spectroscopy*; Academic Press: New York, 1982; pp 93-123.

(A7) Hess, G. D.; Fiedler, T.; Hampel, F.; Gladysz, J. A. *Inorg. Chem.* **2017**, 56, 7454-7469.

(A8) FAB, 3-NBA, *m/z* (relative intensity, %); the most intense peak of the isotope envelope is given.

(A9) The situation with this ion is similar to that described in footnote 48 of section 2.

(A10) *APEX3*, Bruker AXS Inc., Madison, WI, USA, 2012.

(A11) Sheldrick, G. M. *SADABS*, Bruker AXS Inc., Madison, WI, USA, 2001.

(A12) (a) Sheldrick, G. M. *Acta Cryst.* **2008**, *A64*, 112-122. (b) Sheldrick, G. M. *Acta Cryst.* **2015**, *A71*, 3-8. (c) Sheldrick, G. M. **2015**, *C71*, 3-8.

(A13) Spek, A. L. *J. Appl. Cryst.* **2003**, *36*, 7-13.

(A14) (a) Hooft, R. W. W. *Collect*; data collection software; Nonius BV: Delft, Netherlands, 1998. (b) Otwinowski, Z.; Minor, W. Processing of X-ray diffraction data

collected in oscillation mode. In *Methods in Enzymology*; Carter, C. W., Jr.; Sweet, R. M., Eds.; Macromolecular Crystallography, Vol. 276, Part A; Academic Press: New York, 1997; pp 307-326.

(A15) (a) Cromer, D. T.; Waber, J. T. International Tables for X-ray Crystallography, Table 2.2 A. Kynoch Press, Birmingham, England. 1974. (b) Ibers, J. A.; Hamilton, W. C. *Acta Crystallogr.* **1964**, *17*, 781-782.

(A16) Dolomanov, O. V.; Bourhis, L. J.; Gildea, R. J.; Howard, J. A. K.; Puschmann, H. *J. Appl. Cryst.* **2009***, 42*, 339-341.

(A17) Frisch, M. J.; Trucks, G. W.; Schlegel, H. B.; Scuseria, G. E.; Robb, M. A.; Cheeseman, J. R.; Scalmani, G.; Barone, V.; Mennucci, B.; Petersson, G. A.; Nakatsuji, H.; Caricato, M.; Li, X.; Hratchian, H. P.; Izmaylov, A. F.; Bloino, J.; Zheng, G.; Sonnenberg, J. L.; Hada, M.; Ehara, M.; Toyota, K.; Fukuda, R.; Hasegawa, J.; Ishida, M.; Nakajima, T.; Honda, Y.; Kitao, O.; Nakai, H.; Vreven, T.; Montgomery, J. A., Jr.; Peralta, J. E.; Ogliaro, F.; Bearpark, M.; Heyd, J. J.; Brothers, E.; Kudin, K. N.; Staroverov, V. N.; Kobayashi, R.; Normand, J.; Raghavachari, K.; Rendell, A.; Burant, J. C.; Iyengar, S. S.; Tomasi, J.; Cossi, M.; Rega, N.; Millam, J. M.; Klene, M.; Knox, J. E.; Cross, J. B.; Bakken, V.; Adamo, C.; Jaramillo, J.; Gomperts, R.; Stratmann, R. E.; Yazyev, O.; Austin, A. J.; Cammi, R.; Pomelli, C.; Ochterski, J. W.; Martin, R. L.; Morokuma, K.; Zakrzewski, V. G.; Voth, G. A.; Salvador, P.; Dannenberg, J. J.; Dapprich, S.; Daniels, A. D.; Farkas, Ö.; Foresman, J. B.; Ortiz, J. V.; Cioslowski, J.; Fox, D. J. *Gaussian 09, Revision D.01*; Gaussian, Inc., Wallingford CT, **2009**.

(A18) Becke, A. D. *Phys*. *Rev*. *A* **1988**, *38*, 3098-3100.

(A19) Becke, A. D. **1993**, *98*, 5648-5652.

(A20) Lee, C.; Yang, W.; Parr, R. G. *Phys*. *Rev*. *B* **1988**, *37*, 785-789.

(A21) Hariharan, P. C.; Pople, J. A. *Theor*. *Chim*. *Acta*, **1973**, *28*, 213-222.

(A22) Peterson, K. A.; Shepler, B.C.; Figgen, D.; Stoll, H. *J. Phys. Chem. A* **2006**, *110*, 13877-13883.

(A23) Peterson, K. A.; Figgen, D.; Goll, E.; Stoll, H.; Dolg, M. *J. Chem. Phys.* **2003**, *119*, 11113-11123.

(A24) Grimme, S.; Ehrlich, S.; Goerigk, L. *J. Comput. Chem.* **2011**, *32*, 1456-1465.

(A25) Dassault Systèmes BIOVIA, Materials Studio, 6.0, San Diego: Dassault Systèmes, 2017.

(A26) The specific parameters used with the Forcite module were as follows: NVT ensemble with random initial velocities, initial temperature of 300 K, mid-cycle temperature of 700 K, 10 heating ramps per cycle, 100 dynamic steps per ramp. Thus, the total number of steps was 100,000. The sampled structures were automatically geometry optimized after each cycle using the smart algorithm with a fine convergence tolerance (energy of 0.0001 kcal/mol, force of 0.005 kcal/mol·Å, displacement of 0.00005 Å, maximum of 10,000 iterations; the time steps associated with the annealing were 1.0 fs frames).

(A27) Macrae, C. F.; Bruno, I. J.; Chisholm, J. A.; Edgington, P. R.; McCabe, P.; Pidcock, E.; Rodriguez-Monge, L.; Taylor, R.; van de Streek, J.; Wood, P. A. **2008**, *41*, 466-470.

APPENDIX B

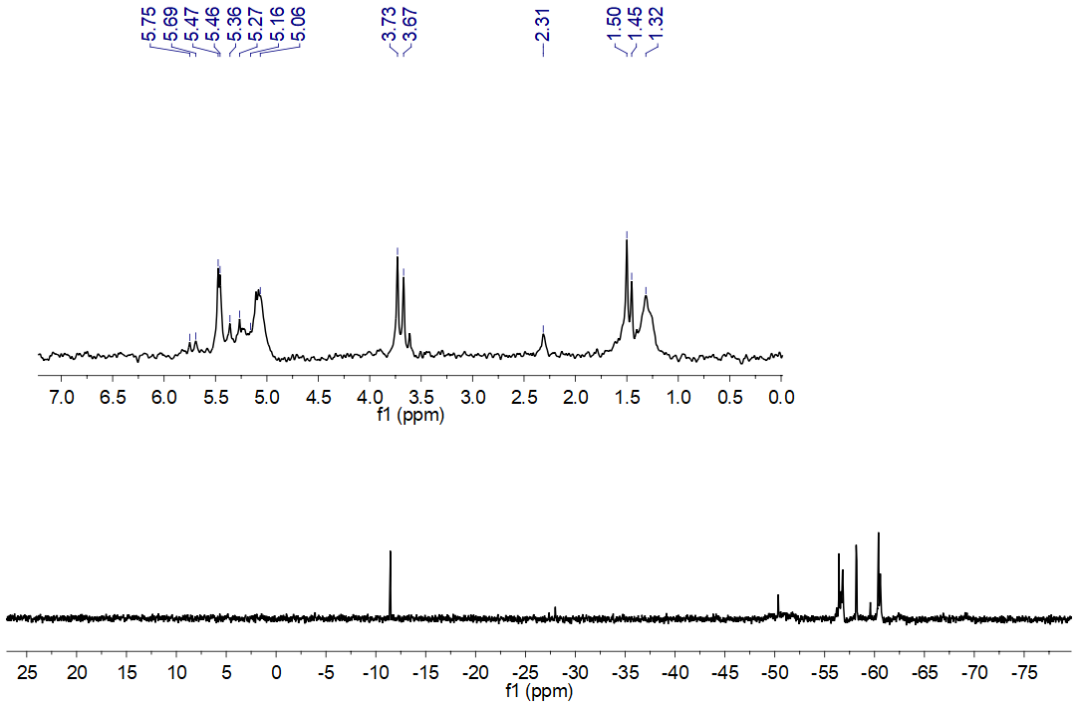

Figure B-1. $^{31}P\{^{1}H\}$ NMR spectrum ($CDCl_3$) of the soluble crude product following partial completion of the metathesis step in Scheme 5 in section 3.

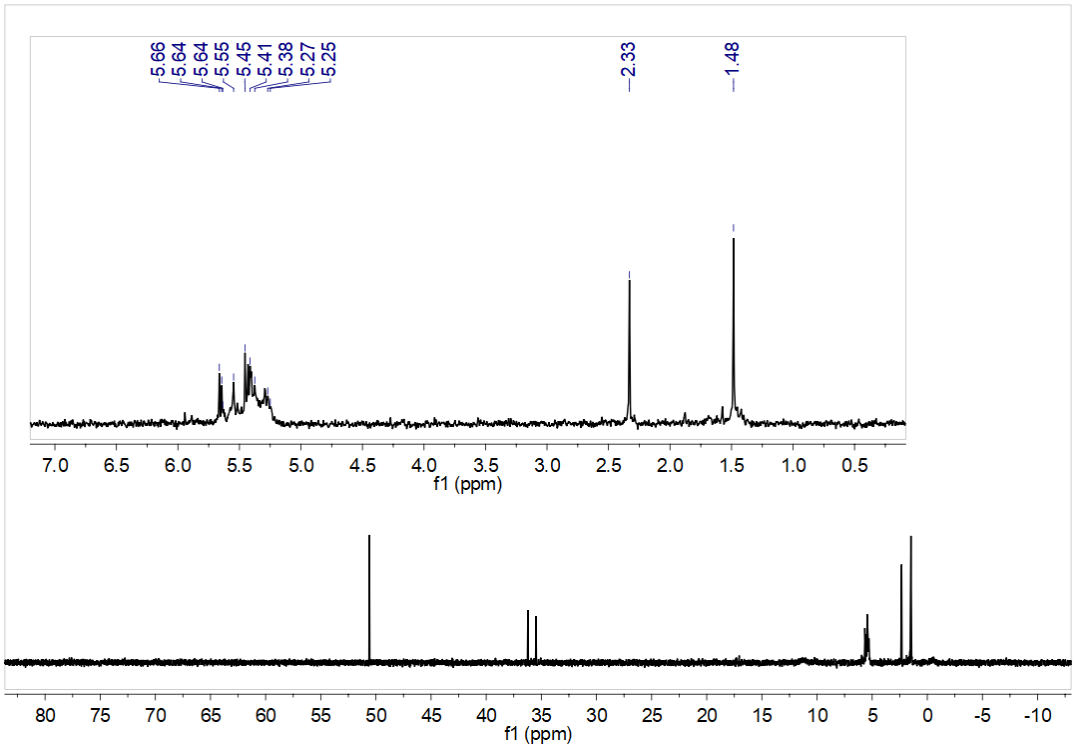

Figure B-2. $^{31}P\{^{1}H\}$ NMR spectrum ($CDCl_3$) of the soluble crude product following completion of the metathesis step in Scheme 5 in section 3.

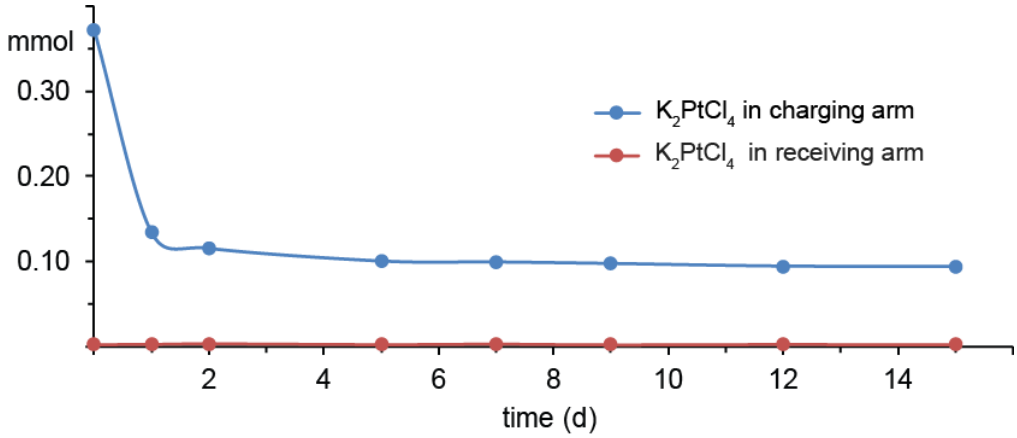

Figure B-3. Disappearance of K_2PtCl_4 (0.372 mmol) from the charging arm (•) and appearance of K_2PtCl_4 in the receiving arm (•; 2.45 mmol KCl) using DMPE (0.368 mmol) in the CH_2Cl_2 phase.

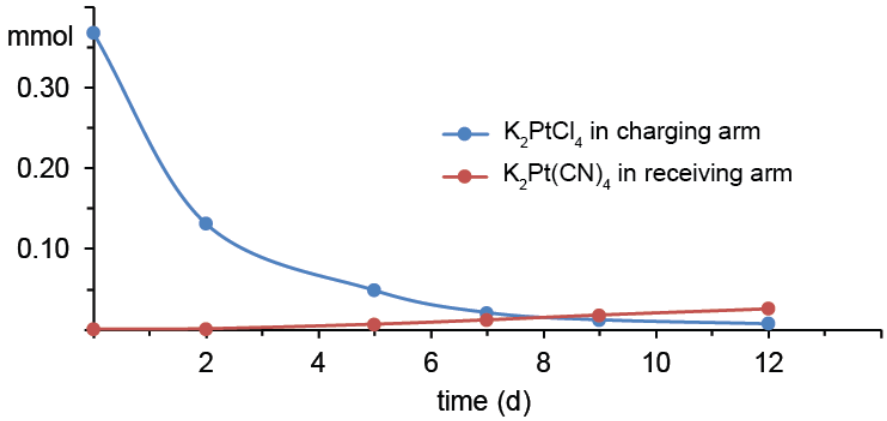

Figure B-4. Disappearance of K_2PtCl_4 (0.368 mmol) from the charging arm (•) and appearance of $K_2Pt(CN)_4$ in the receiving arm (•; 3.69 mmol KCN) using DMPE (0.245 mmol) in the CH_2Cl_2 phase.

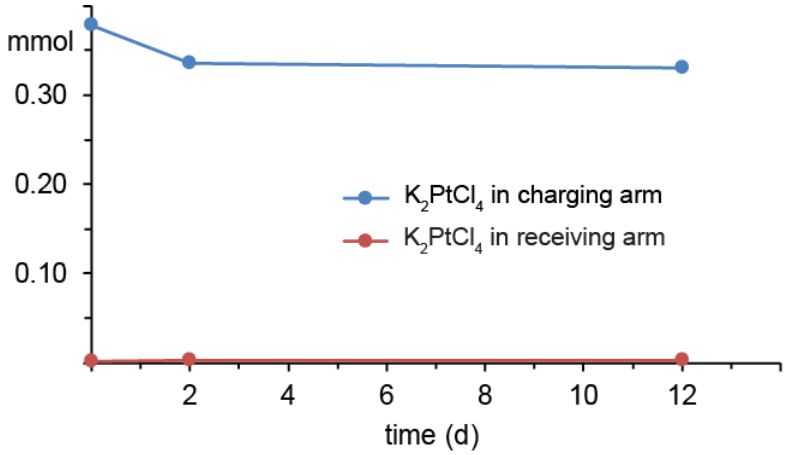

Figure B-5. Disappearance of K_2PtCl_4 (0.379 mmol) from the charging arm (•) and appearance of K_2PtCl_4 in the receiving arm (•; 3.77 mmol KCl) using (*n*-Oct)$_3$P (0.247 mmol) in the CH_2Cl_2 phase.

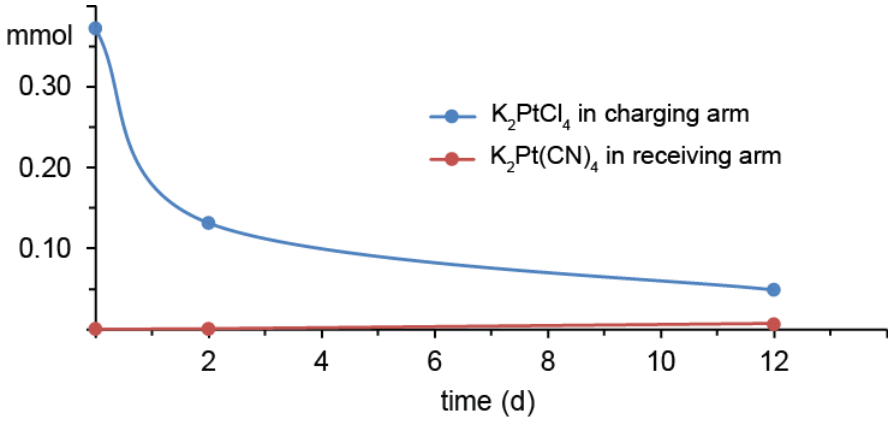

Figure B-6. Disappearance of K_2PtCl_4 (0.372 mmol) from the charging arm (•) and appearance of $K_2Pt(CN)_4$ in the receiving arm (•; 3.63 mmol KCN) using (*n*-Oct)$_3$P (0.247 mmol) in the CH_2Cl_2 phase.

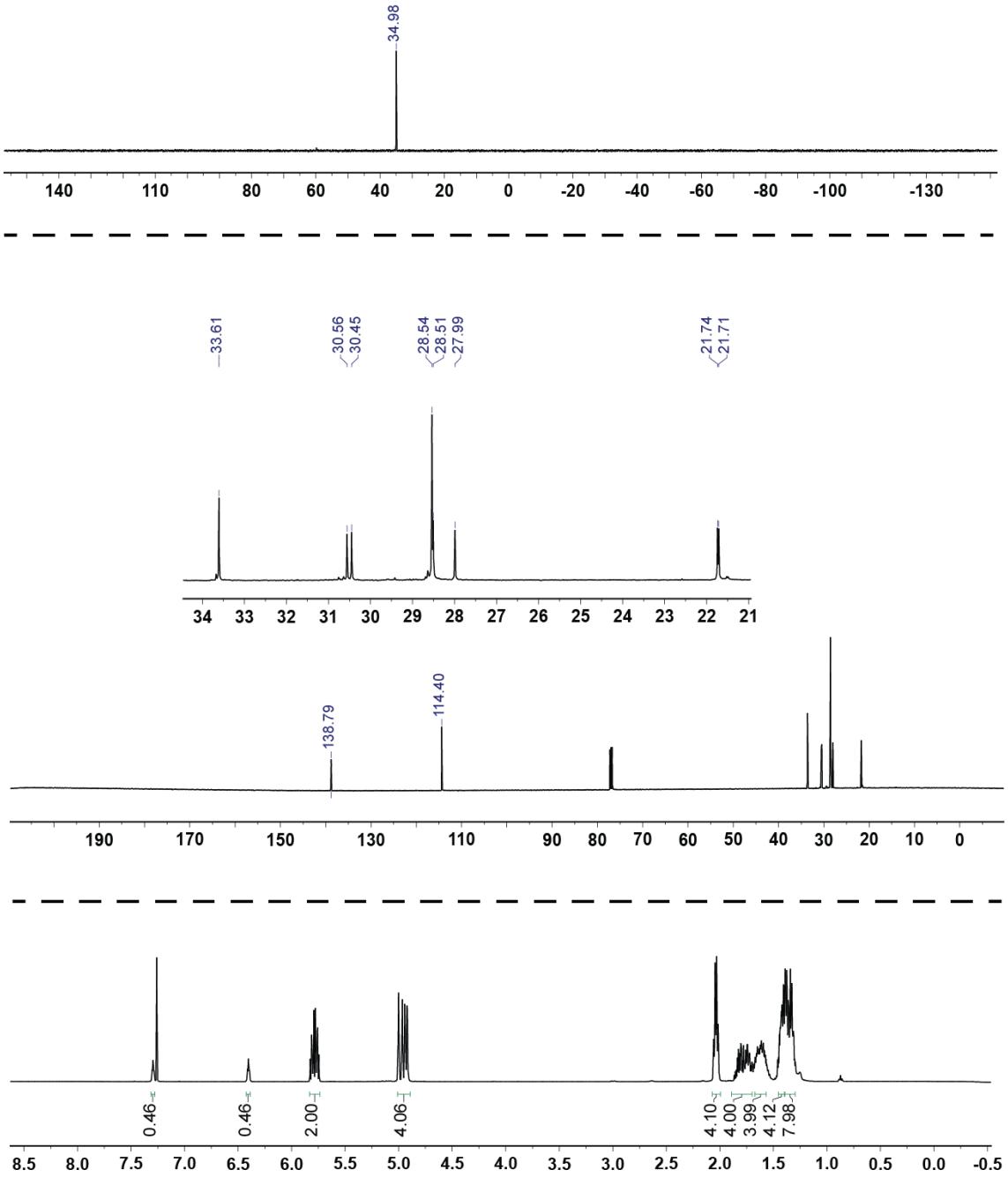

Figure B-7. NMR spectra of **2c** in $CDCl_3$: $^{31}P\{^1H\}$ (top), $^{13}C\{^1H\}$ with inset expanding the aliphatic carbon signals (middle), ^1H (bottom).

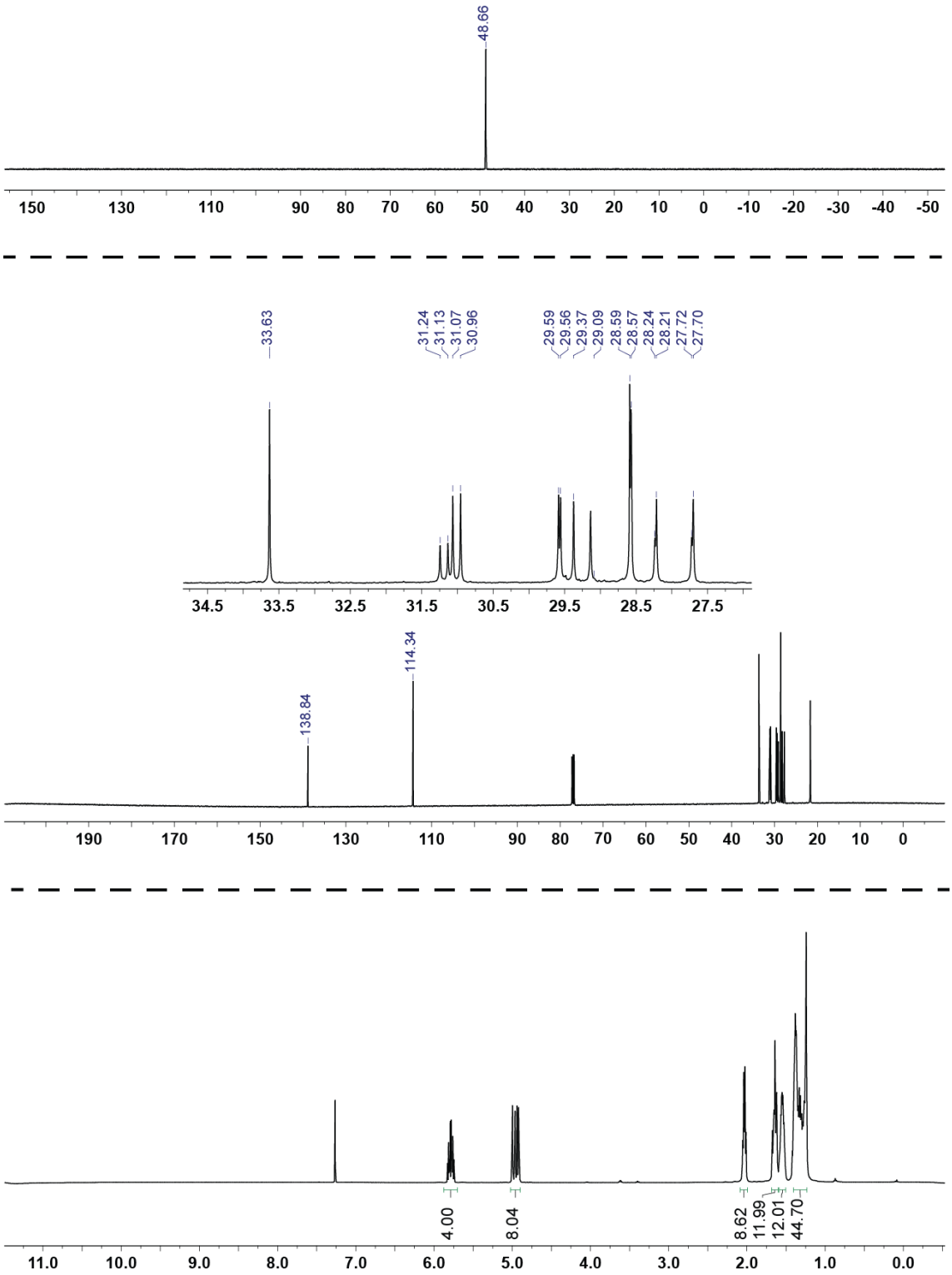

Figure B-8. NMR spectra of **3cd'** in $CDCl_3$: $^{31}P\{^1H\}$ (top), $^{13}C\{^1H\}$ with inset expanding the aliphatic carbon signals (middle), ^1H (bottom).

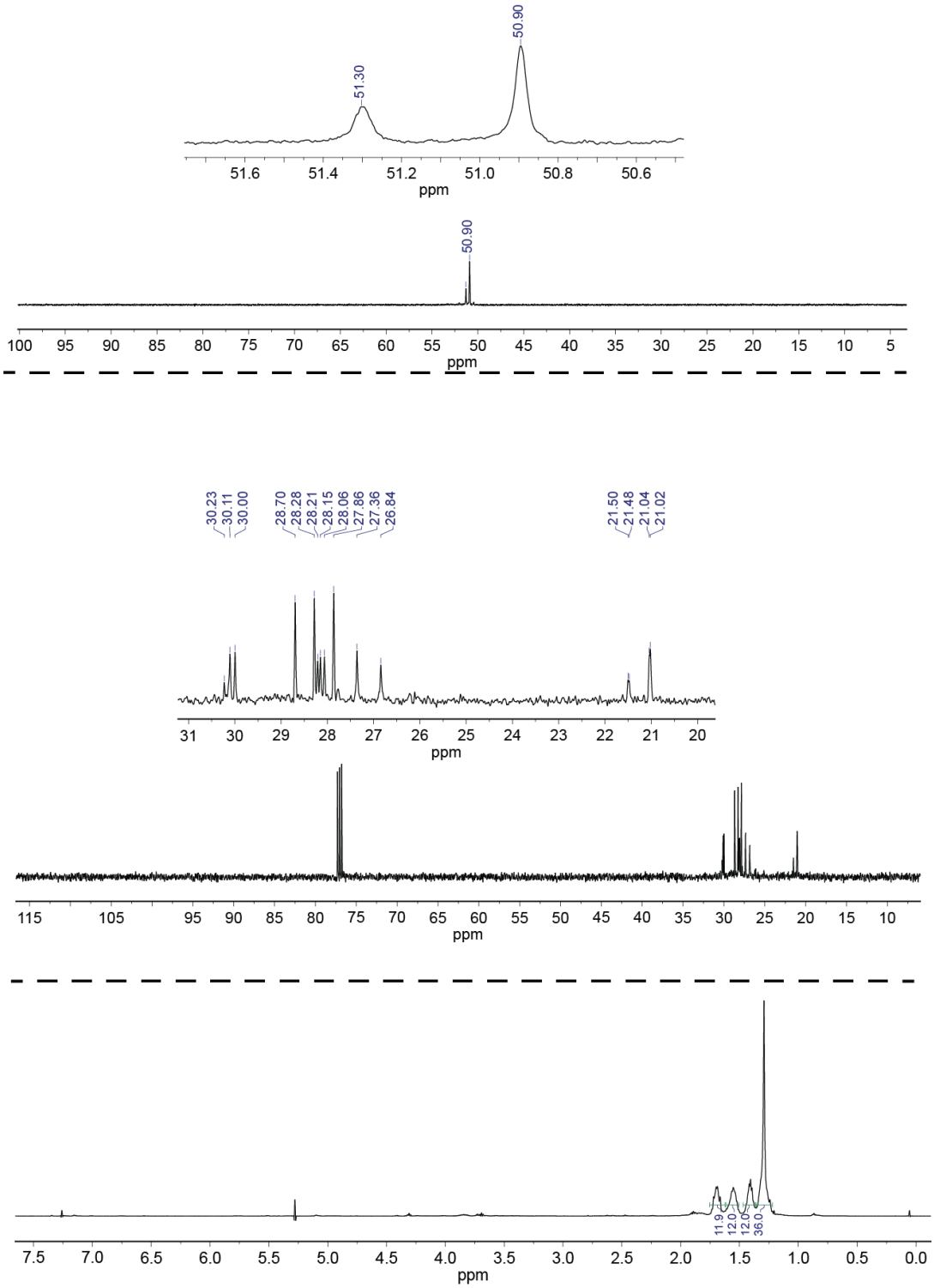

Figure B-9. NMR spectra of **4bc'** in $CDCl_3$: $^{31}P\{^1H\}$ (top), $^{13}C\{^1H\}$ with inset expanding the aliphatic carbon signals (middle), ^1H (bottom).